Potentiel thérapeutique de la modulation de la transition epithélio-mésenchymateuse via le ciblage de nétrine 1 dans le cancer

Melanie Bellina

Université Claude Bernard Lyon 1

THÈSE DE DOCTORAT DE
L'UNIVERSITE CLAUDE BERNARD LYON 1

Ecole Doctorale N° 340
Biologie moléculaire intégrative et cellulaire

Discipline : Oncologie

Soutenue publiquement le 20/10/2023, par :
Mélanie Jessica BELLINA

Potentiel thérapeutique de la modulation de la transition épithélio-mésenchymateuse via le ciblage de nétrine 1 dans le cancer

---

Devant le jury composé de :

Prof. Moyret-Lalle Caroline	UCBL1, Lyon	Présidente
Dr. Pannequin Julie	IGF, CNRS, Montpellier	Rapportrice
Dr. Roman-Roman Sergio	Institut Curie, Paris	Rapporteur
Dr. Savagner Pierre	Gustave Roussy, CNRS, Paris UCBL1, Lyon	Examinateur
Prof. Bernet Agnès		Directrice de thèse
Dr. Ducarouge Benjamin	NETRIS Pharma, Lyon	Co-encadrant
Dr. Mehlen Patrick	CRCL, Lyon	Invité

UNIVERSITE CLAUDE BERNARD - LYON 1

Président de l'Université	**M. le Professeur Frédéric FLEURY**
Président du Conseil Académique	M. le Professeur Hamda BEN HADID
Vice-président du Conseil d'Administration	
Vice-président du Conseil Formation et Vie Universitaire	M. le Professeur Christophe VITON
Vice-président de la Commission Recherche	M. le Professeur Philippe CASSAGNAU
Directeur Général des Services	M. Pierre ROLLAND

COMPOSANTES SANTE

Faculté de Médecine Lyon Est – Claude Bernard	Directeur : M. le Professeur G. RODE
Faculté de Médecine et de Maïeutique Lyon Sud – Charles Mérieux	Directeur : M. le Professeur P. PAPAREL
Faculté d'Odontologie	Directeur : M. le Professeur J.-C. MAURIN
Institut des Sciences Pharmaceutiques et Biologiques	Directeur : M. le Professeur C. DUSSART
Institut des Sciences et Techniques de la Réadaptation	Directeur : M. le Professeur J. LUAUTE

COMPOSANTES ET DEPARTEMENTS DE SCIENCES ET TECHNOLOGIE

Institut National Supérieur du Professorat et de l'Education	Directeur : M. P. CHAREYRON
Institut Universitaire de Technologie Lyon 1	Directeur : M. le Professeur M. MASSENZIO
Institut de Sciences Financière et d'Assurances	Directeur : M. N. LEBOISNE
Observatoire de Lyon	Directeur : Mme. la Professeure I. Daniel
Polytech Lyon	Directeur : M. le Professeur E. PERRIN
UFR Sciences et Techniques des Activités Physiques et Sportives	Directeur : M. le Professeur G. BODET
UFR Chimie, Mathématique, Physique	Directeur : M. le Professeur B. ANDRIOLETTI
UFR Biosciences	Directeur : Mme. la Professeure K. GIESLER
Génie Electrique des Procédés	Directeur : Mme. la Professeure R. FERRIGNO
Informatique	Directeur : Mme. la Professeure S. BOUAKAZ BRONDEL
Mécanique	Directeur : M. M. BUFFAT

Due to my fluency and a greater ease for writing in English, the following manuscript has been entirely formulated in the language of Shakespeare, with the exception of the review presented in the first chapter of my introduction written during the COVID-19 pandemic lockdown and which has been published in the French scientific magazine "médecine/sciences", and therefore written in French.

Du fait de ma fluidité et de mon aisance en anglais, ce manuscrit a été entièrement rédigé dans la langue de Shakespeare, à l'exception d'une revue présentée dans le premier chapitre de l'introduction qui a été rédigée en français pendant le confinement de la pandémie COVID-19, et qui a été publié dans le magazine scientifique « médecine/sciences ».

ACKNOWLEDGEMENTS

Throughout the past 4 years during which my thesis was carried out, I have come across a plethora of people that have impacted my work and my life in many different ways. I would like to take a couple of pages to thank some of them for their particular impact in the incredible experience that my adventure as a PhD student has been.

I would first of all like to thank the members of my jury for evaluating my work and for their benevolence during my thesis defence: Prof Caroline Moyret-Lalle, Dr. Pierre Savagner, Dr. Julie Pannequin and Dr. Sergio Roman-Roman. I'd like to especially thank Dr. Pannequin and Dr. Roman-Roman who also committed some extra time to review my manuscript and give me their feedback. I also thank Dr. Julie Caramel and Dr. Ievgenia Pastuschenko for being part of my Thesis Monitoring Committee and for their feedback on the advancement of my thesis project. It has been a pleasure interacting with you all.

I'd like to thank Dr. Patrick Mehlen for welcoming me in his laboratory and in NETRIS Pharma, and for his trust during my thesis. I'd like to also thank Prof. Agnès Bernet, my thesis director, for her mentoring throughout these past 4 years. Your unfailing determination and belief in the project have enabled it to culminate in not one but 2 publications in Nature (amongst other papers). A PhD student could not wish for a better outcome of their hard work. Maybe it is true that it is "dans le rush que l'on fait des belles histoires…". Thank you also to Dr. Benjamin Ducarouge, my thesis co-supervisor, for your advice and help in the EMT project. You have enabled me to develop essential skills in experimentation and critical thinking that will for sure be of great use for the rest of my career.

My work would not have been of such value without the participation of all of our collaborators. Thank you first of all to the team of Dr. Xavier Dolcet, in particular Dr. Raul Navaridas. Thank you for welcoming me to the Institut de Recerca Biomedica de Lleida, and for letting me learn from you. You along with all the other team members (Aida, Maria, Cris, Pol, Manel, Anna, Carlos (y Maia), Gisela y Anna) have welcomed me with open arms and made me feel like one of team for the entire duration of my stay. It has been one of my favourite adventures of my thesis. Congratulations for those who have since then graduated and moved on to the next chapter of your careers, I wish you all the best and hope our paths will eventually cross again. Thank you to Prof. Cedric Blanpain and his team, especially Dr. Justine Lengrand for passing the torch on to me as you moved on to carry out your post-doc where your valuable work has definitely brought this project to the next level. Thank you for your support, friendship, and encouragement. Thank you, Prof. Darren Carpizo, Anthony Casabianca, and Dr. Stephany Fiore for your work on everything relating to the extracellular vesicles. Thank you also to Yohann Coute, Elizabeth Errazuriz-Cerda and Prof. Alain Brisson for all your precious advice and work on the extracellular vesicles as well. Thank you, Dr. Frédéric Catez, and Dr. Anne Vincent for your support on the EV isolations and for letting me periodically monopolise some of your lab space. Thank you Prof. Hichem Mertani and Dr. Mounira Chalabi for your help on mastering the invasion experiments. You have all been so very kind and helpful.

The life experience that was my thesis would not have been the same without the amazing team of colleagues and friends that have been there through the ups and downs.

Thank you, Dr. Laure Bougarel, for having welcomed me in your office and been of great support throughout the tough times that a thesis can be. You have kept me motivated and pushed me

to grow as a person. Thank you for the many many (many) conversations, the fashion shows, the pep talks, and your friendship.

Thank you, Dr. Camille Victoor (sounds so fancy!). I'm grateful to fate for having allowed us to live this experience together. You have been a key player in the preservation of my mental health. Here's to our brainstorming sugar breaks, your positive attitude, the beginning of our scientific modelling careers, your enormously kind heart, our movie marathons, and so much more…

Thank you, David Neves, for your mentoring and patience as I slowly but surely got accustomed to being around and working on our little furry (and unfurry) friends, as well as supporting me in multiple other experimentations. The broadness of your scientific knowledge never ceases to amaze me. Thank you also for the coffee breaks, the songs stuck in my head, the pep talks, and the salsa chats (I'm still waiting to be invited for a dance...).

Thank you, Dr. Emilie Branche, for your investment in the progression of my project as your feedback has been of valuable help, especially regarding my thesis defence. Thank you for your support and humour, it has been a true pleasure.

Thank you to the other PhD students of NETRIS Pharma for your kindness and support: Nerea Muñoz, Amélie Bécar, Ruxanda Chira, Nicolas Braissand. Thank you for your time and for all the lunch breaks (hold on tight, you're doing great). Thank you to Dr. David Goldschneider for his help and advice on anything relating to molecular biology and for the late-night crash course on gene cloning. Thank you, Victoria Billecocq, for ensuring a safe and benevolent work environment, you enable us students to feel good and taken care of which is all we could as for. And thank you to all the interns that I have had the pleasure of interacting with, notably Romeo Berger for his implication on my project.

I'd also like to thank the members of Dr. Patrick Mehlen's team, notably Nicolas Rama for his work on everything bioinformatic, and Laurent Fattet for his participation in the EMT project. Thank you also to all the other students I've had the pleasure of getting to know, some a bit more than others, and share some great moments, may they be of scientific nature or of a more social and personal aspect. Thank you to the PhD veterans that are now scattered throughout the globe: Ambroise (I hope I get to sleep on your couch in San Diego soon), Mélissa, Anna-Rita, Verena and Mathieu. Thank you to the ones still grinding hard: Lisa, Maeva, Thomas, Sonia, and Silvia. And thank you to all the others: Céline, Aurélie, Kristina, Laura, Valentin, Antoine, Erivan and of course, Sarah who has been of especially great support outside of the lab, may it be at home or at the other end of the world. I shall keep in mind our Marseille weekend, the ski trips, the after-works, the unfortunate COVID Christmas, and many other lovely memories.

I must also take the time to thank all my support system outside of the laboratory who has enabled me to recharge and stay focused, keeping my head above water.

Thank you to all the Covidiotas and to the Slide association, to Justine for our one-on-one quarterly updates, and to Alice who I've had the pleasure of meeting during my time as a teaching staff and has greatly participated in the growth of my desire to make education part of my career plan. Thank you all for your time, your cheerfulness and support.

A very big thank you also to my partner Alejandro Salinas Ruiz for sticking by me during this challenging time. Thank you for your patience, your kindness, your cooking, your motivation, your reassurance, and your ability to make me smile and bring some lightness back into life when times got a little tough.

And finally, thank you to my mother Marie Bellina who, despite not totally understanding what I've been doing for the past decade, has been infinitely supportive, patient, loving, and understanding. Thank you also to the rest of my close family for cheering me on: Jeremy, Jonathan, Coralie, and Jeanne, as well as my extended family. And thank you to my late father Jacques Bellina for, as he always liked to say, passing his brain onto me. From childhood you have pushed all your

kids to work hard, and I believe I also have you to thank for getting to the point I am today. This work is dedicated to you.

Mélanie Bellina

Lyon, 19th January 2024

To my father.

Therapeutic potential of the modulation of the epithelial to mesenchymal transition via netrin 1 blockade in cancer

Résumé du travail de thèse

La nétrine 1 (NTN1) est une molécule sécrétée initialement découverte dans les années 1940 pour son implication dans le développement du système nerveux via le guidage des axones commissuraux. Le laboratoire dans lequel j'ai effectué mon travail de thèse dirigé par le Dr. Patrick Mehlen a montré que la réactivation, voire surexpression, de l'expression de NTN1 à l'âge adulte est associée au développement de nombreux cancers agressifs. Liée à l'activation de nombreuses voies de signalisation impliquées dans la modulation de l'inflammation, la prolifération, la survie, et la migration cellulaire, son ciblage thérapeutique présente un potentiel dans le traitement cancéreux. En 2016, la start-up française NETRIS Pharma, issue du laboratoire, a développé un anticorps monoclonal humanisé dirigé contre NTN1. Cet anticorps inhibe l'interaction de NTN1 avec son récepteur à dépendance Uncoordinated-5B (UNC5B), induisant la mort des cellules par apoptose. Testé en essai clinique de phase I sur de multiples indications cancéreuses avancées à métastatiques, l'anticorps a prouvé sa non-toxicité et montré une efficacité chez l'Homme. De plus, nos travaux sur des biopsies métastatiques de patientes atteintes de cancer de l'endomètre réalisées au cours de cet essai clinique, complétés par l'analyse des modèles précliniques *in vitro* et *in vivo* de cette pathologie, ont mis en évidence un nouvel effet du traitement sur le profil épithélial et mésenchymateux des cellules cancéreuses.

Les travaux réalisés au cours de ma thèse et présentés dans ce manuscrit démontrent l'effet du ciblage de NTN1 par un nouvel anticorps humanisé sur la mort des cellules tumourales ainsi que sur l'épithélialisation des tumeurs, conduisant à l'inhibition de la transition des cellules tumourales vers des phénotypes et fonctions cellulaires mésenchymateuses. Cet effet est également associé à une modification de l'infiltrat immunitaire et des cellules stromales, tout cela couplé à une sensibilisation des tissus cancéreux à des traitements standards de type chimio-thérapeutiques. Ces résultats ont permis la publication de deux articles dans la revue Nature.

Ma thèse a été financée par une Convention industrielle de formation par la recherche (Cifre) du ministère de l'Enseignement Supérieur de la Recherche et de l'Innovation, en étroite collaboration entre le laboratoire du Dr. Mehlen au CRCL et de la start-up NETRIS Pharma.

Summary of thesis work

Netrin 1 (NTN1) is a secreted molecule initially discovered in the 1940s for its implication in the development of the neural system through the guidance of commissural axons. The laboratory in which I conducted my thesis work under the direction of Dr. Patrick Mehlen showed that the reactivation of NTN1 expression in adulthood and its overexpression is associated with the development of numerous aggressive cancers. Due to its induction of manifold signalling pathways implicated in the modulation of inflammation, proliferation, survival and cell migration, its therapeutic targeting offers great potential in the treatment of cancer. In 2016, the French biotech start-up NETRIS Pharma that arose from the laboratory, developed a monoclonal humanized antibody directed against NTN1. This antibody inhibits the interaction of NTN1 with its dependence receptor Uncoordinated-5B (UNC5B), triggering the death of cells through the induction of apoptosis. Tested in phase I clinical trials on multiple advanced and metastatic cancer indications, the antibody has proven its absence of toxicity and its efficacy in humans. Furthermore, our work on metastatic endometrial cancer patients' biopsies carried out over the course of the clinical trial, along with preclinical *in vitro* and *in vivo* models of this disease, have highlighted the effect of the treatment on the epithelial and mesenchymal profile of cancer cells.

The work conducted over the course of my thesis and presented in this manuscript demonstrates the effect of NTN1 targeting by this antibody on the death of tumour cells as well as the epithelialization of tumours, leading to the inhibition of mesenchymal cellular properties, associated with a modulation of the immune infiltrate and of stromal cells. Altogether, these effects are also linked to a sensitization of cancer tissues to standard chemotherapy treatment options.

My thesis was financed by an industrial convention of formation by research (Cifre) from the Ministry of Higher Education and Research, in close collaboration between the laboratory of Dr. Mehlen and the NETRIS Pharma start-up.

Table of Contents

List of abbreviations

3DCRT	Three-Dimensional Conformal Radiation Therapy
AE	Adverse Event
AKT	protein kinase B
AOM	Azoxymethane
APC	Antigen Presenting Cell
ARID	AT-Rich Interaction Domain
ATP	Adenosine TriPhosphate
BAF	Barrier-to-Autointegration Factor
BMI	Body Mass Index
BRRS	Bannayan-Riley-Ruvalcaba Syndrome
CAF	Cancer Associated Fibroblast
CDR	Complementarity-Determining Region
cfDNA	cell-free DesoxyriboNucleic Acid
CRCL	Cancer Research Centre of Lyon
CS	Cowden Syndrome
CSC	Cancer Stem Cells
CT	Computerized Tomography
ctDNA	circulating tumour DesoxyriboNucleic Acid
CTNNB1	Catenin Beta 1
CXCL	C-X-C motif chemokine Ligand
DBD	DNA-Binding Domain
DCC	Deleted in Colorectal Cancer
DLT	Dose Limiting Toxicity
DNA	DeoxyriboNucleic Acid
DSS	Dextran Sodium Sulfate
EBRT	External Beam Radiation Therapy
EC	Endometrial Cancer
ECM	Extra-Cellular Matrix
EEC	Endometrioid Endometrial Carcinoma
EGF	Epidermic Growth Factor
ELISA	Enzyme-Linked ImmunoSorbent Assay
EMT	Epithelial to Mesenchymal Transition
EMT-TF	Epithelial to Mesenchymal Transition Transcription Factor
EPCAM	Epithelial Cell Adhesion Molecule
EV	Extracellular Vesicle
FAK	Focal Adhesion Kinase
FGF	Fibroblast Growth Factor
FGFR	Fibroblast Growth Factor Receptor

FIGO	International Federation of Gynaecology and Obstetrics
FIH	First-In-Human
FLRT2	Fibronectin Leucine-rich Repeat Transmembrane protein 2
FSH	Follicle Stimulating Hormone
FZD	Frizzled receptor
G1/G2/G3	Grade 1 / Grade 2 / Grade 3
GnRH	Gonadotropin hormone-Releasing Hormone
GOG	Gynaecologic Oncology Group
GSK	Glycogen Synthase Kinase
GTP	Guanosine triphosphate
HDR	High Dose Rate
HGF	Hepatocyte Growth Factor
HIF	Hypoxia-Inducible Factor
HNPCC	Hereditary Nonpolyposis Colorectal Cancer
HR	Hormone Receptor
IARC	International Agency for Research on Cancer
IgG1	Immunoglobulin G1
IL	InterLeukine
IMRT	Intensity-Modulated Radiation Therapy
IRR	Infusion Related Reaction
JAK	Janus Kinase
KRAS	Kirsten Rat Sarcoma virus
LDR	Low Dose Rate
LH	Luteinizing Hormone
LS	Lynch Syndrome
LVSI	LymphoVascular Space Invasion
mCRM	modified Continual Reassessment Method
MDM2	Mouse Double Minute 2 homolog
MLH1	MutL Homolog 1
MMAC1	Mutated in Multiple Advanced Cancers 1
MMP	Matrix MetalloProteinase
MMR	MisMatch Repair
MMRd	MisMatch Repair deficiency
MRI	Magnetic Resonance Imaging
MSH	MutS Homolog
MSI	Microsatellite instability
mTOR	mammalian Target Of Rapamycin
NEEC	Non Endometrioid Endometrial Cancer
NFkB	Nuclear Factor kappa B
NK	Natural Killer
NTN1	Netrin 1

OS	Overall Survival
p53abn	p53 abnormal
PD-1	Programmed Death protein 1
PDGF	Platelet Derived Growth Factor
PDGFR	Platelet Derived Growth Factor Receptor
PD-L1	Programmed Death Ligand 1
PFS	Progression Free Survival
PHD	Plant HomeoDomain
PHF2	Plant Homeodomain Finger 2
PI3K	Phosphoinositide 3 Kinase
PI3KCA	Phosphatidylinositol-4,5-Bisphosphate 3-Kinase Catalytic Subunit Alpha
PIK3R1	Phosphoinositide-3-Kinase Regulatory Subunit 1
PIP2	Phosphatidylinositol 4,5-bisphosphate
PIP3	Phosphatidylinositol (3,4,5)-trisphosphate
PMN-MDSC	PolyMorphoNuclear Myeloid-Derived Suppressor Cell
PMS2	PMS1 homolog 2
POLE	DNA POLymerase Epsilon (catalytic subunit)
POLEmut	DNA POLymerase Epsilon mutated
PORTEC	Post Operative Radiation Therapy in Endometrial Carcinoma
PR	Partial Response
PS	*PTEN*-related Proteus Syndrome
PTEN	Phosphatase and TENsin homolog
Q2W	Quality to be delivered every 2 Weeks
RAS	RAt Sarcoma virus
RET	REarranged during Transfection
RH	Hormone Receptor
RNA	RiboNucleic Acid
RP2D	Recommended Phase 2 Dose
SAE	Serious Adverse Event
SD	Stable disease
SERM	Selective Estrogen Receptor Modulators
SH2	Src Homology 2
STAT	Signal Transducer and Activator of Transcription
TAM	Tamoxifen
TCF-LEF	T-Cell Factor - Lymphoid Enhancer Factor
TCGA	The Cancer Genome Atlas
TF	Transcription Factor
TGFb	Transforming Growth Factor beta
TNFa	Tumour Necrosis Factor alpha
TNM	Tumour Node Metastasis staging system
UNC5B	UNCoordinated 5B

VEGF	Vascular Endothelial Growth Factor
VEGFR	Vascular Endothelial Growth Factor Receptor
VMAT	Volumetric Modulated Arc Therapy
WHO	World Health Organization
ZEB	Zinc Finger E-Box Binding Homeobox
ZSCAN12	Zinc finger and SCAN domain containing 12

List of figures

INTRODUCTION

SUPPLEMENTARY DATA

ANNEX

Introduction

CHAPTER 1
Netrin 1, a novel therapeutic target in cancer

In the early 2000s, Patrick Mehlen's laboratory developed the hypothesis of dependence receptors. These refer to receptors that are dependent on the binding of their ligand to ensure the survival of cells. Not only does this interaction lead to positive cellular outcomes such as that of survival and proliferation, but the receptors show a singular duality in the intracellular messages they provoke. In the absence of their ligand, the conformation of dependence receptors triggers a negative signalling cascade, ultimately resulting in cell death.

Over the years, more and more dependence receptors and their associated ligands have been identified, and their potential in cancer therapeutical targeting has also gained in interest. One of these dependence receptor ligands, a secreted molecule named netrin 1 (NTN1), was brought to light for its overexpression in many aggressive cancers, thus preventing tumour cell death. NTN1 was initially described for its role in axonal guidance during embryogenesis by Serafini et al., close to a decade prior to Dr. Mehlen's hypothesis as a ligand of dependence receptors. The reactivation of NTN1 expression in adults not only prevents natural cell death during cells proliferation that occurs when the amount of receptors becomes greater than the amount of ligand, but also triggers the positive signal ensuing from the binding of the ligand to the receptor such as survival, proliferation, and cell migration. For tumour cells, this confers them better survival properties, making them more prone to form aggressive tumours. From this idea of targeting the couple ligand/dependence receptor to trigger cancer cell death emerged the biotech NETRIS Pharma in 2008 (a spin-off from the laboratory; https://www.netrispharma/com) that developed a novel therapy compound inhibiting the interaction of NTN1 with its main dependence receptor UNC5B.

This chapter will review various aspects of NTN1 biology in cancer. In the first instance of this chapter is presented a review article written and published in "médecine/sciences" in 2022 during my thesis, compiling the functional characteristics of the NTN1 molecule, and the potential effects of a novel targeted therapy against NTN1 that could lead to promising results both as stand-alone therapy and in combination with conventional anti-cancer treatments.

médecine/sciences 2022 ; 38 : 351-8

La nétrine-1, une nouvelle cible antitumorale

Mélanie Bellina, Agnès Bernet

› La nétrine-1, une molécule sécrétée mise en évidence pour son rôle de guidage au cours de l'embryogenèse, a été également décrite pour être surexprimée dans de nombreux cancers agressifs. Elle est le ligand de récepteurs dits « à dépendance », à l'origine, chez l'adulte, de la survie, de la prolifération et de la migration de différents types cellulaires, ce qui confère aux cellules cancéreuses des propriétés avantageuses leur permettant de se développer sous forme de tumeurs agressives. Une stratégie thérapeutique consiste à inhiber l'interaction de la nétrine-1 avec son récepteur, ce qui déclenche la mort des cellules par apoptose. Cet article présente une revue des caractéristiques fonctionnelles de cette molécule et les effets potentiels d'une nouvelle thérapie ciblée sur la nétrine-1, dont la combinaison avec les traitements conventionnels pourrait être des plus prometteurs. ‹

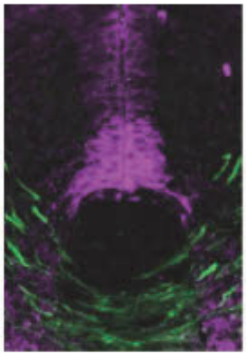

Centre de recherche en cancérologie de Lyon (CRCL), Centre Léon Bérard, 28 rue Laennec, 69008 Lyon, France.
agnes.bernet@lyon.unicancer.fr
melanie.bellina@lyon.unicancer.fr

Ces deux dernières décennies ont vu émerger des traitements révolutionnaires contre les cancers. Les années 1990 ont en effet permis la mise au point des thérapies ciblées qui, comme leur nom l'indiquent, ciblent et bloquent spécifiquement l'anomalie portée par la cellule cancéreuse. Depuis 2013, l'immunothérapie, qui réactive l'infiltrat immunitaire contre les cellules tumorales, est venue offrir une nouvelle arme pour le traitement de nombreux cancers. Cependant, au fil des années, les thérapies ciblées et les immunothérapies semblent avoir atteint un plateau en termes d'efficacité. Le nombre de patients répondeurs à chaque approche thérapeutique n'augmente plus, mettant en évidence la nécessité de combiner différents traitements. Aujourd'hui, 90 % des cas de décès par cancer sont imputables au développement de métastases et aux récidives liées à la résistance de certaines cellules tumorales aux traitements. Il est donc absolument nécessaire de continuer à développer de nouvelles thérapies s'attaquant aux cellules capables d'induire des récidives et à l'origine des métastases. Une nouvelle thérapie, récemment développée par un laboratoire français, pourrait s'adresser à ce type de cellules. Celle-ci cible la nétrine-1, une molécule de guidage sécrétée, active au cours du développement embryonnaire, notamment celui du système nerveux, qui semble être anormalement surexprimée dans la plupart des cancers agressifs. Nous proposons de présenter dans cette revue cette molécule dont l'activité au cours du développement embryonnaire serait réactivée lors de la formation des tumeurs. Nous évoquerons également les effets potentiels d'une telle thérapie ciblée qui pourrait être combinée aux différents traitements conventionnels pour renforcer l'efficacité des thérapies anticancéreuses.

Vignette (© Juan Antonio Moreno Bravo et Alain Chédotal).

La nétrine-1 et ses récepteurs

Découverte dans le cerveau embryonnaire de poulet en 1994, la nétrine-1 est l'homologue vertébré de UNC-6 (*uncoordinated-6*) mis en évidence quelques années plus tôt chez le nématode *Caenorhabditis elegans* [1]. La conservation des résidus les plus importants impliqués dans les sites de liaison de la nétrine-1 à ses récepteurs suggère une importance fonctionnelle du couple ligand/récepteur pour l'ensemble des espèces. En effet, la nétrine-1 appartient à une famille de protéines très conservées de la drosophile à l'homme. Codée par le gène *Ntn1*, la nétrine-1 est une protéine de 70 kDa [2], composée de trois domaines distincts : un domaine N-terminal et un domaine central (comportant trois répétitions de type *epidermal growth factor-like*, V1, V2 et V3) homologues aux domaines des lamininines, et un domaine C-terminal de charge positive, spécifique d'une famille plus large de nétrines (NTR) *(Figure 1A)*. Chez les vertébrés, la famille des nétrines est constituée de six membres dont quatre sont sécrétés (nétrine-1, -3, -4 et -5) et deux sont ancrés dans la membrane

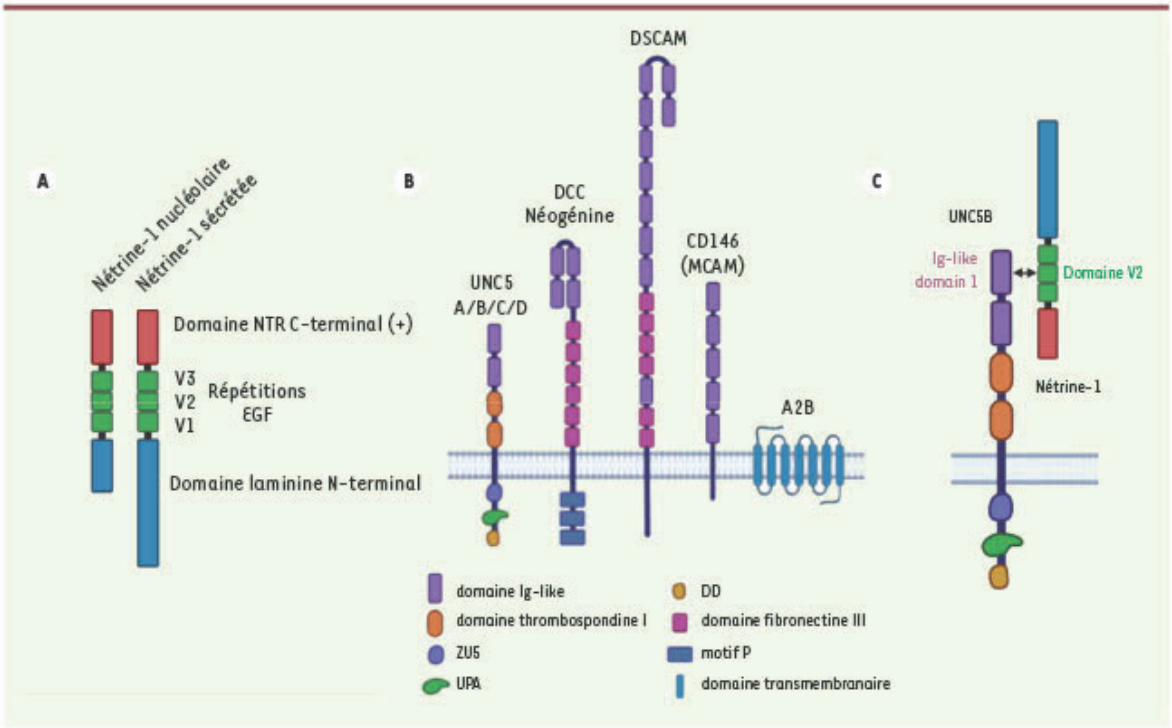

Figure 1. ***La nétrine-1 et ses récepteurs. A.*** Structure protéique de la nétrine-1 et de son isoforme tronquée à localisation nucléolaire. Les différents domaines sont indiqués. ***B.*** Structure protéique des récepteurs de la nétrine-1. Les récepteurs fixant la nétrine-1 sont représentés avec leurs différents domaines. DCC (*deleted in colorectal cancer*) et néogénine ont une séquence comprenant 49 % d'identité en acides aminés, et sont composés de quatre domaines immunoglobuline (*Ig-like*) qui, comme pour UNC5B (*unc-6 netrin receptor B*), interagissent avec la nétrine-1. A2B (*adenosine receptor 2B*) est constituée de sept domaines transmembranaires. Son activité est relayée par des protéines G. ***C.*** Interaction entre UNC5B et nétrine-1 *via* le domaine Ig-like 1 de UNC5B et le domaines EGF V2 de la nétrine-1. DD : domaine de mort ; EGF : *epidermal growth factor* ; NTR : nétrines.

plasmique (nétrine-G1 et G2) [2]. Au sein du domaine NTR spécifique des nétrines, cinq sous-domaines ont été identifiés, dont un motif d'adhérence cellulaire et un motif de localisation nucléolaire aboli dans la nétrine-1 sécrétée. La nétrine-1 possède également une isoforme qui n'est pas sécrétée. Cette isoforme, dont le domaine laminine à son extrémité N-terminale est tronqué, en raison de la présence d'un promoteur alternatif cryptique dans le gène *Ntn1*, se retrouve dans les nucléoles de certaines cellules cancéreuses où elle pourrait jouer un rôle pro-tumoral en altérant la synthèse des ribosomes [3].

La nétrine-1 est considérée comme une protéine sécrétée qui interagit avec deux familles de récepteurs transmembranaires appartenant à la superfamille des immunoglobulines (Ig) : la famille des *Deleted in Colorectal Cancer* (*DCC*) qui comprend DCC et néogénine, et la famille des récepteurs UNC5 (*uncoordinated-5*) composée de UNC5A, UNC5B, UNC5C et UNC5D *(Figure 1B)* [4]. La structure cristallographique de l'interaction entre nétrine-1 et UNC5B a été élucidée. Elle a révélé une interaction entre le domaine V2 de la nétrine-1 et le domaine Ig1 d'UNC5B auquel il se lie *(Figure 1C)* [5]. Certains effets dus à cette interaction pourraient néanmoins impliquer d'autres récepteurs comme A2B (*adenosine receptor 2B*), DSCAM (*down syndrome cell adhesion molecule*) ou CD146 (ou MCAM [*melanoma cell adhesion molecule*] / Muc18 [mucine 18]) *(Figure 1B)* [6-8], même si peu de travaux ont finalement confirmé la pertinence de ces possibles récepteurs alternatifs. Outre ces récepteurs, la nétrine-1 peut également se lier à d'autres protéines, comme les intégrines $\alpha 6\beta 4$ et $\alpha 3\beta 1$, ou les protéoglycanes héparanes sulfates [9,10]

La nétrine-1, un ligand des récepteurs à dépendance

Les récepteurs DCC et UNC5A, -B et -C, sur lesquels se fixe la nétrine-1, ont été décrits comme les prototypes des récepteurs à dépendance, des protéines membres d'une famille à double fonctionnalité, dont un tout dernier membre, c-kit, a récemment été décrit [11]. En présence de leurs ligands, ces récepteurs induisent un signal dit « positif » qui conduit la cellule à proliférer ou à migrer. En son absence, ils induisent un signal « négatif » de mort cellulaire par apoptose. La cellule qui exprime ce type de récepteurs à sa surface devient ainsi dépendante de la présence du ligand pour survivre *(Figure 2)* [4]. Le mécanisme permettant

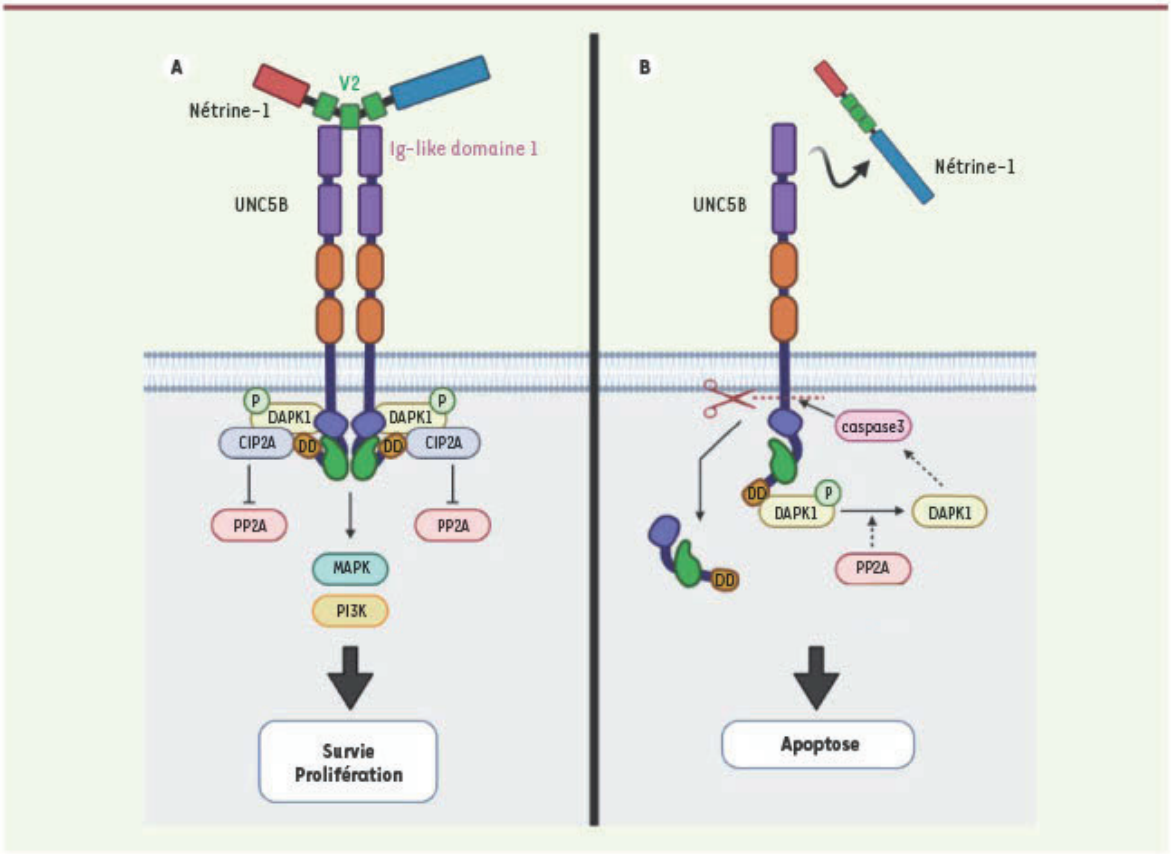

Figure 2. ***Double signalisation des récepteurs à dépendance : UNC5B et nétrine-1. A.*** L'interaction du domaines V2 de la nétrine-1 avec le domaine *Ig-like* 1 de UNC5B permet le blocage de l'apoptose et l'activation des voies des MAPK (MAPKinases) et des PI3K (*phosphoinositide 3 kinases*), assurant survie et prolifération cellulaire. ***B.*** En l'absence de fixation de la nétrine-1, UNC5B (*unc-5 netrin receptor B*) subit un changement de conformation et adopte une organisation intracellulaire ouverte, ce qui permet à la caspase 3 alors activée de cliver le domaine intracellulaire de UNC5B au niveau de l'Asp 412, libérant le domaine de mort (DD) et induisant l'apoptose.

cette dualité de fonction commence à être décrit dans le cas de la nétrine-1 et du récepteur à dépendance UNC5B. En effet, la fixation de la nétrine-1 entraîne la multimérisation de UNC5B qui adopte alors une conformation intracellulaire dite « fermée », bloquant son clivage protéolytique par les caspases, et permettant son interaction avec une forme phosphorylée de DAPK1 (*death-associated protein kinase 1*) inactive. Ainsi liée à DAPK1 phosphorylé, l'extrémité C-terminale intracellulaire de UNC5B interagit avec CIP2A (*cellular inhibitor of PP2A*), ce qui le protège de la déphosphorylation par PP2A (protéine phosphatase 2). L'interaction de la nétrine-1 avec UNC5B stimule les voies des MAPK (*mitogen-activated protein kinases*) et des PI3K (*phosphoinositide 3-kinases*), des voies de survie et de prolifération cellulaires *(Figure 2A)*. En l'absence de nétrine-1, UNC5B est sous forme d'un monomère et adopte une conformation intracellulaire dite « ouverte », permettant à son extrémité C-terminale de lier PP2A qui active alors DAPK1 par déphosphorylation, et rend possible le clivage de son domaine intracellulaire par la caspase 3, libérant un domaine de mort (DD) *(Figure 2B)* à l'origine de l'apoptose de la cellule [4]. Des mécanismes moléculaires assez différents sont observés pour UNC5A, C et la néogénine, mais ils impliquent tous un clivage par les caspases [4].

La nétrine-1 au cours du développement et chez l'adulte

En raison de son interaction avec les différents récepteurs qui la fixent, la nétrine-1 a été étudiée en ce qui concerne son implication dans le développement embryonnaire. Elle promeut en effet la croissance et l'orientation des axones de certains neurones, tels que les neurones commissuraux [12] (➜).

(➜) Voir la Synthèse de P. Mehlen et N. Rama, *m/s* n° 3, mars 2007, page 311

Son rôle le plus documenté est celui d'une molécule bifonctionnelle, jouant des rôles opposés d'attraction ou de répulsion des neurones,

selon les récepteurs qui sont exprimés par les cellules avec lesquelles elle interagit. Son activité ne semble pas se limiter au développement du système nerveux. Il a en effet été proposé que la nétrine-1 soit impliquée dans différents processus, tels que l'angiogenèse [13], l'innervation artérielle sympathique *via* sa sécrétion par les cellules musculaires lisses artérielles, la migration des cellules du mésoderme, le développement des organes branchés (glande mammaire, poumon, oreille interne et pancréas) [14, 15], le développement du système optique ou celui des structures crâniofaciales [16]. Il est cependant important de noter que malgré son implication probable dans ces différentes fonctions, les souris dont le gène codant la nétrine-1 a été délété, ne montrent pas de défaut d'angiogenèse, ni d'anomalie importante de développement de ces organes.

Si son rôle primordial est reconnu dans le développement embryonnaire, l'expression de la nétrine-1 n'est pas formellement démontrée dans l'organisme adulte, en dehors du système nerveux ; on ignore en effet à ce jour les fonctions précises de la nétrine-1 chez l'adulte. La protéine semble cependant être réexprimée lors de certains processus réactionnels, comme au cours d'une ischémie cérébrale ou lors de la survenue d'une lésion hépatique [17, 18]. Des travaux suggèrent qu'elle pourrait jouer un rôle important au cours de la reprogrammation / différenciation des cellules [19] (➜). Chez l'adulte, un des rôles supposés de la nétrine-1, sous sa forme sécrétée, dont les taux en condition physiologique normale sont faibles, pourrait être la protection des tissus contre une prolifération excessive. Une division cellulaire excessive et incontrôlée conduirait en effet à l'impossibilité pour la nétrine-1 de se fixer à ses récepteurs dont le nombre serait alors trop important. Cette absence de liaison de la protéine entraînerait ainsi l'apoptose des cellules surnuméraires. C'est pour cette raison que les récepteurs à dépendance, dont les prototypes sont les récepteurs fixant la nétrine-1, ont été décrits comme des suppresseurs de tumeurs conditionnels [20].

(➜) Voir la Nouvelle de P. Mehlen et F. Lavial, *m/s* n° 3, mars 2016, page 241

La nétrine-1 et le développement tumoral

La capacité des récepteurs à dépendance à induire la mort des cellules quand la quantité de ligand présente dans l'environnement est réduite serait donc un mécanisme de prévention du développement tumoral. Les cellules cancéreuses parviennent pourtant à contourner ce mécanisme, soit en invalidant la voie apoptotique par inactivation des récepteurs ou des voies de signalisation associées, soit en surproduisant le ligand de façon autocrine ou paracrine, assurant ainsi une saturation des récepteurs spécifiques [4]. L'ensemble de ces processus a été retrouvé dans les cellules tumorales, et la surproduction de nétrine-1 comme ligand semble être la voie privilégiée des cellules cancéreuses, cette surproduction apportant probablement un avantage supplémentaire, lié à l'augmentation du signal positif induit par le couple nétrine-1/récepteur. Une surexpression de nétrine-1 a en effet été observée dans de nombreux types de cancers, dans des proportions différentes selon les tissus *(Figure 3)*.

Les cellules cancéreuses se caractérisent par leur pouvoir de survie et de prolifération, des capacités qui mettent en jeu de multiples voies intracellulaires. La nétrine-1 pourrait, lors de sa fixation à son récepteur, activer les voies de signalisation à l'origine de cette prolifération cellulaire, telles que les voies PI3K / AKT (protéine kinase B) et ERK (*extracellular signal-regulated kinases*) [36-38], tout en favorisant l'échappement des cellules à l'apoptose induite par le signal de mort généré par son récepteur UNC5B. Cet échappement à la mort cellulaire en présence de nétrine-1 a été expliquée par l'expression accrue de Mdm2 (*mouse double minute 2 homolog*), un inhibiteur de TP53, une protéine suppresseur de tumeur [39]. La surproduction de nétrine-1 pourrait également permettre aux tumeurs d'assurer le développement de leur propre réseau vasculaire. En effet, la nétrine-1 est exprimée en condition d'hypoxie, ce qui permet la mise en place d'une néo-angiogenèse, non seulement en bloquant l'apoptose induite par son récepteur UNC5B, mais également par l'implication des voies angiogéniques reposant sur ERK et sur la PKC (protéine kinase C) [13, 40, 41]. La nétrine-1 et ses récepteurs, UNC5B et néogénine, ont également été décrits pour leur rôle dans le maintien de la pluripotence cellulaire. Ce mécanisme, qui participe à l'agressivité tumorale, attribue aux cellules cancéreuses un caractère « cellule souche » par l'activation de la voie des MAPK et de la voie Wnt, permettant ainsi la résistance des cellules aux thérapies classiques et les récidives, voire la mise en place de métastases [40]. Une expression importante de la nétrine-1 est en effet associée aux caractères migratoires et invasifs des cellules cancéreuses, des caractères propres aux cellules métastatiques. Ces caractéristiques se traduisent par la réinitialisation des capacités migratoires et invasives des cellules présentes lors du développement, ou accidentellement acquises *de novo* lors des processus de cicatrisation, notamment lors de la réactivation de la transition épithélio-mésenchymateuse (EMT) [42].

La motilité cellulaire implique une réorganisation du cytosquelette d'actine. Cette réorganisation pourrait être induite soit directement dans les cellules tumorales, par des signaux intracellulaires liés à l'interaction de la nétrine-1 avec ses récepteurs [38], soit de manière plus indirecte, *via* l'activation de facteurs de transcription comme NF-κB (*nuclear factor-κB*) [43] et CREB (*cAMP-response element binding protein*) [44], soit encore par l'action de co-activateurs transcriptomiques, comme YAP (*yes-associated protein*) [33] avec, pour conséquence, l'expression et la sécrétion de métalloprotéases et d'interleukines qui favorisent la dégradation de la matrice extracellulaire, promouvant ainsi la formation de métastases [44].

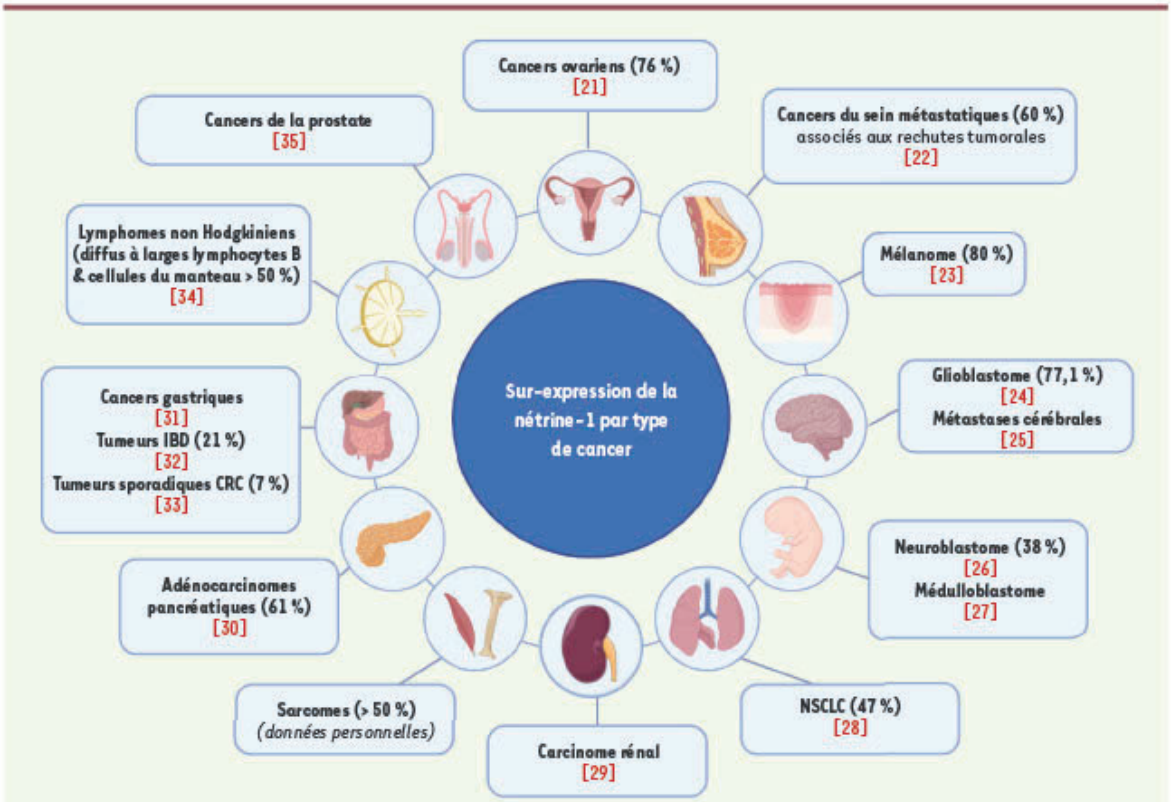

Figure 3. ***La nétrine-1 est surexprimée dans de nombreux types de cancers.*** Les types de cancers dans lesquels une surexpression de la nétrine-1 a été mise en évidence sont indiqués ainsi que les références associées. Lorsqu'il est disponible, le pourcentage de tumeurs surexprimant la nétrine-1 est mentionné entre parenthèses. IBD : *inflammatory bowel disease* ; CRC : *colorectal cancer* ; NSCLC : *non-small cell lung carcinoma*.

La nétrine-1 et le microenvironnement tumoral

L'inflammation et le développement tumoral sont intimement liés et les liens entre nétrine-1 et inflammation sont nombreux. La non-résolution d'une inflammation générée à la suite d'une lésion physique, chimique ou infectieuse, ou d'une réponse immunitaire incontrôlée, peuvent profondément perturber le microenvironnement cellulaire et favoriser le développement tumoral. Un lien direct a été montré entre le facteur de transcription NF-κB, qui régule plusieurs gènes codant des protéines de l'inflammation, et le promoteur du gène codant la nétrine-1. En effet, un contexte inflammatoire à l'origine de l'activation de NF-κB permettrait la transcription du gène codant la nétrine-1 avec pour conséquence l'inhibition du rôle de suppresseur de tumeurs des récepteurs à dépendance, favorisant ainsi le développement des tumeurs [43].

La nétrine-1 a cependant, selon les cellules et les tissus concernés, un rôle bivalent dans les phénomènes inflammatoires. En effet, elle serait impliquée dans de nombreuses maladies, telles que l'ischémie, l'obésité ou les maladies cardiovasculaires comme l'athérosclérose. La conséquence de l'augmentation de son expression dans ces maladies dépendrait de la cellule qui l'exprime. Par exemple, dans le cadre d'une ischémie du rein, du poumon ou du cœur, l'augmentation d'expression de nétrine-1, sécrétée par les cellules endothéliales en condition d'hypoxie, permettrait une protection des risques liés à l'inflammation en maintenant la fonction de barrière des vaisseaux, atténuant ainsi l'afflux et l'adhérence de monocytes circulants, de même que l'infiltration leucocytaires, dans les tissus [45-47]. Cette augmentation de nétrine-1 serait aussi impliquée dans le maintien de la barrière hémato-encéphalique, protégeant le système nerveux central d'une inflammation [48].

Lors de l'inflammation, un effet direct de la surexpression de la nétrine-1 sur la survie des cellules, telles que les cellules endothéliales, les cardiomyocytes ou les cellules tubulaires du rein, a été observé. Cet effet n'est pas sans rappeler la fonction de blocage de la mort liée aux récepteurs à dépendance. Dans l'obésité et l'athérosclérose, la présence de nétrine-1 produite par les macrophages présents dans les tissus adipeux

et les plaques d'athérosclérose, favoriserait leur rétention et leur accumulation [47, 49]. Récemment, il a d'ailleurs été montré, chez la souris, que la perte de l'expression de nétrine-1 dans les macrophages réduisait l'inflammation et la résistance à l'insuline associée à l'obésité [50].

En dehors de l'environnement inflammatoire qu'elles rencontrent, d'autres éléments facilitent le développement tumoral des cellules cancéreuses, en particulier les CAF (*cancer-associated fibroblasts*). En effet, des CAF, cultivés en présence de cellules tumorales, sécrètent la nétrine-1 ainsi que des cytokines qui induisent, dans les cellules cancéreuses, un phénotype « souche » plus agressif [51].

La nétrine-1, une nouvelle cible thérapeutique et un marqueur potentiel

En raison de sa sécrétion, de sa surexpression dans de nombreuses tumeurs, et de son rôle dans l'inflammation et sur la plasticité cellulaire, la nétrine-1 apparaît comme une cible de choix pour une nouvelle thérapie ciblée antitumorale. De nombreux essais d'interférence, altérant la liaison de la nétrine-1 avec ses récepteurs, réalisés sur plusieurs types de tumeurs, que ce soit *in vitro* ou *in vivo* chez la souris, ont révélé un effet inhibiteur sur la croissance tumorale et le développement de métastases, non seulement du fait de l'inhibition de la voie positive, la migration et l'invasion cellulaire [36], mais aussi par induction de la mort cellulaire par apoptose des cellules cancéreuses. Ces effets ont été observés en monothérapie, mais également lors d'essais réalisés en association avec des chimiothérapies conventionnelles ou des agents déméthylants *(Tableau I)* [22, 52]. Récemment, un premier essai clinique de phase I, évaluant un anticorps monoclonal humanisé dirigé contre la nétrine-1, a été conduit chez des patients atteints de cancers solides avancés et métastatiques. Outre le fait qu'aucune toxicité n'ait été observée, des signes tangibles d'efficacité sur les lésions et la survie des patients, sans récidive, ont été mis en évidence, permettant d'espérer la mise en place d'une nouvelle thérapie anti-cancéreuse [53].

Un aspect important de la nétrine-1 est son rôle potentiel comme biomarqueur prédictif de la présence de cancers, de leur évolution et de l'efficacité du traitement administré. De nombreuses études rapportent une corrélation entre la présence de nétrine-1 dans les fluides biologiques et l'agressivité des tumeurs associées [31]. Cependant, la plupart des résultats relatés dans la littérature doivent être soumis à une certaine réserve [54]. En effet, les tests utilisés dans les études (tests immunoenzymatiques de type ELISA [*enzyme-linked immunosorbent assay*]), ne permettent pas d'évaluer spécifiquement la présence de nétrine-1, ni de quantifier les taux de la protéine dans les fluides biologiques [27, 29, 31]. Toutefois, les techniques de marquage de tumeurs par immunohistochimie ou par analyse des ARN messagers réalisées sur les tumeurs primaires, ont montré que des valeurs élevées de nétrine-1 ou d'ARNm codant cette protéine, étaient corrélées à un mauvais pronostique dans l'adénocarcinome du pancréas et les cancers de l'ovaire [21, 30], faisant de la nétrine-1 un nouveau biomarqueur potentiel pour ces types de cancers.

Conclusion

Il apparaît désormais que la nétrine-1 participe au développement de tumeurs en se fixant à ses récepteurs à dépendance, faisant de cette protéine un nouveau candidat pour une thérapie ciblée. La nétrine-1 est une molécule qui participe au développement embryonnaire ; elle ne serait pas la seule molécule à être réactivée et détournée de son rôle au cours du développement, pour contribuer au processus pathologique tumoral. D'autres molécules, comme les sémaphorines, seraient en effet capables, par leur pouvoir attractant ou répulsif, de jouer un rôle important dans l'angiogenèse, l'inflammation et la tumorigenèse. La réactivation de ces molécules serait ainsi un avantage pour la cellule tumorale mais aussi pour la régulation du microenvironnement de la tumeur, notamment en agissant sur l'attractivité ou la répulsion de certaines cellules du système immunitaire, comme les lymphocytes, les macrophages ou les cellules endothéliales et les fibroblastes [55]. Ces molécules de guidage pourraient jouer un rôle dans le maintien des cellules tumorales à l'état de cellules souches, un phénomène qui joue un rôle central dans la résistance aux thérapies classiques. Cibler ce type de molécule représente donc une stratégie prometteuse et innovante, en monothérapie ou en combinaison avec les chimiothérapies, la radiothérapie ou les immunothérapies. Des tests cliniques de phase II en combinaison avec les traitements standards ont récemment débuté dans le cancer de l'endomètre et du col de l'utérus, et devraient permettre d'évaluer l'efficacité de ce type de traitement. Les analyses des échantillons issus des patients devraient permettre également de préciser le rôle de la nétrine-1 et de caractériser les voies de signalisation qui lui sont associées. ◊

SUMMARY

Netrin-1, a novel antitumoral target

Netrin-1, a secreted molecule that was first described for its role in guidance during embryogenesis, was then brought to light for its overexpression in a large number of aggressive cancers. Netrin-1 is a ligand of "dependence receptors". In adults, the interaction between Netrine-1 and these receptors triggers the survival, proliferation, and migration of different cell types. This will confer better survival properties to tumor cells, making them more prone to form aggressive tumors. A recently developed novel therapy aims at inhibiting the binding of Netrin-1 to these receptors in order to trigger cell death by apoptosis. This article presents a review of the functional characteristics of the Netrin-1 molecule, and the potential effects of a novel targeted

Agent interférant	Type de cancer	Effet sur les tumeurs	Références
Anticorps monoclonal anti-nétrine-1	Côlon, NSCLC, sein, lymphomes de type ABC et leucémie myéloïde chronique	– Inhibition de la croissance tumorale – Induction de la mort cellulaire – Combinaison avec une chimiothérapie efficace	[22, 34, 51]
siARN anti-nétrine-1	Glioblastome, poumon, neuroblastome, mélanome, médulloblastome	– Inhibition de la croissance tumorale – Inhibition de la prolifération, de la survie, de l'invasion, de la migration – Inhibition de l'angiogenèse – Réduction des métastases – Induction de la mort cellulaire – Combinaison avec une chimiothérapie efficace	[23, 24, 26, 27, 42, 52]
shARN anti-nétrine-1	Prostate, hépatocarcinome	– Inhibition de prolifération, survie, invasion, migration	[35,37]
TRAP-nétrine-1 (domaine extracellulaire des récepteurs DCC ou UNC5A)	Poumon, pancréas	– Inhibition de la croissance tumorale – Réduction des métastases – Induction de la mort cellulaire	[28, 52]

Tableau I. Utilisation d'agents interférant avec la nétrine-1. Ce tableau reprend l'ensemble des traitements interférant avec la nétrine-1 dans différents modèles de cancer, et leurs effets associés. ABC : *activated B cell* ; DCC : *deleted in colorectal cancer* ; UNC5B : *unc-5 netrin receptor B* ; NSCLC : *non small cell lung carcinoma* ; TRAP : fusion des ectodomaines des récepteurs à dépendance fixant la nétrine-1 à une région Fc d'IgG.

therapy against Netrin-1 that could lead to very promising results in combination with conventional anti-cancer treatments. ◊

LIENS D'INTÉRÊT

Les auteures déclarent n'avoir aucun lien d'intérêt concernant les données publiées dans cet article.

RÉFÉRENCES

1. Serafini T, Kennedy TE, Galko MJ, *et al.* The netrins define a family of axon outgrowth-promoting proteins homologous to C. elegans UNC-6. *Cell* 1994 ; 78 : 409-24.
2. Rajasekharan S, Kennedy TE. The netrin protein family. *Genome Biol* 2009 ; 10 : 239.
3. Delloye-Bourgeois C, Goldschneider D, Paradisi A, *et al.* Nucleolar localization of a netrin-1 isoform enhances tumor cell proliferation. *Sci Signal* 2012 ; 5 : ra57.
4. Negulescu A-M, Mehlen P. Dependence receptors – the dark side awakens. *FEBS J* 2018 ; 285 : 3909-24.
5. Grandin M, Meier M, Delcros JG, *et al.* Structural Decoding of the Netrin-1/UNC5 Interaction and its Therapeutical Implications in Cancers. *Cancer Cell* 2016 ; 29 : 173-85.
6. Liu G, Li W, Wang L, *et al.* DSCAM functions as a netrin receptor in commissural axon pathfinding. *Proc Natl Acad Sci U S A* 2009 ; 106 : 2951-6.
7. Tu T, Zhang C, Yan H, *et al.* CD146 acts as a novel receptor for netrin-1 in promoting angiogenesis and vascular development. *Cell Res* 2015 ; 25 : 275-87.
8. Stein E, Zou Y, Poo M, *et al.* Binding of DCC by netrin-1 to mediate axon guidance independent of adenosine A2B receptor activation. *Science* 2001 ; 291 : 1976-82.
9. Stanco A, Szekeres C, Patel N, *et al.* Netrin-1-alpha3beta1 integrin interactions regulate the migration of interneurons through the cortical marginal zone. *Proc Natl Acad Sci USA* 2009 ; 106 : 7595-600.
10. Matsumoto Y, Irie F, Inatani M, *et al.* Netrin-1/DCC signaling in commissural axon guidance requires cell-autonomous expression of heparan sulfate. *J Neurosci* 2007 ; 27 : 4342-50.
11. Wang H, Boussouar A, Mazelin L, *et al.* The Proto-oncogene c-Kit Inhibits Tumor Growth by Behaving as a Dependence Receptor. *Mol Cell* 2018 ; 72 : 413-25.e5.
12. Mehlen P, Rama N. Nétrine-1 et guidage axonal – Signalisation et traduction asymétrique. *Med Sci (Paris)* 2007 ; 23 : 311-5.
13. Castets M, Mehlen P. Netrin-1 role in angiogenesis: to be or not to be a pro-angiogenic factor? *Cell Cycle* 2010 ; 9 : 1466-71.
14. Brunet I, Gordon E, Han J, *et al.* Netrin-1 controls sympathetic arterial innervation. *J Clin Invest* 2014 ; 124 : 3230-40.
15. Murray MJ. The Role of Netrins and Their Receptors in Epithelial Mesenchymal Plasticity during Development. *Cells Tissues Organs* 2017 ; 203 : 71-81.
16. Hardy H, Prendergast JG, Patel A, *et al.* Detailed analysis of chick optic fissure closure reveals Netrin-1 as an essential mediator of epithelial fusion. *Elife* 2019 ; 8.
17. Schlegel M, Köhler D, Körner A, *et al.* The neuroimmune guidance cue netrin-1 controls resolution programs and promotes liver regeneration. *Hepatology* 2016 ; 63 : 1689-705.
18. Tang T, Gao D, Yang X, *et al.* Exogenous Netrin-1 Inhibits Autophagy of Ischemic Brain Tissues and Hypoxic Neurons via PI3K/mTOR Pathway in Ischemic Stroke. *J Stroke Cerebrovasc Dis* 2019 ; 28 : 1338-45.
19. Mehlen P, Lavial F. Le facteur nétrine-1 régule la reprogrammation cellulaire vers l'état pluripotent. *Med Sci (Paris)* 2016 ; 32 : 241-4.
20. Mazelin L, Bernet A, Bonod-Bidaud C, *et al.* Netrin-1 controls colorectal tumorigenesis by regulating apoptosis. *Nature* 2004 ; 431 : 80-4.
21. Papanastasiou AD, Pampalakis G, Katsaros D, *et al.* Netrin-1 overexpression is predictive of ovarian malignancies. *Oncotarget* 2011 ; 2 : 363-7.
22. Grandin M, Mathot P, Devailly G, *et al.* Inhibition of DNA methylation promotes breast tumor sensitivity to netrin-1 interference. *EMBO Mol Med* 2016 ; 8 : 863-77.
23. Kaufmann S, Kuphal S, Schubert T, *et al.* Functional implication of Netrin expression in malignant melanoma. *Cell Oncol* 2009 ; 31 : 415-22.
24. Sanvoranart T, Supokawej A, Kheolamai P, *et al.* Targeting Netrin-1 in glioblastoma stem-like cells inhibits growth, invasion, and angiogenesis. *Tumour Biol* 2016 ; 37 : 14949-60.
25. Harter PN, Zinke J, Scholz A, *et al.* Netrin-1 Expression Is an Independent Prognostic Factor for Poor Patient Survival in Brain Metastases. *PLoS One* 2014 ; 9 : e92311.
26. Delloye-Bourgeois C, Fitamant J, Paradisi A, *et al.* Netrin-1 acts as a survival factor for aggressive neuroblastoma. *J Exp Med* 2009 ; 206 : 833-47.
27. Akino T, Han X, Nakayama H, *et al.* Netrin-1 promotes medulloblastoma cell invasiveness and angiogenesis, and demonstrates elevated expression in tumor tissue and urine of patients with pediatric medulloblastoma. *Cancer Res* 2014 ; 74 : 3716-26.
28. Delloye-Bourgeois C, Brambilla E, Coissieux M-M, *et al.* Interference with netrin-1 and tumor cell death in non-small cell lung cancer. *J Natl Cancer Inst* 2009 ; 101 : 237-47.
29. Ramesh G, Krawczeski CD, Woo JG, *et al.* Urinary netrin-1 is an early predictive biomarker of acute kidney injury after cardiac surgery. *Clin J Am Soc Nephrol* 2010 ; 5 : 395-401.
30. Link B-C, Reichelt U, Schreiber M, *et al.* Prognostic implications of netrin-1 expression and its receptors in patients with adenocarcinoma of the pancreas. *Ann Surg Oncol* 2007 ; 14 : 2591-9.

RÉFÉRENCES

31. Kefeli U, Yildirim ME, Aydin D, *et al.* Netrin-1 concentrations in patients with advanced gastric cancer and its relation with treatment. *Biomarkers* 2012 ; 17 : 663-7.
32. Paradisi A, Maisse C, Coissieux MM, *et al.* Netrin-1 up-regulation in inflammatory bowel diseases is required for colorectal cancer progression. *Proc Natl Acad Sci USA* 2009 ; 106 : 17146-51.
33. Yin K, Dang S, Cui L, *et al.* Netrin-1 promotes metastasis of gastric cancer by regulating YAP activity. *Biochem Biophys Res Commun* 2018 ; 496 : 76-82.
34. Broutier L, Creveaux M, Vial J, *et al.* Targeting netrin-1/DCC interaction in diffuse large B-cell and mantle cell lymphomas. *EMBO Mol Med* 2016 ; 8 : 96-104.
35. Chen H, Chen Q, Luo Q. Expression of netrin-1 by hypoxia contributes to the invasion and migration of prostate carcinoma cells by regulating YAP activity. *Exp Cell Res* 2016 ; 349 : 302-9.
36. Jin X, Luan H, Chai H, *et al.* Netrin-1 interference potentiates epithelial-to-mesenchymal transition through the PI3K/AKT pathway under the hypoxic microenvironment conditions of non-small cell lung cancer. *Int J Oncol* 2019 ; 54 : 1457-65.
37. Han P, Fu Y, Liu J, *et al.* Netrin-1 promotes cell migration and invasion by down-regulation of BVES expression in human hepatocellular carcinoma. *Am J Cancer Res* 2015 ; 5 : 1396-409.
38. Yin K, Wang L, Zhang X, *et al.* Netrin-1 promotes gastric cancer cell proliferation and invasion via the receptor neogenin through PI3K/AKT signaling pathway. *Oncotarget* 2017 ; 8 : 51177-89.
39. Huang Q, Hua HW, Jiang F, *et al.* Netrin-1 promoted pancreatic cancer cell proliferation by upregulation of Mdm2. *Tumour Biol* 2014 ; 35 : 9927-34.
40. Huyghe A, Furlan G, Ozmadenci D, *et al.* Netrin-1 promotes naive pluripotency through Neo1 and Unc5b co-regulation of Wnt and MAPK signalling. *Nat Cell Biol* 2020 ; 22 : 389-400.
41. Liu J, Li J. PKCα and Netrin-1/UNC5B positive feedback control in relation with chemical therapy in bladder cancer. *Eur Rev Med Pharmacol Sci* 2020 ; 24 : 1712-7.
42. Zhang X, Cui P, Ding B, *et al.* Netrin-1 elicits metastatic potential of non-small cell lung carcinoma cell by enhancing cell invasion, migration and vasculogenic mimicry via EMT induction. *Cancer Gene Ther* 2018 ; 25 : 18-26.
43. Paradisi A, Maisse C, Bernet A, *et al.* NF-kappaB regulates netrin-1 expression and affects the conditional tumor suppressive activity of the netrin-1 receptors. *Gastroenterology* 2008 ; 135 : 1248-57.
44. Lee S-J, Jung YH, Oh SY, *et al.* Netrin-1 induces MMP-12-dependent E-cadherin degradation via the distinct activation of PKCα and FAK/Fyn in promoting mesenchymal stem cell motility. *Stem Cells Dev* 2014 ; 23 : 1870-82.
45. Ly NP, Komatsuzaki K, Fraser IP, *et al.* Netrin-1 inhibits leukocyte migration in vitro and in vivo. *Proc Natl Acad Sci U S A* 2005 ; 102 : 14729-34.
46. Rosenberger P, Schwab JM, Mirakaj V, *et al.* Hypoxia-inducible factor-dependent induction of netrin-1 dampens inflammation caused by hypoxia. *Nat Immunol* 2009 ; 10 : 195-202.
47. Gils JM van, Derby MC, Fernandes LR, *et al.* The neuroimmune guidance cue netrin-1 promotes atherosclerosis by inhibiting the emigration of macrophages from plaques. *Nat Immunol* 2012 ; 13 : 136-43.
48. Podjaski C, Alvarez JI, Bourbonniere L, *et al.* Netrin 1 regulates blood-brain barrier function and neuroinflammation. *Brain* 2015 ; 138 : 1598-612.
49. Ramkhelawon B, Hennessy EJ, Ménager M, *et al.* Netrin-1 promotes adipose tissue macrophage retention and insulin resistance in obesity. *Nat Med* 2014 ; 20 : 377-84.
50. Sharma M, Schlegel M, Brown EJ, *et al.* Netrin-1 Alters Adipose Tissue Macrophage Fate and Function in Obesity. *Immunometabolism* 2019 ; 1 .
51. Sung P-J, Rama N, Imbach J, *et al.* Cancer-Associated Fibroblasts Produce Netrin-1 to Control Cancer Cell Plasticity. *Cancer Res* 2019 ; 79 : 3651-61.
52. Paradisi A, Creveaux M, Gibert B, *et al.* Combining chemotherapeutic agents and netrin-1 interference potentiates cancer cell death. *EMBO Mol Med* 2013 ; 5 : 1821-34.
53. Cassier P, Eberst L, Courbebaisse Y, *et al.* 4390 : A first in human, phase I trial of NP137, a first-in-class antibody targeting netrin-1, in patients with advanced refractory solid tumors. *Annals of Oncology* 2019 ; 30 : v159.
54. Bruikman CS, Zhang H, Kemper AM, *et al.* Netrin Family: Role for Protein Isoforms in Cancer. *J Nucleic Acids* 2019 ; 2019 : 3947123.
55. Nakayama H, Kusumoto C, Nakahara M, *et al.* Semaphorin 3F and Netrin-1: The Novel Function as a Regulator of Tumor Microenvironment. *Front Physiol* 2018 ; 9 : 1662.

TIRÉS À PART

A. Bernet

CHAPTER 2
Targeting netrin 1 in endometrial cancer: the NP137 antibody

2.1. NP137: an anti-NTN1 humanized antibody

2.1.1. NP137 development

In the hopes of reactivating cancer cell death in cancer models prone to NTN1 overexpression, NETRIS Pharma developed the NP137 antibody, a humanized monoclonal antibody directed against NTN1. The first spin-off of the Centre Léon Bérard and the Cancer Research Centre of Lyon (CRCL) in France based their drug development on the cellular mechanisms identified by the Apoptosis, Cancer and Development research team directed by Dr. Patrick Mehlen.

NP137 is a humanized IgG1 immunoglobulin of 150 kDa. It is derived from the 4C11 murine antibody produced through hyperimmune mouse immunization with recombinant human NTN1. The 4C11 clone was selected for its high affinity to NTN1, its inhibition of NTN1 binding to its dependence receptor Uncoordinated 5B (UNC5B) shown by competitive ELISA tests, its ability to induce cell death, its pharmacokinetic profile in mouse plasma and its precise epitope sequence. As a matter of fact, Pepscan epitope mapping allowed to pin down the interaction domain of NTN1 and NP137 to a sequence of 8 overlapping peptides within the V2 domain of NTN1, coinciding with the interaction domain of NTN1 with UNC5B (*figure 1*) [1]. To generate NP137, the hypervariable sequences of the murine complementarity-determining regions (CDR) of 4C11 were grafted onto coding regions of human heavy and light chain structures, fused to standard human constant IgG1 regions (*figure 1*). The antibody's preclinical efficacy and its precise binding site were published in 2016 by our laboratory and reported by Grandin et al. [1].

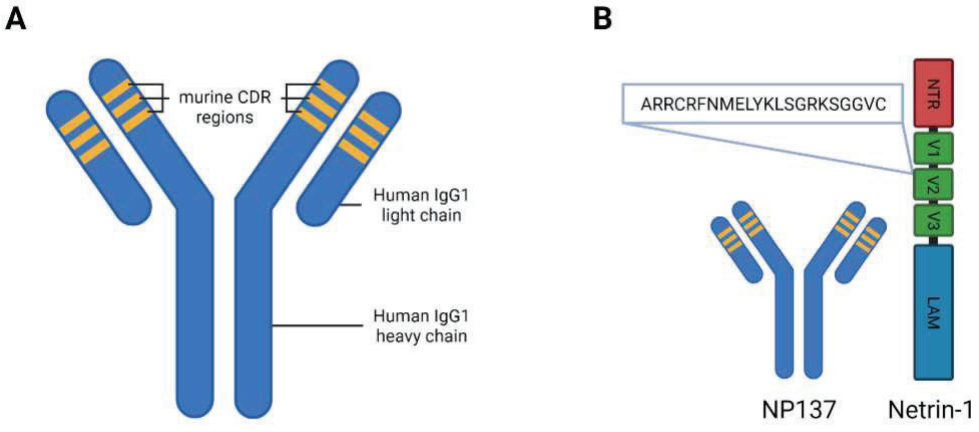

Figure 1: Schematic representation of the NP137 antibody and its interaction with NTN1. ***A.*** *NP137 is a type G1 humanized monoclonal antibody with hypervariable murine CDR regions derived from the 4C11 mouse anti-human recombinant NTN1.* ***B.*** *NP137 interacts with the 22 amino acid sequence described within the V2 domain of NTN1 [1].*

Just like previous therapeutic strategies targeting dependence receptors have shown, a lot of *in vitro* and *in vivo* preclinical studies demonstrated the potential of anti-NTN1 compounds (such as

siRNA against NTN1 and decoy receptors) and the antibody NP137 to inhibit tumour development and growth in cancer-induced mouse models like chronic inflammation-associated colorectal adenocarcinoma using the azoxymethane (AOM)/dextran sodium sulfate (DSS) model, and different cancer cell xenografts in nude mice (lung, ovarian and leukaemic) [1]. Together, these data supported the potential therapeutic benefit of NP137 in NTN1 overexpressing cancers. To go further and investigate its efficacy in humans, toxicology assays were conducted in both mice and cynomolgus monkeys to evaluate the potential toxic and adverse events (AE) related to NP137 administration. Toxicology studies showed no clinical, haematological, or biochemical signs of toxicity in both animal models at doses up to 100 mg/kg, hence validating its use in a phase I clinical trial by the ANSM (*Agence Nationale de Sécurité du Médicament et des produits de santé*) in November 2016 (https://classic.clinicaltrials.gov/ct2/show/NCT02977195).

2.1.2. A First-In-Human phase I clinical trial

Following preclinical validation, the humanized anti-NTN1 antibody underwent phase I clinical trial, the first step in testing a new treatment in humans, to evaluate its safety and tolerability in humans, its recommended dose, and assess its pharmacokinetic, pharmacodynamic and preliminary anti-tumoural activity. The NP137 phase I clinical trial was a "First-In-Human (FIH)" study targeting locally advanced or metastatic solid tumours of all cancer indications. Patients' recruitment was defined following strict inclusion/exclusion criteria (*annex 1*) and took place in 3 French centres: the Centre Léon Bérard in Lyon, the Institut Claudius Régaud in Toulouse and the Institut de Cancérologie de l'Ouest in Nantes.

The study unfolded in 3 stages (*figure 2*):

- **Dose escalation** to define the maximum tolerated dose (MTD) and a recommended phase II dose, as well as identify pharmacodynamic biomarkers in a biological cohort.
- **1st extension** focusing on gynaecological tumours due to the promising results from the endometrial and cervix indications.
- **2nd extension** focusing on hormone receptor positive (HR+) endometrial tumours.

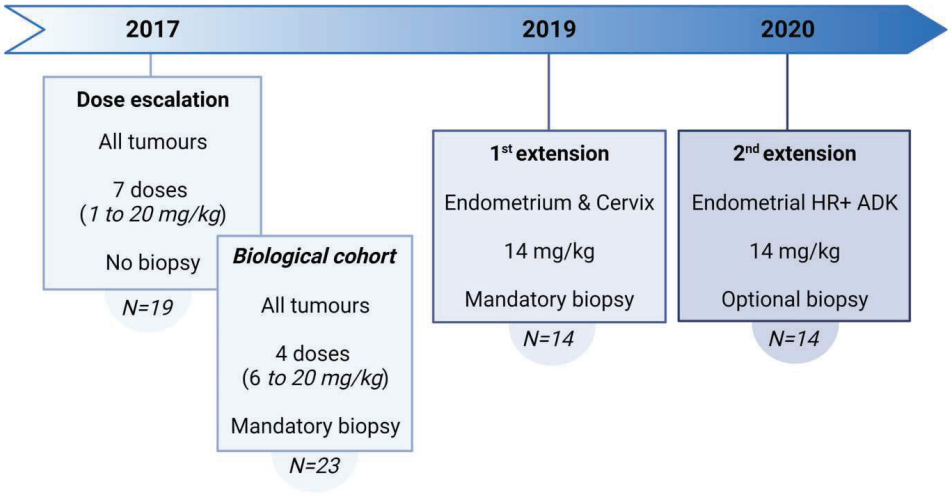

Figure 2: Schematic representation of the NP137 phase I clinical trial chronology.
HR+: Hormone receptor positive, ADK: adenocarcinoma.

2.1.2.1. Dose escalation

Dose escalation happened in two stages (*figure 3*). Firstly, 19 patients were enrolled (16 women and 3 men) using a rapid titration design characterized by a rapid initial escalation phase and in patient dose escalation. Rapid titration allows to drastically reduce the number of patients receiving low doses of the product and the duration of a phase I clinical trial, and provides a substantial increase in the information obtained. Rapid titration was followed by a modified continual reassessment method (mCRM), where the relationship between the dose of the drug and the likelihood of the receiving patient to have a dose limiting toxicity (DLT) is assumed. In total, 7 doses of NP137 were tested at concentrations varying from 1 to 20 mg/kg, with administration every 2 weeks on groups of patients of varying number. Very low concentration doses of 1 to 2 mg/kg were tested on just one patient, while concentrations of 4 to 20 mg/kg were tested on groups of 3 to 4 patients. An additional 23 patients were enrolled (15 women and 8 men) in a "biological" cohort in order to have paired metastatic biopsies for ancillary studies that could help extend our knowledge through the comparison of samples before and after treatment. These patients received NP137 at dose levels declared safe, starting at 6 mg/kg up to 14 mg/kg.

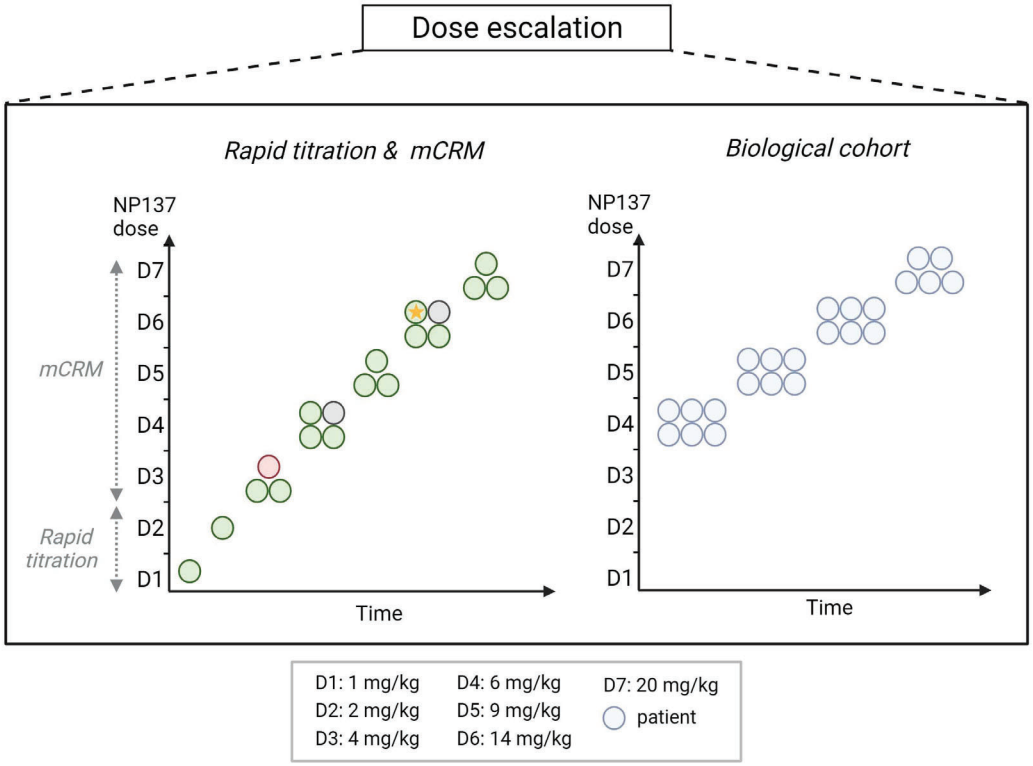

Figure 3: Schematic representation of the rapid titration and mCRM design and subsequent biomarker cohorts of the dose escalation of the NP137 phase I clinical trial.

(Left)19 patients (represented by circles) were enrolled in the dose escalation, and (right) an additional 23 in the biological cohort. In the rapid titration, patients showing good toleration to the treatment are represented by green circle, with the one patient that showed partial response to treatment being represented with an additional gold star, those showing poor to moderate outcome are represented in red circle, while non-evaluable patients are represented in grey circles, corresponding to patients that did not receive the full 2 cycles of NP137 required for this part of the trial. Rapid titration allows the rapid enrolment of patients at very low drug doses until the occurrence of a Grade ≥2 drug-related AE, when the model then switches to a mCRM design where 3 patients must show good tolerability to the dose before moving up in concentration. Poor to moderate reactions are acceptable, but if a serious reaction is observed in a patient, the dose they received is considered as the MTD and the escalation stops.

Following the completion of the dose escalation in January 2019, safety and efficacy data of the initial dose escalation indicated a good tolerability of the treatment, with an excellent safety profile showing no major serious adverse events (SAEs) or DLTs in the total of 42 patients that received the treatment. The most related AEs were infusion related reactions (IRRs) lower than grade II for 57% of patients (which were reduced with premedication), and fatigue for 35% of patients. Out of the 36 solid tumour patients of various primary tumour sites who had a follow-up RECIST[1] 1.1 to measure the response of their tumours to the treatment, 6 patients showed stable disease (SD) at 3 months (cancer indication of pancreas, ovary, cervix and endometrium), with one of the ovarian cancer responses considered as SD of more than a year at 6 mg/kg of NP137 by on site reviewing was later determined as PR by central reviewing. Quite remarkably, one endometrial cancer (EC) patient showed a partial response (PR) as early as after 6 weeks and still after 6 months of treatment at 14 mg/kg, characterized by a shrinkage of more than 50% of her hepatic metastatic lesions. Based on the pharmacokinetic data, the target saturation demonstrated by the administration of 14 mg/kg of NP137 every 2 weeks (Q2W) established it as the recommended dose for phase II. Due to the particularly promising results in gynaecological patients, a first extension was opened targeting endometrial and cervical cancer patients at the dose of 14 mg/kg.

2.1.2.2. Extension cohorts

A first extension…

To go further and investigate the clinical efficacy of NP137, a first extension of 14 patients with an even 50/50 distribution of EC and cervical/uterine cancer cases was opened to analyse the pharmacodynamics of NP137. This extension focused on gynaecological tumours, as these indications had shown the best clinical outcomes in the dose escalation. Patients underwent mandatory biopsies before and after 2 cycles of treatment to analyse the underlying NP137 mechanism in humans.

The first extension was carried out along the Gehan design, that stipulates that if at least 20% of patients show a positive response to the treatment, then there is a 95% likelihood that a therapeutic response will be observed by treating as little as 14 patients. As expected, following the first gynaecological extension of the study, patient clinical result analysis showed 50% of patients with a stable disease at 6 weeks, and 29% with a stable disease at 3 months post-treatment (*figure 4*).

… and a second extension

Ancillary studies of biopsy samples from the first extension cohort showed two things. Firstly, one of the most differentially expressed genes before and after treatment in patients responding to NP137 was the trefoil faction 3 gene (*TFF3*), which has been reported overexpressed in EC, notably in association with oestrogen (ER) and progesterone receptor (PR) [2]. Secondly, according to these patients' files, they also happened to be hormone receptor positive (HR+) patients, suggesting HR+ EC patients may show a greater benefit to NP137 treatment. Therefore, a second extension cohort was opened on the same design model as the first one, enrolling only EC patients, including 14 HR+ EC patients, with optional biopsies to facilitate patient inclusion (6 patients were successfully biopsied and out of them 2 underwent paired biopsies before and after 2 cycles of treatment). Clinical

[1] RECIST = Response Evaluation Criteria In Solid Tumours

response analysis of patients displayed 23% of patients with stable disease at 3 months after treatment initiation (*figure 4*).

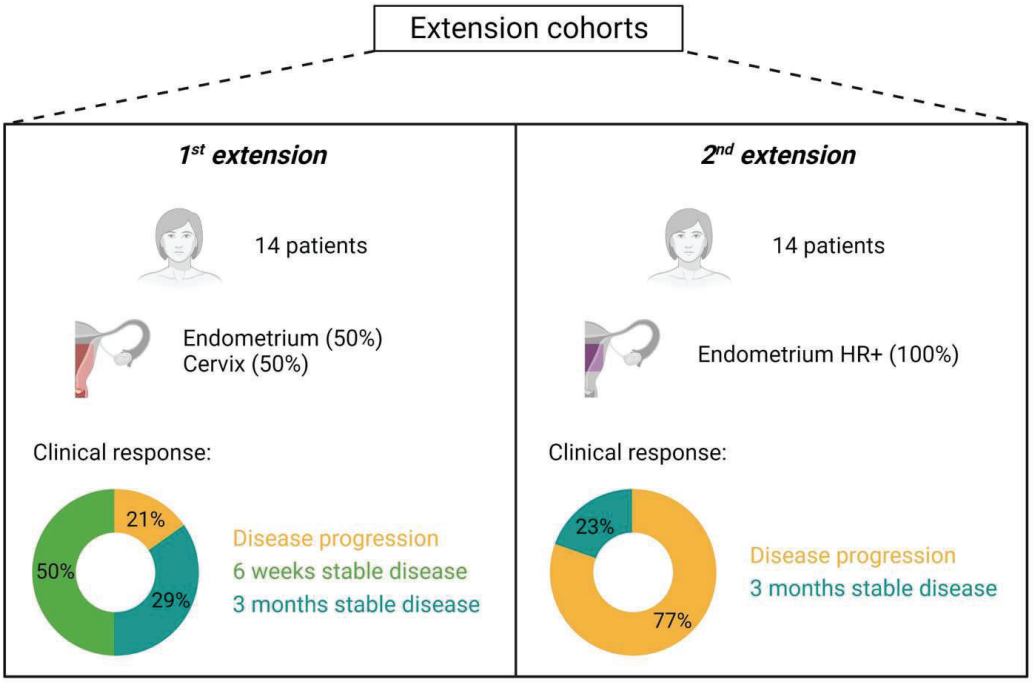

Figure 4: Diagram representation of NP137 phase I extension cohorts with patient population and clinical response.

In the 14 patients recruited in the first extension cohort composed of 7 endometrial and 7 cervical cancer patients, 21% were unresponsive to treatment, while 50% showed a stable disease after 6 weeks of treatment, and 29% showed stable disease after 3 months of treatment. As for the second extension cohort composed of 14 hormone receptor expressing endometrial cancer patients, only 23% showed a stable disease after 3 months of treatment, and 77% were unresponsive.

The opening of extension cohorts to investigate in depth the cellular impact of NTN1 blockade in endometrial and cervical cancers displayed yet again great promise as nearly 80% of patients showed a positive outcome, unlike the second extension investigating the potential implication of hormone receptors in endometrial cancer as only a small minority demonstrated stable disease after treatment. In summary,

2.1.2.3. Ancillary studies

Alongside the determination of drug tolerance and patient clinical response to NP137, biological cohort patients underwent paired biopsies, before and on treatment (after 1 month of treatment with the anti-netrin-1 compound), to investigate the molecular and cellular impact of NTN1 blockade on tumours. Global RNA sequencing analysis on the entire samples of 12 paired pre- and on-treatment biopsies enabled the discovery of a phenotypical shift of tumours to a more epithelial profile following NP137 treatment after only two injections of NP137. These ancillary studies were the basis of my investigations and will therefore be further developed in the "Results" portion of this manuscript. Moreover, one patient from the 2nd extension cohort was biopsied in Lyon in the CLB, and the recovery of fresh material allowed us to realize single cell RNA sequencing analysis, giving us very important results for the understanding of the mechanisms (see "Results" portion of the manuscript).

2.1.3. In summary…

The NP137 phase I clinical trial has proven the compound's safety at a recommended phase II dose of 14 mg/kg as apart from some IRRs of low grade and fatigue, no SAEs were observed after NP137 injection. Regarding the compound's efficacy, patients of various cancer indications showed positive outcomes of stable disease and partial remission, notably in cases of gynaecological cancers. Remarkably, one endometrial cancer patient's liver metastasis had shrunk by more than 50% after 6 months of NP137 treatment. Their results are further described in the Cassier et al. article in the "Results" portion of the manuscript.

CHAPTER 3
Endometrial cancer

The uterus is subdivided into 4 compartments: from top to bottom, we find the fundus, the corpus, the isthmus and the cervix (*figure 5*). The corpus itself is composed of 3 layers of tissues : the serosa or perimetrium constituting the outmost layer, the myometrium which is the intermediate muscle layer composed of smooth muscle cells, and the endometrium, the inner luminal lining of the uterus (*figure 5*) [3].

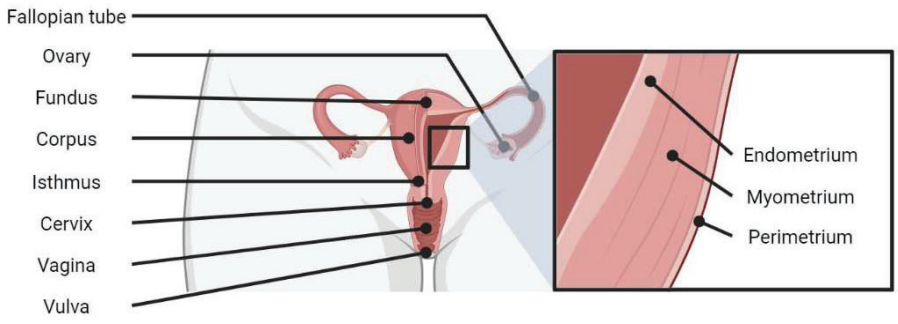

Figure 5: The female reproductive system

The uterus communicates with the ovaries through the fallopian tubes connected to the fundus of the uterus, and with the vagina through the cervical canal beneath the isthmus. The corpus is the larger part of the uterus that expands during pregnancy and is lined with a luminal endometrial layer of tissue, surrounded by myometrium and perimetrium.

The endometrium is the functional layer of the uterus that responds to hormonal input. Its thickness varies based on hormonal stimulation throughout the reproductive cycle, originating from multiple sources: the hypothalamus, the pituitary glands, and the ovaries. Pulsatile release of gonadotropin hormone-releasing hormone (GnRH) synthesized in the hypothalamus binds GnRH receptors in gonadotropic cells in the anterior pituitary gland. Upon the G protein-coupled receptor stimulation, gonadotrophic cells synthesize luteinizing hormone (LH) and follicle-stimulating hormone (FSH) gonadotropins, and alter gonadotrophic cell organization, leading to the extension of cellular projections towards the surrounding vasculature, increasing the cells' secretory impact. The intensity of GnRH pulse release impacts the nature of synthesized hormone released: high GnRH pulse frequencies favour LH secretion, whereas low GnRH pulse frequencies favour that of FHS. LH and FSH travel through the bloodstream to reach the ovaries, where FSH ensures oestrogen production by ovarian granulosa cells, and LH the androgen production in theca cells and progesterone synthesis in luteal cells. Oestrogen and progesterone then carry out a negative feedback loop to the hypothalamus, inhibiting GnRH pulses [4]. Histologically speaking, these variations in steroid hormones expression translate at the tissue levels through alteration of the uterine tissue organization and cell proliferation (*figure 6*).

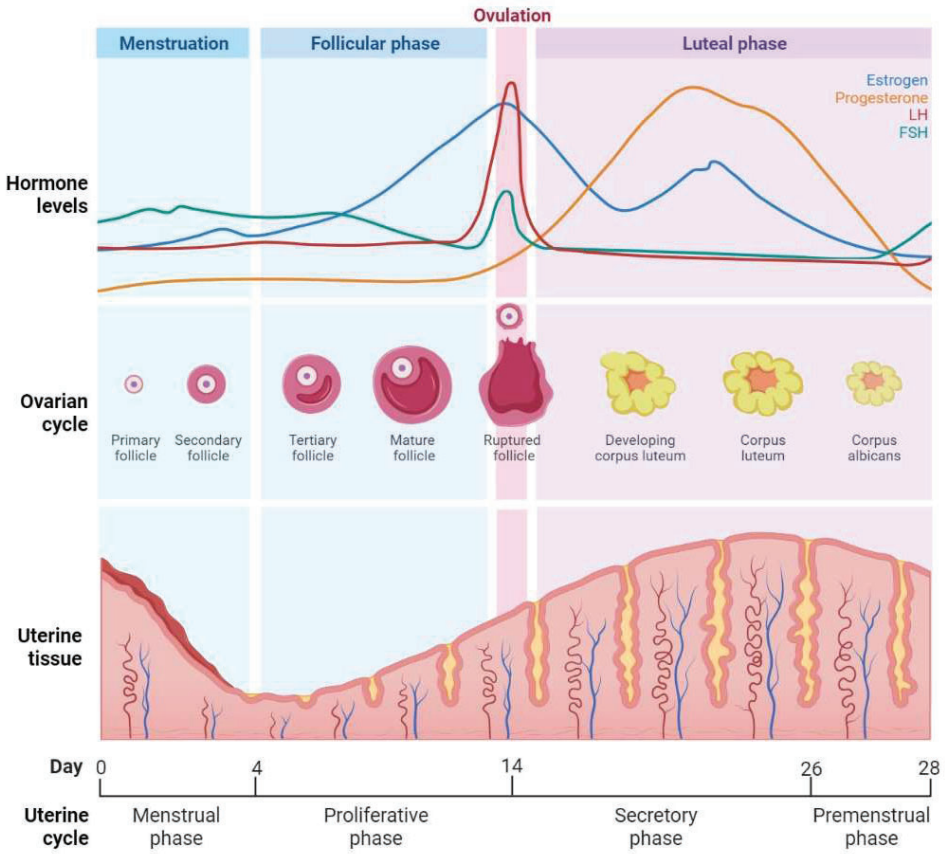

Figure 6: The female menstrual cycle

The menstrual cycle is driven by variations in hormones controlled by the hypothalamus, pituitary glands and ovaries. The synthesis of oestrogen by granulosa cells composing the follicles in the ovaries promotes the proliferation of endometrial cells in preparation for embryo implantation, this is known as the proliferative phase of the cycle. Once a follicle ruptures to release its oocyte at ovulation, there is a switch in hormone secretion as progesterone expressed by luteal cells of the corpus luteum becomes the dominant hormone during the secretory phase. If no pregnancy ensues, a drop in hormone secretion during the premenstrual phase leads to the shedding of the endometrial layer known as menstruation.

3.1. Statistics, clinical description, and diagnosis.

Cancer of the uterine corpus is the 2nd most commonly occurring gynaecological cancer worldwide behind cervical cancer, with an average age of diagnosis at 60 years. Over 90% of uterine corpus cancers are endometrial, originating in the epithelial layer of the uterine tissue, while the rest known as uterine sarcomas develop in the smooth muscle or connective tissue of the uterus. When endometrial carcinoma (EC) is detected at early stages, it is of good prognosis, with a 5-year relative survival rate of 72 to 96% depending on its localization and tissue invasion. However, once EC spreads to distant sites, the 5-year relative survival rate drastically drops to 20% [5]. Abnormal vaginal bleeding is the most common and early clinical manifestation of EC concerning 90% of affected women, whether it be characterized by change in period cycles, bleeding in between periods or bleeding after menopause [6]. Due to the high prevalence of clinical symptoms, screening for EC is not a widespread custom, and considered only in high-risk populations. The clinical evaluation consists of a physical and pelvic examination and followed by a transvaginal ultrasound to determine endometrial thickness and possibly abdominal ultrasound to identify any concomitant adnexal pathologies, defined as lumps in tissues neighbouring the uterus. If the need for biopsy is established, curettage or hysteroscopy to obtain endometrial tissue for histopathological diagnosis is carried out,

where the tumour type and grade of lesion is determined [7]. A variety of less invasive approaches have been developed over the years showing promising results in the detection of genomic biomarkers for early EC screening, such as blood sampling, uterine lavage and cervicovaginal fluid collect [8–17]. For example, DNA derived from the tumour fraction of plasma cell free DNA, also called ctDNA, serves a promising role in early detection of EC through the evaluation of a 4 genes panel composed of catenin beta 1 (CTNNB1), Kirsten rat sarcoma virus (KRAS), phosphatase and tensin homolog (PTEN) and phosphatidylinositol-4,5-bisphosphate 3-kinase catalytic subunit alpha (PI3KCA) [18].

3.2. Aetiology and risk factors

3.2.1. High fat diet and type 2 diabetes

Obesity and a sedentary lifestyle significantly contribute to the risk of developing EC, especially type 1 or endometrioid EC. As a matter of fact, a population-based study evaluated that 34% of worldwide corpus uteri cancers are attributable to high BMI [19]. Indeed, adipocytes have the capacity to convert androgens to oestradiol thanks to aromatase activity, which stimulates endometrial proliferation. Hence, obese women, due to an excess of adipocytes, are at higher risk of endometrial hyperplasia and ultimately cancer development [20]. Not only does adipose tissue favour the proliferation of cells, but it also ensures an inflammatory environment by the expression of leptin, an anorexigenic pro-inflammatory hormone capable of activating the leptin receptor on immune cells. In turn, these cells synthesize inflammatory cytokines that further recruit circulatory immune cells such as macrophages, lymphocytes, and neutrophils. Altogether, the environmental change in immune cells and the altered phenotype of adipose tissue promote hormone and metabolic changes that, side by side with inflammation, create a hotspot for tumour development [21]. Furthermore, while adapting to increasing levels of free fatty acids constantly released from adipose tissue within the intra-abdominal fat store, the metabolism adapts through an induced resistance to insulin. As tissues shift towards an increased storage of fats for energy production, they become less able to metabolize glucose, and along with the resistance to insulin, glucose concentrations increase, a cause for type II diabetes [22]. Although the molecular link between diabetes and EC isn't clear, a systemic review and meta-analysis of a total of 22 cohort and case-control studies confirmed the significantly increased risk of diabetic patients to develop EC [23].

3.2.2. Exposure to oestrogens: parity, infertility, and late menopause.

Quantity meta-analysis evaluating the relationship between parity and EC risk showed giving birth was associated with an inverse risk of developing EC [24]. This effect may be explained by the hormonal shift during pregnancy to a high progesterone low oestrogen environment, protecting the endometrial tissue from malignancy. Indeed, unlike oestrogen, progesterone reduces cell proliferation and stimulates cell differentiation. Therefore, the absence of gestation enables an unopposed oestrogenic exposition of the endometrium, leading to higher risk of hyperplasia and downstream cancer development. However, that does not mean women unable to bear children are off the hook. As a matter of fact, after adjusting for nulliparity, the evaluation of infertility and incident EC risk indicates women reporting infertility share an increased risk of developing EC [25]. Be that as it may, the use of fertility drugs for women struggling with infertility does not significantly increase their risk of cancer [26]. Prolonged exposition to oestrogen also concerns women presenting a late onset of menopause, as with the loss of follicles also comes a change in sex hormones expression. During the menopausal transition (also known as perimenopause), the ovaries go into

senescence, characterized by the elevation of FSH and concomitant decrease in ovarian oestrogen production, discontinuing the negative feedback control of GnRH pulses which in turn become more frequent [27]. As a result, the endometrial tissue atrophies, the uterus diminishes in size and the vaginal epithelium loses its cornified layer of cells. Considering women with late onset of menopause have a longer lifetime exposure to oestrogens, one may wonder whether age at menopause may be associated with EC. A Chinese retrospective study from 2022 showed that type 1 endometrioid EC is significantly higher in premenopausal patients, while type 2 serous EC is higher in post-menopausal patients, data consistent with the previously described estrogenic dependent and independent characteristics of endometrioid and serous EC respectively [28]. Additionally, a meta-analysis report evaluating the causal connection between age at menopause and EC development risk not only corroborated the link, but also indicated that high BMI, early onset of menses and high parity were associated with late onset of menopause [29].

3.2.3. Concomitant treatment: tamoxifen and hormone replacement therapy

In menopausal women, hormone replacement therapy helps alleviate symptoms associated with the loss of sex hormones production that comes with the depletion of the finite pool of ovarian follicles, such as hot flushes, night sweats and mood swings. It also helps with the prevention of osteoporosis, as oestrogen deficiency is a major factor in its pathogenesis at menopause [30]. Initially, hormone replacement therapy was limited to the administration of oestrogens. However, treatment options changed to incorporate synthetic progestins like medroxyprogesterone acetate, as retrospective studies demonstrated the correlation between unopposed oestrogen exposure and heightened risk of cancer development such as EC and breast cancer [31]. In the category of hormone-related treatments, tamoxifen is another culprit involved in EC development, but with a curious Janus-headed action. Tamoxifen is a selective oestrogen receptor modulator for the prevention and treatment of oestrogen receptor positive breast cancers. It acts by competing with oestradiol for receptor binging and hence blocking its inducing role in breast cancer [32]. However, tamoxifen is also associated with EC development in a time usage-dependent manner, meaning that it is the accumulation of tamoxifen administration over time that drives cancer development, rather than the dose administered in itself. No explanation has yet been found to explain the molecular mechanisms for the dual effect of tamoxifen dependent of tissues (protective in the breast, but harming to the uterus) [33].

3.3. Staging and grading

To recommend the best course of treatment to EC patients, doctors use an array of diagnostic tests to determine a cancer's stage and grade, based on clinical evaluations and information obtained after sample collection during biopsy. The collected information enables practitioners to establish a risk stratification of the disease, in other words, assign a risk status to patients to orientate care and improve health outcomes.

3.3.1. Clinical staging

A variety of cancer staging systems exist to determine the clinical staging of EC based on clinical examination, imaging and biopsies carried out during diagnosis. The most widely used of them all is the Tumour-Node-Metastasis (TNM) staging system. In this system, each letter stands for a specific indicator: T refers to the size and the extent of the primary tumour, N to the number of surrounding lymph nodes that have been invaded by cancer cells, and M to the metastatic nature or not of the

cancer (*annex 2*). Comparable to the TNM staging method, the International Federation of Gynaecology and Obstetrics (FIGO) has established their own staging of gynaecological cancers named FIGO staging, based on the invasiveness of the tumour in proximal or distant organs and lymph nodes. It categorizes EC into 4 stages, although a binary grading is recommended by the World Health Organization (WHO), regrouping FIGO grade I and II cancers in a low-grade category, and FIGO grade III and IV in a high-grade category (figure 7, annex 3):

- Stage I: the tumour is confined to the endometrial glands of the corpus uteri.
- Stage II: the tumour has spread to the endometrial stroma but stays confined within the uterus.
- Stage III: the tumour has spread to local or regional tissues like the vagina and the pelvic and para-aortic lymph nodes.
- Stage IV: the tumour has metastasized to regional organs within the pelvis such as the bladder and the bowel, or has invaded distant sites such as the lungs or the brain.

Clinical staging alone is not sufficient to classify EC. Tumours must undergo microscopical anatomopathological evaluation to help doctors determine the best course of patient care.

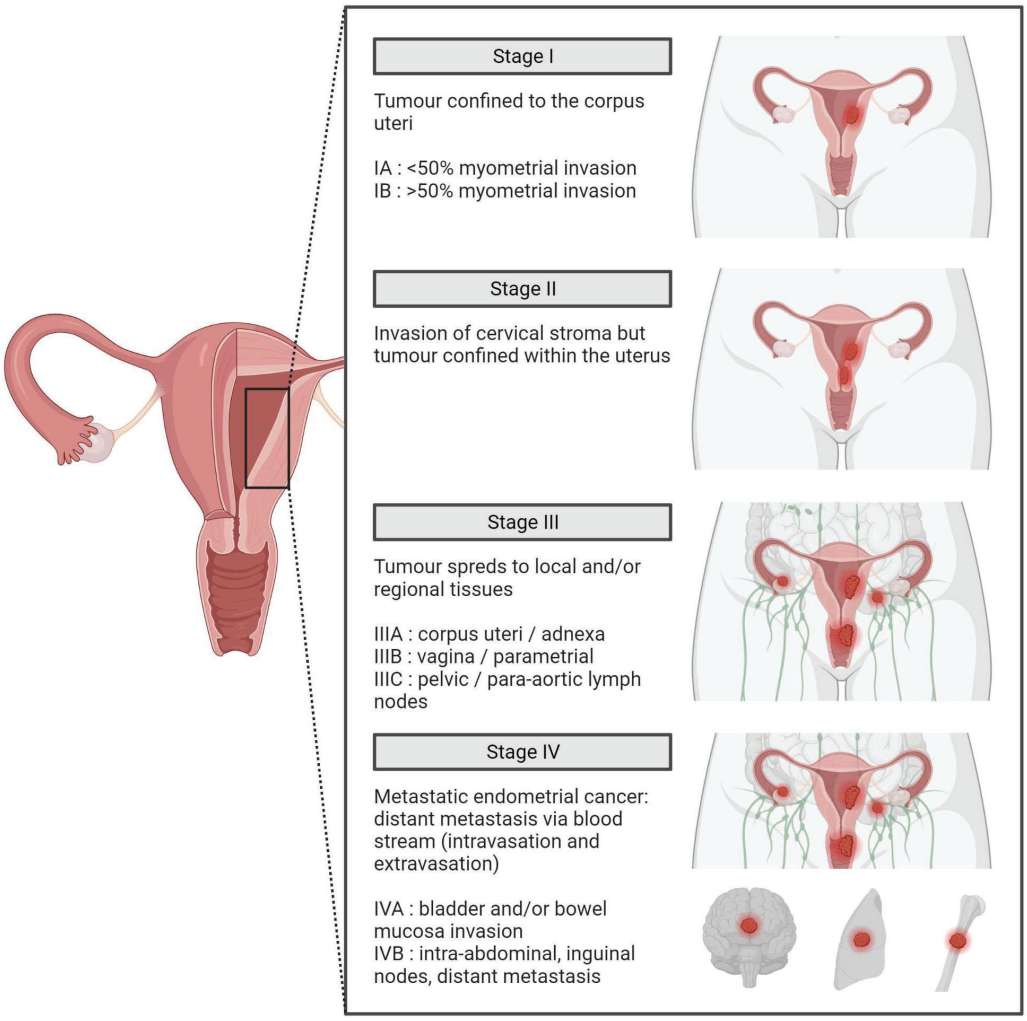

Figure 7: FIGO staging of EC

EC progression is divided into four stages, from the tumour confined to the uterine corpus (stage I) that invades the cervical stroma (stage II) then loco regional tissues (stage III) before reaching distant organs after circulating through the bloodstream (stage IV).

3.3.2. Histopathologic grading

Histopathological grading determined by microscopic analysis is based on the degree of glandular complexity of the endometrial tissue, whether it be luminal infolding, budding, papillae (with or without psammoma bodies) and cribriforming. EC is typically divided into 3 histological groups based on the tissue architecture, regarding neoplastic cell arrangement in solid sheets within the tumour samples known as solid growth patterns (*figure 8*):

- Grade 1 (G1) tumours present well differentiated cells, with less than 5% of non-squamous or non-morular solid growth pattern.
- Grade 2 (G2) tumours present moderately differentiated cells, with 6 to 50% of non-squamous or non-morular solid growth pattern.
- Grade 3 (G3) tumours present poorly differentiated cells, with more than 50% of non-squamous or non-morular solid growth pattern.

The presence of cytologic atypia such as nuclear pleomorphism, irregular chromatin clumping, and prominent nucleoli increases the grading by 1 level.

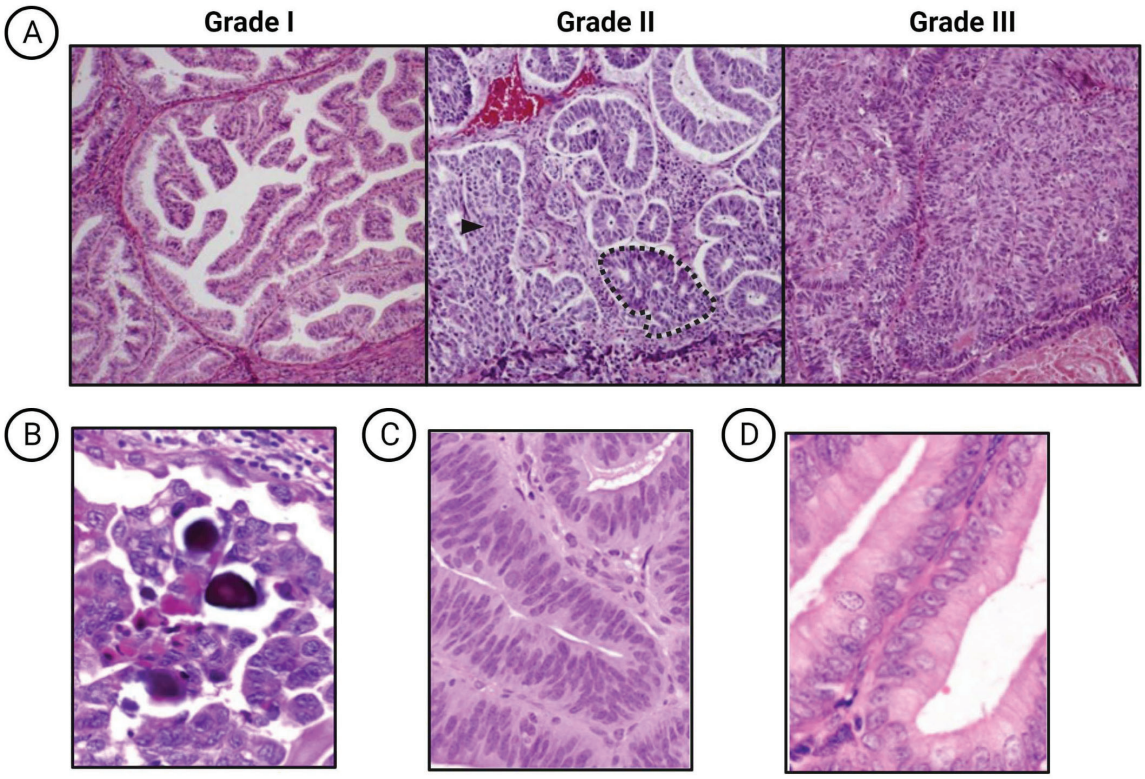

Figure 8: Histology of endometrial carcinoma

(A) Grade I EC (left) is characterized by branching glands with maze-like lumen indicating an architecture of folded sheets of neoplastic epithelium, while grade II EC (middle) shows solid growth (black arrow), cribriform areas (outlines in a black dotted line) along with tightly packed glands, and grade III EC (right) shows a great majority of solid growth. (B,C,D) ECs can also present (B) are round calcifications known as psammoma bodies, and (C,D) cytologic atypia characterized by loss of nuclear polarity, nuclear enlargement and rounding, and prominent nucleoli.

3.3.3. Classification

3.3.3.1. Histopathology-based type I vs type II

In 1983, Bokhman proposes an EC classification based on clinical, metabolic and endocrine characteristics of tumours, dividing ECs into 2 groups [34]:

- **Type I** ECs accounting for 80 to 90% of cases were associated with obesity, endometrial hyperplasia, excess oestrogen expression, oestrogen and progesterone receptor expression, well differentiated cells and were of an overall favourable prognosis.

- **Type II** ECs accounting for 10 to 20% of cases were associated with absence of endocrine and metabolic anomalies, atrophic endometrium, weak or null hormone receptor expression, poorly differentiated cells and were of an overall rather poor prognosis.

While the Bokhman classification system has advanced understanding of ECs and provided a valuable framework for studies, the imperfections of the dualistic model revealed themselves throughout the years. The design didn't account for the heterogeneity within each of the established types, or in the evolution of population characteristics such as biological, genetic, and pathological features, or the effects of hormone replacement therapy. To counter these shortcomings, a new classification of ECs was published in the 4th edition of the WHO Classification of Tumours. This new model allowed for better stratification of patients based on histopathological criteria (*table X*). Hence, 5 new groups were established in the 2014 publication: endometrioid carcinoma, serous carcinoma, clear cell carcinoma, carcinosarcoma and other mixed or unclassified tumours.

Endometrioid carcinoma, which accounts for 70 to 80% of all ECs is characterized histologically by confluent glands with little to no intervening stroma, cribriform[2] or micro-acinar[3] configurations and complex papillary, micropapillary or villoglandular structures. Cytologically speaking, cells and nuclei appear enlarged, with nuclear rounding with large nucleoli, a loss of cellular polarity and cytoplasmic eosinophilia. This type of EC is known to arise in younger women with a defined precursor lesion such as hyperplasia or intraepithelial neoplasia (EIN), and is considered to be oestrogen dependent, very much like type I EC described by Bokhman.

Serous carcinoma which accounts for 5 to 10% of ECs is on the other hand usually observed at later stages of disease progression, in postmenopausal women, and with no dependency to oestrogen, much like type II EC described by Bokhman. Serous carcinoma frequently arises on the surface of endometrial polyps in a background of atrophic endometrium and is histologically characterized by cells presenting nuclear hyperchromasia[4], irregular nuclear contours, irregular coarse chromatin and prominent cherry red nucleoli, with possible cytoplasmic vacuoles.

Clear cell carcinoma, adenocarcinoma and other mixed tumours are considered to be rare, representing each less than 5% of gynaecological carcinomas. We will not go into the detail of their characterization in this manuscript.

[2] Describing something perforated or sieve-like.
[3] Arranged as a ball around a small sac-like distension of the lumen of a gland (acinus).
[4] Cells in which the nuclei appear to be dark, smudges or opaque when stained.

3.3.3.2. Genomic mutation profiles

In 2020, the 5th edition of the WHO Classification of Tumours updated its criteria for EC classification, taking into account the findings of The Cancer Genome Atlas (TCGA) analysis of immunohistochemical and mutational profiles of endometrial tumours published in 2014 [35]. With exome sequencing, they established a novel classification of EC tumours integrating somatic nucleotide substitutions, microsatellite instability and somatic copy number alterations. Based on these findings, tumours were stratified into four groups, three of which group a majority of endometrioid type I EC and characterized by one marker: *PTEN* inactivating mutations.

PTEN

PTEN is a tumour suppressor gene located on chromosome 10 at the q23.31 locus [36]. Short for "phosphatase and tensin homologue deleted from chromosome 10", it is also known as MMAC1 for "mutated in multiple advanced cancers", a name quite descriptive of its discovery and ultimately its function [37]. PTEN is mostly known for its inhibition of the PI3K/AKT pathway by dephosphorylation of PI3K's effector PIP3 into PIP2 in the cytoplasm [38]. It also has a role in the cell nucleus to which it translocates to regulate gene expression and induce DNA repair, and also shows an intricate interplay with the tumour immune microenvironment where it prevents the secretion of immunosuppressive chemokines and prevents the formation of a reactive stroma with pro-tumourigenic activity [39,40]. PTEN function is altered in 13.5% of human cancers, with genomic alterations being most frequently observed in endometrial cancer (35%), as well as glial tumours, prostate cancer, melanoma, non-small small-cell lung cancer and breast cancer [41,42]. In sporadic tumours, *PTEN* loss of heterozygosity is observed at higher frequency than biallelic inactivation [43]. However, PTEN mutation can also be inherited as it is the case for PTEN Hamartoma Tumour syndrome, an autosomal dominant disease characterized by benign tissue malformations and germline PTEN pathogenic variants. Clinically speaking, this syndrome encompasses a variety of others such as Cowden syndrome (CS), Bannayan-Riley-Ruvalcaba syndrome (BRRS), *PTEN*-related Proteus syndrome (PS) and PTEN-related Proteus-like syndrome [44]. Patients affected by the disease are prone to develop various cancers like breast, thyroid, kidney, endometrium, colon, and melanoma tumours. Indeed, 21 to 28% of PTEN Hamartoma Tumour syndrome patients develop EC with no specific age at appearance.

3.3.3.2.1. Ultra-mutated (or POLE)

Presenting an unusually high mutational burden (232.10^{-6} mutations/Mb) but microsatellite stability, ultra-mutated tumours are genomically characterized by mutations of the catalytic subunits of the DNA polymerase epsilon (POLE) involved in DNA replication and repair. In addition, this group is also marked by inactivating mutations of *PTEN* (94%) and mutations of PI3K regulatory and catalytic subunits (65% and 71% respectively) in favour of the pathway's stimulation. Despite representing a majority of grade 3 endometrioid ECs (EECs), ultra-mutated tumours have the best prognosis of the 4 groups (figure 9).

POLE & PODL1

DNA replication in eukaryotes is carried out by three DNA polymerases: polymerase alpha, delta, and epsilon [45]. Polymerase alpha initiates replication at origins and Okazaki fragments, while polymerase delta (POLD) and polymerase epsilon (POLE) follow through with the bulk replication of DNA [46]. POLD and POLE possess both polymerase and 3' to 5' exonuclease proofreading activity, ensuring genomic stability through DNA replication and repair [45,47]. According to a 2019 meta-analysis on POLE and POLD1 (the catalytic subunit of POLD) mutations in their exonuclease

domain in an array of cancer types, EC is the second most affected cancer with POLE and POLD1 mutations after skin cancer nonmelanoma, with POLE mutations being the most common of the two [48]. Due to the characteristic mutation signature (COSMIC signature 10), the enhanced immune response, good clinical outcome and high mutational profile of POLE mutated ECs (with frequently over 100 mutations per megabase), POLE ultra-mutated EC was proposed as a distinct subgroup of endometrial carcinomas in the latest WHO classification [49].

PI3K

Out of all human cancers, EC has the strongest rates of alterations within the PI3K pathway. According to TCGA analysis, the most frequently altered associated genes are those encoding the 110 kDa catalytic subunit of type I PI3K called PIK3CA, an alteration ubiquitous of all mutational profiles of EC, and the 85 kDa regulatory subunit of type I PI3K called PIK3R1 [50,51]. PIK3R1 binds to the SH2 intracellular domain of activated tyrosine kinase receptors and acts as a scaffold that mediates the binding of PIK3CA [52]. Activated PIK3CA then carries out the phosphorylation of PIP2 into PIP3 at the cell membrane which leads to a cascade of intracellular signalling resulting in cellular growth, metabolism, proliferation, survival, migration apoptosis and angiogenesis [52,53]. Not only does the alteration of these PI3K subunits result in an aberrant activation of the pathway, but *PIK3CA* is frequently commutated with the most altered gene in EC that just so happens to be a negative regulator of the PI3K pathway: *PTEN* [53].

3.3.3.2.2. Hyper-mutated (or MSI)

This group bears as lower mutational burden than the ultra-mutated group (18.10^{-6} mutations/Mb), but a much greater microsatellite instability. Most of them presented mismatch repair deficiency (MMRd) due to methylation of their *MLH1* promoter, along with frequent mutations of *KRAS and ARID1A.* Despite being exclusively comprised of endometrioid tumours, this group is unspecific to tumour grade, and presents a fairly intermediate prognosis (figure 9).

MMR deficiency

Lynch syndrome (LS) accounts for 2 to 3% of all EC cases. Previously known as hereditary nonpolyposis colorectal cancer (HNPCC), LS is an autosomal dominant inherited disease caused by germline pathogenic variants in MMR genes (*MLH1, MSH2, MSH6, PMS2*). Due to the germline nature of the mutations, disease development requires a somatic inactivation of the second allele by loss of its heterozygosity or promoter methylation. More rarely, cases of hypermethylation by constitutional deletion of *EPCAM* (adjacent to *MSH2*), constitutional hypermethylation (de novo or inherited) and deletions or inversions creating nonfunctional genes, gene fusions or gene inactivation have also been reported. The loss of genomic stability normally maintained thanks to MMRs leads to microsatellite instability (MSI) and an increased susceptibility to tumoural development within the colon, rectum, endometrium, ovaries, breast, urinary tract, stomach, hepatobiliary tract, small bowel and brain. Individuals with relatives diagnosed with LS are considered high risk for EC development, and therefore prioritized for EC screening. Turcot syndrome is also linked to MMR mutation. However, contrary to LS, MMR deficiency is here constitutional, due to biallelic hereditary mutations in MMR genes. Due to the inheritance of both mutated alleles, patients develop cancers at an earlier age like childhood haematological or cerebral tumours, along with LS associated cancers such as EC. MMR deficiency is not necessarily hereditary, it can also originate from somatic MMR gene mutation which is referred to as Lynch-like, and homozygous methylation of the MLH1 gene promoter, which is classified as sporadic. In total, MMR deficient patients all origins considered represent 20 to 30% of EC.

KRAS

KRAS mutations are observed in 35% of hypermutated endometrial tumours [51]. RAS proteins are small GTPases that are implicated in the transduction of growth factor receptor signals [54]. Amongst its 3 members, we find the Kirsten rat sarcoma viral oncogene (*KRAS*), evenly expressed in tissues except for a shortlist including the uterus where it is overexpressed [54]. *KRAS* is located at chromosome 12 (12p12.1), and the generated protein tethers to cell membrane growth factor receptors to transduce its intracellular signalling, therefore regulating the proto-oncogenic pathways MAPK and PI3K/AKT [55]. Oncogenic mutations in the *KRAS* gene permanently activates the RAS molecules, thus perturbing the intrinsic biochemical properties of these pathways and increasing their activity, favouring cellular proliferation and survival [56]. The most common cancer associated mutations affect *KRAS*, showcasing a mutation rate of more than 10% in EC [57]. 85 different mutations of *KRAS* have been reported, the most common one, constituting 90% of *KRAS* mutations, is the alteration of a guanine to adenine in exon 2 [35]. It is also the most frequent form of *KRAS* mutation in EC and is pathway specific, as it is associated with mismatch repair deficiency signatures [58].

ARID

Members of the AT-rich interactive domain (ARID) family are DNA binding proteins that specifically target AT rich DNA sequences [59]. ARID1A, also known as BAF250A [60], is an integral member of the human BAF complex that impacts chromatin remodelling and transcription initiation and elongation. ATPases from the BAF complex modulate the accessibility of DNA to TFs and the transcriptional machinery through nucleosome remodelling [59,61]. Additionally, ARID1A is involved in double-strand break repairs, homologous recombination and a multitude of pathways including (but not limited to) PI3K, immune checkpoints, KRAS, p53, etc [61]. ARID5B on the other hand, also known as modulator recognition factor 2 (MCF2), acts through the formation of a complex with phosphorylated PHD finger protein 2 (PHF2) to target promoters where PHF2 may demethylate histone H3, also regulating gene expression [62]. ARID5B is found to be mutated in 11% of endometrioid carcinomas, while ARID1A loss-of-function mutations have been recorded in 6% of human malignancies, including 37% of hypermutated ECs, but also 42% of copy number low ECs [51,61].

3.3.3.2.3. Copy number low (or MSS)

Although these tumours' mutation frequency was nearly a tenfold lower than hyper-mutated tumours ($2.9x10^{-6}$ mutations/Mb), their mutational landscape was quite similar, aside from a higher frequency of *CTNNB1* mutations (52%). Majorly composed of grade 1 and 2 endometrioid tumours, this group also presented a fairly intermediate prognosis. Due to its increased progesterone receptor expression, this group may be more responsive to hormonal therapy (figure 9).

CTNNB1

The *CTNNB1* gene encodes beta-catenin, a pro-tumoural protein that has 2 great roles: one nuclear and one cytoplasmic, regulated by the Wnt signalling pathway. When Wnt is stimulated by environmental factors such as TGFb, its binding to its receptors LPR5/6 and FZD at the cell membrane enables the destruction of the AXIN/APC complex, responsible for the phosphorylation and degradation of cytoplasmic beta-catenin by ubiquitination. Beta-catenin can therefore ensure its cytoplasmic and nuclear function. By binding directly to E-Cadherin (CDH1) and indirectly to actin filaments from the cytoskeleton (through interaction with alpha-catenin), beta-catenin participates in cell-to-cell adherence junctions. By translocating to the nucleus, beta-catenin binds the TCF-LEF

transcription factors (TFs) which induces the expression of proto-oncogenes such as Slug, Fibronectin, c-Myc, Cyclin D1, etc… [63]. 20-25% of ECs show *CTNNB1* mutations, constituting 50% of copy number low ECs [51,64]. Since many pathological mutations of beta-catenin have been localized at the exon 3 of *CTNNB1* on as phosphorylation sites, it is possible to hypothesize that an altered phosphorylation of beta-catenin could lead to its cellular accumulation and nuclear translocation, inducing aberrant expression of EMT related proto-oncogenes, and in addition, modified function of beta-catenin could affect its cellular adhesion function, leading to loss of cell-to-cell contact and promoting cellular motility [64].

3.3.3.2.4. Copy number high (or serous-like)

Regrouping the quasi-entirety of serous EC and a few grade 3 EEC, this cluster showed the worst prognosis of them all. With the highest rate of somatic copy number alterations, these tumours were specifically characterized by aberrant p53 expression due to mutation of *TP53* (90%), which corroborated with cell cycle deregulation through great transcriptional activity (also exemplified by *MYC, PI3K* and *CDKN2A*). Additionally, copy number high tumours showed very little *PTEN* mutations (11%) and MSI (6%) compared to the other groups (figure 9).

P53

Specific to the copy number high subtype of ECs, p53 mutation is also the most common mutation of all human cancers, present in more than 50% of cancers [51,65]. The majority of p53 mutations are missense, the most common being in the DNA-binding domain (DBD) of the protein, affecting just one amino acid yet sufficient to alter the protein's function altogether [66]. P53 is typically kept at low levels in healthy tissue thanks to its negative regulation by mouse double minute 2 (MDM2), and activated following endogenous and exogenous stressful stimuli, triggering a plethora of cellular responses to maintain homeostasis. Missense mutations of P53 lead to the loss of its tumour-suppressive properties and a gain of pro-tumoural functions implicated in cellular proliferation, metastasis, tumoural microenvironment reprogramming, genomic instability, cell differentiation and stemness, metabolic reprogramming, immune suppression and therapy resistance [65]. In EC, multiple studies have found that patients with p53 mutation show poorer clinical outcomes than their p53 wild type counterparts from the same group based on the EC classification of 2014. Hence, its addition as a marker for mutational profile classification of EC hopes to improve clinical outcomes by adjusting treatment strategies for affected patients [67].

In summary, the new classification system integrating mutational profiles of tumours allows a better stratification of patients, which along with FIGO staging allows their categorization into risk groups that guide the choice of treatment (annex 3). Although each group has specific biomarker expression that play a part in their classification such as *POLE* mutation for ultra-mutated tumours, MMR deficiency for hyper-mutated tumours, or *CTNNB1* mutation for copy number low tumours and *p53* mutations for serous-like tumours, one major marker remains specific to all endometrioid ECs: *PTEN* mutation.

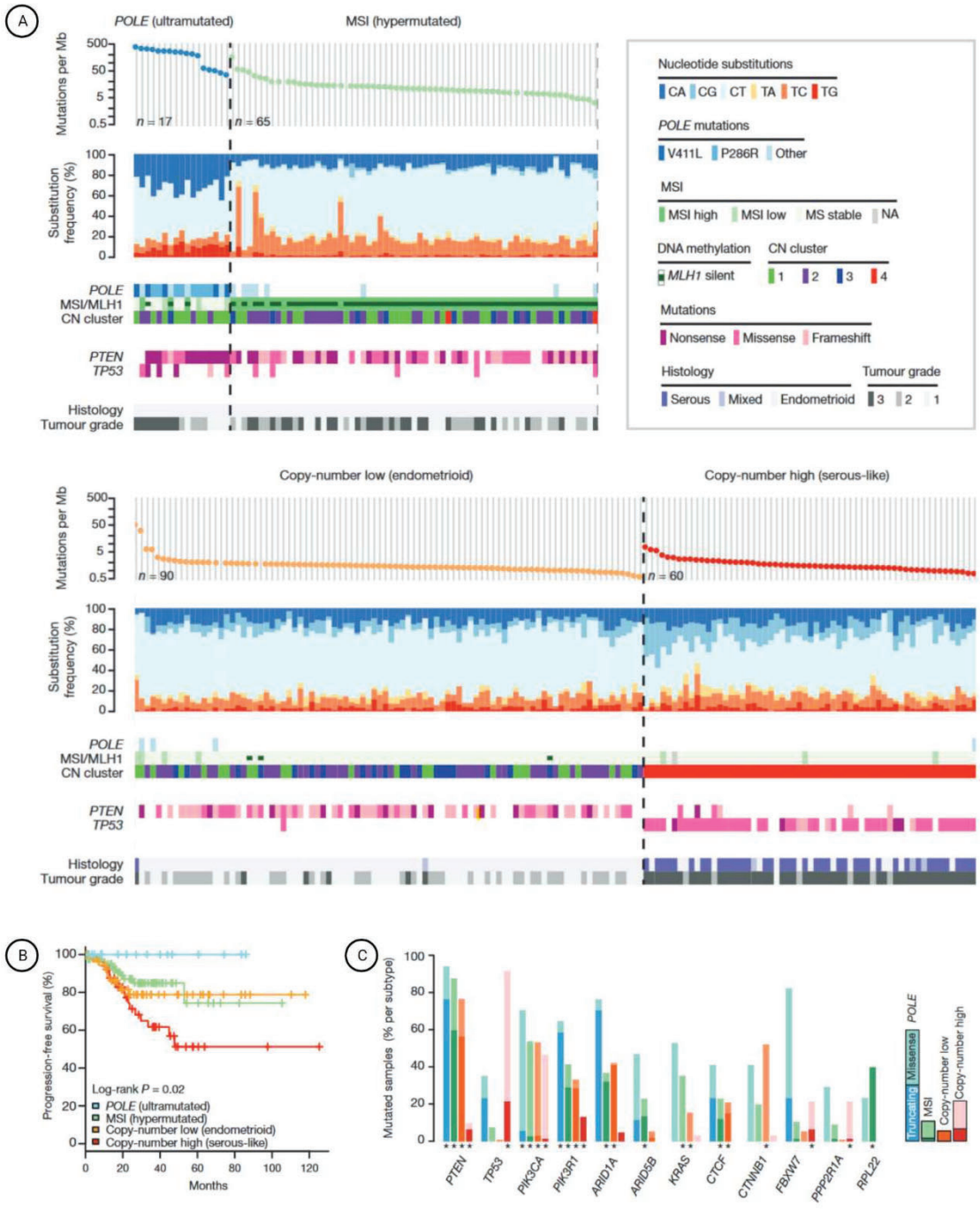

***Figure 9: Mutation spectra across EC** [51].*

(A) Mutation frequencies (vertical axis, top panel) plotted for each tumour (horizontal axis). Nucleotide substitutions are shown in the middle panel, with a high frequency of C-to-A transversions in the samples with POLE exonuclease mutations. CN: copy number. (B) POLE-mutant tumours have significantly better progression-free survival, whereas copy-number high tumours have the poorest outcome. (C) Recurrently mutated genes are different between the four subgroups. Shown are the mutation frequencies of all genes that were significantly mutated in at least one of the four subgroups (: FDR < 0.05).*

3.4. EC treatments and their limitations

3.4.1. Surgery

With its 5-year survival rate of 93% for early-stage cancer patients, surgery is today the standard go-to treatment for the management of EC. Different options are available for patients, depending on the extent of cancer dissemination, which can be carried out though minimally invasive approaches (vaginal, robotic, laparoscopic) to facilitate patient recovery due to diminished pain, blood loss and scarring. All procedures rely on the removal of cancer invaded genital tissues. When the cancer is localized within the corpus uteri, a simple or total hysterectomy is usually conducted. If the cancer has also invaded the cervix, then practitioners opt for a radical hysterectomy, taking out the cervix as well. A unilateral or bilateral salpingo-oophorectomy is conducted in addition to the radical hysterectomy, depending on whether one or both ovaries are also compromised. As detection of lymph node metastasis determines the staging of cancer and the ulterior administration of adjuvant treatment, an evaluation of lymph node status is recommended in patients with high grade EC, FIGO stage ≥ IB or non-endometrioid histology. Additionally, complementary procedures such as pelvic washing, omentectomy (the removal of abdominal fatty tissue) and cytoreductive surgery (removal of cancer sites in the abdominal cavity for advanced patients) are carried out to ensure the total removal of cancer cells and reduce metastasis in the peritoneal cavity.

3.4.2. Radiotherapy

Radiotherapy is a treatment option available at multiple times in cancer care management: it can either be considered as a neo-adjuvant form of treatment before surgery with the intention of shrinking the tumour to obtain complete resection with clear margins, or an adjuvant treatment to limit risk of cancer recurrence after surgery, or even as a palliative approach when a cure is no longer a possibility, but patient quality of life could benefit from it. Whatever the case may be, 2 forms of radiation are available for patients: external beam radiation therapy (EBRT), or internal radiation also known as brachytherapy.

3.4.2.1. EBRT and brachytherapy

With the discovery of X-rays in 1895 by Röntgen, the clinical use of radiation was quickly put to the test and is now utilized as a form of curative care for a variety of cancers [68]. EBRT utilizes high-energy photons of 6 to 25 MV administered in a fractionated manner and directed against tissues in order to damage cellular DNA. In oncology, radiation exploits the fragilized DNA repair system of cancer cells and their higher replication rate compared to that of healthy tissue, specifically targeting them and inducing their death [69]. A great variety of EBRT techniques are available, but the most commonly used for gynaecological tumours are 3-dimensional conformal radiotherapy (3DCRT), intensity modulated radiotherapy (IMRT), and volumetric modulated arc therapy (VMAT), which all share a common adverse effect, that of radiation diffusion to neighbouring organs, leading to the development of gastro-intestinal toxicities and secondary malignancies (figure 10) [69].

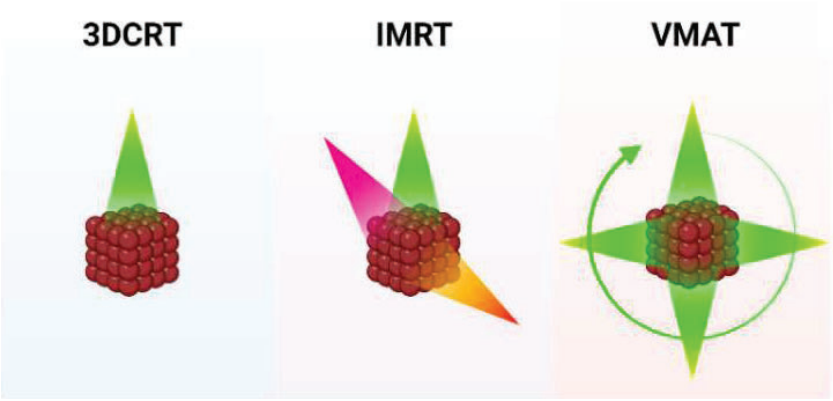

Figure 10: External beam radiation therapy techniques most used as adjuvant gynaecological therapy techniques and their beam orientations.

3DCRT: 3-dimensional conformal radiotherapy uses a single beam that targets the tumour, guided by CT imaging. IMRT: Intensity modulated radiotherapy uses multiple beams of varying intensities to target the tumour. VMAT: Volumetric modulated arc therapy uses a full 360-degree rotation of beams at lower doses of radiation to target the tumour to limit off target radiation of neighbouring tissues.

Internal radiation or brachytherapy, on the other hand, consists of the insertion of radioactive material directly into the body, close to the tumour. Back in the mid-1900s, practitioners conducted brachytherapy by inserting radium tubes inside patients' uterine cavity until maximum capacity was reached [70]. Over time, the technique has greatly improved and has become the most commonly used adjuvant treatment option for EC management, notably reducing the risk of vaginal recurrence, especially for intermediate or high-intermediate-risk patients due in part to the limited associated toxicity and adverse effects compared to EBRT [71]. Since 2012, brachytherapy has been preferentially administered by high-dose-rate administration of iridium 192 in a fractionated manner, allowing surrounding tissues to recuperate from radioactive induced damage between sessions and specifically targeting cancer cells through the progressive accumulation of radiotherapy [72].

3.4.2.2. Which adjuvant therapy to choose: EBRT, Brachytherapy, or both?

Low-risk patients do not benefit from adjuvant radiotherapy as much as higher risk patients. As a matter of fact, EBRT shows greater risk of secondary cancer development for younger, low-risk patients [73–76]. As for intermediate- and high-risk stratified cases, studies comparing the efficacy of EBRT and vaginal brachytherapy (VBT) alone and in combination showed that EBRT greatly reduced loco-regional cancer recurrence along with metastasis but didn't do much concerning overall survival when compared to VBT [76,77]. However, it is important to note that EBRT induced greater adverse side effects, notably acute and late toxicity, reduced quality of life as well as rectal and bladder functions [73,75,76]. Therefore, the use of EBRT is now limited to high-risk patients, sparing them from the latter described adverse effects, making brachytherapy the go-to adjuvant therapy option for high intermediate risk patients [78]. As for lower risk patients, no adjuvant radiotherapy is recommended as data show no additional benefit to the post-surgical resection of tumours [79,80].

3.4.3. Chemotherapy

Similarly to radiotherapy, chemotherapy is also available to patients as a neo-adjuvant, adjuvant or palliative form of treatment. For EC, the most common types of chemotherapy that have been used are doxorubicin, cisplatin, paclitaxel, carboplatin, and docetaxel, each aiming at arresting the cancer

cell cycle through varying mode of actions. Cisplatin, carboplatin and doxorubicin are all DNA intercalating agents that block cell division through the binding of DNA bases (*figure 11*) [81]. Unlike doxorubicin however, cisplatin and carboplatin are both synthetic platinum compounds [82]. They differ in that carboplatin has a longer lasting effect, as it displays a diminished reactivity with DNA and stays longer in the body. However, carboplatin is much less toxic than cisplatin, which allows the use of greater amounts of carboplatin and for longer periods of time [82]. As for paclitaxel and docetaxel, they are taxane compounds that also block cell division, but through their interference with the cell cytoskeleton (*figure 11*). Unlike docetaxel, paclitaxel has a dose-dependent effect, where higher doses will rather lead to chromosome mis-segregation before anaphase and the subsequent death of daughter cells lacking important DNA information [83]. These taxane compounds also differ in the side effects they engender. Paclitaxel is linked to neurological issues whereas docetaxel is associated with nail toxicity and fluid retention, neutropenia being the most frequent DLT for both [83,84].

3.4.3.1. Chemotherapy combinations for EC

Based on GOG trials aiming to identify the best chemotherapeutic approach for the management of EC, the standard of care until 2002 for intermediate to high-risk patients was a combination of doxorubicin and cisplatin. This decision regarded previous studies showing a benefit of this combination in comparison with single agent therapy and doxorubicin-paclitaxel combination with reference to overall survival and progression free survival, and toxicity profiles respectively [85]. The later addition of paclitaxel to the standard doxorubicin-cisplatin combination resulted in improved clinical outcomes as increased objective response, progression free survival and overall survival, but came with greater adverse reactions including neutropenia and neurotoxicity. Due to the efficacy and tolerability of paclitaxel-carboplatin combination in ovarian cancer, its effect was investigated in EC and showed similar effects to the previous chemotherapeutic trio with diminished neurotoxicity. Carboplatin and paclitaxel have hence become the new standard regimen of chemotherapy treatment for EC (figure 11) [85,86].

3.4.3.2. Chemotherapy and radiotherapy: the more, the merrier?

The combination of chemotherapy with radiotherapy, also known as concomitant or sequential chemoradiation, is proposed as an adjuvant treatment for some higher-risk patients only. There is indeed no evidence supporting chemotherapy as an adjuvant therapy option for low-risk patients. Studies comparing the efficacy of chemotherapy compared to chemoradiation for patients of all stages showed no significant differences in patient overall survival and progression free survival [87,88]. When focusing on advanced patients, the GOG-122 and PORTEC-3 trials both found that chemotherapy in combination with chemoradiation or alone may improve overall survival (OS) and progression free survival (PFS) compared to radiotherapy, but also show worsened acute toxicity and number of AEs [89,90].

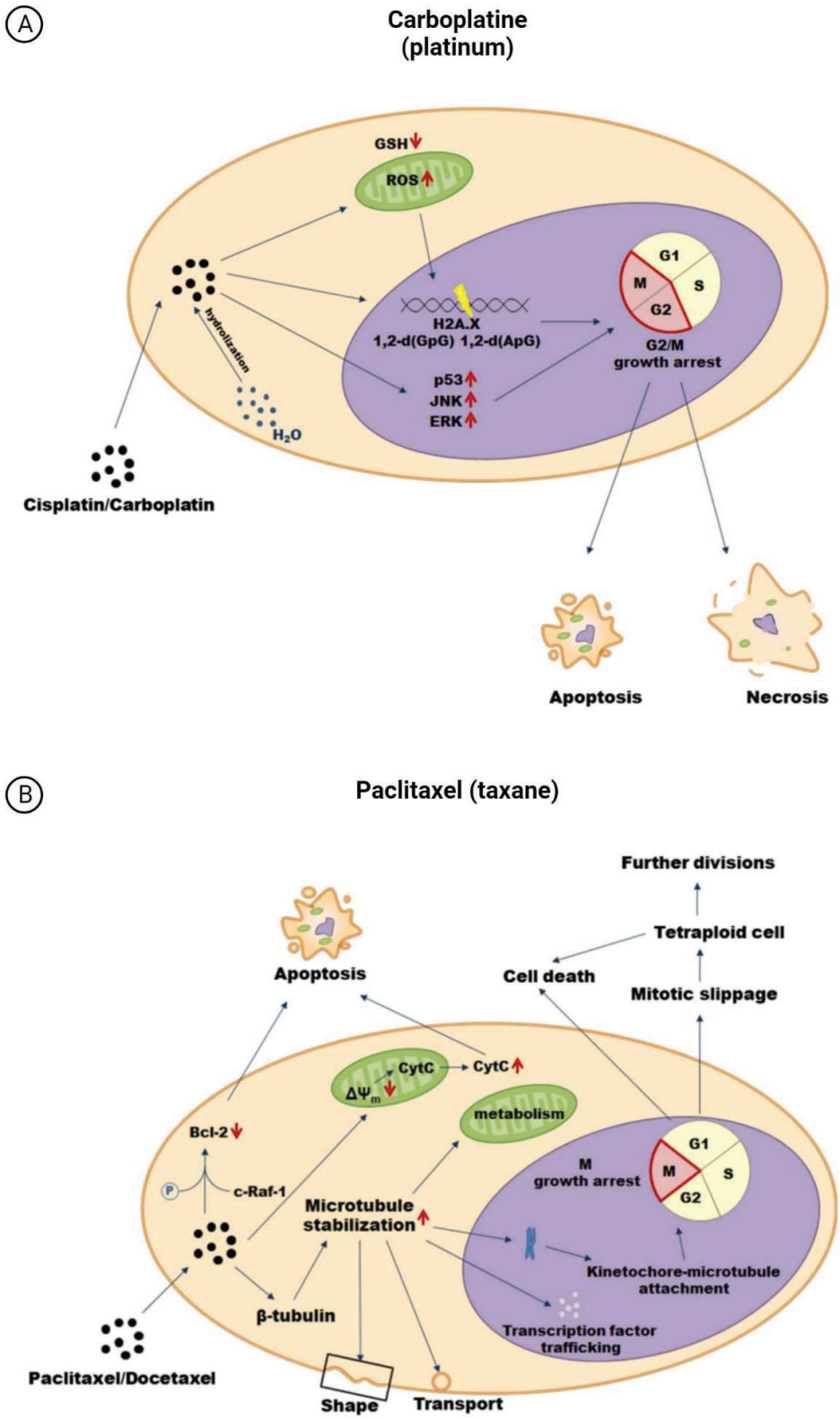

Figure 11: Carboplatin and Paclitaxel mechanism of action in cancer cells *[91].*
(A) Carboplatin intercalates in cell DNA, interfering with DNA replication and RNA transcription by binding DNA-associated enzymes, possibly triggering the apoptosis pathway through accumulated DNA damage. (B) Paclitaxel targets the mitotic phase of cell division by enabling polymerization of microtubules but blocking their depolarization, effectively obstructing the mitotic cell checkpoint.

3.4.4. Targeted therapy in EC

The 2 main kinds of targeted therapies in EC are that of monoclonal antibodies and small molecule inhibitors. Antibodies target specific proteins in and around tumours, while small molecular inhibitors can target intracellular effectors.

3.4.4.1. Small molecules

Hormone treatment

Different types of hormonal treatments exist for the management of EC. All have the same goal: alter the sex hormones balance to prevent cell proliferation in the endometrium (*figure 12*). Three main kinds of hormone treatments for EC are available: progestogens like medroxyprogesterone acetate (MPA), selective estrogenic receptor modulators (SERMs) like tamoxifen, and aromatase inhibitors [92]. These types of treatments are indicated for patients with low-grade carcinomas of endometrioid histology or slow progressing diseases, where chemotherapy is not an option [93].

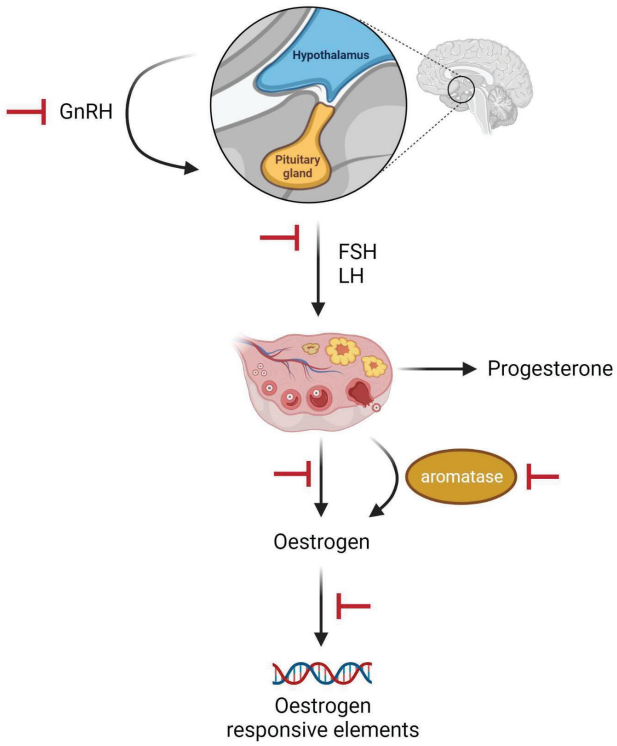

Figure 12: Hormonal therapies to counter gynaecological cancer progression.
Hormonal therapy to target EC can take place through the blocking of the GnRH communication between the hypothalamus and pituitary glands, through the blocking of LH and FSH secretion by the pituitary glands, through the inhibition of estradiol production by the ovaries, and through the blocking of oestrogen receptor signalling that normally induces the expression of pro-tumoural genes (figure adapted from Mitra et al. 2022 [94]*).*

Multi-kinase inhibitor

As an inhibitor of tyrosine kinases, Lenvatinib inhibits various signalling pathways such as angiogenesis, cell proliferation, and ultimately tumour growth. Its anti-angiogenic effect is due to its binging of the VEGF receptors at the cell surface. As for the blockade of cell proliferation, it is due to its binding to other cell surface receptors such as fibroblast growth factor receptors (FGFRs),

platelet-derived growth factor receptor (PDGFR) and the KIT and RET receptors [95]. By binding these receptors, Lenvatinib prevents the phosphorylation of downstream signalling effectors, effectively blocking pathologically dysregulated signalling pathways such as PI3K/AKT/mTOR (*figure 13*). Lenvatinib is generally administered to advanced or recurrent EC cases [96,97]. Indeed, in a recent phase III clinical trial, its combination with an immunotherapy targeting cell cycle progression called Pembrolizumab compared to chemotherapy alone shows an increase of PFS to 7.2 months compared to 3.8, and an increased OS of 18.3 months compared to 11.4 months for advanced EC patients [98].

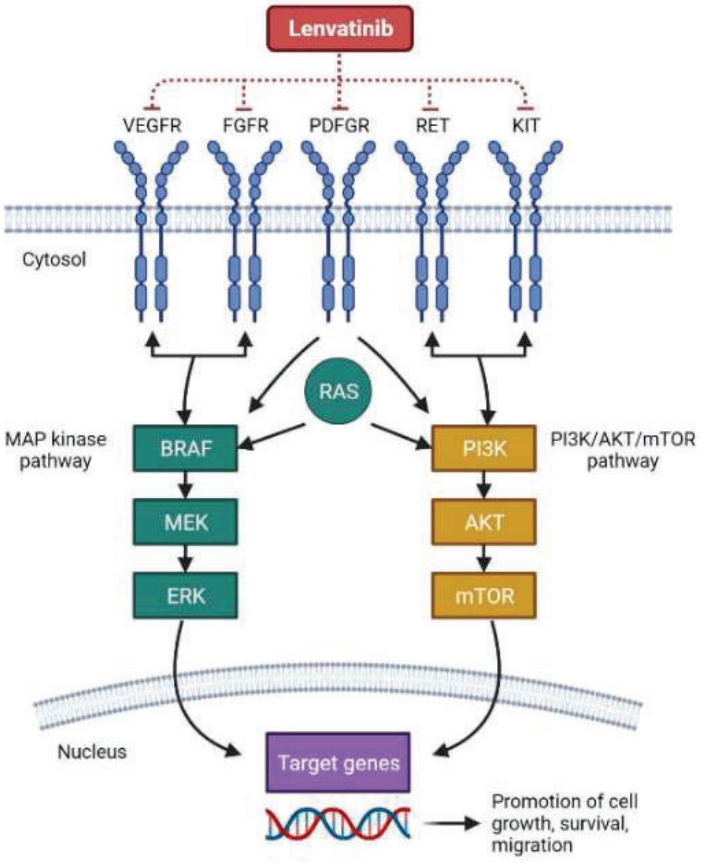

Figure 13: Lenvatinib mechanism of action.

The two major signalling pathways MAPK and PI3K/AKT/mammalian target of rapamycin (mTOR) are targeted by Lenvatinib through its inhibition by direct binding to membrane bound tyrosine kinase receptors, therefore blocking their downstream activation of genes implicated in pro-tumoural function such as cell growth, survival and migration. Figure adapted from Rehman et al. 2021 [95].

3.4.4.2. Immunotherapy

Immune checkpoint inhibitors

Pembrolizumab (Keytruda®) is a humanized monoclonal IgG antibody directed against programmed cell death protein receptor 1 (PD-1) expressed at the surface of lymphocytes. This receptor acts as an immune checkpoint, essentially preventing T lymphocytes from attacking cells that present its ligand PD-L1 at its surface, such as other immune cells. Certain tumours however have high expression of PD-L1, therefore high jacking this T cell tolerance to proliferate and develop cancers hiding in plain sight. By binding with PD-1, pembrolizumab enables the activation of T-cell-mediated immune responses against tumour cells [99,100]. It has shown a high efficacy when

administered in combination with standard Carboplatin and Paclitaxel chemotherapy in advanced MMR deficient EC patients, with a PFS of 74% compared to 38% with chemotherapy alone [101]. Pembrolizumab is usually administered to EC patients that cannot be cured with surgery or radiotherapy and that are non-respondent to chemotherapy.

Angiogenesis inhibitors

To ensure a procurement of nutrients and oxygen, tumours require the development of a blood supply. The over expression of vascular endothelial growth factor (VEGF) mediated in part by hypoxia-regulated genes such as hypoxia-inducible factor (HIF) [102], guides vascular permeability during vasculogenesis and angiogenesis via its binding to its receptors VEGFR1 and VEGFR2 at the surface of target cells. Bevacizumab (Avastin®) binds VEGF directly, inhibiting its interaction with VEGRs and all the canonical signalling therefore induced, essentially starving the tumour (*figure 14*). This antibody is approved for the treatment of gynaecological cancers such as cervical and ovarian cancers, but it is being tested in multiple clinical trials for EC indication. Since 2015, clinical trials have shown a significant benefice of the combination of Bevacizumab with Paclitaxel/Carboplatin compared with the standard treatment for advanced EC, although the rate of AEs was quite high [103].

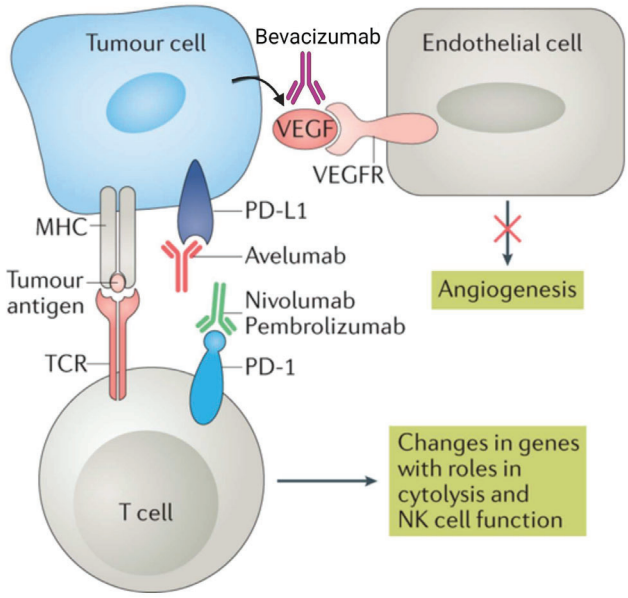

Figure 14: Mechanisms of action of agents used in combination therapies.
Combination of VEGF inhibition by Bevacizumab or Axitinib and PD-1 or PD-L1 inhibition by Pembrolizumab, Nivolumab or Avelumab enables the blockade of angiogenesis and the activation of T cell mediated immune response to target tumour development.

3.5. Combined treatment response based on molecular classification

Since the publication of the TCGA data in 2013 proposing a novel classification of ECs based on molecular profile, great efforts have been made to integrate this information in clinical diagnostic evaluation and patient care. Multiple trials have put to light the influence of molecular classification in patient response to standard treatments.

As an example, we will look at the PORTEC-1 and -2 trials that after investigating post-operative radiation therapy for EC had concluded that high-intermediate risk patients (determined by clinico- pathological stratification) could effectively be treated with vaginal brachytherapy as

opposed to low-intermediate patients where such treatment could be omitted. When further stratifying the high-intermediate risk patients by molecular subgrouping, significant variability in prognosis was exposed, with p53 mutant patients showing the worst prognosis (*figure 15*) [104]. Another example resides in the review of the GOG-86P trial, a phase II study of frontline combinations of chemotherapy with targeted therapies for advanced EC. Analysis of *P53* mutation and patient outcome showed that *P53* mutated tumour bearing patients had longer PFS when treated with chemotherapy combined with bevacizumab rather than Temsirolimus (with a median PFS of 12,5 and 8,2 months respectively) [105].

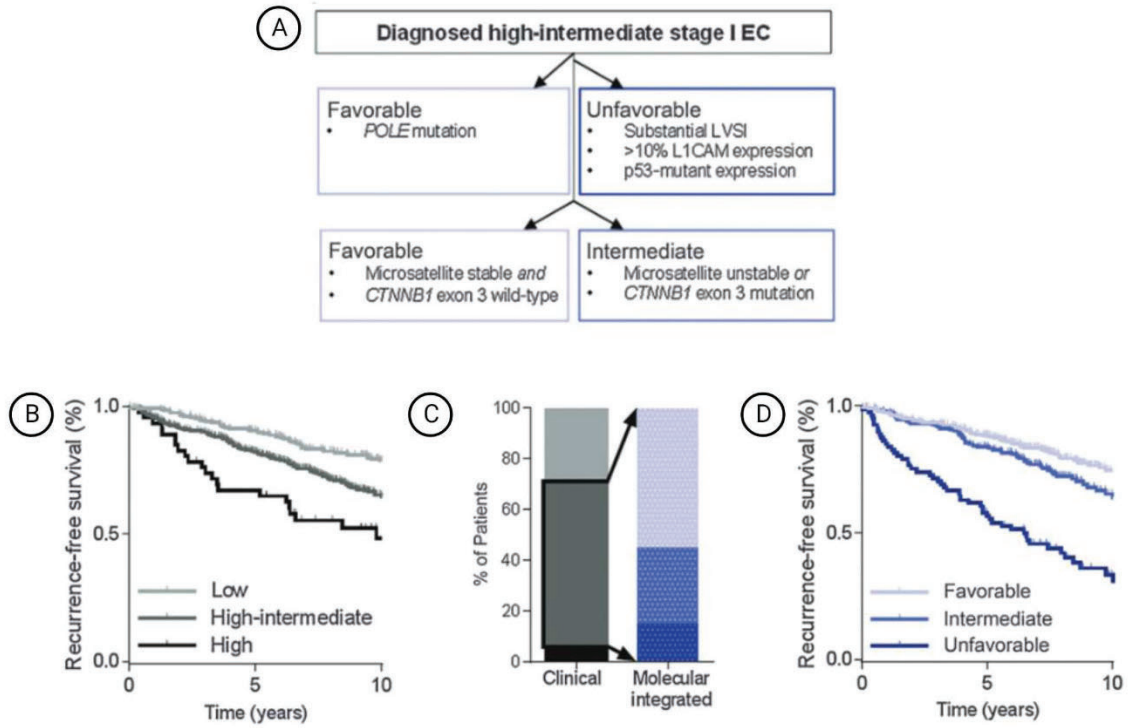

Figure 15: Molecular integrated risk assessment.

(A) *Flow chart of the molecular integrated risk model.* ***(B)*** *recurrence-free survival of clinical risk assessment in early-stage EC (n ¼ 834, P < 0.001).* ***(C)*** *bar chart of the proportion of clinically low-, high-intermediate-, and high-risk patients based on central pathology review (left) and the proportion of clinically high-intermediate risk patients reclassified into favourable, intermediate, and unfavourable molecular integrated risk groups.* ***(D)*** *recurrence-free survival of molecular integrated risk assessment in early-stage high-intermediate risk EC (n ¼ 546, P < 0.001)* [104].

Presently, there is a great deal of EC trials investigating disease response to treatments based on molecular stratification with the aim to better EC patient care [106], such as the PORTEC-4a study, a phase III randomized trial which investigates molecular-profile-based versus standard recommendations for adjuvant radiotherapy in women with early-stage EC [107].

3.6. EC murine study model

With their comparable lifetime risk for developing tumours along with their easy accessibility and quick data production, mice are a go-to animal study in the oncologic research field. Although mice and humans certainly do not look alike, they both remain mammals. The development of an inducible transgenic mouse model of EC progression has allowed us to investigate the effects of NP137 treatment on endometrial tissue histology and molecular markers' expression.

3.6.1. The mouse reproductive system

3.6.1.1. Anatomy, histology, and sex hormone physiology

The mouse and human reproductive system share similar general organization, although their morphology and size differ. Where the human uterus is pyriform, possessing one uterine cavity, mice possess a bicornuate uterus, composed of two uterine horns, each connected by an oviduct leading to an ovary at the top, and joining caudally to form the cervical canal (*figure 16*). Histologically speaking, we find common structures in mice compared to humans: an endometrial surface composed of an epithelial luminal layer of simple columnar to pseudostratified columnar epithelial cells, and an endometrial stroma of connective tissue interspersed with endometrial glandular epithelia. In mice, oestradiol levels are undetectable before 7 days after birth, and progressively increase, reaching a peak around 1 month of age, correlating with the start of murine cycles and puberty. As for progesterone, blood levels are slightly elevated at birth but strongly decline around day 7 after birth. Ovarian production of progesterone starts around day 10 with levels increasing around 1 month and reaching their peak around 2 months [108].

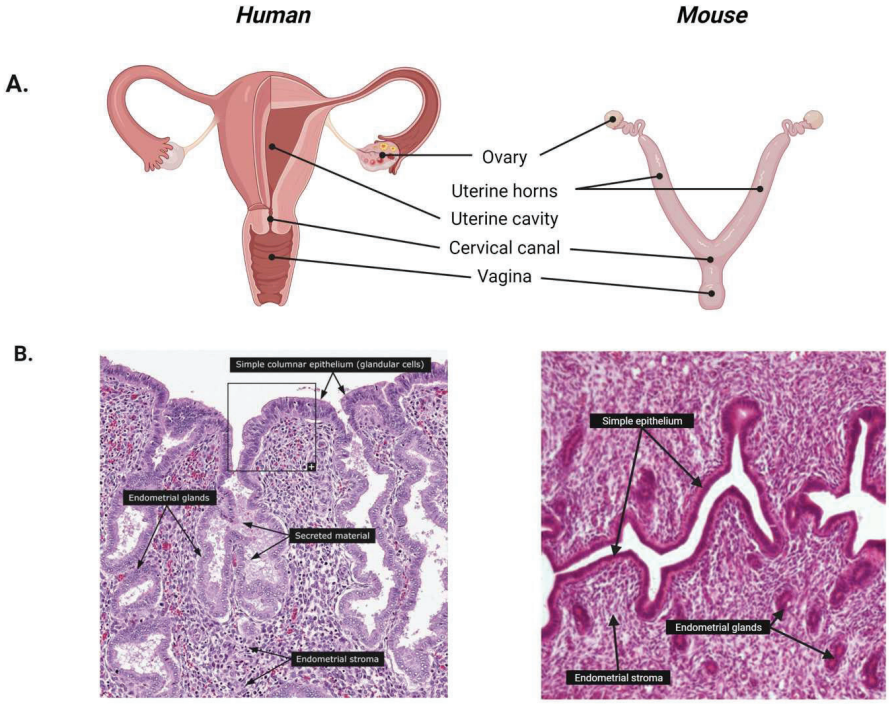

Figure 16: Comparative of the human and murine female reproductive organ anatomy and histology.

(A) Comparative of human and murine female reproductive organ anatomy (B) Human (left) and murine (right) uterine histology share common structures such as a uterine cavity bordered by an endometrial simple epithelial luminal layer and stroma interspersed with epithelial glands.

3.6.1.2. The oestrous cycle

The main comparison between the oestrous cycle of the mouse (exception made for the spiny mouse model) and the menstrual cycle of humans is the absence of murine menstruation. Indeed, mice do not menstruate nor undergo menopause. In their 4-to-5-day reproductive cycle (unless interrupted by pregnancy) that starts around 26 days after birth, the murine reproductive system is subject to 4 cyclic phases comparable to those of humans: proestrus, oestrus, metestrus, and dioestrus (*figure 17*). During proestrus, follicular development is initiated as the ovarian corpus luteum from

the previous cycle regresses and levels of progesterone decrease and oestrogen increase. Mice then enter oestrus, characterized by a surge of LH due to high circulating levels of oestrogen, ultimately resulting in ovulation. The following phase is metestrus, where a new corpus luteum develops under the influence of LH, producing increasing levels of progesterone that inhibit LH release. Eventually, dioestrus marks the start of the regression of the corpus luteum, accompanied by a suppression of progesterone which progressively releases its blocking action on oestrogen.

Aside from steroid concentration variations throughout the reproductive cycle, multiple other modifications arise within the rodent's organism; throughout the cycle, vaginal smears or lavages demonstrate changes in cell composition with varying levels of leucocytes, nucleated and cornified epithelial cells, urine samples show varying levels of proteins, lipids and carbohydrates all dependent on oestradiol and progesterone concentrations, and histological examinations of uterine cross and longitudinal sections portray shifts in epithelial cell morphology and organization, cell cycle progression, cell degeneration, immune cell infiltration, stromal oedema and luminal dilatation [109].

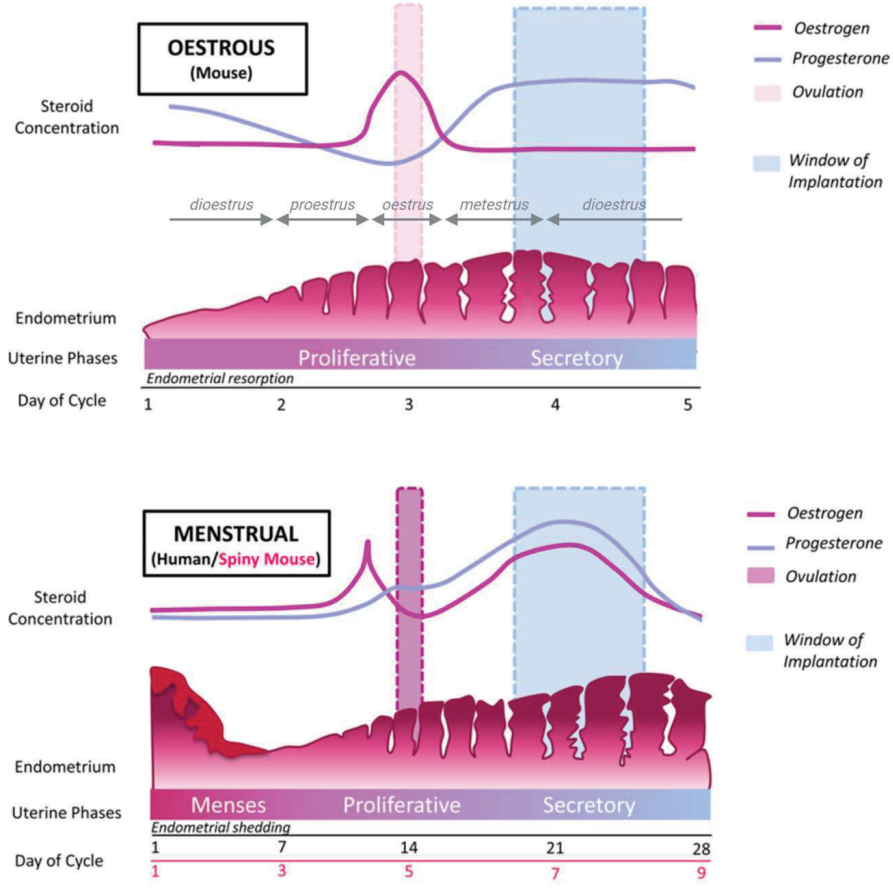

Figure 17: Comparative of the murine and human endometrial cycle.

In oestrous species like most mice, ovulation is triggered by seasonal cues, and a decline in progesterone leads to endometrial resorption. In menstruating species like humans, breeding is year-round and rapid withdrawal of progesterone leads to endometrial shedding, also known as menstruation. (adapted figure [110]*)*

3.6.2. An inducible PTEN knock-out mouse

The most common mouse models used in preclinical studies for EC are *PTEN*-knockout (KO) mice, where a heterozygous loss of function is induced, as homozygous excision of *PTEN* leads to embryonic lethality. In these models, generated neoplasms are not limited to the endometrial tissue

as they are also observed in the breast, the prostate, the thyroid glands, the gastrointestinal tract, and lymphoid tissues [111]. To study the effect of NP137 on an inducible murine model of EC, we turned to Dr. Xavier Dolcet's research team, as they had developed a Tamoxifen induced *PTEN* knock-out mouse. This mouse model was born from the breeding of a Tamoxifen induced CAG-Cre-ER^{T} recombinant mouse with a *PTEN* floxed one. Due to the use of the chicken actin promoter (CAG) which is ubiquitously expressed, neoplasms induced in these mice are not specific to the endometrium as PTEN loss due to Cre-ERT recombination after tamoxifen injection is observed in multiple other epithelial tissues including the endometrium, the thyroid, the liver, the colon, the kidneys, and the lungs. Through the generation of a CAG-Cre-ERT mT/mG mouse model where cells lacking Cre-ERT expression showed only red fluorescence (Tomato) while those having undergone Cre-mediated excision showed green fluorescence (GFP), they demonstrated that in their mouse model, stromal tissue and well as lymphoid and hematopoietic organs such as the spleen and the bone marrow do not display any Cre recombination activity (*figure 18*). Heterozygous loss of *PTEN* in these mice leads to the development of endometrial hyperplasia and eventually intra-epithelial carcinoma as early as 3 weeks post tamoxifen injection [112]. In addition to an endometrial involvement, female mice also thyroid nodular hyperplasia (figure 18).

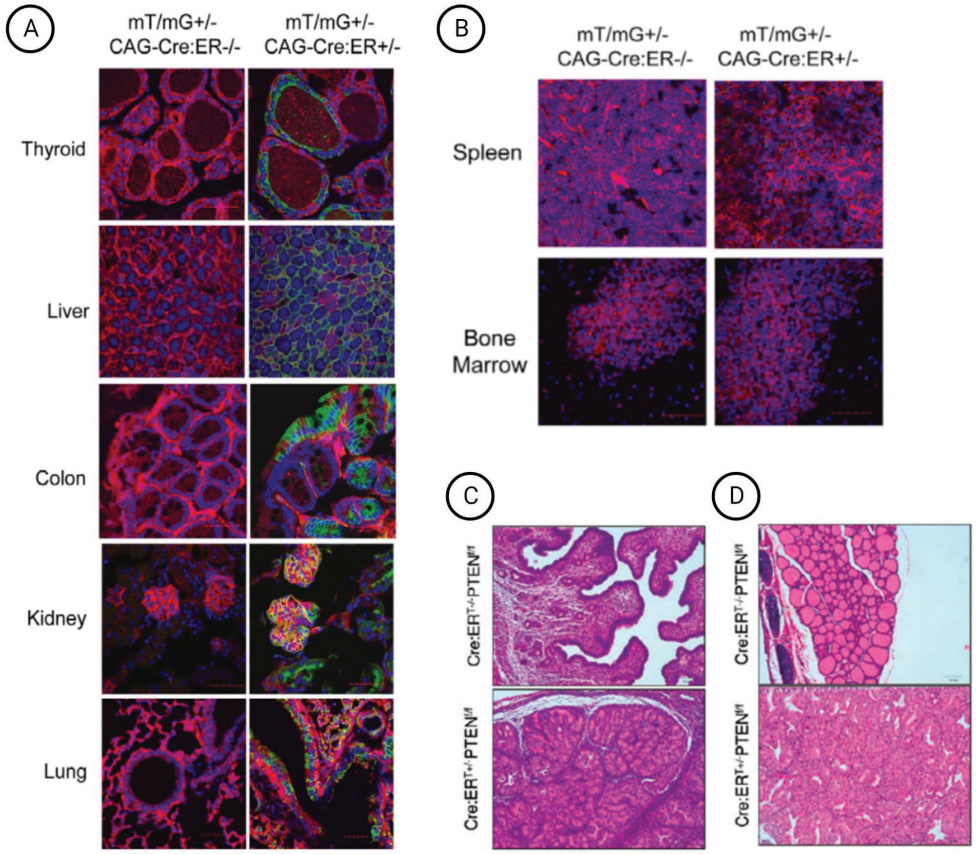

Figure 18: Activity of tamoxifen-induced PTEN deletion by Cre-ERT recombinase

(AB) Representative confocal images corresponding to organs of the double fluorescent mT/mG reporter mice containing (A) epithelial tissues (thyroid, liver, colon, kidney and lung) showing green fluorescence after tamoxifen injection and (B) hematopoietic and lymphoid organs (bone marrow and spleen). Note the absence of green fluorescence. (C) Representative images of haematoxylin and eosin staining of the uterus from PTEN proficient (top panel) or deficient (bottom panel) mice. (D) Representative images of haematoxylin and eosin staining of the thyroid from PTEN proficient (top panel) or deficient (bottom panel) mice. Figure adapted from Mirantes et al. 2013 and Dosil et al. 2017 [112,113]

CHAPTER 4
The epithelial to mesenchymal transition at the root of EC resistance and recurrence

The epithelial-to-mesenchymal transition (EMT) is a transitory and reversible biological process that enables polarized epithelial cells to undergo multiple biochemical changes leading to the acquisition of a mesenchymal phenotype [114]. These biochemical changes lead to a cellular shift in morphology and function, as cells transform from an epithelial, immobile, polarized and closely confined phenotype to very motile and fibroblastic like mesenchymal cells of spindle shape [115]. The reversibility of the process is revealed by the mesenchymal-to-epithelial transition (MET), where cells convert from a mesenchymal phenotype back to an epithelial one [114]. Throughout our lifespan, 3 types of EMT occur in our organism, classified according to their physiological consequence (figure 19).

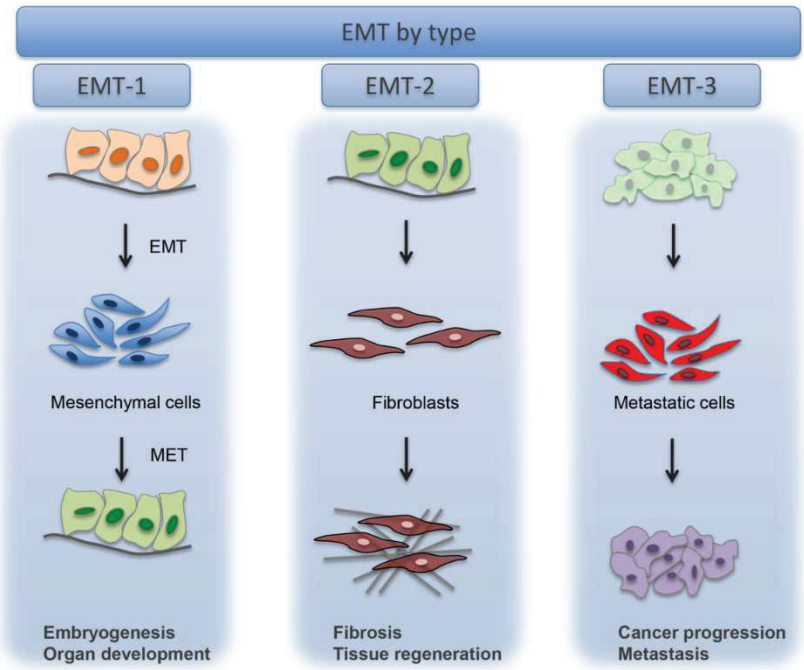

Figure* 19*: Types of EMT.

Three types of EMT are recognized, depending on the phenotype of the output cells. Type 1 EMT is seen when primitive epithelial cells transition into mesenchymal cells that form the diaspora of the basic body plan following gastrulation or neural crest migration. These mesenchymal cells either undergo MET to form secondary epithelial cells or apoptosis. Type 2 EMT is seen when secondary epithelial cells or endothelial cells populate interstitial spaces with resident or inflammation-induced fibroblasts, the latter during persistent injury. Type 3 EMT is part of the metastatic process, whereby epithelial tumour cells leave a primary tumour nodule, migrate to a new tissue site, and reform as a secondary tumour nodule [116,117].

Type 1 EMT: Embryonic development

During embryonic development, EMT enables the final differentiation of cellular types and the formation of organ structure through three sequential rounds of EMT referred to as primary, secondary and tertiary EMT, interspersed by rounds of MET to allow the final differentiation of cells [118]. Primary EMT first occurs during gastrulation giving rise to mesoderm, endoderm, and ectoderm, as well as during the migration of neural crest cells of vertebrates. As for secondary EMT,

it enables the formation of multiple tissues and organs including somites, the palate, the pancreas, the liver and the reproductive tracts. Finally, tertiary EMT is in charge of the heart's development.

Type 2 EMT: Tissue regeneration and organ fibrosis

Dependent on inflammation-inducing injuries to be initiated, type 2 EMT is expressed over extended periods of time throughout our lives to resolve tissue damage. Associated with wound healing and tissue regeneration, sometimes also organ fibrosis when inflammation does not attenuate over time, therefore leading to organ destruction [114]. Physiological wound healing is also a process familiar to the female reproductive system, consisting of de- and re-epithelialization processes which share similarities with EMT and MET to heal the epithelial layer of the ovaries and the endometrium after ovulation and during menstruation respectively [119].

Type 3 EMT: Cancer progression and metastasis

Necessary for the transformation of neoplastic cells at the tumour front to acquire migratory and invasive properties in order to forsake primary tumours, travel through the blood stream and form distant metastatic colonies, type 3 EMT is a pathology-associated process unlike type 1 and 2 which are physiological. This type of EMT will be described further in depth in this chapter of the manuscript.

4.1. EMT function in cancer

Functionally speaking, EMT in cancer can be simplistically resumed into four basic steps, which involve many molecular processes from its initiation up until its completion [120]: i. Cellular loss of baso-apical polarization, ii. Cellular individualization, iii. Cellular motility, and iv. Cellular invasiveness, leading to cellular dissemination (*figure 20*). The occurrence of all of these processes during EMT in cancer cells ultimately provide them with tumoural associated functions such as the ability to migrate and invade to disseminate, stem-like features for the formation of metastasis, as well as cytotoxic drug resistance [114].

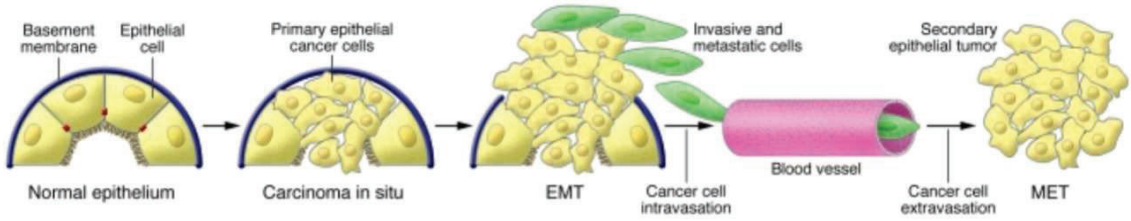

***Figure 20: Contribution of EMT to cancer progression** [114].*

Progression from normal epithelium to invasive carcinoma goes through several stages, from the loss of epithelial cell polarity and their detachment from the basement membrane that also changes in composition, altering cell-ECM interactions and signalling networks. Thereupon, EMT facilitates the malignant invasion of tumour cells by enabling their entering the circulation and consequent exit at a remote site to form metastases which may involve MET and therefore a reversion to an epithelial phenotype.

The initiation of EMT requires the activation of specific TFs that negatively regulate the expression of membrane bound proteins implicated in cellular adhesion. This regulation gives rise to a reorganization of cellular junctions such as tight junctions, adherens junctions, desmosomes and hemi-desmosomes, in favour of a detachment of cells from the basal membrane. Additionally, TFs also regulate the expression of cytoskeleton associated proteins and cell-to-matrix adhesion molecules, switching the basal-apical polarity of epithelial cells to a front-rear polarity, typical of

mesenchymal cells and important for the initiation of migration. To enable cells to migrate through a densely packed heterogenous microenvironment known as the extracellular matrix (ECM), TFs also promote the remodelling of the ECM by the production of new compounds like the pro-migratory FN1 or by its degradation with enzymes such as metalloproteases (MMPs) that pave cells a way to the circulation as single cells or collective clusters using vascularisations located away from the primary tumour or within the tumour mass [121,122]. It has been observed that in primary tumours, it is the peripheral tumour cells that exhibit EMT phenotypes such as loss of epithelial marker expression and cell to cell junctions but gain of mesenchymal markers, suggesting that peripheral tumour cells compose the invasive front, promoting the cancer's dissemination at distant sites [123]. Once cells reach the circulation, the risk of anoikis[5] is countered by the activation of EMT in circulating tumour cells (CTCs) which ensures their survival in the peripheral system [124,125]. These CTCs show cancer stem cell hallmarks such as self-renewal and multilineage differentiation capacity, enabling them to develop colonies in distant sites [126]. Their presence in peripheral blood in multiple cancer indications has been associated with decreased PFS and OS [127–129]. Cells having successfully colonized distant tissues after extravasation make use of EMT associated stem properties of self-renewal as well as the reverse process of MET for the formation of metastases (*figure 21*) [130]. The modulation of signalling pathways implicated in these morphological and functional changes is in part regulated by intrinsic factors (such as TFs), and in part induced by extrinsic factors, such as the composition of the ECM in chemokines and stromal cells such as immune cells, endothelial cells, neural cells, and fibroblastic cells known as cancer associated fibroblasts (CAFs).

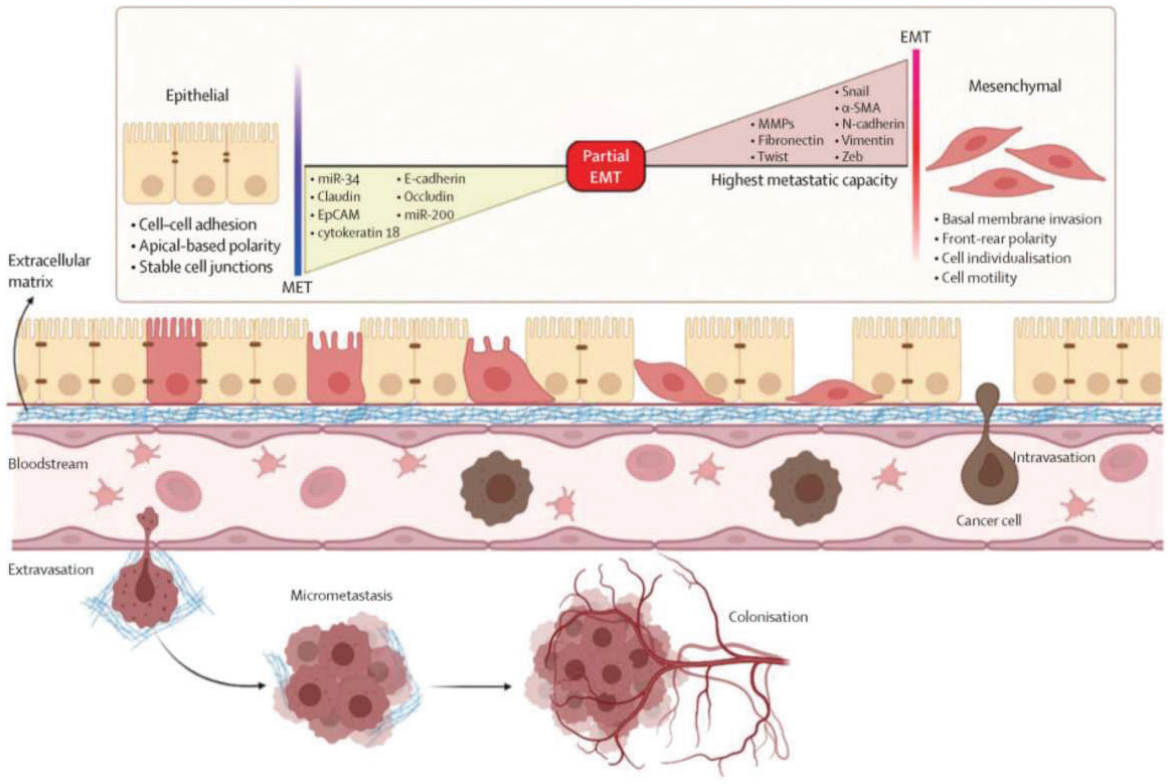

***Figure 21: Overview of cancer EMT and its associated cellular functional and transcriptional impact** [131].*

The blue and red bars present the level and intensity of gene expression. EMT and MET are non-binary reversible processes that emphasize the plasticity of cells to transit along these two states. Cells with

[5] apoptosis induced by a lack of cellular adhesion.

more epithelial features and less mesenchymal conversions have the highest malignancy. α-SMA=α-smooth muscle actin. EMT=epithelial–mesenchymal transition. MET=mesenchymal–epithelial transition. mIR=microRNA. MMPs=matrix metalloproteinases.

In the following paragraphs, we will overview how cancer associated EMT is regulated by intracellular and extracellular actors and the various biomarkers of EMT routinely used for the monitoring of its progression in cancer. To conclude, we will talk about how EMT is involved in the resistance and recurrence of EC in the face of standard treatments.

4.2. Regulation of EMT

4.2.1. Transcriptional regulation

TFs are some of the best-characterized mediators of EMT. These proteins can regulate specific gene expression, generally through the binding to the DNA of their promoter and enhancer regions. Certain TFs such as Snail (Snail1), Slug (Snail2), Twist1, ZEB1 and ZEB2 have been identified as involved in the regulation of the transcription of genes specifically involved in EMT processes, and therefore dubbed "EMT-TFs" [132]. Their activity can also be modulated through the formation of complexes with coactivators and corepressors. In the following paragraphs, we will go over the implication of the classical EMT TFs in EMT and EC, as well as cite some less common TFs that will be mentioned in the "Results".

Snail family: Snail and Slug belong to the large family of zinc finger TFs, and repress the expression of epithelial genes like that of CDH1, claudins and occludin, all implicated in cell to cell junctions [133,134]. If we take the example of cadherins, the repression of E-cadherin and activation of N-cadherin during the cadherin switch of cell during EMT is carried out by the direct binding of Snail and Slug to their promoters, notably on the multiple E-box domains [135]. The silencing of CDH1 does not alone induce loss of cellular polarity, as Snail also represses the expression of Crumbs3, another protein essential in epithelial morphogenesis [136]. Beyond epithelial gene regulation, Slug is also described to be implicated in the promotion of cell survival and the induction of metastatic phenotype. Indeed, Snail and Slug upregulation has been related to poor prognosis in a variety of cancer indications, including ovarian and colorectal cancer, and Snail genes have been found to be largely overexpressed in thyroid metastases [137–139].

Twist family: Twist proteins belong to the family of basic helix loop helix TFs, which are mainly expressed during embryogenesis and in certain precursor cells only hereinafter [140]. Their expression is reactivated in tumour cells that use them to induce EMT and promote cancer development and metastasis. Indeed, Twist expression is associated with worse patient prognosis as it promotes tumour invasion through the downregulation of CDH1 which reduces cell adhesion and the upregulation of multiple mesenchymal markers such as vimentin, N-cadherin and fibronectin which promote cellular motility [141,142].

ZEB family: Like Snail and Slug, ZEB1 and ZEB2 also belong to the zinc family of TFs that bind E-box domains on the promoter regions of target genes [143], and much like Twist proteins, they actively repress epithelial cell markers and activate mesenchymal biomarker, hence mediating EMT [144]. In fact, Snail and Twist proteins can together control ZEB1 expression levels, which in turn suppresses the expression of epithelial polarity maintenance genes such as CHD1 and Crumbs3 [145,146]. As a result, the expression of both ZEB1 and ZEB2 have been associated to poor prognosis in various indications of cancer [147–149].

The overexpression of these EMT-TFs has frequently been observed in EC in link with reduced expression of epithelial markers such as E-cadherin, a key regulator of cell-to-cell adhesion [150]. ZEB2, Snail and Slug have all been associated with aggressive clinical characteristics of EC, notably higher stage, grade, histology, myometrial invasion, lymph node involvement and metastasis [151]. Additionally, Slug expression in EC is also associated with a decreased 5-year OS [151]. However, these EMT-TFs are not the sole transcriptional regulators implicated in EC progression. For example, Sal-like 4 (SALL4), a TF implicated in the maintenance of pluripotent embryonic stem cells, also happens to be overexpressed in EC, promoting the expression of the mesenchymal marker N-cadherin and the activity of c-Myc, another well described oncogenic TF [152]. Transcriptional regulation of EMT is also observed through the downregulation of tumour suppressive TFs such as grainyhead like 2 (GRHL2) which is essential in the development and function of epithelial tissues. Its expression is often times downregulated in cancers due to the hypermethylation of its promoter regions [153,154]. Not only has it been identified as an activator of epithelial gene transcription (such as that of *CDH1*), but it also binds promoter regions of other EMT-TFs to negatively regulate their expression like ZEB1, therefore liberating their oppression on the transcription of other epithelial markers [155]. Its hypermethylation and therefore inhibition has been associated with ovarian endometriosis [153].

4.2.2. The microenvironment composition

The tumour microenvironment is a complex milieu that participates in the promotion of cancer progression through the maintenance of a hypoxic and inflammatory surrounding. It is composed of both cellular and non-cellular components that all play a role in the progression of cancer and EMT.

4.2.2.1. Non-cellular components: extracellular matrix and extracellular vesicles

Extracellular matrix (ECM)

Providing a physical scaffold for tumour cells, the ECM is key in the promotion of tumour cell dissemination. Stiffness of the ECM dependent on the organization of the ECM has a great impact on the promotion of EMT. Indeed, increased matrix rigidity has been shown to be responsible for the promotion of positive cellular signalling of survival and tumour growth, and also promote the transition of epithelial cancer cells to a more mesenchymal phenotype in multiple cancer models [156,157]. The ECM is composed of collagen, fibronectin, elastin and laminin secreted by cellular components of the tumour microenvironment, such as CAFs. Additionally, a plethora of pro-tumoural and EMT inducing factors are deposited in the ECM and utilized by tumour cells to promote cancer progression, such as growth factors (TGFb, EGF) and angiogenic factors (VEGF) (*annex 4*).

Extracellular vesicles (EVs)

Identified in circulating body fluids and transporting proteins and nucleic acids representative of the secreting cells, the use of tumour derived EVs has gained increasing interest for disease diagnostic and monitoring [158–160]. Whether they be micro-vesicles or exosomes arising from the budding of the plasma membrane or the endosomal membrane respectively, they both ensure the transportation of cellular cargo into the microenvironment [161]. Their release by tumour cells as well as stromal cells such as CAFs enables pro-tumoural EVs to act on neighbouring tumour cells, tumour microenvironment and long-range metastasis formation where they have been described to create a niche promoting the proliferation of disseminating tumour cells [162,163]. Although some reports have demonstrated the potential of tumour derived EVs to exhibit anti-tumoural properties through the induction of apoptosis or the enhancement of tumour immunity [164–166], growing evidence suggests their potential as tumour promoters, notably through the triggering of the EMT

process, increasing the invasiveness of tumours in multiple cancer models [167–169]. This effect is ensured through their transfer of pro-tumoural functional proteins and nucleic acids such as miR-19a which downregulated the tumour suppressor PTEN, the oncogenic mutants of EGFR and Ras, or the TGFb cytokine [170–172].

4.2.2.2. Cellular components: immune and stromal cells

Immune cells

Macrophages are important modulators of tumours progression and exist under two phenotypes: M1 anti-tumour macrophages, and M2 tumour associated macrophages (TAMs) that promote tumour progression [173]. As CAFs, these cells also secrete factors implicated in EMT, like TNFa, IL6 and TGFb which are able to activate the NFkB signalling pathway implicated in the maintenance of inflammation-induced cancer cell migration and invasion. Indeed, NFkB is capable of stabilizing the expression of Snail by inhibiting its phosphorylation by GSK3, therefore ensuring its localization in cells to carry out the modulation of EMT-related gene expression [174]. TGFb secretion along with IL10 secretion by TAMs also carry out an immunosuppressive effect which promotes regulatory T cell activity and inhibition of T lymphocytes activity and dendritic cell maturation [175]. Additionally, TAMs' immune suppressive effect can also be carried out through their expression of PD-L1 that acts upon T cell exhaustion through the PD-L1/PD-1 inhibitory pathway [175].

Stromal cells

Cancer Associated Fibroblasts (CAFs) are the main component of the tumour stromal compartment. They are a heterogenous group of activated fibroblasts whose origin is still today being disputed. They can derive from epithelial cells, endothelial cells, adipocytes, pericytes, stellate cells or fibroblasts. Their expression is correlated with the remodelling of the ECM, the suppression of anti-tumour immunity and the progression of cancer. These functions are notably carried out through their expression of secretory factors that promote tumourigenesis, notably through the stimulation of EMT [176,177]. These include growth factors (TGFs, PDGF, FGF, HGF and EGF) as well as interleukins (1b, 6, 11) and chemokines (CXCL1, 12, CCL5). The secretion of these factors affects cancer cells as well as regulates immune cells. As an example, the expression of CAF-derived IL6 is known to activate the JAK/STAT3 signalling pathway that is implicated in the stimulation of cell proliferation of cancer cells and angiogenesis through the implication of matrix metalloproteases (MMPs) that degrade the basement membrane to facilitate infiltration [178]. In regard to EMT, STAT3 activation in cancer cells promotes the expression of the EMT-TFs Snail and Twist, which in turn induce the secretion of inflammatory cytokines, forming a positive feedback loop [179]. Additionally, this STAT3 activation in immune infiltrating cells can also negatively regulate them, ensuring an immunosuppressive environment favourable for the development of cancer [180]. The malignant transition of epithelial cells to a mesenchymal phenotype also implicates an increased expression of molecules involved in the adhesion of cells to the extracellular matrix (ECM). In tumours, fibronectin, a 440 kDa dimeric glycoprotein implicated in these matrix anchoring functions, is majorly expressed by CAFs present in the tumour's microenvironment [181]. Fibronectin expression by these CAFs organizes the ECM to form a scaffold that helps cells to anchor themselves to it and migrate away from the primary tumour [182]. This migration is also possible due to fibronectin's activation of the cancer cell's Focal Adhesion Kinase (FAK) pathway via its binding to cellular integrins that releases metalloproteases (MMPs) responsible for ECM remodelling, facilitating cellular invasion [183]. In addition to migration/invasion, fibronectin is also implicated in the stimulation of cell proliferation and angiogenesis [184,185].

4.3. Markers of EMT progression in cancer

The progression of EMT can be experimentally monitored through transcriptomic and cell behaviour analysis (*annex 5*). Variations in the expression levels of certain cell surface and cytoskeletal markers are indicative of the cellular advancement along the EMT spectrum, that is the downregulation of cell-to-cell junctions with a switch in junction molecule expression from E- to N-cadherin and the reversal of cytosolic intermediate filaments from keratin to vimentin. Such variations are induced in part by the transcriptional regulation of genes following the activation of the EMT-TFs described previously (Snail1/2, Twist1, ZEB1/2). As tumours are not only composed of tumour cells but also of a complex microenvironment, it is important to also consider differently expressed matrix associated molecules. The following paragraphs will present the various types of molecular changes observed in tumours related to the progression of EMT and EC.

4.3.1. Tumour cell morphology and tissue organization

4.3.1.1. Cadherins

Cell-to-cell contact in epithelial tissues is assured by three types of interactions: from apical to basal localization, we find tight junctions that connect plasma membranes, adherens junctions that join actin filaments, and desmosomes that join intermediate filaments [186]. Cadherins form a group of membrane associated glycoproteins that mediate these interactions through the formation of calcium dependent homophilic junctions. They promote contact formation between cells through their clustering and the recruitment of associated proteins to increase cell to cell contact and reduce surface tensions. They also enable the reorganization of cells' cytoskeleton dependent on the type of cadherin implicated along with the associated actomyosin linked effectors to further reduce tension. To mediate cell coupling, cadherins anchor themselves to the actin cytoskeleton through the formation of a complex with beta- and alpha-catenin which allows them to transmit to the cytoskeleton any forces of mechanical load [187,188].

Epithelial cadherin (E-cadherin) and Neural cadherin (N-cadherin), two classical type I cadherins encoded by *CDH1* and *CDH2* on chromosomes 16 and 18 respectively, are key components of the cadherin superfamily that drive tumourigenesis through their implication in EMT. Although they share a similar structure composed of five extracellular cadherin repeats, a transmembrane domain and a cytoplasmic domain tethered to the actomyosin cytoskeleton, they carry out contradictory effects. As a matter of fact, a hallmark of EMT is the early loss of E-cadherin expression in favour of N-cadherin also known as the "cadherin switch" (*figure 22*), which is associated with increased migratory and invasive cell behaviour and worse patient prognosis. For example, E-cadherin trans-binding allows the recruitment of actomyosin skeleton effectors such as PIP3 that enables the activation of Rac1 implicated in the maintenance of apico-basolateral cell polarity, or p120-catenin that downregulates RhoA implicated in the stimulation of actomyosin contractility [189]. The activation of Rac1 by N-cadherin trans-binding on the other hand stimulates the formation of membrane protrusions at points of cell to cell contact, while RhoA is activated, rendering cells with a more motile phenotype [190]. Additionally, N-cadherin extracellular domain ligation also triggers the PI3K/AKT pathway implicated in the stimulation of cell survival.

In the endometrium, E-cadherin and catenin expression vary throughout the cycle. During the proliferative phase, E-cadherin and cytoplasmic beta-catenin expression are increased in glandular cells as well as stromal cells, as cellular contacts are required to maintain an epithelial structural

integrity replicating that of glands. However, during the secretory phase, E-cadherin and cytosolic beta-catenin expression decrease along with the strength in cellular bonds as the tissue prepares for the menstrual phase breakdown [191]. Loss of E-cadherin expression also impacts intracellular effectors such as beta-catenin which when bound E-cadherin at the plasma membrane participates in the maintenance of epithelial tissue organization, but when free in the cytoplasm and nucleus stimulates cell proliferation through the Wnt pathway cytosolically, and through the stimulation of CDK1 expression when in the nucleus. This nuclear localization of beta-catenin has been linked to loss of E-cadherin expression has also been observed in normal endometrium [191]. As for N-cadherin, its expression in normal endometrium has been associated to progenitor glandular cells that show greater self-renewal properties and located in the base of glands, close to the myometrium [192].

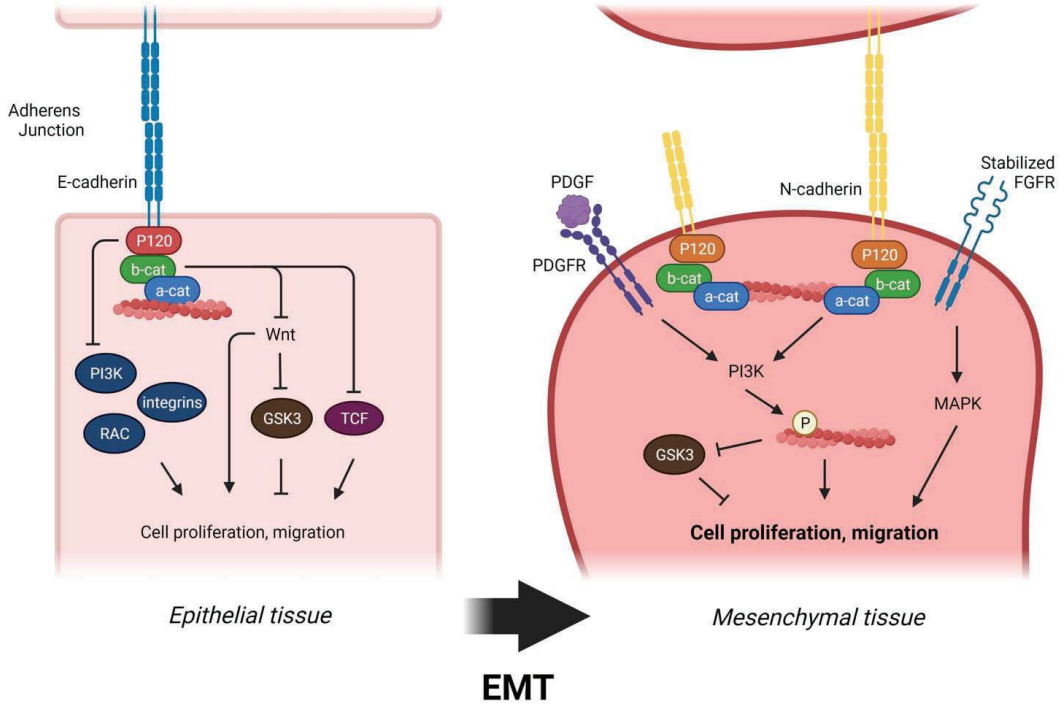

Figure 22: Functions of E-cadherin and N-cadherin

(Left) E-cadherin junctions form the stable adherens junction and enable strong cell–cell contact. As p120 catenin and β-catenin are strongly bound to the E-cadherin complex, they are not available to activate Wnt/β-catenin pathway and P13K pathway. (Right) N-cadherin junction enables the stabilization of fibroblast growth factor receptor (FGFR) which leads to activation of MAPK/ERK pathway and activates the PI3K pathway in association with PDGFR to enhance cell survival and migration. PI3K = Phosphoinositide-3-kinase; RAC = Ras-related C3 Botulinum Toxin Substrate; GSK3 = Glycogen Synthase Kinase 3; TCF = T-cell Factor; PDGFR: Platelet-derived Growth Factor Receptor; FGFR: Fibroblast Growth Factor Receptor; MAPK = Mitogen-activated Protein Kinase; ERK = Extracellular Signal-regulated Kinases. (Figure adapted from Loh et al. 2019 [193]*).*

When investigating these proteins' expression in cancerous endometrium, it is observed that not only does E-cadherin expression decrease in pathological samples compared to normal proliferative phase endometrial glands, but also that this decrease intensifies along with tumour aggressivity and the degree of disease progression [191,194,195]. Additionally, N-cadherin expression is observed to be increased in EEC and its precursor lesions in comparison with healthy proliferative endometrium [196]. Furthermore, N-cadherin expression in EC is also linked with higher FIGO staged and lower histological differentiation of tumours, and its expression in primary tumours is heightened at the

tumour front compared to the main mass of primary tumours [197], supporting the idea that EMT is initiated at the tumour front to favour cancer progression and metastasis.

4.3.1.2. EpCAM

Short for epithelial cell adhesion molecule, EpCAM is another transmembrane glycoprotein expressed in epithelial cells and implicated in cellular junctions. Its coding sequence localized on human chromosome 2 encodes a 40 kDa protein expressed at the basolateral membrane of most epithelial tissues [198]. EpCAM carries out both a functional and signalling role. From a functional point of view, EpCAM forms homophilic intercellular adhesions (in proximity to those formed by E-Cadherin) through the interaction of its intracellular domain with cytoskeletal alpha-actin, ensuring epithelial integrity and cellular aggregation [199]. As for the signalling aspect of its functions, intramembrane proteolysis of EpCAM releases both its intracellular (EpICD) and ecto-domain (EpEX) that serve specific EMT-related functions; EpICD translocated to the cell nucleus where it serves a transcriptional regulator role, while EpEX may serve as a ligand of epidermal growth factor receptor (EGFR) (*figure 23*). The released EpICD has been shown to associate with other intracellular effectors like beta-catenin to form DNA binding complexes, inducing oncogenic gene transcription [200]. For example, has a role in the maintenance of stemness due to its binding to downstream effectors of the Wnt signalling pathway, well described for its implication in cell stemness maintenance and self-renewal, therefore modulating the expression of cell stemness-associated genes such as *c-MYC, SOX2, KL4 and NANOG* [201].

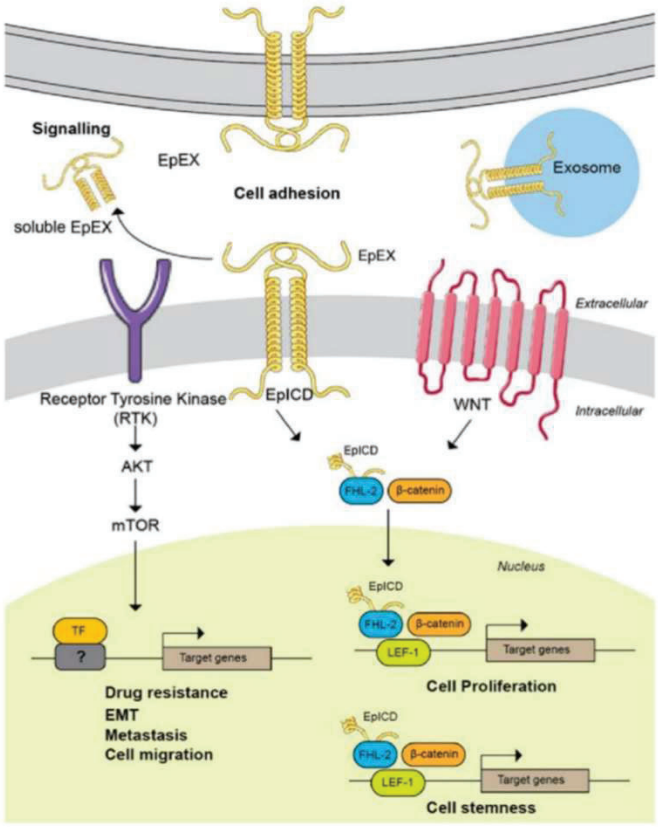

***Figure 23: EpCAM localization and modulation of its downstream targets in cancer** [202].*
The membrane bound EpCAM undergoes regulated intermembrane proteolysis that leads to the secretion of solubilized extracellular domain, EpEX and the liberation of cytoplasmic intracellular domain, EpICD. The cytoplasmic EpICD forms a transcriptional complex with WNT signalling

downstream effector to activate genes that are associated with cells proliferation and stemness maintenance. The solubilized EpEX acts as a ligand to stimulate the oncogenic signalling pathways like the PI3K/AKT/mTOR via its binding to receptor tyrosine kinase and activates the expression of genes involved in supporting cancer cells' growth and fitness. The membrane bound EpCAM can also function in promoting cell adhesion, as well as being expressed on the exosome surface to mediate cell-cell communication.

In EC, low EpCAM expression is linked with bad prognosis and is associated with advanced stages and metastasis [203]. In the endometrium, oestrogen signalling is a known stimulator of cell proliferation, and a factor implicated in the development of EC. Oestrogen receptor alpha expression has shown to be correlated with EpCAM expression through the stimulation of its promoter activity, as has EGF. Furthermore, EGF treatment has shown to induce the proteolysis of EpCAM and EpICD nuclear internalization which regulates the expression of junction proteins (upregulation of mesenchymal genes and down regulation of epithelial genes) [204]. Morphologically speaking, EpCAM proteolysis also renders EC cells with greater elasticity and lower adhesive function [204]. The loss of expression of membrane bound EpCAM in favour of its proteolysis is a major player in the promotion of EMT in EC. Additionally, some cases of Lynch syndrome-associated EC induced by the inactivation of MSH2 sue to EPCAM deletion have been reported [205].

4.3.2. Tumour cell cytoskeletal organization

4.3.2.1. Cytokeratins and vimentin

The migratory capacity of cells acquired with EMT is in part ensured by the remodelling of their intracellular network that is the cytoskeleton [206]. The latter is composed of multiple filaments that maintain its integrity: intermediate filaments which form a diverse family of molecules, microfilaments which are mainly actin, and microtubules which are primarily tubulin. Intermediate filaments are the main regulators of cell morphology, and their organization within cells is regulated by the nature of cell junctions and adhesion structures. Within the intermediate filament group, some components are common to all cell types, such as laminins which provide nuclear support in cells, while others are cell type specific like cytokeratin (CK) and vimentin [207]. Humans possess 54 functional *CK* genes distributed on chromosomes 12 and 17 [208]. They possess a highly conserved central domain known as the "rod" which is crucial for filament assembly, and vary in their "head" and "tail" domains. CKs are divided into 2 groups: type I acidic and type II basic that must be expressed together to form proper filaments also known as hetero-tetramers [209]. CKs are expressed in epithelial cells where they ensure cell to cell adhesion by associating with desmoplakin in desmosomes at the cell periphery, as well as proper basolateral localization of E-cadherin for the formation of adherens junctions presented previously. Additionally, CKs also maintains cell shape within tissues as they form a filamentous cytoplasmic network capable of mechano-sensing and resistant to mechanical stress. As cells undergo EMT, CK expression is downregulated, but doesn't necessarily disrupt the cell's cytoskeleton as vimentin is upregulated to take over some of CK's responsibilities [210]. Vimentin is a type III intermediate filament protein of 57 kDa encoded on the human chromosome 10 that shares structural and functional similarities with CKs. Vimentin is composed of a "head", a "rod" and a "tail" domain, but unlike CKs, vimentin assembles to form homo-tetramers [207,211]. Vimentin structure is dynamic in cells, constantly changing shape and cellular localization. Proteins can assemble into filaments that form an intracellular network that, like CKs, extends from the nuclear membrane to the plasma membrane where it (unlike CKs) directly binds integrin beta 3 or stay in a soluble form predominantly in the cell periphery. Through an increase in vimentin expression, mesenchymal cells are capable of modulating cellular elasticity in response to external forces, as well as mediating cellular motility [212]. Indeed, mesenchymal

migrating cells which possess a front-rear polarity (as opposed to the baso-apical polarity of epithelial cells), require the assembly and disassembly of actin filaments respectively at the front leading edge and at the rear of cells, a process which is regulated by Vimentin [213–215]. Vimentin also influenced tubulin function by enhancing the front-rear polarity of cells (*figure 24*).

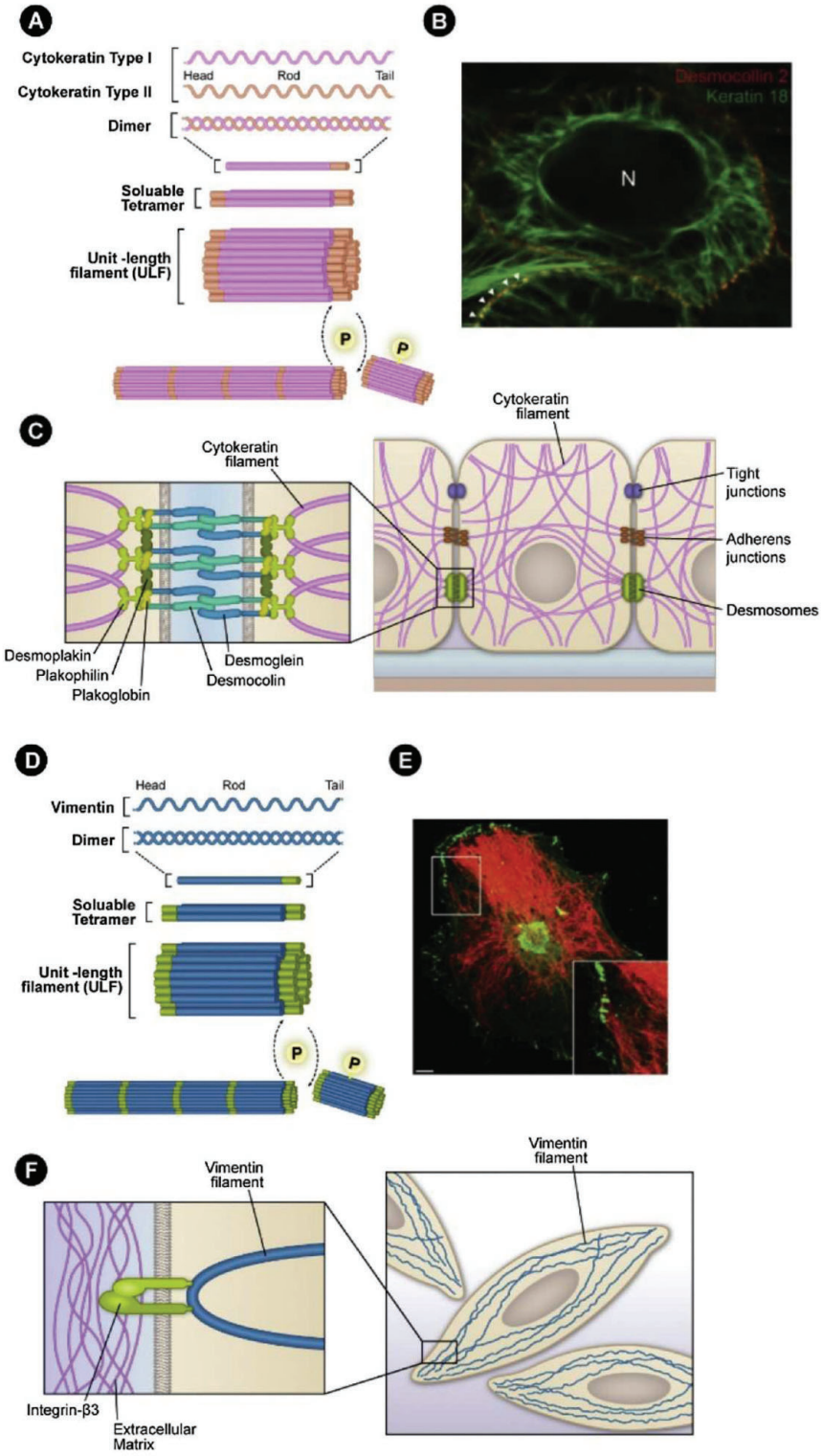

Figure 24: Filamentous assembly and localization of cytokeratin and vimentin *[216].*
A) *Cytokeratin assembly initiates with type I and type II heterodimer formation. The heterodimers combine to form soluble tetramers that interact to form ULFs made up of eight monomers. ULFs are then assembled in a phosphorylation-dependent manner into 10-nm filaments.* ***B)*** *Survey fluorescence micrograph of MDCK cells that express YFP-labeled desmocollin (red) and mRFP-labeled human*

cytokeratin 18 (green). Image reprinted with permission from Quinlan et al., J. Cell Sci*., 130, 3437-3445 (2017).* ***C)*** *Schematic of cytokeratin distribution in an epithelial cell with cell-cell adhesion processes. Zoomed inset shows the protein-protein interactions between cytokeratin filaments and desmosomes.* ***D)*** *Vimentin assembles as homodimers that combine to form soluble tetramers and then ULFs made up of eight monomers. ULFs are then assembled in a phosphorylation-dependent manner into filaments.* ***E)*** *Transformed human bone marrow endothelial cells stained for integrin β3 (green) and vimentin (red). Image reprinted with permission from Bhattacharya et al.,* J. Cell Sci*., 122, 1390-1400 (2009).* ***F)*** *Schematic of vimentin distribution in a mesenchymal cell. Zoomed inset indicates the vimentin filament interaction with β3 integrin that anchors the filament to the extracellular matrix.*

Throughout the menstrual cycle, the vimentin and CK expression profile varies in the uterine tissue. Vimentin expression is highest in the proliferative phase while CK is low, but the tables turn in the late secretory phase, where vimentin expression decreases and CK increases. During the early secretory phase however, CK and Vimentin are co-expressed, a phenomenon that is often observed in EC [217,218]. This overlapping expression of CK and vimentin in cancer cells is characteristic of EMT, providing cells with a higher level of tumourigenesis than fully mesenchymal or fully epithelial cells as tumour cells are able to collectively migrate and disseminate as clusters [219]. Loss of CK expression in cancers including EC has been linked to more aggressive tumours [220]. As for vimentin, in a variety of cancers including ovarian and breast cancer, high vimentin expression is correlated with poor clinical outcome, making it a molecular target in cancer therapy [221–223]. However, low vimentin expression in low-grade cases that is a prognostic factor of worst OS and PFS [224,225]. Indeed, ECs compared to ovarian cancers are vimentin positive, with a slightly higher expression in endometrioid type I EC than serous and clear cell type II EC [226,227].

4.3.2.2. Endocytic trafficking and HOOK1

The previously described alteration of epithelial cell morphology, structure and organization bring in to play multiple intracellular effectors and signalling pathways. For example, the loss of E-cadherin expression during EMT results from transcriptional regulation but also protein degradation through modulation of endocytosis. Indeed, normal epithelial cells use endocytosis of E-Cadherin to recycle it and form new adherens junctions, while cancer cells undergoing EMT steer the endocytic pathway towards lysosomal degradation [228]. Endocytic recycling or degradation involves various effectors that see their expression modulated in EMT, such as the hook microtubule tethering protein 1 (HOOK1) that plays a key role in endocytic recycling [229]. HOOK1 is a coiled coil cytosolic protein of 84 kDa encoded on chromosome 1 that attaches to microtubules through its N-terminal domain and to organelles with its C-terminal domain [230]. HOOK1 interacts with members of the Rab GTPase family involved in endocytosis, linking the endocytic vesicle trafficking to the microtubule cytoskeleton [231]. From a pathological standpoint, its expression is associated with PFS in primary tumours of luminal A subtype breast cancer, and its downregulation in cancer has been shown to promote carcinoma malignancy and EMT progression [232–234].

4.4. EMT associated signalling pathways.

A plethora of complex and interconnected signalling pathways are known to be implicated in the promotion of EMT and in the progression of EC, as recapitulated in *figure 25*. For the sake of clarity and brevity, the following paragraphs will focus on the MAPK, PI3K, mTOR and hypoxia signalling pathways often dysregulated in EC and subject to PTEN regulation. Indeed, the frequent mutation or deletion of PTEN in EC leads to the deregulation of these pathways. The latter will be mentioned and/or investigated to some extent in the “Results” and “Discussion” portions of the manuscript.

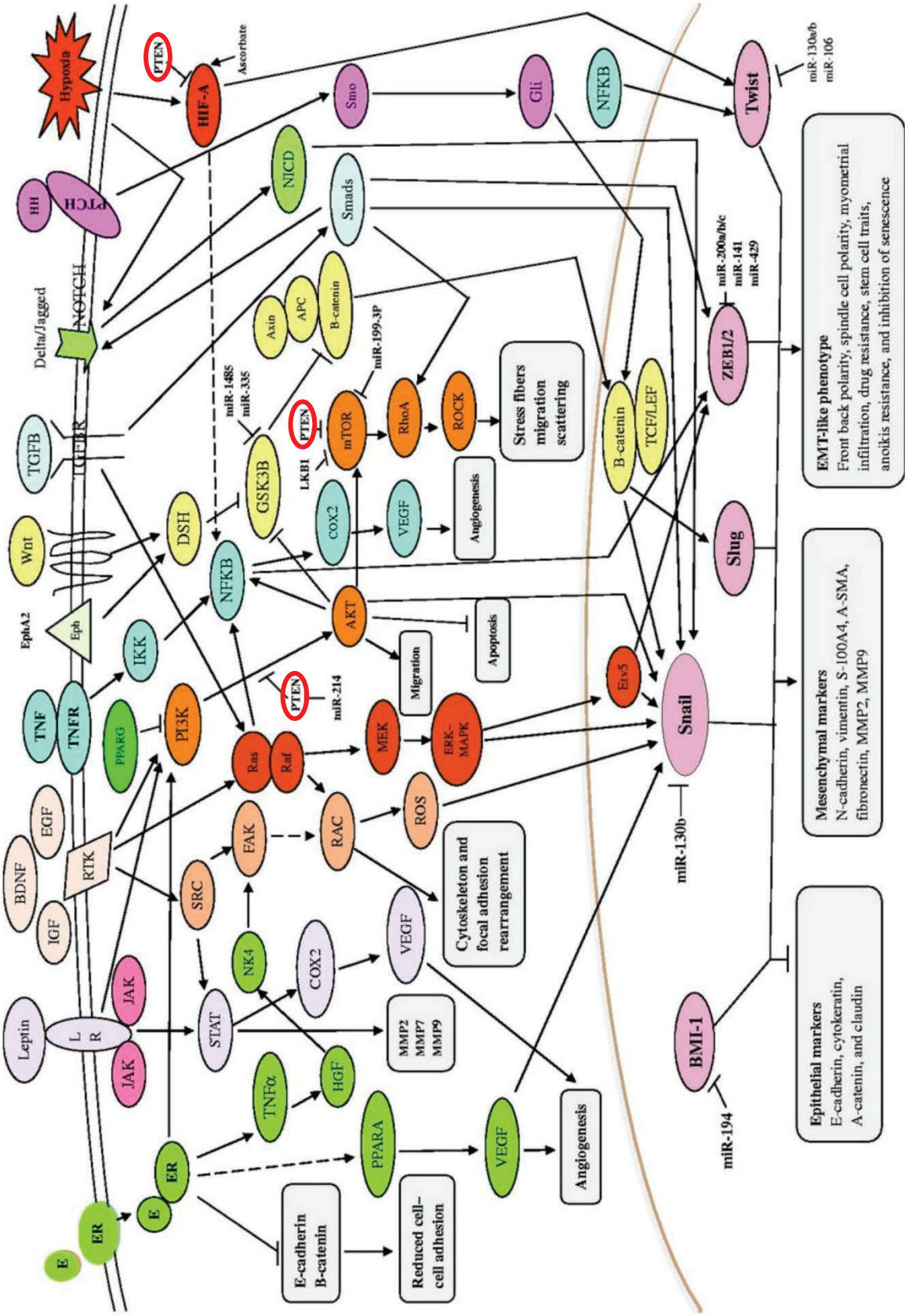

Figure 25: Schematic illustration of the major molecular pathways and transcription factors associated with the EMT program in EEC [235].

The main pathways (Leptin/LR, RTK, TNF/TNFR, Wnt, TGFB, Notch, Ptch, Hypoxia) associated with EMT and EC are described, and most are interconnected as shown by arrows, and regulated by PTEN

expression circled in red. These pathways all target the transcription of the transcription factors linked to the EMT, Snail, Slug, Zeb1/2 and Twist. Several microRNAs also regulate the EMT inducing signalling pathways and the core EMT regulators. Sharp arrows denote activation and blunt arrows indicate inhibition. Dotted lines indicate the presence of intermediate signalling molecules (not shown). End points of the EMT program are boxed.

4.4.1. PI3K/AKT

The PI3K/AKT pathway is a well described central mechanism in the initiation and progression of cancer through the promotion of cell growth and survival that also plays an important role in the control of EMT and stem cell features. As briefly presented in "Chapter 2", PI3K is a cytosolic kinase whose activity can be promoted through the binding of its regulatory subunit by membrane-bound receptor tyrosine kinases (RTKs) such as EGFRs or IGFRs which auto-phosphorylate tyrosine residues in their cytoplasmic region following the binding of exogenous growth factors and interleukins respectively. PI3K can also be activated through the endogenous binding of small Ras-related GTPases such as RAS to its catalytic subunit [236]. Negatively regulated by the phosphatase activity of PTEN, PI3K enables the accumulation of PIP3 at the plasma membrane which in turn recruits AKT that, when phosphorylated by also recruited PDK1, regulates downstream effectors including mammalian target of rapamycin (mTOR) [237], glycogen synthase kinase 3 (GSK3) [238]., bcl-2-associated death (BAD) [239], breast cancer type 1 susceptibility protein (BRCA1) [240].

As previously presented, aberrant activation of this pathway by mutation of the PI3K subunits and of its negative regulator PTEN are common genetic hallmarks of EC. However, additional factors can come to play in the aberrant upregulation of the PI3K/AKT pathway in EC. Indeed, EGFR, a RTK which acts upstream of PI3K and whose expression is negatively correlated with that of epithelial markers but positively with that of mesenchymal markers, is often observed to be overexpressed in EC [241,242]. EGFR has been shown to stimulate EMT in EC cell lines, as its activation led to an increase in EMT-TF Snail expression and concomitant decrease in E-cadherin expression [243]. Insulin growth factors (IGFs) have also an impact on EEC progression as the overexpression of their receptor has shown to activate the PI3K/AKT signalling pathway, leading to the induction of endometrial hyperplasia [244]. Additionally, insulin receptors' expression has also been observed at higher levels in advanced stages of EC, as was that of phosphorylated (and therefore activated) AKT [245,246]. In accordance with this, the targeting of this pathway in advanced or recurrent EC has shown potential in the improvement of patient PFS [247].

4.4.2. Mammalian target of rapamycin (mTOR)

Member of larger complexes called mTORC1 and mTORC2, its function is regulated either directly through PIP3 recruitment and activation of mTORC2, or indirectly regulated by AKT whose phosphorylation inhibits TSC2 and PRAS40, negative regulators of mTORC1 [248]. This complex is responsible for the phosphorylation and subsequent activation of substrates implicated in protein synthesis, cell cycle progression, invasion and metastasis [237]. As downstream effectors of the PI3K pathway, the deregulation of the latter and of PTEN have major consequences on mTOR whose activity is selectively upregulated in ECs as evidenced by nuclear expression of phosphorylated mTOR [249,250]. Furthermore, it has also been correlated with poor clinical outcome, as the expression of nuclear phosphorylated mTOR has been linked with tumour aggressiveness (as it is highly observed in poorly differentiated tumours, and those that show lymph node involvement), as well as shorter PFS and OS [251].

4.4.3. MAPK/ERK

The mitogen-activated protein kinase (MAPK) signalling, also known as Ras/RAF/MEK/ERK signalling pathway, is a key regulator of cell proliferation, differentiation, and survival. When activated by extracellular signals such as EGF binding to its TKR, Ras GTPase oncoproteins in their active GTP-bound state interact with multiple effectors such as RAF kinases, promoting their translocation to the plasma membrane where they are fully activated following dimerization and release of their auto-inhibition by phosphorylation [252,253]. Once activated, RAF kinases are able to phosphorylate and activate mitogen-activated protein kinase (MEK), whose predominant downstream target is extracellular-signal-regulated kinases (ERK) [254]. ERKs have multiple targets positively regulated by direct or indirect phosphorylation. They can translocate to the nucleus where they stimulate in response to cellular stress, growth factors, cytokines and matrix components nuclear substrates such as TFs implicated in transcriptional regulation, chromatin remodelling, cell cycle progress, motility and EMT [254,255].

ERK activity also modulates tissue structure through the downregulation of gap junction communications, induced by the phosphorylation of connexin 43 [256]. As a matter of fact, ERK activation induced global changes of mRNA expression during EMT, notably an upregulation of transcripts implicated in focal adhesions, cell-matrix interactions and organization of the ECM, all essential aspects of gained cell motility, a hallmark of EMT progression [257]. Additionally, it has been observed that the MAPK/ERK pathway has as strong link with oestrogen signalling and therefore hormone dependent gynaecological cancers like EC. Indeed, progesterone signalling mediation (through the expression of mitogen-inducible gene 6) suppressing that of oestrogen in the uterus has shown to negatively correlate with ERK phosphorylation during tumour progression [258]. Additionally, ERa expression following MAPK/ERK stimulation of RSK serves as a positive feedback loop for the activation of MAPK signalling, promoting the development of EC [259]. However, conflicting data regarding ERK in EC has been brought to light. Although phosphorylated MAPK is observed to be more highly expressed in EC tumours compared to non-neoplastic tissues and ERK inhibition in PTEN deficient mice demonstrating phosphorylated ERK expression in tumours has shown to suppress EC progression, Mizumoto et al. have highlighted a positive correlation between phosphorylated ERK expression in EC and favourable patient prognosis, a process Ras-independent, suggesting an alternative activation and signalling path for ERK [258,260,261]. Finally, KRAS mutation, often observed in cancer and associated with EMT progression, is also an indicator of early EC development: with a mutation frequency of 10 to 30%, it marks the transition of endometrial hyperplasia to EC and the invasive potential of low grade tumours [262–264].

4.4.4. Hypoxia

Hypoxia, or the deprivation of oxygen, is a major feature of solid tumours. Not only has it been associated with poor patient prognosis due to its induction of tumour progression through the promotion of neovascularization, cellular invasiveness, stem cell-like properties and even resistance to treatment, but it has also been linked to EMT progression [265]. Indeed, under hypoxic conditions, the TF hypoxia inducible factor 1 (HIF-1) is able to form stable interactions using its oxygen-regulated subunit HIF-1a with coactivators such as cAMP to activate the transcription of oncogenic EMT inducing factors [266]. Such effect is negatively regulated by the tumour suppressor PTEN, as shown in figure 25 [267]. According to the study of Feng et al., HIF-1 overexpression has been observed in 65% of primary ECs where it has been demonstrated to act upon EMT TF regulation.

Indeed, high HIF-1 expression has been correlated to high Twist levels, which in turn ensures the downregulation of the epithelial E-Cadherin protein [268].

4.5. EMT related EC resistance to therapy

In the case of EC, EMT status has been identified as a predictive factor of patient survival. Tanaka and colleagues corroborated previously observed mechanisms associated to EMT and cancer progression specifically in EC through the noted overexpression of EMT-TFs Snail and Slug along with the increased expression of CDH1 in cancer cells forming the invasive front of tumours [269]. They also highlighted the correlation between EMT-TF expression and lymph node metastasis, as well as patient overall survival (OS). EMT related therapy resistance in cancer is due in part to cancer cells' ability to increase the efflux of drugs, to slow down their speed of replication, and to avoid the induction of apoptosis. In addition to this, the modulation of their ECM also enabled them to survive despite treatment, as they are able to suppress the immune response by altering their immunosuppressive molecular expression and that of infiltrating tumour cells.

In EC, the observed EMT induction in cells responsible for cancer development and bad progression is also at the root of therapy resistance. For instance, oestrogen signalling cascades at the source of EC development and progression induce ZEB1 expression, described for its implication in EMT promotion [270]. This induced EMT may provide cancer cells with stem like properties, such as an enhanced ability to repair DNA damaged caused by chemo or radiotherapy [144]. ZEB1 is not the only EMT-TF implicated in therapy resistance as SNAIL and SLUG that are also a promoter of cancer resistance and recurrence to treatment are found to be overexpressed in EC study models [151,271,272]. EMT additionally impacts resistance to targeted therapies. Indeed, it has been observed that hormone receptor deregulation is associated with resistance to hormone therapy, and that disease-free survival of EC patients is correlated with hormone receptor expression [273,274]. EMT is implicated in such a resistance, as it is a down-regulator of progesterone receptor expression in endometrial lesions [275].

More generally, accumulating evidence indicates that conventional therapies often fail to eradicate carcinoma cells via activation of the EMT programme, thereby permitting CSC-mediated clinical relapse. The activation of the EMT programme is mainly due to micro-environmental changes during tumourigenesis with the critical contributions made by tumour resident and recruited cells stromal cells that can be categorized into three major classes: angiogenic vascular cells, infiltrating immune cells, and CAFs [276].

The rate of EC recurrence has been reported to be between 13 and 17% [277]. With a world incidence of approximately 420 000 individuals as estimated by the international agency for research on cancer (IARC) in 2020 [278], we can estimate that cancer relapse should concern more than 60 000 patients world-wide. Targeting EMT in ECs may provide a valuable solution for these cases, through direct effect on tumour development and metastasis, or through the re-sensitisation of cells to standard therapy options. The development of treatment strategies to directly target the EMT programme is also needed to prevent the malignant progression of all carcinomas, in order to improve therapeutic strategies and prevent resistance by any carcinoma cells.

Results

Project rationale & Results

When I started out my thesis, preliminary data concerning the biological cohort patient samples of the phase I clinical trial testing NP137 in advanced solid tumours had just brought to light through bulk and single cell RNA (scRNA) sequencing an effect on the epithelialization of metastatic lesions (as shown in the upcoming "Results" portion of the manuscript). This data was based on bulk and scRNA sequencing of sampled tissues using different Pan-Cancer EMT gene signatures "NES Hallmark EMT" and the one published in 2016 by Mak *et al.* (*annex 6 and 7*) [279]. Around the same time, Prof. Cedric Blanpain's research team in Brussels (Belgium) contacted us as they had observed a link between NTN1, UNC5B and EMT in their mouse model of spontaneous squamous skin carcinoma as well. As a result, a collaboration between our laboratories developed, leading to the submission and acceptance of two research articles for publication in Nature. In line with the data produced by Dr. Stephany Fiore during her thesis demonstrating the delivery of NTN1 by EVs in cancer cells, a second collaboration emerged with Dr. Darren Carpizo's research team from Rochester (USA) who has demonstrated the potential of NTN1 treated EVs to promote metastatic foci development in mice. Our collaborative work also enabled the submission of a research article for publication in Cell Reports.

As announced previously, the work I have produced over the course of my thesis has been partly published in three articles that I will briefly present below, along with my contribution to each one of them. Additional generated data regarding these articles to answer reviewer's interrogations does not appear in the papers, but will nonetheless be presented in the section "Supplementary Data".

Article synopsis & author contribution

- **Article 1: "Netrin 1 blockade inhibits tumour growth and EMT features in endometrial cancer."** – Published in Nature on the 2nd of August 2023.

Authors : Philippe A. Cassier, Raul Navaridas*, **Melanie Bellina***, Nicolas Rama*, Benjamin Ducarouge*, Hector Hernandez-Vargas*, Jean-Pierre Delord*, Justine Lengrand, Andrea Paradisi, Laurent Fattet, Gwenaële Garin, Hanane Gheit, Cecile Dalban, Levgenia Pastushenko, David Neves, Remy Jelin, Nicolas Gadot, Nicolas Braissand, Sophie Léon, Cyril Degletagne, Xavier Matias-Guiu, Mojgan Devouassoux-Shisheboran, Eliane Mery-Lamarche, Justine Allard, Egor Zindy, Christine Decaestecker, Isabelle Salmon, David Perol, Xavi Dolcet, Isabelle Ray-Coquard, Cédric Blanpain, Agnès Bernet and Patrick Mehlen.

This article is a result of a collaborative project with the research team of Dr. Javier Dolcet (Institut de Recerca Biomedica, Lleida, Spain) who has gracefully welcomed me into their laboratory to carry out experiments with a spontaneous EC mouse model they have developed, to test the effect of NP137 alone and in combination with standard chemotherapy agents on EC development. My contribution resides in figures1, 3, extended data figure 2 and extended data figure 7.

- **Article 2: "Pharmacological targeting of netrin-1 inhibits EMT in cancer."** – Published in Nature on the 2nd of August 2023.

Authors: Justine Lengrand, Ievgenia Pastushenko, Sebastiaan Vanuytven, Yura Song, David Venet, Rahul M. Sarate, **Melanie Bellina**, Virginie Moers, Alice Boinet, Alejandro Sifrim, Nicolas Rama, Benjamin Ducarouge, Jens Van Herck, Christine Dubois, Samuel Scozzaro, Sophie Lemaire, Sarah Gieskes, Sophie Bonni, Amandine Collin, Nicolas Braissand, Justine Allard, Egor Zindy, Christine Decaestecker, Christos Sotiriou, Isabelle Salmon, Patrick Mehlen, Thierry Voet, Agnès Bernet, Cédric Blanpain.

This article is a result of the collaborative project with the research team of Prof. Cedric Blanpain (Laboratory of stem cells and cancer, Brussels, Belgium). It portrays the effects of NTN1 targeting with NP137 on EMT progression in a spontaneous EMT mouse model of skin squamous cell carcinoma. My contribution resides in experiments regarding the human EC cell lines, including xenografting experiments, invasion, migration, cell death and cell proliferation assays as presented in extended data 7.

- **Article 3: "Netrin-1 Mediated Feedforward Mechanism Promotes Pancreatic Cancer Liver Metastasis through Hepatic Stellate Cell Activation, Retinoid, and ELF3 Signalling"** – Submitted to Cell Reports in July of 2023.

Authors: Crissy Dudgeon, Anthony Casabianca, Charline Ogier, Chris Harris, **Mélanie Bellina**, Stephany Fiore, Agnes Bernet, Benjamin Ducarouge, David Goldschneider, Xiaoyang Su, Jason Pitarresi, Aram Hezel, Subhajyoti De, Wade Narrow, Fady Soliman, Cory Shields, Debora Barbosa Vendramini-Costa, Orjola Prela, Lan Wang, Igor Astsaturov, Patrick Mehlen, and Darren R. Carpizo.

As part of a complete collaboration with the research team of Dr. Darren Carpizo in pancreatic cancer (University of Rochester Medical Center, Rochester, USA), I carried out the experiments to detect netrin 1 expression at the surface of extracellular vesicles to promote pancreatic cancer liver metastasis as can be seen in figure 5.

Article

Netrin-1 blockade inhibits tumour growth and EMT features in endometrial cancer

https://doi.org/10.1038/s41586-023-06367-z

Received: 22 April 2022

Accepted: 23 June 2023

Published online: 02 August 2023

Open access

Check for updates

Philippe A. Cassier[1], Raul Navaridas[2,15], Melanie Bellina[3,4,15], Nicolas Rama[3,15], Benjamin Ducarouge[4,15], Hector Hernandez-Vargas[5,15], Jean-Pierre Delord[6,15], Justine Lengrand[3,4,7], Andrea Paradisi[3], Laurent Fattet[3], Gwenaële Garin[1], Hanane Gheit[1], Cecile Dalban[1], Ievgenia Pastushenko[7], David Neves[3], Remy Jelin[3,4], Nicolas Gadot[8], Nicolas Braissand[3,4], Sophie Léon[8], Cyril Degletagne[8], Xavier Matias-Guiu[2], Mojgan Devouassoux-Shisheboran[9], Eliane Mery-Lamarche[10], Justine Allard[11], Egor Zindy[11], Christine Decaestecker[11,12], Isabelle Salmon[11,13,14], David Perol[1], Xavi Dolcet[2], Isabelle Ray-Coquard[1,16], Cédric Blanpain[7,16], Agnès Bernet[3,4,16]✉ & Patrick Mehlen[3,4,16]✉

Netrin-1 is upregulated in cancers as a protumoural mechanism[1]. Here we describe netrin-1 upregulation in a majority of human endometrial carcinomas (ECs) and demonstrate that netrin-1 blockade, using an anti-netrin-1 antibody (NP137), is effective in reduction of tumour progression in an EC mouse model. We next examined the efficacy of NP137, as a first-in-class single agent, in a Phase I trial comprising 14 patients with advanced EC. As best response we observed 8 stable disease (8 out of 14, 57.1%) and 1 objective response as RECIST v.1.1 (partial response, 1 out of 14 (7.1%), 51.16% reduction in target lesions at 6 weeks and up to 54.65% reduction during the following 6 months). To evaluate the NP137 mechanism of action, mouse tumour gene profiling was performed, and we observed, in addition to cell death induction, that NP137 inhibited epithelial-to-mesenchymal transition (EMT). By performing bulk RNA sequencing (RNA-seq), spatial transcriptomics and single-cell RNA-seq on paired pre- and on-treatment biopsies from patients with EC from the NP137 trial, we noted a net reduction in tumour EMT. This was associated with changes in immune infiltrate and increased interactions between cancer cells and the tumour microenvironment. Given the importance of EMT in resistance to current standards of care[2], we show in the EC mouse model that a combination of NP137 with carboplatin-paclitaxel outperformed carboplatin-paclitaxel alone. Our results identify netrin-1 blockade as a clinical strategy triggering both tumour debulking and EMT inhibition, thus potentially alleviating resistance to standard treatments.

Netrin-1 is an embryonic, secreted, laminin-related glycoprotein that plays key roles in neuronal navigation, angiogenesis and cell survival[1,3,4]. Netrin-1, which is expressed mainly during embryonic development, has been shown to be re-expressed by both cancer cells and the tumour microenvironment in a large proportion of human neoplasms[1,5]. Specifically this has been shown to occur in inflammation-associated colorectal cancer[6,7], metastatic breast cancer[8], lung cancer[9], neuroblastoma[10], lymphoma[11] and melanoma[12]. In preclinical models mimicking these diseases, interference between netrin-1 and its receptors was sufficient to trigger cancer cell death and induce tumour growth inhibition[1,5,11,12]. Based on these findings, a monoclonal antibody (mAb) neutralizing netrin-1 and blocking the netrin-1–UNC5B interaction, dubbed NP137, was developed[13] and underwent preliminary safety and efficacy assessment in patients with advanced solid tumours in a Phase 1 trial (NCT02977195). Owing to some objective responses observed in gynaecological cases during the dose-escalation phase, the extension phase of the trial was enriched in patients carrying endometrial tumours. A specific cohort has also been established, with mandatory biopsies

[1]Centre Léon Bérard, Departement de Recherche Clinique, Centre de recherche en cancérologie de Lyon INSERM U1052-CNRS UMR5286, Université de Lyon, Université Claude Bernard Lyon1, Centre Léon Bérard, Lyon, France. [2]Basic Medical Sciences Department Oncological Pathology Group, Institut de Recerca Biomèdica de Lleida, Universidad de Lleida, Lleida, Spain. [3]Apoptosis, Cancer and Development Laboratory – Equipe labellisée 'La Ligue', LabEx DEVweCAN, Institut PLAsCAN, Centre de Recherche en Cancérologie de Lyon INSERM U1052-CNRS UMR5286, Université de Lyon, Université Claude Bernard Lyon1, Centre Léon Bérard, Lyon, France. [4]Netris Pharma, Lyon, France. [5]Centre de Recherche en Cancérologie de Lyon, INSERM U1052-CNRS UMR 5286, Centre Léon Bérard, Claude Bernard Lyon 1 University, Lyon, France. [6]Institut Claudius Regaud, IUCT-Oncopole, Toulouse, France. [7]Laboratory of Stem Cells and Cancer, WEL Research Institute, Université Libre de Bruxelles, Brussels, Belgium. [8]CRCL Core facilities, Centre de Recherche en Cancérologie de Lyon (CRCL) INSERM U1052-CNRS UMR5286, Université de Lyon, Université Claude Bernard Lyon1, Centre Léon Bérard, Lyon, France. [9]Hospices Civils de Lyon, Department of Pathology, Lyon, France. [10]Department of Pathology, IUCT-Oncopole, Toulouse, France. [11]DIAPath, Center for microscopy and molecular Imaging, Université Libre de Bruxelles, Gosselies, Belgium. [12]Laboratory of Image Synthesis and Analysis, Ecole Polytechnique-Université libre de Bruxelles, Brussels, Belgium. [13]Departement of Pathology, Erasme University Hospital, Université Libre de Bruxelles, Brussels, Belgium. [14]Centre Universitaire Inter Régional d'Expertise en Anatomie pathologique Hospitalière (CurePath), Jumet, Belgium. [15]These authors contributed equally: Raul Navaridas, Melanie Bellina, Nicolas Rama, Benjamin Ducarouge, Hector Hernandez-Vargas, Jean-Pierre Delord. [16]These authors jointly supervised this work: Isabelle Ray-Coquard, Cédric Blanpain, Agnès Bernet, Patrick Mehlen. ✉e-mail: agnes.bernet@lyon.unicancer.fr; patrick.mehlen@lyon.unicancer.fr

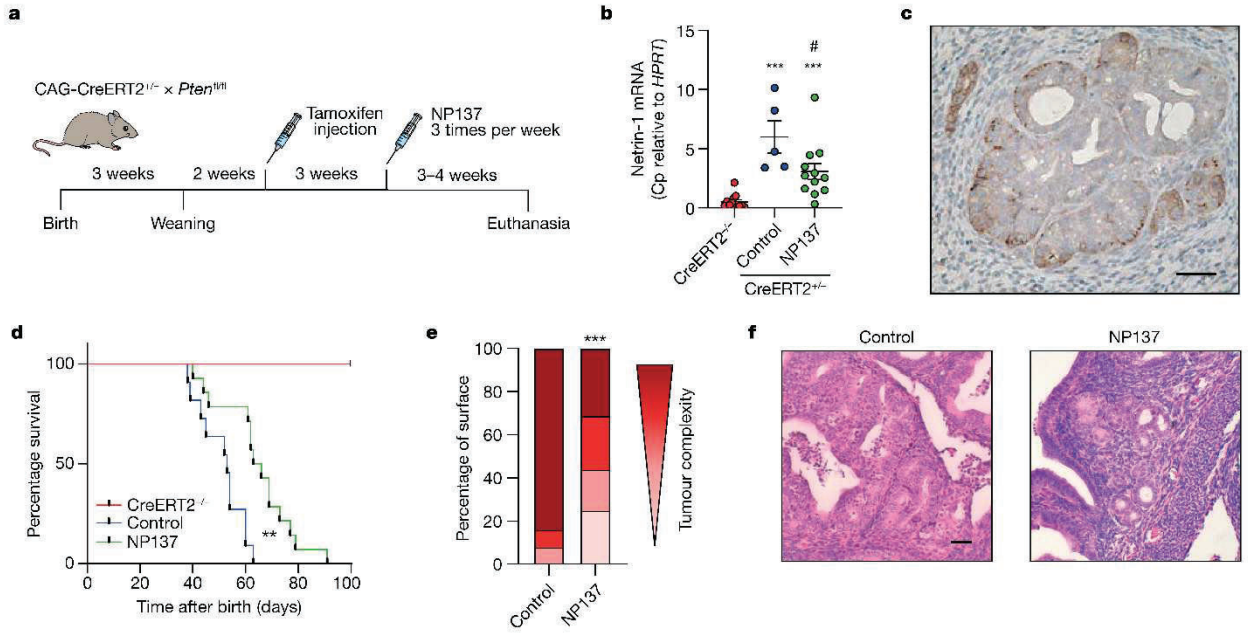

Fig. 1 | Netrin-1 blockade inhibits endometrial adenocarcinoma progression in preclinical models. a, Diagram showing the experimental strategy used to induce *Pten* deletion into CAG-CreERT2$^{+/-}$ *Pten* f/f mice using tamoxifen injection and either treatment with NP137 or control. Mice were euthanized if they experienced breathing difficulties[15]. **b**, Relative messenger RNA expression of netrin-1 as defined by RT–qPCR in the endometrium of CreERT2$^{-/-}$ animals ($n = 12$) and in tumours induced following *Pten* deletion (tamoxifen injection) in CreERT2$^{+/-}$ *Pten* f/f mice intraperitoneally treated with NP137 (10 mg kg^{-1}) ($n = 12$) and in control ($n = 5$). Bars are mean ± s.e.m.; data normalized to *HPRT* gene; Cp, crossing point. ***$P < 0.001$ CreERT2$^{+/-}$ versus CreERT2$^{-/-}$ and $^{\#}P = 0.0284$ NP137 versus control by Mann–Whitney two-sided test. **c**, Representative netrin-1 IHC analysis of EC in CreERT2$^{+/-}$ *Pten* f/f mouse following 6 weeks of tamoxifen injection. Scale bar, 100 µm. **d**, Kaplan–Meier curves indicating percentage survival for normal mice (CreERT2$^{-/-}$, red, $n = 8$), *Pten*-deleted mice treated with NP137 (green, $n = 14$) and control (blue, $n = 11$). **$P < 0.01$ by Mantel–Cox test. **e**, Quantification by pathologists of endometrial lesions, presented by tumour complexity (progressively darker colour from hyperplasia through mild, then moderate, endometrial intraepithelial neoplasia to adenocarcinoma) between control mice ($n = 12$) and those treated with NP137 mAb ($n = 16$). ***$P < 0.001$ by chi-squared test and Fisher's two-sided exact test. **f**, Representative images of H&E staining of uterus from mice killed at week 6 of tamoxifen injection, those treated with NP137 and control. Scale bar, 50 µm.

before and after treatment, for translational research. Preliminary data from this trial were disclosed at the 2019 ESMO meeting[14], but the trial is still ongoing, with patients continuing to receive treatment, and results will be fully reported after final analysis. In this article we report translational data generated in parallel with the Phase 1 study including patients with endometrial cancer and provide a series of preclinical and biopsy data demonstrating that NP137 not only reduces tumour cell number but also triggers inhibition of epithelial-to-mesenchymal transition (EMT) features, which ultimately increases tumour sensitivity to chemotherapy.

Netrin-1 and endometrial adenocarcinomas

We analysed netrin-1 expression by quantitative PCR with reverse transcription (RT–qPCR) in a cohort of 72 human endometrial tumours (Supplementary Table 1a). As shown in Extended Data Fig. 1a, netrin-1 is significantly upregulated in endometrial adenocarcinoma (EC) without specific change in grades or subtypes (Extended Data Fig. 1b,c). Its main receptor, UNC5B, was also found to be expressed more in tumour tissues than in normal endometrium (Extended Data Fig. 1a–c) while DCC, another netrin-1 receptor, is expressed neither in normal endometrium nor endometrial cancer. Netrin-1 (and UNC5B) positivity was monitored in most endometrial tumours by immunohistochemistry (IHC) (Extended Data Fig. 1d).

We thus moved to a preclinical model recapitulating the development of EC, using the genetically engineered, temporally controlled *Pten* f/f-deleted mouse model (namely, the tamoxifen-inducible CAG-CreERT$^{+/-}$ promoter), which has been shown to develop EC in situ rapidly, as well as thyroid hyperplasia[15] (Fig. 1a). We thus treated control and *Pten*-deleted mice for 3–4 weeks with NP137 (10 mg kg^{-1}, three times per week) and analysed netrin-1 expression and tumour progression. As shown in Fig. 1b,c, netrin-1 was upregulated in mouse tumours following deletion of *Pten*, and this upregulation was decreased following NP137 treatment. Of interest, NP137 was associated with decreased development of endometrial tumours (Extended Data Fig. 2a) and increased survival (Fig. 1d; note that there was no extension of the study after 7 weeks following *Pten* deletion because most mice showed breathing difficulties or other ailments due to development of thyroid tumours). Pathologists observed a decreased number of cancer cells following NP137 treatment (Fig. 1e) and healthier endometrial tissue (Fig. 1f). Similarly, antitumour activity was also observed in the thyroids of mice treated with NP137 (Extended Data Fig. 2b–e). These results indicate that targeting netrin-1 in EC inhibits tumour progression.

Objective response in a patient with EC

Based on previous results suggesting that netrin-1 blockade is a viable therapeutic strategy in cancer, a netrin-1-blocking antibody was developed for clinical use[13] and is undergoing Phase I/II evaluation. We extracted efficacy data for 14 patients with EC from the ongoing Phase 1 study (Supplementary Table 1b,c). In this study, NP137 was administered once every 2 weeks (Q2W) as monotherapy until clinical/radiological progression. As shown in Fig. 2a and Extended Data

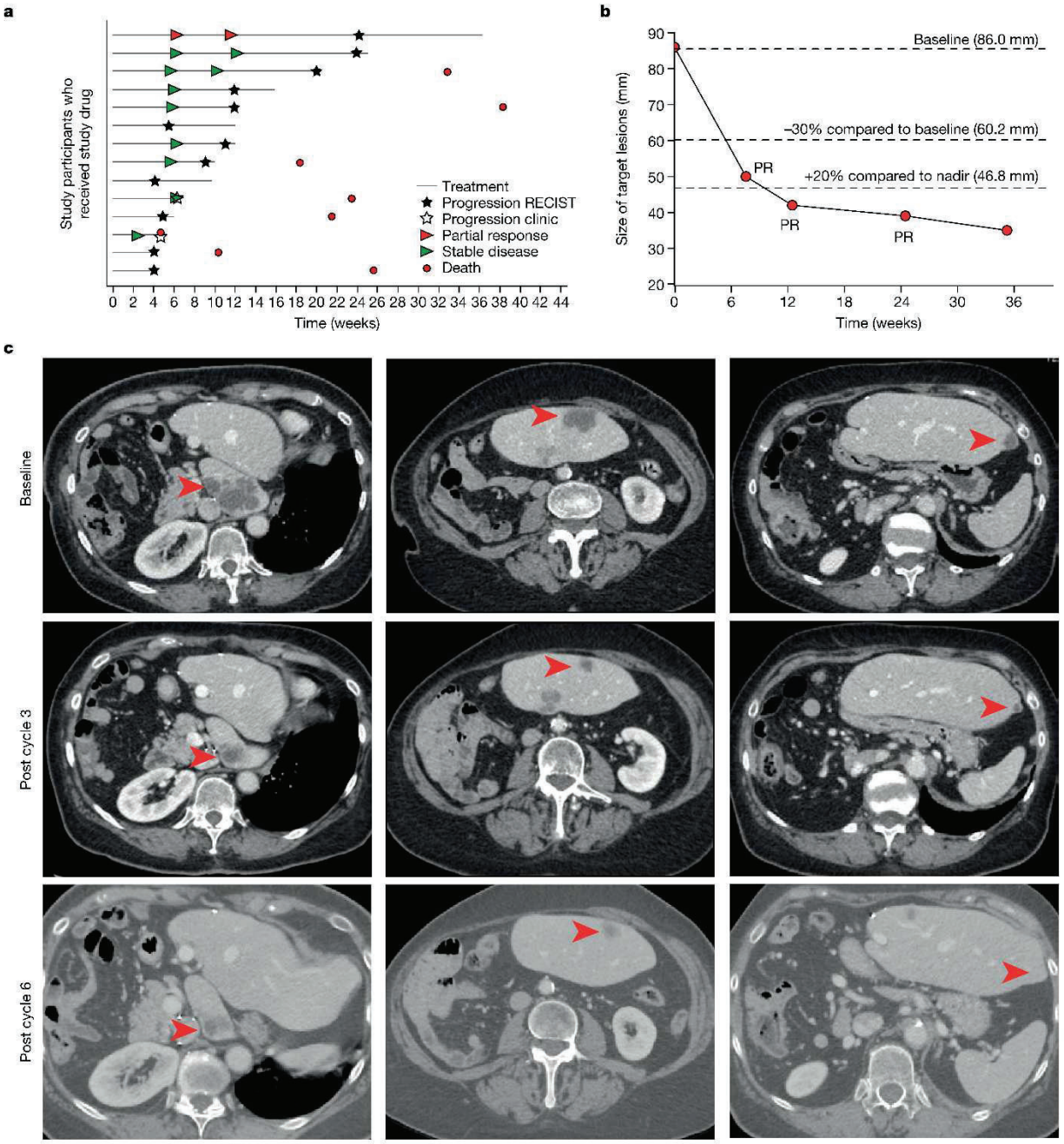

Fig. 2 | Clinical response in patients with EC following NP137 treatment. **a**–**c**, Fourteen patients (median age, 68.3 years (44.7–80.6); ECOG performance status 0, $n = 5$; ECOG performance status 1, $n = 9$) who had advanced or metastatic stage IV EC and were previously treated with a median of three (2.0–6.0) systemic treatment lines before inclusion were treated with NP137 (14 mg kg^{-1}, $n = 11$ patients or 20 mg kg^{-1}, $n = 3$ patients) with a median of 5.5 injections (2.0–17.0). **a**, Each bar represents one patient. Best responses to treatment are presented based on investigator review (according to protocol). Filled stars, radiological progression as per RECIST v.1.1; hollow stars, clinical progression as per investigator assessment; red arrowheads, partial response according to RECIST v.1.1; green arrowheads, stable disease according to RECIST v.1.1; red circles, death. **b**, Graph presenting the size evolution of target lesions (sum of two liver target lesions) from patient no. 02-004 treated intravenously with 14 mg kg^{-1} NP137 Q2W. Tumour response was assessed as partial response (PR) at 6 weeks and then at 3, 6 and 9 months; −30% reduction in target lesions size compared to baseline indicates partial response according to RECIST v.1.1. A dotted line showing the 20% increase in target lesions size compared to the nadir (minimum lesions size upon NP137 treatment) is also indicated. **c**, Abdominal transversal scans presenting liver metastasis at baseline, C3D1 (post cycle 3) and C6D1 (post cycle 6) from patient no. 02-004. Red arrowheads indicate lesions of interest.

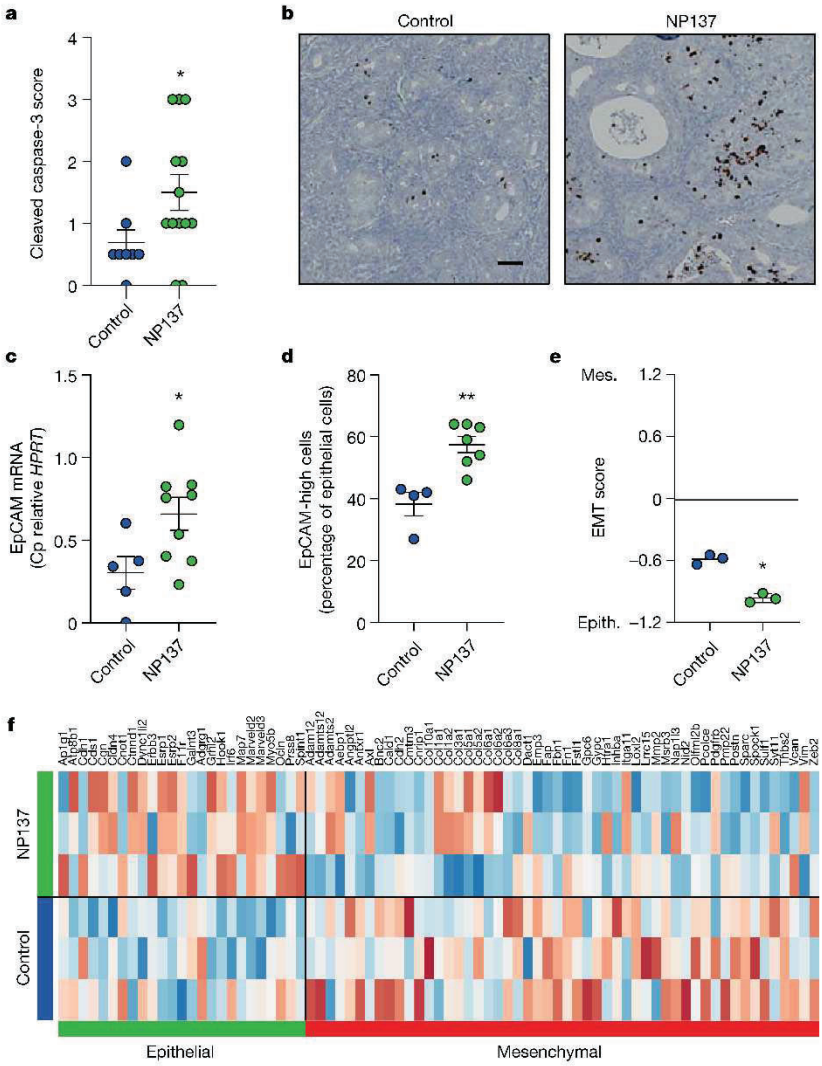

Fig. 3 | Netrin-1 blockade triggers apoptosis and EMT inhibition in a preclinical mouse model. a, Quantification of cell death using cleaved caspase-3 IHC in control ($n = 8$) and NP137 ($n = 13$)-treated tumours of CreERT2$^{+/-}$*Pten* f/f mice. Bars are mean ± s.e.m.; $^{*}P = 0.0389$ by Mann–Whitney two-sided test. **b**, Representative images of cleaved caspase-3 staining of **a**. Scale bar, 100 µm. **c**, Relative mRNA expression of EpCAM epithelial marker by RT–qPCR in mouse tumours, control ($n = 5$) and NP137 ($n = 9$). Bars are mean ± s.e.m., data normalized to *HPRT* gene; $^{*}P = 0.032$ by Mann–Whitney two-sided test. **d**, Percentage of EpCAM high-expressing cells in control tumours ($n = 4$) versus NP137-treated ($n = 7$) as assessed by IHC. Bars are mean ± s.e.m.; $^{**}P = 0.0061$ by Mann–Whitney two-sided test. **e**, EMT score (mouse orthologues of epithelial (epith.) or mesenchymal (mes.) signature from ref. 20) analysis derived from RNA-seq data, between control ($n = 3$) and NP137 ($n = 3$)-treated mice. Bars are mean ± s.e.m.; $^{*}P = 0.05$ by Mann–Whitney one-sided test. **f**, Heatmap derived from RNA-seq data showing expression of EMT genes; control ($n = 3$) and NP137 ($n = 3$). Note that epithelial genes were upregulated under NP137-treated condition whereas mesenchymal genes were downregulated.

Table 1a, no dose-limiting toxicity was observed and more than half of the patients (8 out of 14) had disease control (stable disease) as best response (best overall response, stable disease, 57.1%). In addition, a 74-year-old female patient with advanced EC had a RECIST1.1-defined partial response (patient no. 02-004; Supplementary Table 1b). The original diagnosis for this patient showed an endometrioid origin, a microsatellite stable phenotype, and expression of CK7, PAX8 and oestrogen receptors but no expression of CK20 or progesterone receptor. Before administration of NP137 she had received multiple therapeutic attempts, including adjuvant radiotherapy and carboplatin-paclitaxel followed by lurbinectedin as first-line treatment for metastatic disease, and a second attempt with carboplatin-paclitaxel, but had progression of liver metastases despite these therapeutics.

A positron emission tomography–computed tomography (PET–CT) scan, performed at inclusion, confirmed intense uptake of fluorodeoxyglucose (before C1D1). She received 14 mg kg^{-1} intravenous NP137 Q2W and underwent a PET–CT scan at 6 weeks (that is, post cycle 3 of NP137), showing partial response according to RECIST v.1.1 with a 51% reduction in target liver lesions (Fig. 2b,c and Extended Data Table 1b). Partial response was confirmed on PET–CT scan at 3 months (Fig. 2c) and then again at 6 months, when size reduction of target lesions reached 55% (Extended Data Table 1b). This patient eventually experienced disease progression after 17 cycles of NP137 and went on to receive additional therapy, including letrozole A, immunotherapy and tamoxifen, without experiencing additional objective response.

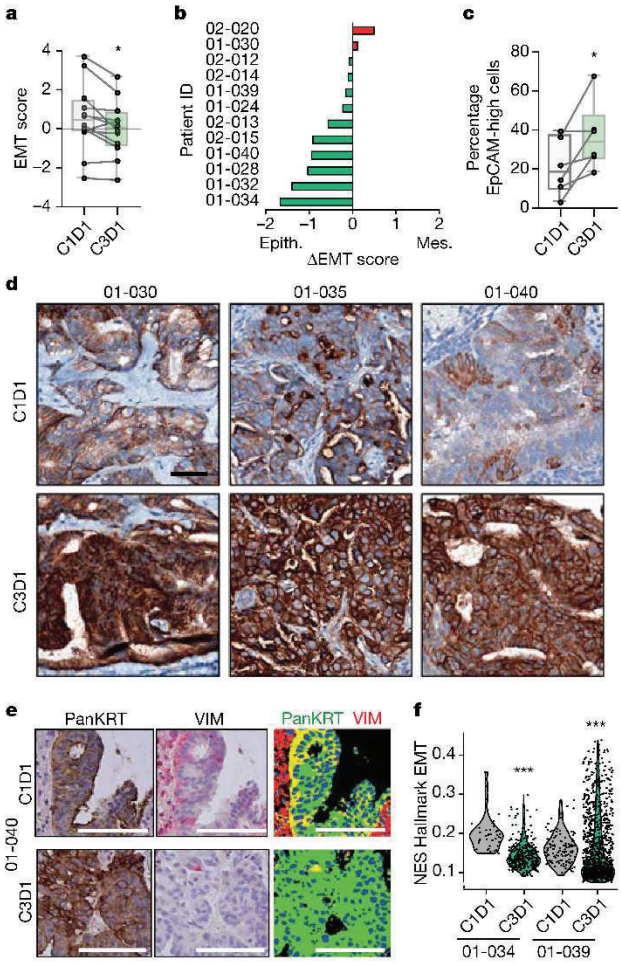

Fig. 4 | NP137 treatment inhibits EMT in patients with EC. a, Diagram showing EMT score calculated with Mak's signature[20] from RNA-seq of biopsies before (C1D1) and following two cycles of NP137 (C3D1) treatment ($n = 12$). Boxplots represent mean (25th–75th), whiskers range from minimum to maximum values and paired samples are identified on single-value representation; *$P = 0.0161$ by two-sided t-test. **b**, Swimmer plots showing individual evolution of EMT score for each patient; ΔEMT is the EMT score at C3D1 minus that at C1D1; ΔEMT < 0 means evolution towards epithelial phenotype (green) and >0 towards mesenchymal (red). **c**, Percentage of EpCAM high-expressing cells in C1D1 versus C3D1 biopsy samples as identified by IHC; *$P = 0.0313$ by Wilcoxon two-sided test ($n = 6$ patients). Boxplots represent mean (25th–75th), whiskers range from minimum to maximum values and paired samples are identified on single-value representation. **d**, Representative IHC of EpCAM in tumours in C1D1 and C3D1 for patient nos. 01-030, 01-035 and 01-040. Scale bar, 50 µm. **e**, Representative images of pancytokeratin (PanKRT) and vimentin (VIM) expression (colocalization of pancytokeratin (green) and vimentin (red) in the merged picture, right) in primary endometrial adenocarcinoma from patient no. 01-040 before and after NP137 treatment. Scale bars, 50 µm. Quantifications were performed on the full slides and similar results were observed for patient nos. 01-030 and 01-034. **f**, Analysis of tumour cell compartment in patient nos. 01-034 and 01-039 by Visium spatial gene expression. Violin plot of EMT UCell normalized enrichment score (NES) from tumoural histologically selected Visium spot between cells of C1D1 and C3D1 biopsy. ***$P < 0.01$ by Mann–Whitney two-sided test.

Netrin-1 blockade inhibits tumour EMT

To gain insight into the underlying mechanisms that link netrin-1 blockade to tumour growth inhibition we first analysed, based on the hypothesized mode of action of netrin-1 blockade, whether tumour growth inhibition was associated with tumour cell death in *Pten* f/f tumours treated with NP137. As shown in Fig. 3a,b, NP137 increased cancer apoptosis as measured by IHC on active caspase-3. We next performed RNA-seq of *Pten* f/f mouse tumours treated with NP137 versus untreated. Among the pathways/genes modulated following NP137 administration, we noted a decrease in EMT-related genes following treatment. Several in vitro studies have suggested the involvement of netrin-1 in EMT[16–19], often associated with the PI3K/AKT pathway, which is frequently altered in endometrial cancer[17,18]. We then investigated whether NP137 might impact tumour EMT in the *Pten* f/f mouse model. We first assessed EpCAM epithelial marker expression in control versus NP137-treated tumours, and observed a statistically significant increase of this epithelial marker in NP137-treated tumours (Fig. 3c,d). To gain a more general view of tumour gene expression we then utilized a commonly used pancancer EMT signature[20] that can be employed to determine EMT score[20]. We observed that treatment with NP137 decreased EMT score (Fig. 3e), associated with decreased expression of mesenchymal genes and increased expression of epithelial genes (Fig. 3f). These preclinical data support the view that netrin-1 blockade has a dual action on tumour cells: triggering of cancer cell death and inhibition of EMT features, rendering overall NP137-treated tumours more epithelial.

We next determined whether the inhibition of EMT features observed in the preclinical models also occurs in patients treated with NP137. In the NP137 Phase 1 trial, among patients with EC described above, paired biopsies were collected at inclusion (C1D1) and after 1 month of treatment with the anti-netrin-1 compound (that is, just before the third infusion of NP137 (C3D1)). Bulk RNA-seq was successfully performed on 12 paired pre- and on-treatment biopsies (Supplementary Table 1b) and, as shown in Fig. 4a,b, two injections of NP137 were found sufficient to trigger a significant decrease in the pancancer EMT score described above, indicating an overall more epithelial phenotype of the tumour in patients after 1 month of treatment with NP137. The shift toward a more epithelial phenotype was confirmed by increased EpCAM IHC staining in tumour samples from patients treated with NP137 (Fig. 4c,d). We also observed a decrease in the proportion of tumour cells coexpressing pancytokeratin and vimentin (Fig. 4e).

Of interest, when analysing changes in EMT score between baseline and on-treatment biopsies we observed that samples from patients who had disease progression as their best response on NP137 (progressive disease at first evaluation at 6 weeks) failed to show variation in EMT score. Conversely, there was a statistically significant decrease in EMT score in samples from patients who had disease control (at least stable disease at 6 weeks; Extended Data Fig. 3a).

To demonstrate more formally that the bulk change in EMT score seen with NP137 treatment in patients was occurring specifically in cancer cells, as a first approach we used the 10x Visium spatial gene expression system compatible with formalin-fixed, paraffin-embedded (FFPE) tissues. Two pairs of C1D1/C3D1 FFPE sections from two patients with EC were analysed (Extended Data Fig. 3b,c) and spatial gene expression profiling was performed in pathologist-selected regions of interest where only cancer cells could be identified by haematoxylin and eosin (H&E) staining. In both cases, EMT score was strongly decreased at C3D1 compared with C1D1 (Fig. 4f). Thus in patients, after 1 month of treatment with NP137, remaining cancer cells showed decreased EMT features compared with their pretreatment status.

To extend these studies to the single-cell level we performed 3′ single-cell RNA-seq (10x Genomics Next GEM 3′ kit) directly on fresh biopsies obtained at inclusion (C1D1, 9,216 cells) in the NP137 trial and after 1 month of treatment (C3D1, 7,159 cells) from a patient with advanced EC (patient no. 01-040; Supplementary Table 1b and Fig. 5a).

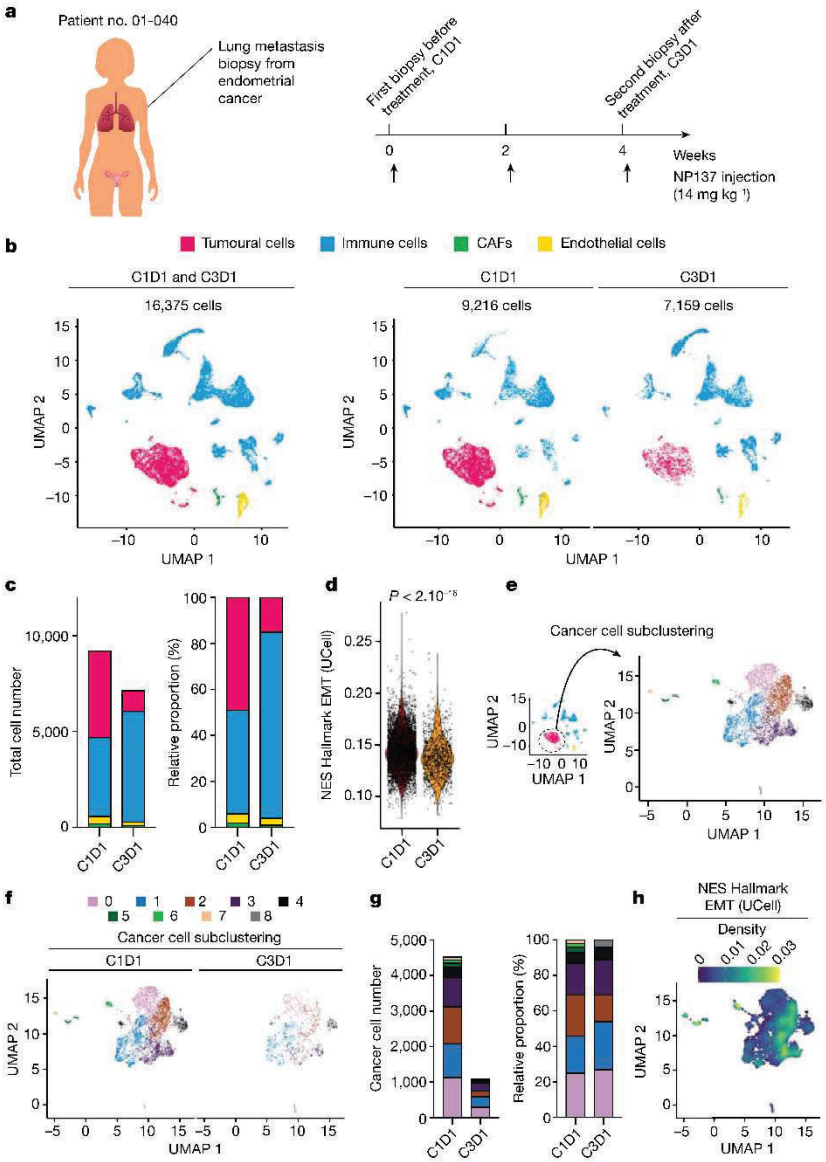

Fig. 5 | Single-cell RNA-seq analysis pre and post biopsy of a patient with EC. **a**, Illustration of patient no. 01-040 with two lung metastasis biopsies—one before treatment (C1D1), and one after two cycles of NP137 treatment (C3D1). **b**, Uniform manifold approximation and projection (UMAP) plot of 16,375 cells from two lung metastasis biopsies (left) or before treatment with 9,216 cells (C1D1, middle) and after treatment with 7,159 cells (C3D1, right), coloured by their four major cell types. **c**, Composition of major cell types in C1D1 and C3D1 biopsies. Left, total cell numbers in each condition; right, proportion of cells in each sample (note that cancer cell number decreased markedly after treatment). Colour coding as in **b**. **d**, Violin plot of EMT UCell enrichment score between cells of C1D1 and C3D1 biopsy (two-sided Wilcoxon test, $P < 2.10^{-16}$). **e**, UMAP plot of subclustered cancer cells from the whole integrated dataset (C1D1 + C3D1). **f**, UMAP plot of subclustered cancer cells before and after treatment. **g**, Composition of cancer cell clusters in C1D1 and C3D1 biopsies. Left, cell numbers; right, proportion of cells in each sample (note that cancer cell number decreased markedly after treatment). **h**, Density plot of EMT UCell enrichment score showing clusters 2/3 with strong EMT enrichment (note that cluster 2 decreased after treatment (**g**, right)).

Unsupervised clustering showed the presence of different cell populations including tumour cells (expressing EpCAM, PGR and TFF3—all markers of ECs[21]), immune cells (marked by CD45 (PTPRC) expression), cancer-associated fibroblasts (CAFs, marked by αSMA (ACTA2)) and endothelial cells (PECAM1 positive) (Fig. 5b and Extended Data Fig. 4a,b).

Treatment with NP137 led to a statistically significant decrease in the tumour cell compartment (Fig. 5b,c and Extended Data Fig. 4b). The proportion of tumour cells following anti-netrin-1 treatment was 3.19 times lower after two cycles of NP137 (Extended Data Fig. 4b). Of interest, in addition to the net decrease in cancer cells we noted a statistically significant decrease in EMT score in the whole tumour compartment, indicating an overall more epithelial phenotype associated with NP137 treatment (Fig. 5d). We also performed unbiased differential expression and pathway analysis only in tumour cells (Extended Data Table 2). Remarkably, EMT was the most significant term, with downregulation following exposure to NP137 (Extended Data Table 2). Of interest, while following NP137 treatment, most of the subcompartments of tumour cells decreased in a similar way and we noted that tumour cluster 2, which had the strongest decrease, also showed a high EMT score (Fig. 5e–h; note that clusters 5–7, with high

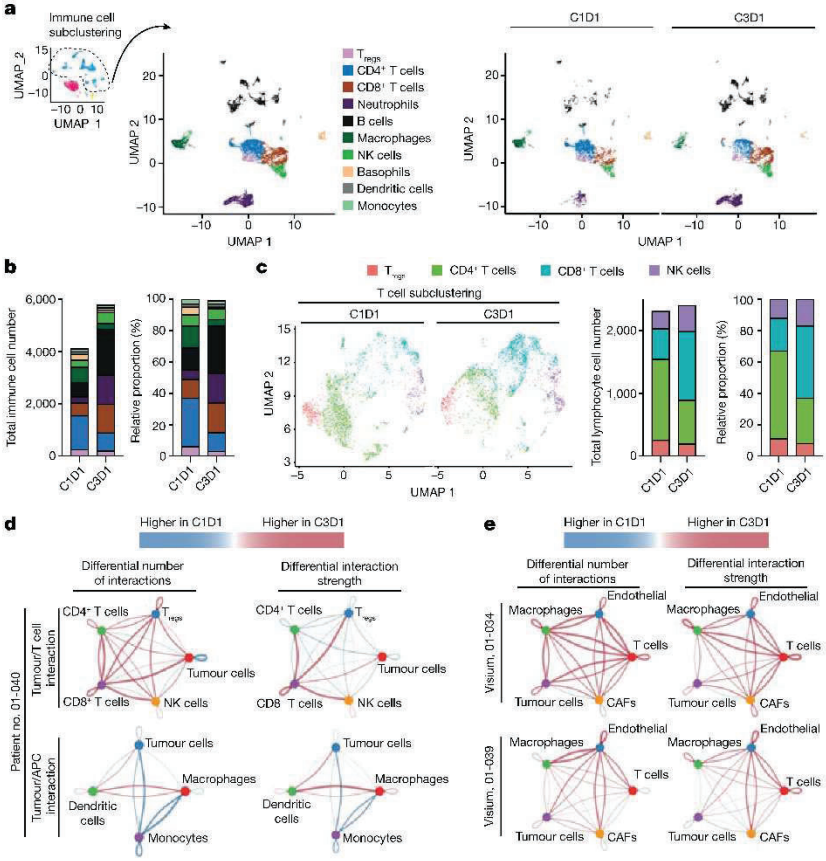

Fig. 6 | Immunological changes observed from single-cell RNA-seq analysis pre and post biopsy of a patient with endometrial adenocarcinoma. **a**, UMAP plots of subclustered immune cells from the whole integrated dataset (C1D1 + C3D1) for patient no. 01-040, illustrating the composition of major immune cell clusters in C1D1/C3D1 biopsies (left) or separately for C1D1 and C3D1 (right). **b**, Number (left) and proportion (right) of immune cell types in each sample. **c**, Left, UMAP plot of subclustered lymphocyte/NK cells from the whole integrated dataset (C1D1 and C3D1). T regulatory cells (T_{regs}) were determined according to the markers shown in Extended Data Fig. 5b. Middle, right,composition of T/NK cell clusters in C1D1 and C3D1 biopsies; cell number (middle) and proportion of cells in each sample (right). Note that cytotoxic $CD8^+$ T cell number increased after treatment whereas that of $CD4^+$ cells decreased. **d**, CellChat analysis of single-cell assay in patient no. 01-040, showing the differential (C3D1/C1D1) number of interactions (left) and strength of interactions (right) between tumour cells and lymphocytes (top) and between tumour cells and APCs (bottom). **e**, CellChat analysis of Visium assay on patient nos. 01-034 (top) and 01-039 (bottom), showing the differential (C3D1/C1D1) number of interactions (left) and strength of interactions (right) between tumour cells and stromal cells. Line colours indicate higher numbers or strength interactions in C3D1 (red) and C1D1 (blue). Segment size is proportional to the difference in the number or strength of interactions between C3D1 and C1D1.

EMT score, were not detectable following NP137 treatment but we cannot exclude the possibility that they were not captured, because these clusters already had very few cells at C1D1).

The change occurring in the tumoural compartment was also associated with a change in stromal cells (Figs. 5b,c and 6 and Extended Data Figs. 4c–f, 5 and 6a). Of note, NP137 treatment clearly appeared to have an impact on immune cells (Fig. 6a,b and Extended Data Fig. 5a). More specifically, following NP137 treatment we noted an increase in lymphocytes endowed with cytotoxic functions ($CD8^+$ T cells and natural killer (NK) cells; Fig. 6c and Extended Data Fig. 5b). A similar increase in $CD8^+$ cells was also noted in *Pten* f/f mice treated with NP137 (Extended Data Fig. 5c,d). Of interest, following NP137 treatment we noted both in the single-cell analysis from patient no. 01-40 and in the spatial transcriptomic data from patient nos. 01-034 and 01-039 an increase in both the number and strength of interaction between T cells and tumour cells (Fig. 6d,e). In particular, single-cell RNA-seq data showed an increase in the number and strength of interactions between $CD8^+$ T cells and tumour cells (Fig. 6d). A decrease in M2 macrophages was detected (Extended Data Fig. 5e,f), together with an increase in major histocompatibility class I/II antigen presentation (Extended Data Fig. 6a,b). NP137 treatment is associated with more efficient antigen-presenting cells (APCs) because we observed a clear switch from monocytes in C1D1 to dendritic cells in C3D1 interacting with cancer cells (Fig. 6d,e and Extended Data Fig. 6b).

NP137 inhibits chemotherapy resistance

Because of a large body of literature describing EMT as a major cause of chemotherapy resistance[2,22] and because our data suggest that targeting of netrin-1 inhibits EMT, we assessed whether the addition of NP137 to carboplatin-paclitaxel (carbotaxol), the standard-of-care chemotherapy used in clinical settings in endometrial cancer, might enhance the efficacy of carbotaxol alone in the *Pten* f/f mouse model of endometrial adenocarcinoma. As shown in Extended Data Fig. 7, NP137/carbotaxol treatment proved superior to carbotaxol alone, leading to complete responses in mice. Altogether, these preclinical and clinical data demonstrate that a clinical-stage drug both induces tumour cell debulking and triggers a general inhibition of EMT features, which offers the possibility of alleviating resistance to conventional therapies.

Discussion

We provide here documentation of a clinical activity of netrin-1 titration using NP137 as monotherapy. Whereas the interest in targeting netrin-1 in the cancer field is relatively recent[13], this report indicates that targeting netrin-1 in endometrial cancer may be effective. In addition to the generation of a series of data, including analysis of a human cohort and preclinical experiments in mice, we have confirmed a key mechanistic role for netrin-1 in endometrial cancer resistance and progression. We also report a partial response detected in a patient with EC receiving an anti-netrin-1 mAb. This partial response in a human patient, together with decrease in tumour cell counts in mice and marked decrease in tumour cells observed in single-cell RNA-seq analysis of a patient treated with NP137, further support the initial view of the mode of action of the netrin-1 mAb as an inducer of tumour cell death[1,23]. Indeed, netrin-1 was previously considered to be an embryonic secreted molecule re-expressed in cancer settings to promote tumour cell survival[1,8]. NP137, by blocking netrin-1, is theorized as unleashing the pro-death activity of netrin-1 receptor as observed in various preclinical models[11–13,24]. In patients with EC or preclinical models of EC treated with NP137, this is expected to be translated into a decrease in tumour cells.

However, we have shown here that, not only does NP137 induce tumour cell death, but it also appears to impact tumour EMT. Only a few previous studies have suggested that netrin-1 may be implicated in EMT, and these showed only in vitro data[16–19], thus only weakly supportive of a major regulatory effect of netrin-1 on EMT[25]. Tumour EMT, in which tumour cells lose their epithelial characteristics and acquire mesenchymal features, appears to be a key driver of tumour heterogeneity and has been associated with different steps in tumourigenesis such as tumour initiation, progression, metastasis and, more recently, resistance to chemotherapy or immunotherapy[2]. Whereas great progress in the understanding of the role and mechanisms by which EMT regulates these different tumour functions has been achieved, there is still virtually no pharmacological intervention that allows the clinician to alleviate EMT in tumours. It is also fair to say that, to date, because there are no clinical-stage drugs impacting only on EMT features, there is no clinical demonstration that EMT is clinically important. Here we demonstrate, using both preclinical models and pre- and on-treatment biopsies from patients with EC, that systemic treatment with NP137 led to a decrease in tumour EMT features. This inhibition of EMT features is associated with an overall more epithelial phenotype. Given the extreme complexity of tumour heterogeneity, we have not yet demonstrated whether the effect of N137 on tumour EMT is mediated by a direct effect of netrin-1 blockade on cancer cells or whether this effect is due to an indirect effect triggered by changes in the tumour microenvironment. It is likely that these effects are combined, because we have shown using single-cell analysis that changes in EMT features are associated with changes in the tumour microenvironment. Although further confirmation is required, we observed a decrease in cancer-associated fibroblasts, which usually serve as primary source of EMT-inducing molecules[26], and a decrease in protumourigenic M2-like macrophages, which also contribute to EMT by multiple mechanisms[27]. Moreover, we observed an increase in lymphocytes endowed with cytotoxic functions and an increase in both the number and strength of interactions between immune cells and tumour cells associated with more highly efficient APCs. Together this supports the view that NP137, possibly by impacting on EMT, enhances tumour immune response. Whatever the mechanism, because there is an increasing literature describing EMT as a major player in resistance to chemotherapy and immune checkpoint inhibitors[2,28], the observation that treatment with NP137 inhibits features of tumour EMT argues for the clinical assessment of combinations of the anti-netrin-1 mAb with conventional therapies to interfere with tumour progression. This is currently investigated in the Phase 2 GYNET trial (NCT04652076) assessing the safety and efficacy of combining NP137 with carboplatin-paclitaxel and/or pembrolizumab (anti-PD1 mAb) in patients with endometrial or cervical cancer.

Online content

Any methods, additional references, Nature Portfolio reporting summaries, source data, extended data, supplementary information, acknowledgements, peer review information; details of author contributions and competing interests; and statements of data and code availability are available at https://doi.org/10.1038/s41586-023-06367-z.

1. Mehlen, P., Delloye-Bourgeois, C. & Chédotal, A. Novel roles for Slits and netrins: axon guidance cues as anticancer targets? *Nat. Rev. Cancer* **11**, 188–197 (2011).
2. Shibue, T. & Weinberg, R. A. EMT, CSCs, and drug resistance: the mechanistic link and clinical implications. *Nat. Rev. Clin. Oncol.* **14**, 611–629 (2017).
3. Brisset, M., Grandin, M., Bernet, A., Mehlen, P. & Hollande, F. Dependence receptors: new targets for cancer therapy. *EMBO Mol. Med.* **13**, e14495 (2021).
4. Wu, Z. et al. Long-range guidance of spinal commissural axons by netrin1 and sonic hedgehog from midline floor plate cells. *Neuron* **101**, 635–647 (2019).
5. Sung, P.-J. et al. Cancer-associated fibroblasts produce netrin-1 to control cancer cell plasticity. *Cancer Res.* **79**, 3651–3661 (2019).
6. Paradisi, A. et al. NF-κB regulates netrin-1 expression and affects the conditional tumor suppressive activity of the netrin-1 receptors. *Gastroenterology* **135**, 1248–1257 (2008).
7. Paradisi, A. et al. Netrin-1 up-regulation in inflammatory bowel diseases is required for colorectal cancer progression. *Proc. Natl Acad. Sci. USA* **106**, 17146–17151 (2009).
8. Fitamant, J. et al. Netrin-1 expression confers a selective advantage for tumor cell survival in metastatic breast cancer. *Proc. Natl Acad. Sci. USA* **105**, 4850–4855 (2008).
9. Delloye-Bourgeois, C. et al. Interference with netrin-1 and tumor cell death in non-small cell lung cancer. *J. Natl Cancer Inst.* **101**, 237–247 (2009).
10. Delloye-Bourgeois, C. et al. Netrin-1 acts as a survival factor for aggressive neuroblastoma. *J. Exp. Med.* **206**, 833–847 (2009).
11. Broutier, L. et al. Targeting netrin-1/ DCC interaction in diffuse large B-cell and mantle cell lymphomas. *EMBO Mol. Med.* **8**, 96–104 (2016).
12. Boussouar, A. et al. Netrin-1 and its receptor DCC are causally implicated in melanoma progression. *Cancer Res.* **80**, 747–756 (2020).
13. Grandin, M. et al. Structural decoding of the netrin-1/UNC5 interaction and its therapeutical implications in cancers. *Cancer Cell* **29**, 173–185 (2016).
14. Cassier, P. et al. A first in human, phase I trial of NP137, a first-in-class antibody targeting netrin-1, in patients with advanced refractory solid tumors. *Ann. Oncol.* **30**, v159 (2019).
15. Mirantes, C. et al. An inducible knock-out mouse to model cell-autonomous role of PTEN in initiating endometrial, prostate and thyroid neoplasias. *Dis. Model. Mech***6**, 710–720 (2013).
16. Yan, W. et al. Netrin-1 induces epithelial–mesenchymal transition and promotes hepatocellular carcinoma invasiveness. *Dig. Dis. Sci.* **59**, 1213–1221 (2014).
17. Jin, X. et al. Netrin-1 interference potentiates epithelial-to-mesenchymal transition through the PI3K/AKT pathway under the hypoxic microenvironment conditions of non-small cell lung cancer. *Int. J. Oncol.* **54**, 1457–1465 (2019).
18. Zhang, X. et al. Netrin-1 elicits metastatic potential of non-small cell lung carcinoma cell by enhancing cell invasion, migration and vasculogenic mimicry via EMT induction. *Cancer Gene Ther.* **25**, 18–26 (2018).
19. Chen, Y. et al. Bradykinin promotes migration and invasion of hepatocellular carcinoma cells through TRPM7 and MMP2. *Exp. Cell. Res.* **349**, 68–76 (2016).
20. Mak, M. P. et al. A patient-derived, pan-cancer EMT signature identifies global molecular alterations and immune target enrichment following epithelial-to-mesenchymal transition. *Clin. Cancer Res.* **22**, 609–620 (2016).
21. Bignotti, E. et al. Diagnostic and prognostic impact of serum HE4 detection in endometrial carcinoma patients. *Br. J. Cancer* **104**, 1418–1425 (2011).
22. DeConti, R. C. Chemotherapy of squamous cell carcinoma of the skin. *Semin. Oncol.* **39**, 145–149 (2012).
23. Gibert, B. & Mehlen, P. Dependence receptors and cancer: addiction to trophic ligands. *Cancer Res.* **75**, 5171–5175 (2015).
24. Paradisi, A. et al. Combining chemotherapeutic agents and netrin-1 interference potentiates cancer cell death. *EMBO Mol. Med.* **5**, 1821–1834 (2013).
25. Lambert, A. W. & Weinberg, R. A. Linking EMT programmes to normal and neoplastic epithelial stem cells. *Nat. Rev. Cancer* **21**, 325–338 (2021).
26. Sahai, E. et al. A framework for advancing our understanding of cancer-associated fibroblasts. *Nat. Rev. Cancer* **20**, 174–186 (2020).
27. Gonzalez, H., Hagerling, C. & Werb, Z. Roles of the immune system in cancer: from tumor initiation to metastatic progression. *Genes Dev.* **32**, 1267–1284 (2018).
28. Brabletz, S., Schuhwerk, H., Brabletz, T. & Stemmler, M. P. Dynamic EMT: a multi-tool for tumor progression. *EMBO J.* **40**, e108647 (2021).

Methods

Genetically modified mouse model and NP137 administration

Floxed homozygous *Pten* (C;129S4-Ptentm1Hwu/J, hereafter called *Pten* f/f) Cre:ER (B6.Cg-Tg(CAG-CRE/Esr1* 5Amc/J) mice were obtained from the Jackson Laboratory. Cre:ER$^{+/-}$ *Pten* f/f mice were bred in a mixed background (C57BL6; 129S4) by crossing *Pten* f/f and Cre:ER$^{+/-}$ mice. To obtain mice carrying both *Pten* floxed alleles (*Pten* f/f) and a single Cre:ER (Cre:ER$^{+/-}$), Cre:ER$^{+/-}$ *Pten* f/$^{+}$ mice were backcrossed with *Pten* f/f mice. To induce deletion of floxed alleles, tamoxifen (Sigma-Aldrich) was dissolved in 100% ethanol at 100 mg ml^{-1}. Tamoxifen solution was emulsified in corn oil (Sigma-Aldrich) at 10 mg ml^{-1} by vortexing. To induce *Pten* deletion, adult mice (4–5 weeks old) were given a single intraperitoneal injection of 0.5 mg of tamoxifen emulsion (30–35 µg mg^{-1} body weight). Three weeks after tamoxifen injection, mice were treated via intraperitoneal injection of 100 µl of NP137, or its isotypic control NP001 diluted in PBS, at 10 mg kg^{-1} every 2 days. Animal care and housing were in accordance with institutional European guidelines from the CEEA local Ethical committee of Lleida University concerning *Pten* mouse experiments. General behaviour and weight were monitored three times per week and animals were killed in the event of strong alteration or weight loss under 20%. All mice were always killed before terminal tumour progression, and endometrial tissues were analysed blind by a pathologist.

RT–qPCR

Endometrial samples collected in the Biomedical Research institute of Lerida (Spain) were frozen and sent to the Cancer Research Center of Lyon (France) in dry ice. Samples were cryoground to obtain tumour powder, which was processed for total RNA extraction using the Nucleospin RNA Plus kit (Machery-Nagel) according to the manufacturer's instructions. Expression of mRNA was measured using a NanoDrop1000 (Themo Scientific). RNA was retrotranscribed using the T100 ThermoCycler (Bio-Rad) and the iScript cDNA Synthesis Kit (Bio-Rad) according to the manufacturer's instructions. RT–qPCR was performed using LC480 qPCR (Roche) and OneGreen Fast qPCR Premix (Ozyme) according to the manufacturers' instructions.

Bulk RNA-seq

Patient analysis: patient microbiopsy RNA was extracted with the RNA easy FFPE kit (Qiagen). The RNA-seq library was produced from 100 ng of RNA with the Illumina TruSeq Exome kit (RNA Library Prep for Enrichment & TruSeq RNA Enrichment) according to the manufacturer's instructions and then sequenced with an Illumina NovaSeq 6000. FASTQ files were then processed with STAR (v.2.7.10a). Briefly, FASTQ files were mapped to the human reference genome (gencode.v.27) and aligned reads were converted for counting with STAR. The quality of FASTQ files was also checked, by FATSQC (v.0.11.9). RNA-seq analysis was performed with R (v.4.0.3) and the DESeq2 package (v.1.30.1). $\log_2$-Transformed transcripts per million were calculated, and we performed EMT score calculation as previously described[20].

Murine endometrial cancer model: tumours were collected, snap-frozen and cryoground. RNA was extracted with a standard kit (Macherey-Nagel). The RNA-seq library was produced from RNA with Illumina TruSeq Stranded Total RNA Library Prep Human/Mouse/Rat, according to the manufacturer's instructions, then sequenced with Illumina NOVASeq. FASTQ files were processed as described above, except for the reference genome which was Mus_musculus.GRCm38 (GENECODE release 25). Analysis was done with DESeq2 (v.1.30.1) and ggplot (v.3.1.3) packages in R (v.4.0.3). EMT scoring and heatmaps were done with $\log_2$ fragments per kilobase exon per million mapped reads values.

Single-cell RNA-seq

Endometrial metastasis biopsies were dissociated for single-cell RNA-seq using the Tumor Dissociation kit by Miltenyi Biotec (no. 130–095-929). Briefly, the biopsy was placed in RPMI medium in a Petri dish on ice and cut into small pieces (2–4 mm) after removal of necrotic tissue. Pieces were then infused with the RPMI/enzyme mix (Miltenyi Biotec), transferred to a gentleMACS C tube containing RPMI/enzyme mix, attached to the sleeve of the gentleMACS Octo Dissociator and run using the programme 37_h-TDK1. After completion of the programme the cells were spun down at 300*g* for 7 min at 4 °C, resuspended in RPMI, passed through a 70 µm strainer and centrifugation was repeated. The cell pellet was treated with 500 µl of ACK solution for 5 min at room temperature and lysis then stopped with 5 ml of RPMI/10% FBS. After centrifugation, cells were resuspended in 100 µl of RPMI. The number of live cells was determined with a Luna-FL Dual fluorescence cell counter (Logos Biosystems) to obtain an expected cell recovery population of 10,000 cells per channel, loaded on a 10x G chip and run on the Chromium Controller system (10x Genomics) according to manufacturer's instructions. Single-cell RNA-seq libraries were generated with the Chromium Single Cell 3′ v.3.1 kit (10x Genomics, no. PN-1000121) and sequenced on the NovaSeq 6000 platform (Illumina) to obtain around 50,000 reads per cell.

Except when specifically mentioned, all analyses were performed with R/Bioconductor packages, R v.4.2.2 (2022-11-10 r83330) (https://cran.r-project.org/; http://www.bioconductor.org/) in a Linux environment (x86_64-pc-linux-gnu (64-bit)).

Filtered barcoded matrices from single-cell RNA-seq data were imported into R using the Seurat package (v.4.1.1). Doublets were detected with DoubletFinder (v.2.0.3) and filtered out, together with cells showing a low number of features (nFeature_RNA < 500) or a high percentage of mitochondrial genes (above 25%). Seurat functions were used for normalization (SCTransform), merging, dimensional reduction and clustering. Initial cell type identification was based on consensus from several automated cell annotation packages (SciBet' v.1.0, SingleR v.1.10.0 and scType (https://github.com/IanevskiAleksandr/sc-type/blob/master/README.md)). T cell subtypes were visually inspected and manually curated after further annotation with ProjecTILs (v.3.0.3) and the python implementation of CellTypist (v.1.3.0). EMT signature scores were calculated by three methods (Seurat's AddModuleScore function, UCell (v.2.2.0) and AUCell (v.1.18.1)) and using two different gene lists (MsigDb Hallmark EMT pathway and the PanCancer EMT signature[20]). Pathway enrichment analyses were performed with the 'escape' package (v.1.6.0). Additional visualizations were based on functions from Nebulosa (v.1.6.0), Scillus (v.0.5.0) and ggplot2 (v.3.3.6).

Spatial RNA-seq matrices and images were imported into R using the Load10X_Spatial function of the Seurat package. For each sample, only those spots with more than 1,000 features were kept for downstream preprocessing, including SCTransform normalization, dimensional reduction and clustering. Most analyses were performed independently for each sample (without merging or integration). Two strategies were used for cell type annotation: label transfer following integration of the single-cell RNA-seq data described above, and manual annotation using known markers for major cell types.

Inference of cell–cell communication was done with CellChat (v.1.6.0), for both single-cell and spatial RNA-seq data.

Histology and IHC analysis

Cre:ER$^{+/-}$ *Pten* f/f mice were euthanized by cervical dislocation after 3 weeks of NP137 treatment. Endometrial samples were collected and formalin fixed overnight at 4 °C. Tumours were paraffin embedded for further histologic analysis. Paraffin blocks were sectioned at 3 µm and dried for 1 h at 65 °C before the pretreatment procedures of deparaffinization, rehydration and epitope retrieval in the pretreatment module at 95 °C for 20 min in 50× Tris/EDTA buffer. Before staining of sections, endogenous peroxidase was blocked. Representative images were taken with a Leica DMD108 microscope.

Immunohistochemistry was performed on an automated immunostainer (Ventana discoveryXT, Roche) using the rabbit Omni map

DAB Kit. Sections were incubated with specific antibodies targeting EpCAM (no. ab71916, abcam), cleaved caspase-3 (no. 9661, Cell Signaling Technologies), netrin-1 (no. CPA2389, Cohesion Biosciences), Unc5B (no. 13851S, Cell Signaling Technologies) and CD8 (no. 4SM15, eBioscience). Staining was by anti-rabbit horseradish peroxidase, visualized with 3,3′-diaminobenzidine as a chromogenic substrate and counterstained with Gill's haematoxylin. Histological quantifications were performed with Halo software (Indica Labs).

Multiplex IHC

Sequential chromogenic multiplex IHC for vimentin/pancytokeratin (panCK), as previously described, was performed on tumour sections from patients included in the NP137 clinical trial and that were collected at C1D1 and C3D1. Dewaxed 4-µm-thick, paraffin-embedded tissue sections were subjected to two successive steps of IHC on a Ventana discovery XT platform (Ventana, Roche Diagnostics) using the REDMap and DABMap detection systems according to the manufacturer's recommendations. In a first step for vimentin expression, slides were incubated with mouse monoclonal anti-human vimentin for 1 h (mouse, clone V9, Leica, no. NCL-L-VIM-V9, dilution 1:100) and incubated with rabbit monoclonal anti-mouse secondary antibody for 20 min (clone M1gG51-4, abcam, no. 125913, dilution 1:750). The slides were then incubated with biotinylated anti-rabbit secondary antibody for 24 min (Vector Laboratories, dilution 1:200) followed by the addition of the streptavidin–alkaline phosphatase complex. Immunostaining was detected by incubation with naphthol and Fast red. Tissue sections were counterstained with Gill's haematoxylin, dehydrated and mounted. Whole histological slides were digitized at ×20 magnification using a Hamamatsu 2.0 HT scanner. After removal of coverslips, slides were incubated in 100% ethanol until complete erasure of red colour. In a second step, to show panCK expression, the slides were incubated with mouse monoclonal anti-panCK antibody for 1 h (mouse, clone CKAE1AE3, Dako Belgium, no. M351529-2, dilution 1:150) and then with rabbit monoclonal anti-mouse secondary antibody for 20 min. The slides were then incubated with biotinylated anti-rabbit secondary antibody for 28 min (Vector Laboratories, dilution 1:200) followed by the addition of streptavidin–alkaline phosphatase. PanCK immunostaining was detected by incubation with naphthol and Fast red. The IHC slides were counterstained with Gill's haematoxylin, dehydrated, mounted and again digitized. Image processing and analysis for Hynrid EMT score computation were performed using Visiomorph DP 2018.4 to determine vimentin and panCK co-expression in each tissue slide. Briefly, each pair of vimentin- and panCK-labelled virtual slides, which were acquired from the same tissue section, was subjected to image registration. Vimentin- and panCK-positive areas were automatically detected in the aligned virtual slides to evidence their co-expression in tumour cells. This co-expression was evaluated on whole slides at ×10 magnification to take into account potential imperfections. Manual corrections were carried out to exclude irrelevant sample parts, such as necrosis. Cell nuclei negative for both markers were also excluded, to focus only on cytoplasmic areas where colocalization could occur.

Spatial transcriptomics using Visium FFPE technology

FFPE tissue sections were placed on Visium slides and prepared according to the 10x Genomics protocols. After H&E staining, imaging and de-crosslinking steps, tissue sections were incubated with human-specific probes targeting 17,943 genes (10x Genomics, Visium Human Transcriptome Probe Set v.1.0). Probes hybridized on mRNA were captured on Visium slides and a gene xpression library prepared following the provided protocol and sequenced on an Illumina NovaSeq 6000 with 50,000 reads per spot targeted sequencing depth.

For each FFPE section, FASTQ files and histology images were processed using 10x Space Ranger v.2.0 to obtain the gene expression matrix associated with each spot.

Seurat v.4 (https://satijalab.org/seurat/) in R 4.1 was used to perform the analysis. Briefly, filtered matrices were loaded, merged per patient and spots with fewer than 1,000 detected genes were removed. Following SCTransform normalization we subset the tumoural spot according to pathologist spot identification then calculated the EMT gene set enrichment score (escape R package) with the UCell method.

NP137 clinical trial

NP137 is a first-in-human Phase I trial with a dose-escalation part followed by extension cohorts (NCT02977195) conducted in adult patients with advanced or metastatic solid tumours. The dose-escalation part was initiated using an accelerated dose titration with one patient per dose level until the occurrence of a grade 2 or higher drug-related adverse event. Following occurrence of a grade 2 NP137-related adverse event, patients were enrolled in a slower dose-escalation design with at least three patients per dose level using a modified continual reassessment method. Additional patients were enrolled in three biomarker cohorts, at dose levels that had been declared safe, and underwent paired biopsies for pharmacodynamics purposes. In the dose-escalation part, 19 patients were enrolled in seven dose levels (1–20 mg kg^{-1}, intravenous, Q2W). No dose-limiting toxicities were observed and 11 (58%) patients had infusion-related reactions of grade 12 severity, all at doses of 4 mg kg^{-1} and above[14]. Based on available data, 14 mg kg^{-1} Q2W was selected as the recommended Phase 2 dose. Two extension cohorts were opened, including one in patients with hormone receptor-positive EC (enrolment closed in October 2021).

The trial was conducted according to Good Clinical Practice guidelines, the Declaration of Helsinki and relevant French and European laws and directives. All patients provided written informed consent.

Statistical analysis

Statistical analyses were performed on Prism (GraphPad Software). In the figure legends, *n* denotes the total number of replicates. All statistical tests were two-sided. For mouse experiments, statistical methods were not used to predetermine necessary sample size but sample size was chosen based on pilot experiments applying appropriate statistical tests that could return significant results. Survival curves were analysed using the log-rank (Mantel–Cox) test. Population ratios were analysed by chi-squared tests. qPCR expression, caspase-3 IHC and thyroid weights were compared by Mann–Whitney test. For data involving patients, gene expressions and EMT scores were compared by *t*-test.

Reporting summary

Further information on research design is available in the Nature Portfolio Reporting Summary linked to this article.

Data availability

The raw RNA-seq, single-cell RNA-seq and spatial transcriptomic sequencing data of this study have been deposited in Gene Expression Omnibus with accession no. GSE225691. For version control, sharing and reproducibility, all bioinformatic code related to the single-cell analysis is retained in a GitHub repository (https://github.com/hernandezvargash/NP137_single.cell). Source data are provided with this paper.

Acknowledgements We thank D. Bredesen for critical reading of the manuscript. This work was supported by institutional grants from CNRS, University of Lyon, Centre Léon Bérard and from the Ligue Contre le Cancer, INCA, ARC Sign'it and ANR (nos. ANR-10-LABX-0061, ANR-17-CONV-0002 and ANR-18-RHUS-0009). The preclinical experiments were in part supported by PID2019-104734RB-I00 from MCIUN – Ministerio de Ciencia, Innovación y Universidades. I.P. is supported by the FNRS and WEL Research Institute. DIAPath and the Department of Pathology are supported by the Fonds Yvonne Boël. The CMMI is supported by the European Regional Development Fund and the Walloon region. C.B. is supported by the WEL Research Institute, FNRS, TELEVIE, Fondation Contre le Cancer, ULB Foundation, FNRS/FWO EOS (40007513) and European Research Council (ERC AdvGrant 885093).

Author contributions X.D., C.B., A.B. and P.M. designed preclinical experiments. P.A.C., J.-P.D., G.G., H.G., C. Dalban, E.M.-L., D.P., P.M. and I.R.-C. designed the clinical trial and managed patient follow-up and clinical data analysis. R.N., M.B., L.F., D.N., N.B. and X.M.-G. performed and analysed preclinical experiments. N.R., H.H.-V., R.J., S.L. and C. Degletagne processed clinical specimens for single-cell RNA-seq and carried out bioinformatic analysis. A.P., B.D., J.L., L.P., N.G., M.D.-S., J.A., E.Z., C. Decaestecker and I.S. performed analysis on the patient endometrial cohort. A.B. and P.M. wrote the manuscript. All authors read and approved the final manuscript.

Competing interests A.B. and P.M. declare a conflict of interest as founders and shareholders of NETRIS Pharma. D.N., B.D., M.B., J.L. and P.M. declare a conflict of interest as employees of NETRIS Pharma. A.B., A.P. and N.R. declare a conflict of interest as consultants for NETRIS Pharma. No patent has been filed based on this study. The NP137 patent is fully owned by NETRIS Pharma and none of the authors are inventors. The remaining authors declare no competing interests.

Additional information

Supplementary information The online version contains supplementary material available at https://doi.org/10.1038/s41586-023-06367-z.

Correspondence and requests for materials should be addressed to Agnès Bernet or Patrick Mehlen.

Peer review information *Nature* thanks Angela Green and the other, anonymous, reviewer(s) for their contribution to the peer review of this work.

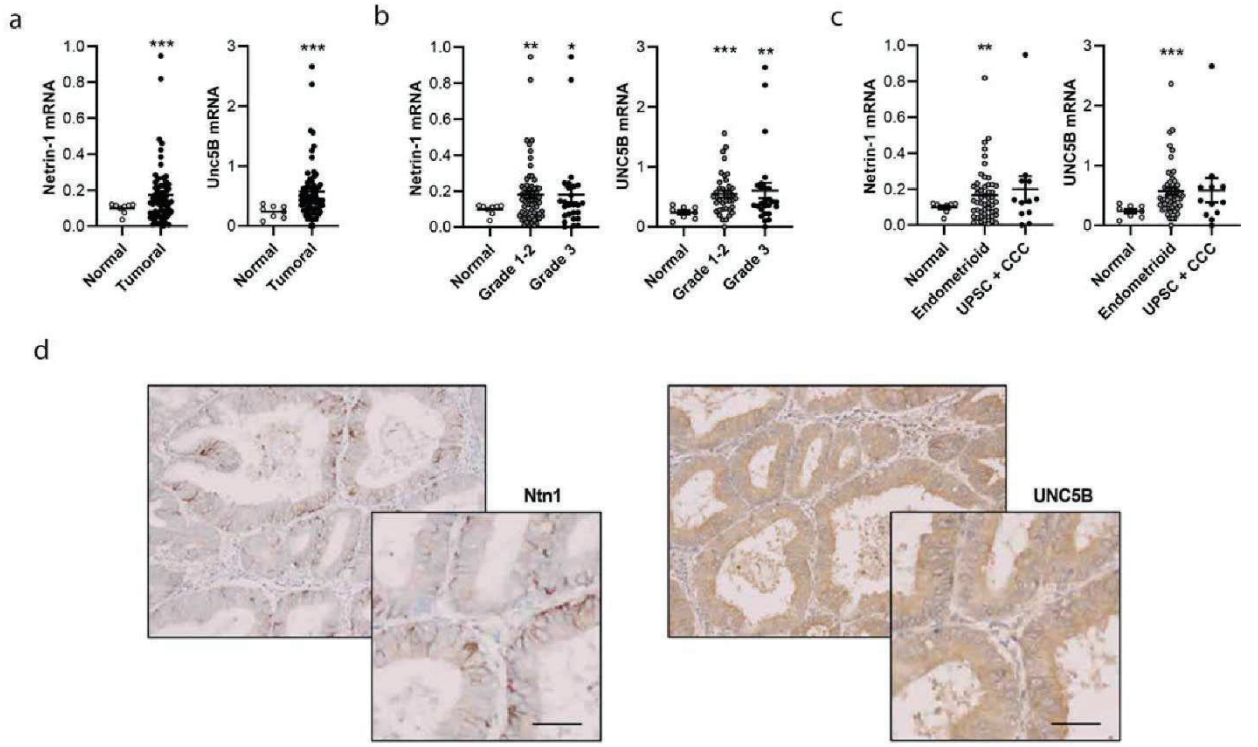

Extended Data Fig. 1 | Netrin-1 and UNC5B are up-regulated in human endometrium adenocarcinoma. a, **b**, **c**, Relative mRNA expression of netrin-1 (left) and UNC5B (right) in patients with endometrial carcinoma (n = 73) compared to unpaired normal tissue (n = 8) (**a**) global expression (*** $P < 0.001$ by T-test one-sided) (**b**) expression reported to grades: Grade1+2 n = 38, Grade 3 n = 26, (** $P = 0.002$ and * $P = 0.038$, respectively normal vs grade 1-2 and grade 3 for Ntn1 and p < 0.001 and ** p = 0.004 for Unc5B by T-test one-sided) (**c**) expression reported to types: Endometrioid n = 51, UPSC+CCC n = 12 (UPSC: Uterine papillary serous carcinoma, CCC: Clear cell carcinoma) (** p = 0.002 and * p = 0.097, respectively normal vs endometrioid and UPSC+CCC for Ntn1 and *** p < 0.001 for Unc5B by T-test one-sided), defined by qRT-PCR (Bars are mean values mean ± s.e.m., data are normalized to TBP, PPIA and GUSB genes). **d**, Representative netrin-1 and UNC5B immunohistochemistry analysis of an endometrioid carcinoma (grade 1). 2x magnification field (bottom right). Scale bar (represented by a line, 100 µm).

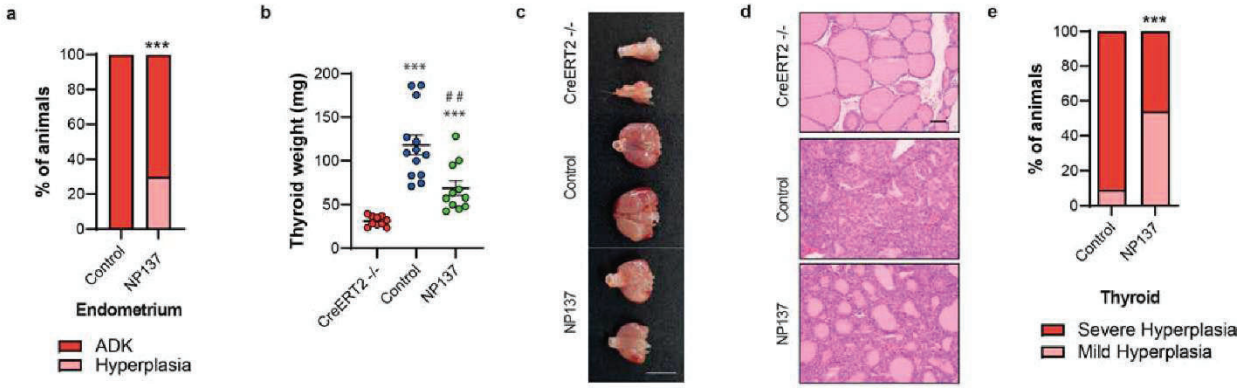

Extended Data Fig. 2 | Netrin-1 blockade impacts tumor growth in a preclinical mouse model. a, Percentage of mice treated with control (n = 12) or NP137 (n = 16), showing hyperplasia or Adenocarcinoma (ADK) of the endometrium. *** $P < 0.001$ by Chi-square test and Fischer's exact test. **b**, Quantification of the thyroid weight in CreERT2−/− mice (n = 10) or after *Pten* deletion (Tamoxifen injection) in CreERT2+/−x *Pten* f/f mice treated with control (n = 13) or NP137 (n = 11). Bars are mean values mean ± s.e.m., *** $P < 0.001$ against CreERT2−/−; ## $P = 0.015$ NP137 against control by Mann-Whitney two-sided. **c**, Representative images of the thyroids in panel **b**. **d**, Representative images of H&E staining of thyroid from mice sacrificed in weeks 5-6 after tamoxifen injection. Scale bar represented by a line, (100 µm) similar observations have been done on the full cohort. **e**, Percentage of mice showing mild or severe hyperplasia of the thyroid in mice treated (n = 16) or not with NP137 (n = 12). *** $P < 0.001$ by Chi-square test and Fischer's exact test.

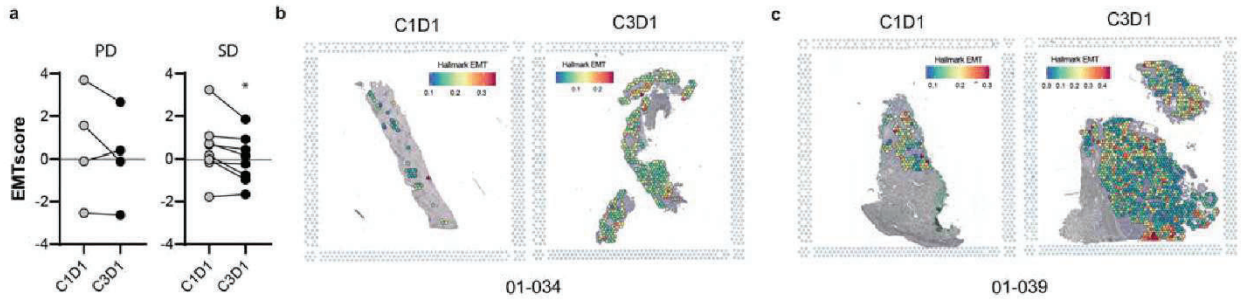

Extended Data Fig. 3 | Pre/post biopsies analysis by bulk RNAseq or Visium Spatial Gene Expression. a. Diagram showing EMT-score calculated with the Mak's signature[20] as in Fig. 4a. Patients are segregated in PD (progression at 6 weeks) and SD (stable disease at least 6 weeks) according to their clinical benefit determined upon centralized review. * $P = 0.0023$; by T-Test two-sided. **b**, **c**, H&E-stained tissue from C1D1 (left panel) and C3D1 (right panel) with EMT score enrichment on Visium tumoral spot by UCell method.

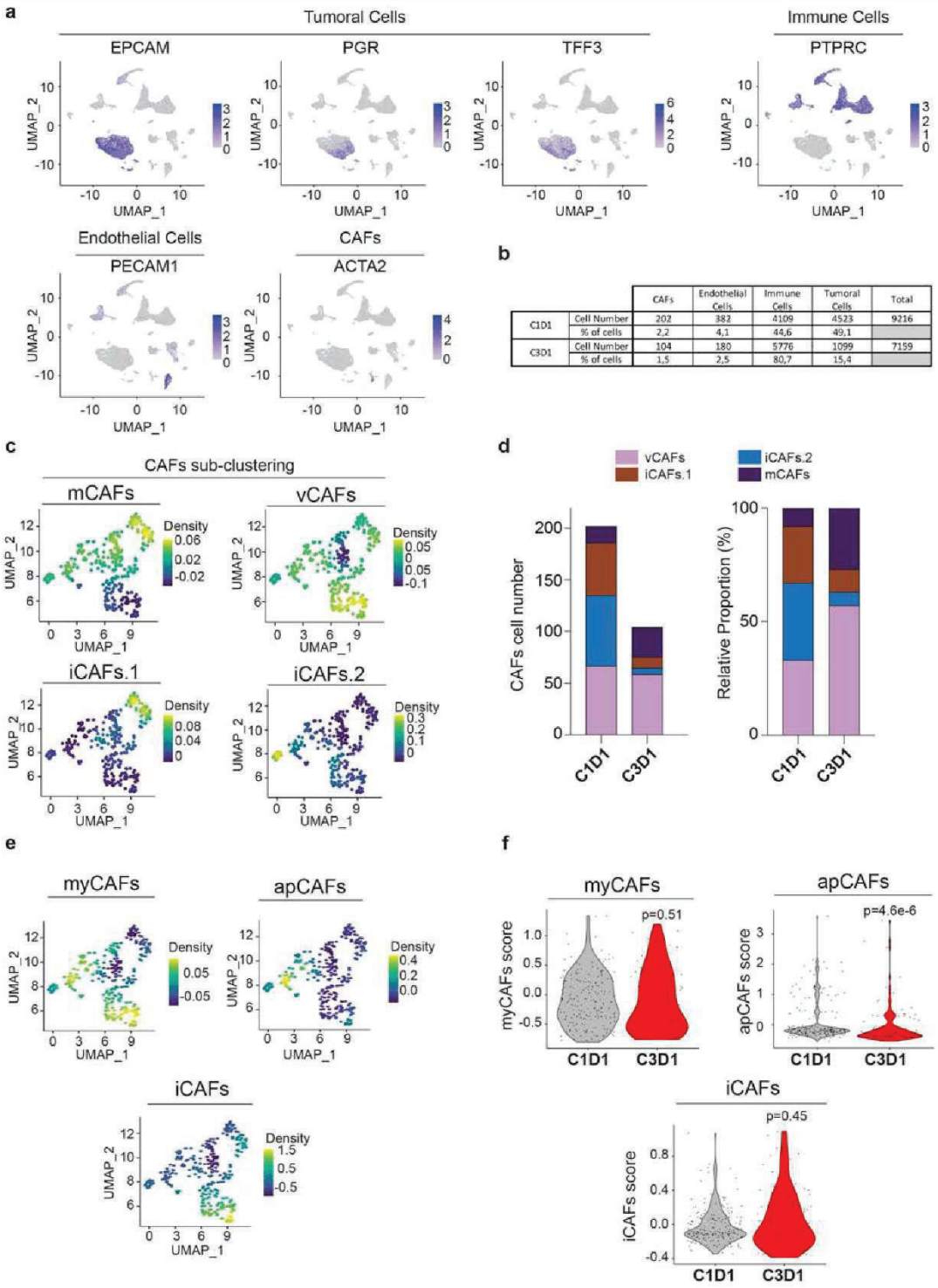

		CAFs	Endothelial Cells	Immune Cells	Tumoral Cells	Total
C1D1	Cell Number	202	382	4109	4523	9216
	% of cells	2,2	4,1	44,6	49,1	
C3D1	Cell Number	104	180	5776	1099	7159
	% of cells	1,5	2,5	80,7	15,4	

Extended Data Fig. 4 | Pre/post biopsies scRNAseq identify global cell types and cancer cell sub-clustering. a, UMAP plot with the 2 integrated samples of patient 01-040 showing the normalized expression of major cell type markers: immune cells (*PTPRC*, also known as *CD45*), endothelial cells (*PECAM*), tumor cells (*EPCAM*, *PGR*, *TFF3*), CAF cells (*ACTA2*). **b**, Table showing the cell number in each cell type. **c**, Identification of CAFs subtypes (markers used: mCAFs: MMP2, DCN, COL12A1, FBLN1; vCAFs : MCAM, COL4A1, COL18A1; iCAFs.1: MUSTN1, TAGLN, S100A4, CXCL2; iCAFs.2: S100A8, CXCL8, SPLI). **d**, CAFs subcluster composition analysis, the left panel shows the total CAFs numbers *per* cluster in each condition and the right panel shows the proportion of CAFs *per* cluster in each samples. **e**, UMAP plot of sub-clustered CAFs showing other CAFs subtypes (markers used: myCAFs: ACTA2, CTGF, POSTN, PDGFR, TGFB1, COL1; iCAFs : IL6, CXCL1, CCL2, PDGFRA, HAS1, FAP, IL11, LIF; apCAFs: H2-AB1, CD74, SAA3). **f**, Violin plot showing CAFs subtypes scores before and after treatment (C1D1 or C3D1) (Wilcoxon test, two-sided).

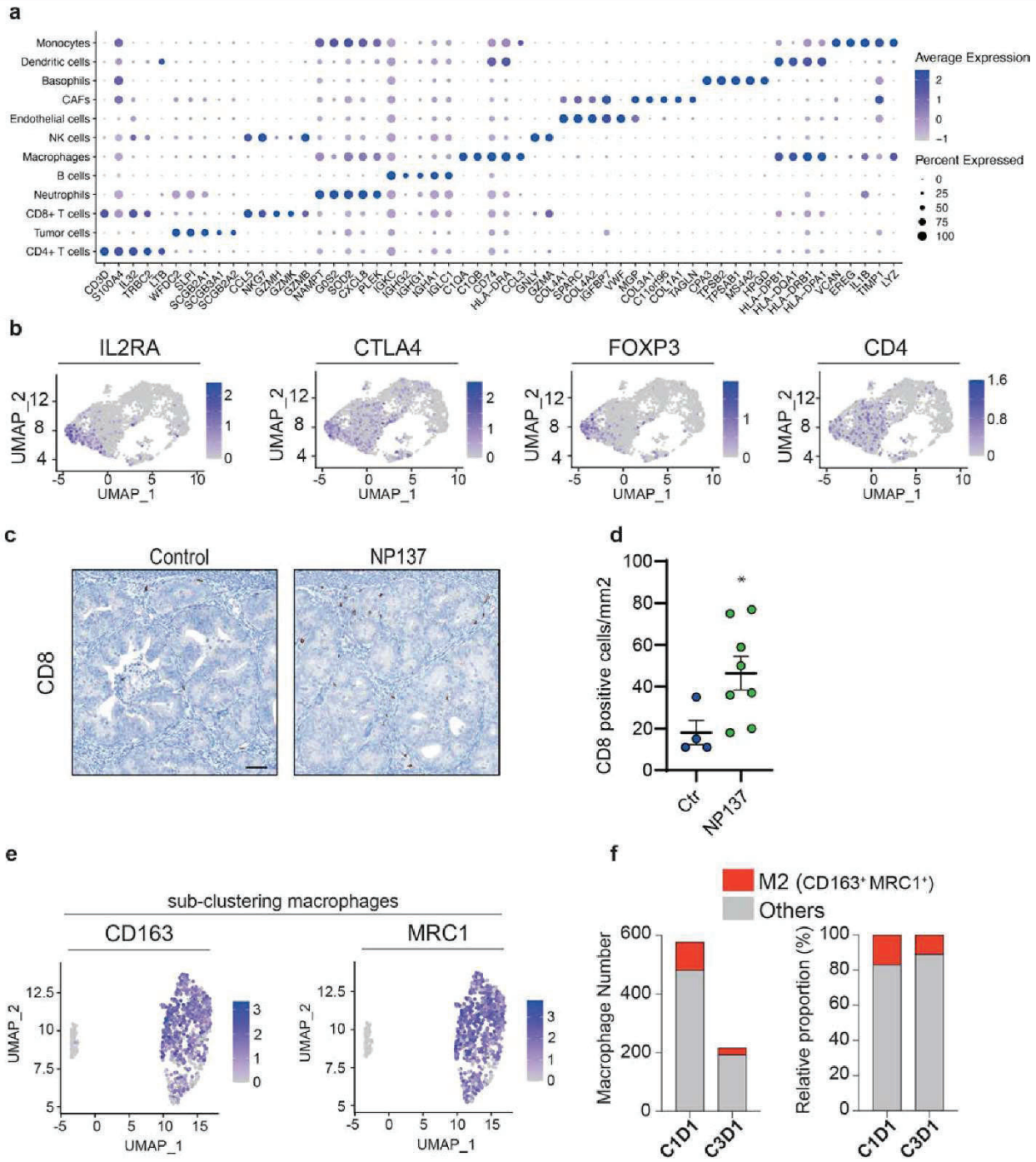

Extended Data Fig. 5 | Pre/post biopsies scRNAseq identify various immune cell types. a, Validation of the cluster annotation with dot plot showing top 5 genes markers that are enriched in clusters which were previously characterized by automatic cell annotation package. **b**, Tregs cluster identification with UMAP plot of sub-clustered lymphocyte showing Tregs expression markers: IL2RA, CTLA4, FOXP3 and CD4. **c**,**d** CD8 detection and quantification by IHC in mouse *Pten* driven tumors treated with control or NP137. **c**, representative image of IHC. Scale bar = 50 µm. **d**, Quantification of CD8 positive cells in control tumors (n = 4) vs NP137 treated (n = 8). Bars are mean values mean ± s.e.m., * $P = 0.0162$ by Mann-Whitney two-sided. **e**, Analysis of M2-macrophages, we used *CD163* and *MRC1* as markers on the UMAP plot of sub-clustered macrophages with the 2 integrated samples. **f**, The 2 panels show the M2 cell type number and the proportion of M2 in each sample compared to the total macrophage number.

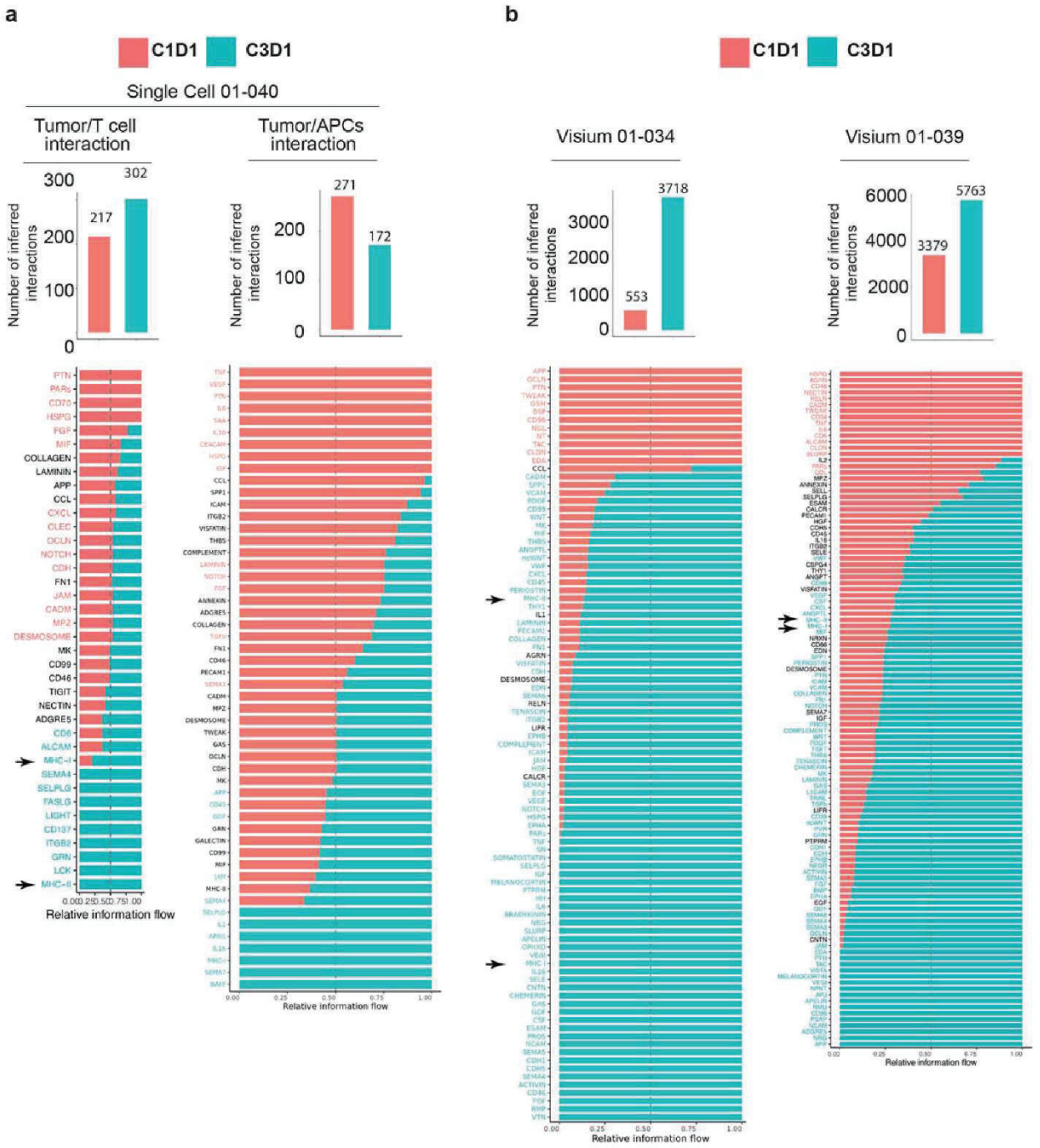

Extended Data Fig. 6 | NP137 treatment impacts tumor cell communication with immune cell types. a, Histograms showing the number of inferred interaction (upper panel) from the single cell RNA seq analysis (patient 01-040) by CellChat packages and (lower panel) the significant genes were ranked based on their differences of overall information flow between C1D1 and C3D1. The left panels investigate the communication between Tumor and lymphocyte cells. The right panels investigate the communication between Tumor and APCs. **b**, Histograms showing the number of inferred interaction (upper panel) from the Visium assays (patients 01-034 and 01-039) by CellChat packages and (lower panel) the significant genes were ranked based on their differences of overall information flow between C1D1 and C3D1. The left and right panels correspond respectively to patient 01-034 and 01-039. Red and green are more enriched in C1D1 and C3D1 sample, respectively. Arrows indicate MHC-I and II genes which expression is enriched in C3D1 samples.

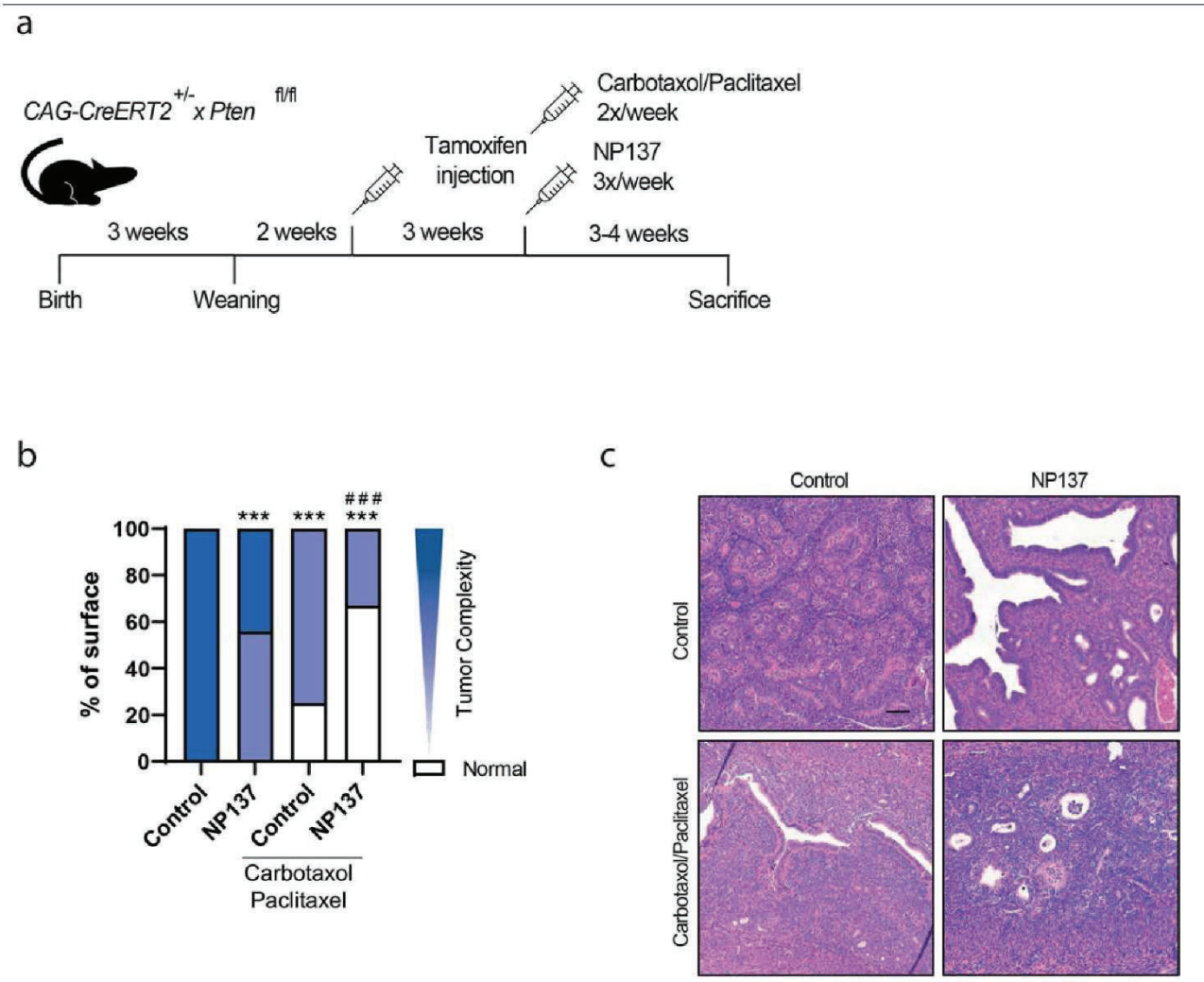

Extended Data Fig. 7 | Combining NP137 and chemotherapy in *Pten* mutant mice. a, Diagram showing the experimental strategy to combine NP137 (10 mg/Kg, I.P. 3x/week) and Carboplatin Paclitaxel (respectively 30 mg/Kg and 15 mg/Kg, I.P. 2x/week) treatments in CAG-CreERT2+/−*Pten* f/f mice. **b**, Quantification by pathologists of the endometrial lesions presented by tumor complexities (progressively darker color from normal through hyperplasia, slight EIN (Endometrial intraepithelial neoplasia), moderate EIN and to adenocarcinoma) between mice treated with control (n = 6) or NP137 Ab (n = 9) alone or in combination with Carboplatin and Paclitaxel (n = 4 and 6). $^{***}P < 0.001$ against control alone; $^{###}P < 0.001$ against control with chemotherapy by Chi-square test and Fischer's exact test. **c**, Representative H&E staining pictures of uterus from mice sacrificed in weeks 5-6 after tamoxifen injection, treated with control or NP137 alone or in combination with chemotherapy. Scale bar (represented by a line, 100 µm).

Extended Data Table 1 | Clinical data for 14 patients with endometrium carcinoma enrolled in NP137 trial

a

Best overall response rate, N (%)	PD :5 (35.7%) SD : 8 (57.1%) PR : 1 (7.1%) CR : 0
Median PFS, months [95% CI]	1.7 [1.0-2.8]
Median OS, months [95% CI]	8.2 [4.2-22.0]

b

		Size (mm)	
		Baseline	6 months
Measurable target lesions	Liver - Segment 3	32	18
	Liver - Segment 1	54	21
	Total size	86	39
	Target lesion response	/	**-54,65%**
Non measurable lesions	Other lesions <10 mm Hepatic micronodules	Present	SD
	Overall response		**PR**

a, Median progression-free survival (mPFS) and overall survival (mOS) are presented with their 95% confidence interval (95% CI). Best overall response is also presented. N: number of patients. **b**, Table resuming target lesion size evolution and non-target lesions from baseline to 6 months of patient no. 02.004. PR indicates partial response, SD indicates stable disease as per RECIST V1.1. PR was identified both by investigator review and by centralized review.

Extended Data Table 2 | Hallmark pathway analysis extracted from scRNAseq from patient 01-040

pathway	T.statistic	p.value	FDR	median.C1D1	median.C3D1
HALLMARK_EPITHELIAL_MESENCHYMAL_TRANSITION	15,08621283	7,7691E-49	3,88455E-47	2859,902814	2557,333021
HALLMARK_KRAS_SIGNALING_UP	10,89278853	7,14057E-27	3,49888E-25	1964,753409	1794,200713
HALLMARK_INFLAMMATORY_RESPONSE	10,86867076	9,87281E-27	4,73895E-25	1748,2871	1514,957989
HALLMARK_ALLOGRAFT_REJECTION	7,727578737	1,79802E-14	8,4507E-13	1988,78895	1846,142848
HALLMARK_TNFA_SIGNALING_VIA_NFKB	7,261371738	5,64195E-13	2,5953E-11	4660,642594	4176,946452
HALLMARK_ANGIOGENESIS	6,444807669	1,50205E-10	6,75921E-09	2234,136723	2027,01566
HALLMARK_MYC_TARGETS_V2	-5,762236091	1,00073E-08	4,40322E-07	2435,810357	2918,108381
HALLMARK_MITOTIC_SPINDLE	-5,691385213	1,49558E-08	6,43098E-07	1967,153804	2686,27385
HALLMARK_PANCREAS_BETA_CELLS	3,908516549	9,64992E-05	0,004052967	417,0240287	316,1166428
HALLMARK_HYPOXIA	3,68650822	0,000234468	0,009613172	3491,409812	3428,984276
HALLMARK_BILE_ACID_METABOLISM	-3,665707628	0,000254695	0,01018782	1829,33146	1961,188447
HALLMARK_COAGULATION	3,335588755	0,000869041	0,033892592	1912,342637	1928,992864
HALLMARK_HEME_METABOLISM	-3,148627486	0,00167075	0,063488493	3238,711742	3721,44776
HALLMARK_INTERFERON_ALPHA_RESPONSE	-3,049864557	0,002327889	0,086131899	3283,54901	3399,451987
HALLMARK_G2M_CHECKPOINT	-2,895796658	0,003831532	0,137935156	2416,049593	2915,670354
HALLMARK_APICAL_JUNCTION	-2,7458895	0,006101202	0,213542077	1388,743328	1722,439069
HALLMARK_KRAS_SIGNALING_DN	2,560282242	0,01055679	0,358930856	-680,7552326	-743,5768364
HALLMARK_PROTEIN_SECRETION	-2,559256895	0,010584129	0,358930856	5640,040155	6385,182383
HALLMARK_PI3K_AKT_MTOR_SIGNALING	-2,501366309	0,012469304	0,399017725	4085,874566	4583,800494
HALLMARK_APICAL_SURFACE	2,176379847	0,029671998	0,91983194	407,1181967	342,6951173
HALLMARK_IL2_STAT5_SIGNALING	2,138112955	0,032646389	0,979391673	3210,59177	3238,777366
HALLMARK_DNA_REPAIR	-2,011303269	0,044466347	1	3609,740607	4182,659808
HALLMARK_NOTCH_SIGNALING	-1,983413577	0,047494329	1	4615,924184	4735,280098
HALLMARK_E2F_TARGETS	-1,861119401	0,062907858	1	2075,635658	2485,895883
HALLMARK_PEROXISOME	-1,817000553	0,069403277	1	3830,402183	4120,63062
HALLMARK_WNT_BETA_CATENIN_SIGNALING	-1,79657145	0,072589624	1	2495,438483	2678,364175
HALLMARK_HEDGEHOG_SIGNALING	-1,763951214	0,077927896	1	624,2516919	874,6034634
HALLMARK_ESTROGEN_RESPONSE_LATE	1,599309062	0,109939184	1	2778,941336	2955,905109
HALLMARK_MYC_TARGETS_V1	-1,489702157	0,136504994	1	8104,536916	8660,058067
HALLMARK_COMPLEMENT	1,487900137	0,1369674	1	2819,288032	2858,325699
HALLMARK_UV_RESPONSE_DN	1,437041114	0,150891191	1	3963,290338	4062,005117
HALLMARK_CHOLESTEROL_HOMEOSTASIS	1,36964528	0,170985619	1	4164,265273	4241,65484
HALLMARK_UNFOLDED_PROTEIN_RESPONSE	-1,27101671	0,203912824	1	5554,678569	5975,614936
HALLMARK_ADIPOGENESIS	-1,196030358	0,231866591	1	4444,980124	4787,913311
HALLMARK_UV_RESPONSE_UP	-1,130703414	0,258348119	1	3885,115301	4208,768301
HALLMARK_XENOBIOTIC_METABOLISM	1,092745793	0,274668132	1	2698,064155	2839,495429
HALLMARK_P53_PATHWAY	-1,049052977	0,294310361	1	3513,341061	3869,132798
HALLMARK_IL6_JAK_STAT3_SIGNALING	1,048127475	0,294730604	1	1592,320532	1657,30633
HALLMARK_FATTY_ACID_METABOLISM	-0,892365818	0,372333035	1	4214,532636	4498,848537
HALLMARK_INTERFERON_GAMMA_RESPONSE	-0,744997223	0,456382113	1	2485,390169	2570,751791
HALLMARK_TGF_BETA_SIGNALING	0,655666664	0,512130741	1	4499,397448	4706,518817
HALLMARK_ANDROGEN_RESPONSE	-0,595282072	0,551736373	1	4940,313557	5249,51218
HALLMARK_APOPTOSIS	0,557575735	0,577209601	1	4378,02934	4634,20245
HALLMARK_GLYCOLYSIS	0,506499357	0,61257711	1	3717,259012	3914,032958
HALLMARK_ESTROGEN_RESPONSE_EARLY	0,44574339	0,655840074	1	2326,192775	2490,176471
HALLMARK_REACTIVE_OXYGEN_SPECIES_PATHWAY	-0,421770238	0,673250846	1	4398,035752	4741,20996
HALLMARK_SPERMATOGENESIS	-0,413693015	0,679151806	1	977,4039552	999,3609945
HALLMARK_MYOGENESIS	0,384453151	0,700690142	1	689,0137412	806,2674031
HALLMARK_OXIDATIVE_PHOSPHORYLATION	0,303810274	0,761313569	1	7776,322168	8210,789505
HALLMARK_MTORC1_SIGNALING	-0,256105086	0,797902561	1	5385,150948	5751,43224

Table presenting a gene set enrichment between C3D1 and C1D1 tumoral cluster cell for all the hallmark gene sets. – Note that HALLMARK_EPITHELIAL_MESENCHYMAL_TRANSITION is the strongest enriched pathway (two-sided student test).

Article

Pharmacological targeting of netrin-1 inhibits EMT in cancer

https://doi.org/10.1038/s41586-023-06372-2

Received: 4 April 2022

Accepted: 26 June 2023

Published online: 02 August 2023

Check for updates

Justine Lengrand[1,2,3,13], Ievgenia Pastushenko[1,13], Sebastiaan Vanuytven[4,5,13], Yura Song[1], David Venet[6], Rahul M. Sarate[1], Melanie Bellina[2,3], Virginie Moers[1], Alice Boinet[1], Alejandro Sifrim[5,7], Nicolas Rama[3], Benjamin Ducarouge[2], Jens Van Herck[4], Christine Dubois[1], Samuel Scozzaro[1], Sophie Lemaire[1], Sarah Gieskes[1], Sophie Bonni[1], Amandine Collin[8], Nicolas Braissand[2,3], Justine Allard[8], Egor Zindy[8], Christine Decaestecker[8,9], Christos Sotiriou[6], Isabelle Salmon[8,10,11], Patrick Mehlen[2,3]✉, Thierry Voet[4,7], Agnès Bernet[2,3]✉ & Cédric Blanpain[1,12]✉

Epithelial-to-mesenchymal transition (EMT) regulates tumour initiation, progression, metastasis and resistance to anti-cancer therapy[1–7]. Although great progress has been made in understanding the role of EMT and its regulatory mechanisms in cancer, no therapeutic strategy to pharmacologically target EMT has been identified. Here we found that netrin-1 is upregulated in a primary mouse model of skin squamous cell carcinoma (SCC) exhibiting spontaneous EMT. Pharmacological inhibition of netrin-1 by administration of NP137, a netrin-1-blocking monoclonal antibody currently used in clinical trials in human cancer (ClinicalTrials.gov identifier NCT02977195), decreased the proportion of EMT tumour cells in skin SCC, decreased the number of metastases and increased the sensitivity of tumour cells to chemotherapy. Single-cell RNA sequencing revealed the presence of different EMT states, including epithelial, early and late hybrid EMT, and full EMT states, in control SCC. By contrast, administration of NP137 prevented the progression of cancer cells towards a late EMT state and sustained tumour epithelial states. Short hairpin RNA knockdown of netrin-1 and its receptor UNC5B in EPCAM$^+$ tumour cells inhibited EMT in vitro in the absence of stromal cells and regulated a common gene signature that promotes tumour epithelial state and restricts EMT. To assess the relevance of these findings to human cancers, we treated mice transplanted with the A549 human cancer cell line—which undergoes EMT following TGFβ1 administration[8,9]—with NP137. Netrin-1 inhibition decreased EMT in these transplanted A549 cells. Together, our results identify a pharmacological strategy for targeting EMT in cancer, opening up novel therapeutic interventions for anti-cancer therapy.

Tumour cells lose their epithelial characteristics and acquire mesenchymal features via EMT. This process is a key driver of tumour heterogeneity and has been associated with tumour initiation, progression, metastasis and resistance to chemotherapy or immunotherapy[2,4–7,10,11]. Although substantial progress has been made towards understanding the role and the mechanisms by which EMT regulates these various aspects of cancer, there are still very few non-genetic pharmacological interventions that enable the inhibition of EMT in primary tumours, decrease their metastatic potential or potentiate the response to anti-cancer therapy.

Netrin-1 is expressed in EMT skin SCC

To identify novel therapeutic strategies that can inhibit EMT, we searched RNA-sequencing (RNA-seq) data from epithelial and mesenchymal tumour cells isolated from a model of SCC in mouse that presented spontaneous EMT[12–14] (*Lgr5-cre^{ER};Kras^{G12D};Trp53^{cKO};Rosa-YFP* (LKPR)) for secreted factors preferentially expressed by mesenchymal EPCAM$^-$ tumour cells compared with epithelial EPCAM$^+$ tumour cells and for which specific therapy targeting the factor was available and currently administered for cancer in humans. We found that the

[1]Laboratory of Stem Cells and Cancer, Université Libre de Bruxelles (ULB), Brussels, Belgium. [2]NETRIS Pharma, Lyon, France. [3]Laboratory Apoptosis, Cancer and Development, Equipe labellisee 'La Ligue', LabEx DEVweCAN, Institute PLAsCAN, Centre de Recherche en Cancérologie de Lyon, INSERM U1052-CNRS UMR5286, Lyon, France. [4]Department of Human Genetics, University of Leuven, KU Leuven, Leuven, Belgium. [5]Laboratory of Multi-omic Integrative Bioinformatics, Center for Human Genetics, KU Leuven, Leuven, Belgium. [6]Laboratory of Breast Cancer Translational Research J.-C. Heuson, Institut Jules Bordet, Hôpital Universitaire de Bruxelles (H.U.B), Université Libre de Bruxelles (ULB), Brussels, Belgium. [7]KU Leuven Institute for Single-cell Omics, KU Leuven, Leuven, Belgium. [8]DIAPath, Center for Microscopy and Molecular Imaging, Université Libre de Bruxelles (ULB), Jumet, Belgium. [9]Laboratory of Image Synthesis and Analysis, Ecole Polytechnique-Université libre de Bruxelles (EPB-ULB), Gosselies, Belgium. [10]Centre Universitaire Inter Régional d'Expertise en Anatomie pathologique Hospitalière (CurePath), Brussels, Belgium. [11]Department of Pathology, Erasme University Hospital, Université Libre de Bruxelles (ULB), Brussels, Belgium. [12]WEL (Wallon ExceLlence) Research Institute, Université Libre de Bruxelles (ULB), Brussels, Belgium. [13]These authors contributed equally: Justine Lengrand, Ievgenia Pastushenko, Sebastiaan Vanuytven. ✉e-mail: patrick.mehlen@lyon.unicancer.fr; agnes.bernet@lyon.unicancer.fr; cedric.blanpain@ulb.be

genes encoding netrin-1 (*Ntn1*) and its receptor UNC5B (*Unc5b*) were overexpressed in EPCAM$^-$ EMT tumour cells compared with EPCAM$^+$ epithelial tumour cells (Fig. 1a,b). Netrin-1 has been shown to regulate tumour progression in multiple cancer models by preventing apoptosis of tumour cells, promoting neoangiogenesis and controlling the pro-tumorigenic cancer-associated function of fibroblasts[15,26]. The therapeutic netrin-1-blocking antibody NP137 is currently being tested in clinical trials for treatment of cancer (ClinicalTrials.gov identifier: NCT02977195).

Netrin-1 overexpression increases EMT

To assess whether netrin-1 promotes EMT, we first overexpressed human netrin-1 in LKPR mice to produce LKPR-NTN1 mice (*Lgr5-cre^{ER};Kras^{G12D};Trp53^{cKO};Rosa-YFP;Rosa-NTN1*) (Extended Data Fig. 1a–c). Following netrin-1 overexpression, we observed an increase in the number of tumours per mouse (Fig. 1c) and the proportion of tumour cells that underwent EMT compared with control mice (Fig. 1d and Extended Data Fig. 1d). As reported previously, EMT is not a binary process—it occurs in a stepwise manner via intermediate EMT states[3,6,7,14,27–29]. Using histological analysis and immunofluorescence, we assessed the effects of netrin-1 overexpression on the different tumour states previously described in this model[14], including epithelial (KRT14$^+$VIM$^-$), hybrid EMT (KRT14$^+$VIM$^+$) and late EMT (KRT14$^-$VIM$^+$). Immunostaining revealed that control skin SCCs were heterogeneous: 20% were epithelial (KRT14$^+$VIM$^-$), 35% exhibited hybrid EMT (KRT14$^+$VIM$^+$) and 45% exhibited full EMT (KRT14$^-$VIM$^+$) (Fig. 1e,f). By contrast, overexpression of netrin-1 led to a significant increase in the proportion of tumours with full EMT (70%) and a decrease in SCCs with epithelial phenotype (3%) (Fig. 1e,f), in good accordance with the quantification of EPCAM expression by fluorescence-activated cell sorting (FACS) (Fig. 1d). These data demonstrate that overexpression of netrin-1 promotes tumour initiation and EMT in a primary model of skin SCC.

Targeting netrin-1 inhibits EMT

Previous in vitro studies have reported upregulation of netrin-1 in several cancers exhibiting EMT[30–33]; however, to our knowledge, the effect of pharmacological inhibition of netrin-1 on EMT in vivo has not been investigated. To assess whether pharmacological inhibition of netrin-1 inhibits EMT, we treated LKPR mice with NP137 four weeks after tamoxifen administration and determined the effect of netrin-1 inhibition on tumour formation and EMT (Extended Data Fig. 1e). NP137 administration three times per week led to a decrease of 50% in the number of SCCs per mouse (Fig. 1g). FACS quantification of the percentage of YFP$^+$EPCAM$^+$ (epithelial) tumour cells and YFP$^+$EPCAM$^-$ tumour cells (those that had been through EMT) showed that NP137 administration decreased the proportion of EPCAM$^-$ tumour cells that underwent EMT (41% in NP137-treated versus 77% in control mice) in primary skin SCCs presenting spontaneous EMT, showing that in the LKPR mouse model, pharmacological targeting of netrin-1 inhibits EMT (Fig. 1h). To determine whether netrin-1 inhibition differentially affects the different EMT states, we used immunofluorescence to assess the proportions of tumour states. NP137 administration increased the proportion of the epithelial state (54% in NP137-treated mice versus 31% in control mice), whereas the proportion of hybrid EMT was unchanged (16% in NP137-treated mice versus 12% in control mice) and the proportion of the late EMT state was decreased (30% in NP137-treated mice versus 56% in control mice) (Fig. 1i,j). These data demonstrate that pharmacological targeting of netrin-1 inhibits EMT in a mouse model of cancer.

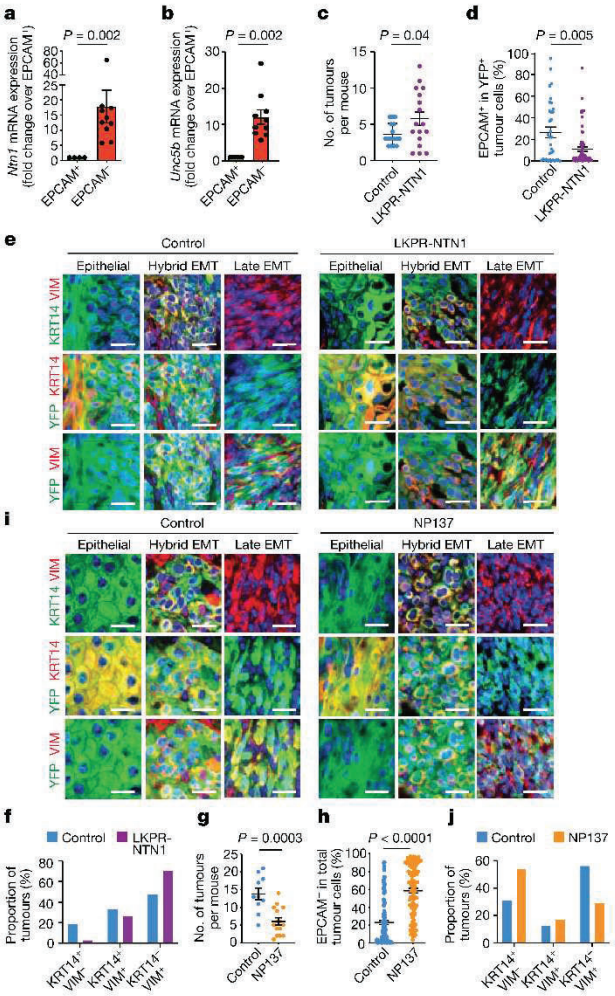

Fig. 1 | Targeting netrin-1 inhibits EMT. a,b, Relative mRNA expression of *Ntn1* (**a**) and *Unc5b* (**b**) in EPCAM$^-$ ($n = 4$) and EPCAM$^-$ ($n = 10$) tumour cells determined by quantitative real-time PCR. Data are mean ± s.e.m., normalized to the *Tbp* gene. Two-tailed Mann–Whitney *U* test. **c**, Dot plot showing the number of tumours in control LKPR ($n = 16$) and LKPR-NTN1 ($n = 17$) mice. Data are mean ± s.e.m. Two-tailed *t*-test. **d**, The proportion of EPCAM$^+$ tumour cells in control LKPR ($n = 34$ tumours from 16 mice) and LKPR-NTN1 ($n = 70$ tumours from 17 mice). Data are mean ± s.e.m. Two-tailed *t*-test. **e**, Co-immunostaining of YFP and KRT14 or vimentin (VIM) in primary control and LKPR-NTN1 tumours ($n = 21$ tumours from 11 control LKPR mice and $n = 34$ tumours from 9 LKPR-NTN1 mice). Scale bars, 20 µm. **f**, The percentage of tumours with epithelial (KRT14$^+$VIM$^-$), hybrid EMT (KRT14$^+$VIM$^+$) and full EMT (KRT14$^-$VIM$^+$) phenotypes ($n = 21$ tumours from 11 control LKPR mice and $n = 34$ tumours from 9 LKPR-NTN1 mice). **g**, Dot plot showing the number of tumours in control ($n = 10$) and NP137-treated ($n = 15$) LKPR mice. Data are mean ± s.e.m. Two-tailed *t*-test. **h**, The proportion of EPCAM$^+$ tumour cells in skin SCC of control ($n = 148$ tumours from 20 mice) and NP137-treated ($n = 117$ tumours from 16 mice) LKPR mice. Data are mean ± s.e.m. Two-tailed *t*-test. **i**, Co-immunostaining of YFP and KRT14 or vimentin in control and NP137-treated skin SCC from LKPR mice ($n = 32$ tumours from 10 control mice and $n = 24$ NP137-treated SCCs from 9 mice). Scale bars, 20 µm. **j**, The percentage of tumours exhibiting epithelial (KRT14$^+$VIM$^-$), hybrid EMT (KRT14$^+$VIM$^+$) and full EMT (KRT14$^-$VIM$^+$) phenotypes ($n = 32$ tumours from 10 control mice and $n = 24$ NP137-treated SCCs from 9 mice).

Targeting netrin-1 inhibits metastasis

EMT has been shown to have an important role in metastasis formation in different mouse models and is associated with resistance to anti-cancer therapy[1,4–6,10,11,34]. We assessed whether pharmacological inhibition of netrin-1 in LKPR mice decreased the formation of primary metastases. NP137 administration strongly decreased the number

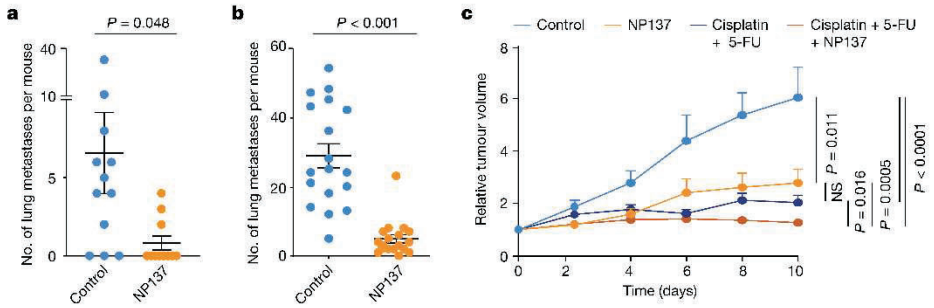

Fig. 2 | Targeting netrin-1 reduces metastasis and sensitizes tumour cells to chemotherapy in skin SCC. a, Dot plot showing the number of spontaneous lung metastases in control ($n = 12$) and NP137-treated ($n = 11$) mice with skin SCC. Data are mean ± s.e.m. Two-tailed t-test. **b**, Dot plot showing the number of lung metastases arising from the intravenous injection of 1,000 EPCAM$^-$ tumour cells ($n = 18$ control-injected mice and $n = 18$ NP137-injected mice). Data are mean ± s.e.m. Two-tailed t-test. **c**, Relative tumour volume over time of control tumours ($n = 29$ from 5 mice) or tumours following therapy with cisplatin plus 5-FU ($n = 58$ from 8 mice), anti-netrin-1 antibody ($n = 29$ from 5 mice) or combined of cisplatin plus 5-FU and anti-netrin-1 ($n = 59$ from 8 mice). Data are mean + s.e.m. Two-tailed t-test. Tumour volumes were normalized to the tumour volume on the first day of chemotherapy.

of lung metastases in LKPR mice (Fig. 2a), suggesting that netrin-1 is important for the formation of spontaneous lung metastases. As the number of tumours was lower in LKPR mice treated with NP137, it is possible that the reduction in the number of lung metastases was a consequence of the reduced number of tumours. To clarify this point, we injected YFP$^+$ tumour cells intravenously and assessed the number of lung metastases following pharmacological netrin-1 inhibition. NP137 administration strongly decreased the number of lung metastases following tail vein injection of FACS-isolated YFP$^+$ tumour cells from LKPR mice, demonstrating that netrin-1 inhibition directly inhibits metastasis formation (Fig. 2b).

NP137 sensitizes cancer cells to chemotherapy

EMT has been shown to promote resistance to chemotherapy in skin SCC[2,35]. To assess whether pharmacological targeting of netrin-1 can sensitize tumour cells to chemotherapy, we treated mice with cisplatin and 5-fluoracil (5-FU), a standard chemotherapy for the treatment of human SCCs[36,37] and assessed the effect of netrin-1 inhibition on the response to chemotherapy. The combination of NP137 with cisplatin and 5-FU significantly potentiated the effect of cisplatin and 5-FU on the inhibition of tumour growth in primary SCCs from LKPR mice (Fig. 2c). These data demonstrate that pharmacological targeting of netrin-1 can decrease cancer traits associated with EMT, including metastasis and resistance to therapy.

Effect of NP137 on stromal cells

To assess comprehensively the effect of netrin-1 inhibition on the different EMT tumour states and the composition of the tumour stroma, we performed single-cell RNA-seq (scRNA-seq) (10x Genomics Chromium) analysis of tumour cells and their associated stromal cells in two control and two NP137-treated primary skin SCCs. Unsupervised clustering revealed the presence of different cell populations in primary skin SCCs (Extended Data Fig. 2), including tumour cells (*Epcam*$^+$*Yfp*$^+$) (Extended Data Fig. 3a,b), immune cells (marked by CD45 (also known as *Ptprc*) coexpression with *Cd86* (myeloid cells), *Cxcr2* (neutrophils) and *Cd3d* (T cells)), cancer-associated fibroblasts (CAFs) (*Acta2*$^+$*Pdgfra*$^+$*Yfp*$^-$) and endothelial cells (*Pecam1*$^+$) (Extended Data Fig. 3c,d). This clustering reveals that *Ntn1* is expressed in EMT tumour cells and CAFs in skin SCC with spontaneous EMT from LKPR mice (Extended Data Fig. 3e).

After integration of the tumour microenvironment across conditions, we observed that NP137 administration decreased the proportion of tumour cells and changed the composition of the tumour stroma, with a relative increase in the proportion of CAFs (Extended Data Fig. 4a–d). Using single-cell compositional data analysis (scCODA) to perform differential abundance analysis, we found no significant difference in the proportions of the different CAF clusters—three myofibroblastic CAFs (myCAF) clusters, two immune (iCAF) clusters and proliferative and glycolysis CAF clusters—or in gene expression within these clusters between two control and two NP137-treated mice (Extended Data Fig. 4e–h). Immunostaining analyses confirmed the relative increase of CAFs following NP137 administration (Extended Data Fig. 4i).

Effect of NP137 on tumour cell states

To assess more specifically the effect of netrin-1 inhibition on tumour states, we clustered YFP$^+$ tumour cells of control and NP137-treated mice at higher resolution (Fig. 3a,b). In control tumours, we identified clusters corresponding to distinct EMT cell states ranging from epithelial (*Epcam*$^+$*Krt14*$^+$*Vim*$^-$), early hybrid EMT (*Epcam*$^-$*Krt14*$^+$*Vim*$^+$), late hybrid EMT (*Epcam*$^-$*Krt14*$^-$*Krt8*$^+$*Vim*$^+$*Pdgfra*$^-$) and late EMT (*Epcam*$^-$*Krt14*$^-$*Krt8*$^-$*Vim*$^+$*Pdgfra*$^+$) (Fig. 3a and Extended Data Fig. 5a). NP137 administration was associated with an increase in the proportion of the epithelial tumour cell state, a similar proportion of early EMT, a decreased proportion of late hybrid EMT and a strong decrease in late EMT compared with the control (Fig. 3b,c and Extended Data Fig. 5b,c). In situ immunofluorescence for KRT14, VIM, KRT8 and PGFRA confirmed the increase in epithelial states and the decrease in late EMT tumour states following NP137 administration (Fig. 3d).

Spatial transcriptomic analysis using 10x Visium revealed the spatial localization of the tumour states identified by scRNA-seq and showed that they were localized in distinct niches, as previously reported[14]. NP137 administration increased the proportion of the epithelial state (*Epcam*$^+$*Krt14*$^+$) and inhibited the occurrence of the late EMT state (*Krt14*$^-$*Krt8*$^-$*Vim*$^+$), blocking EMT progression at the hybrid EMT state (*Krt8*$^+$*Vim*$^+$) (Fig. 3e,f and Extended Data Fig. 6).

To further understand the mechanisms and signalling pathways by which NP137 administration regulates EMT, we performed pathway analyses using MSigDB Hallmark gene sets[38] on the scRNA-seq data. These analyses revealed that the expression of genes associated with EMT, hypoxia, angiogenesis and inflammatory response were all significantly decreased in tumour cells following netrin-1 inhibition (Fig. 3g).

Lineage trajectory analysis revealed that two distinct lineage trajectories could be identified in the control tumour, with a trajectory going from epithelial cells towards hybrid EMT and another trajectory going from the epithelial state towards the late full EMT state (Fig. 4a). NP137-treated tumour cells were characterized by different lineage trajectories, with the disappearance of a trajectory toward the late EMT state expressing a high level of *Aqp1* and the appearance of two new

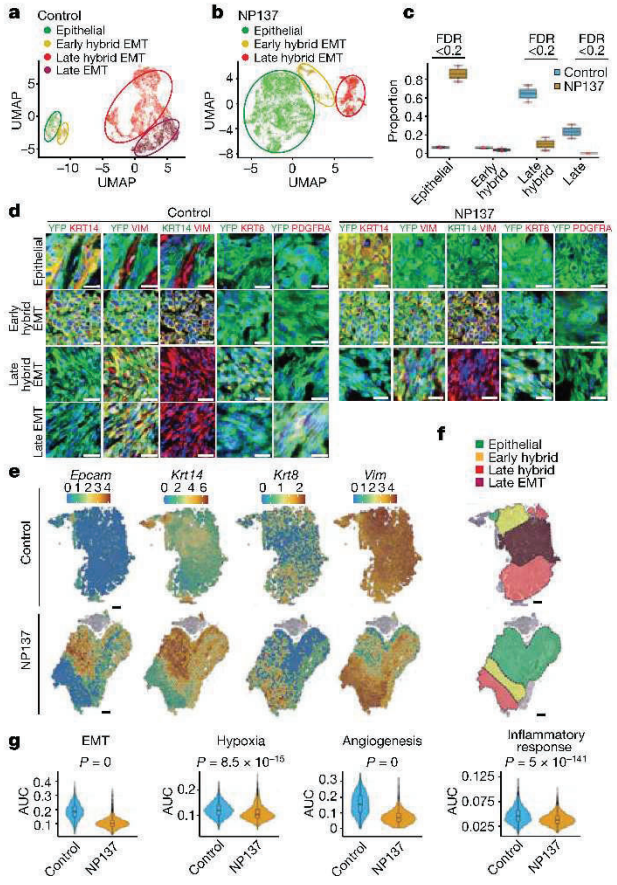

Fig. 3 | Pharmacological inhibition of netrin-1 inhibits late EMT and promotes epithelial tumour states. a,**b**, Uniform manifold approximation and projection (UMAP) plots coloured by EMT state for control (**a**) and NP137-treated (**b**) YFP$^+$ tumour cells from skin SCC. Colours represent the different tumour states. **c**, Box plot depicting the proportion of tumour states for the four samples in control and NP137-treated conditions. Significant changes in proportion are defined as false discovery rate (FDR) <0.2. **d**, Co-immunostaining of YFP and KRT14, KRT8, vimentin and PDGFRA in control (left) and anti-netrin-1 treated (right) skin SCC from LKPR mice, defining areas with different degrees of EMT ($n = 3$ control tumours and $n = 3$ NP137-treated tumours). Scale bars, 20 µm. **e**, Spatial transcriptomics using 10x Visium was conducted on tumour sections of control and NP137-treated mice. Normalized gene expression values are represented as a colour gradient. **f**, Summary of the different areas presenting different tumour states based on the expression of *Epcam*, *Krt14*, *Krt8* and *Vim*: epithelial, *Epcam*$^+$*Krt14*$^+$*Vim*$^-$; early hybrid EMT, *Epcam*$^-$*Krt14*$^+$*Vim*$^+$; late hybrid EMT, *Epcam*$^-$*Krt14*$^-$*Krt8*$^+$*Vim*$^+$; late full EMT, *Epcam*$^-$*Krt14*$^-$*Krt8*$^-$*Vim*$^+$. **g**, Combined box plot and violin plot showing the activity of 4 MSigDB[38] hallmark gene sets (epithelial-to-mesenchymal transition, hypoxia, angiogenesis and inflammatory response) in control ($n = 2$) and NP137-treated ($n = 2$) tumours. The area under the curve (AUC) indicates enrichment of the different hallmark gene sets in NP137-treated tumours relative to control tumours. Two-sided Wilcoxon rank-sum test with Bonferroni correction. In box plots, the centre line represents median, box edges delineate 25th and 75th percentiles and whiskers extend to 1.5 times the interquartile range (IQR).

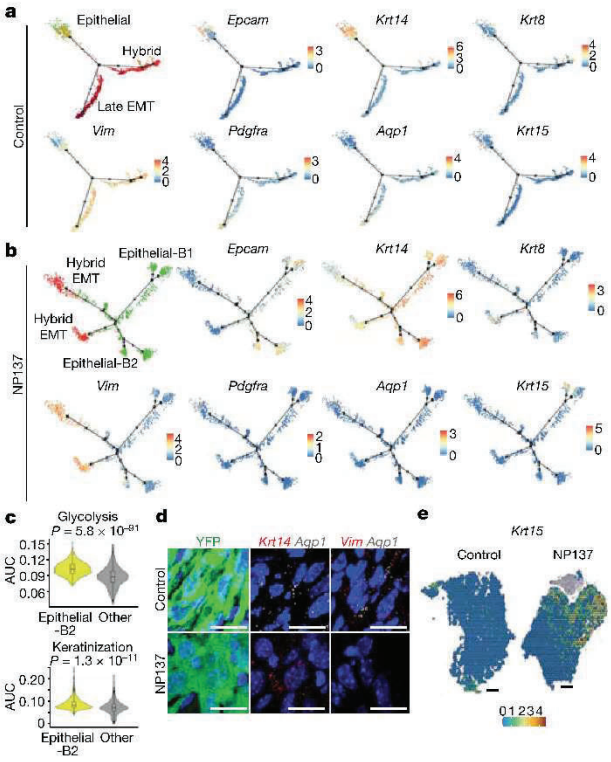

Fig. 4 | Pharmacological inhibition of netrin-1 inhibits late EMT and promotes epithelial differentiation trajectories of tumour cells. **a**,**b**, Pseudotemporal analysis using Monocle2 showing lineage trajectories in control skin SCC showing two EMT trajectories (hybrid and full (late) EMT trajectories) (**a**) and in NP137-treated skin SCC showing the absence of the late EMT trajectory and the appearance of new epithelial trajectories (**b**). Dots represent single cells. Green, epithelial; orange, early hybrid EMT; red, late hybrid EMT; dark red, late EMT. Gene expression is visualized as a colour gradient with blue indicating no expression and red indicating maximum expression. The two new branches detected in the NP137-treated trajectory are labelled epithelial-B1 and epithelial-B2. **c**, Combined box plot and violin plot showing the activity of glycolysis and keratinization gene sets in tumour cells belonging to the new epithelial state and other EMT states based on GO-term analysis in NP137-treated tumours ($n = 2$). The centre line represents median, box edges delineate 25th and 75th percentiles and whiskers extend to 1.5 times the IQR. Two-sided Wilcoxon rank-sum test with Bonferroni correction. **d**, Immunostaining for YFP and RNA in situ hybridization (RNAscope) for *Krt14*, *Vim* or *Aqp1* in control and NP137-treated skin SCCs from LKRP mice ($n = 2$ independent biological replicates). Scale bars, 20 µm. **e**, *Krt15* expression analysis using 10x Visium spatial transcriptomic analysis on tumour sections. Gene expression values are normalized in the control and treated sample and are visualized as a colour gradient. Scale bars, 500 µm.

trajectories towards epithelial states (epithelial-B1 and epithelial-B2), and two hybrid EMT trajectories (Fig. 4b). The epithelial-B1 state was characterized by high expression of *Krt15*, and gene ontology (GO) term enrichment analysis of marker genes of cells belonging to the epithelial-B2 state revealed an upregulation of glycolysis and increased keratinization (Fig. 4b,c).

In situ analysis using RNA fluorescence in situ hybridization and 10x Visium spatial transcriptomics on tumour sections of control and NP137-treated tumours showed a decrease of *Aqp1*-expressing cells (Fig. 4d) and an increase of tumour cells expressing *Krt15* following netrin-1 inhibition, confirming the inhibition of the late EMT trajectory and the increase of epithelial states following NP137 administration (Fig. 4e). Together, these data reveal that EMT is characterized by the presence of different EMT tumour states, with two different differentiation trajectories from the epithelial state towards distinct EMT states, and that pharmacological targeting of netrin-1 inhibits the switch of the epithelial state to the late EMT state and promotes tumour cell differentiation to the epithelial state.

The netrin-1–UNC5B axis promotes EMT

Netrin-1 has been proposed to have a pleiotropic role in cancer, including a cellular autonomous role in tumour proliferation and apoptosis, as well as having a non-cellular autonomous mechanism that regulates tumour growth by controlling tumour angiogenesis and CAF functions[15–26]. Our single-cell analysis shows that NP137 administration modulates the composition of the tumour microenvironment and the proportion of the different EMT tumour cell states. NP137 has been shown to specifically inhibit the interaction of netrin-1 with its receptor UNC5B[39]. To assess whether the regulation of EMT and the promotion of pro-epithelial states by NP137 administration is the consequence of a disruption of a paracrine or autocrine netrin-1–UNC5B signalling axis that directly regulates EMT states, we studied the effect of genetic knockdown of *Ntn1* and *Unc5b* on EMT states in a tumour cell-autonomous manner in vitro in the absence of the tumour microenvironment. EPCAM$^+$ tumour cells isolated by FACS from primary SCCs from LKPR mice and cultured in vitro progressively underwent EMT, as shown by the progressive loss of EPCAM expression by tumour cells (Fig. 5a), with an average of 60% of EPCAM$^+$ switching to become EPCAM$^-$ tumour cells over two weeks in culture. Notably, shRNA-mediated knockdown of *Ntn1* or *Unc5b* resulted in a strong decrease in the ability of EPCAM$^+$ tumour cells to switch to the EPCAM$^-$ EMT phenotype (Fig. 5a). Inhibition of EMT upon shRNA knockdown of *Ntn1* or *Unc5b* was accompanied by a decrease in cell migration that was not further enhanced by NP137 administration (Fig. 5b).

To assess the molecular mechanisms by which netrin-1 and UNC5B signalling regulate EMT, we performed bulk RNA-seq of EPCAM$^+$ tumour cells from control, *Ntn1*-KD and *Unc5b*-KD tumour cells cultured in vitro 6 days after plating of FACS-isolated EPCAM$^+$ tumour cells. More than 50% of the genes that were downregulated or upregulated following *Unc5b* knockdown were also differentially regulated by *Ntn1* knockdown (Fig. 5c), indicating that netrin-1 and UNC5B regulate a similar signalling pathway and transcriptional programme. Consistent with the results of single-cell RNA-seq following NP137 administration, *Ntn1* knockdown and *Unc5b* knockdown promoted the expression of genes associated with the epithelial state (*Krt14*, *Krt15* and involucrin and claudin) (Fig. 5d) and decreased the expression of genes associated with EMT and promoting EMT (*Aqp5*, *Nrp1*, *Nr2f2*, *Twist1* and *Twist2*) (Fig. 5e–g). Together, these data demonstrate that targeting the netrin-1–UNC5B signalling axis in tumour cells decreases EMT and promotes the epithelial state in skin SCC in a cellular autonomous manner independently of the tumour microenvironment.

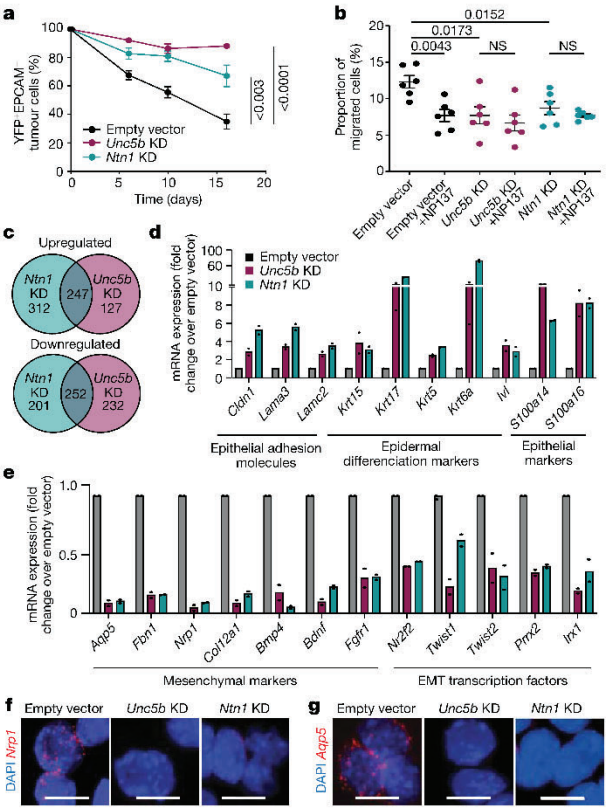

Fig. 5 | Netrin-1 and UNCnc5B knockdown inhibits EMT and promotes the epithelial state. a, EPCAM expression following in vitro culture of FACS-isolated primary EPCAM$^-$ tumour cells transduced with empty vector, or *Ntn1* or *Unc5b* shRNA knockdown (KD) ($n = 8$ independent replicates for empty vector, $n = 6$ independent replicates for *Unc5b* knockdown and $n = 3$ independent replicates for *Ntn1* knockdown). Data are mean ± s.e.m. Two-tailed *t*-test. **b**, The percentage of migrated EPCAM$^-$ cells from LKPR mice quantified by crystal violet staining ($n = 2$ independent replicates, 3 wells per condition). Data are mean ± s.e.m. Two-tailed Mann–Whitney *U* test. **c**, Venn diagram showing the overlap between upregulated and downregulated genes in *Ntn1*-KD and *Unc5b*-KD cell lines. **d**, mRNA expression of upregulated epithelial genes by RNA-seq of EPCAM$^+$ cells 6 days after plating of 100% EPCAM$^+$ tumour cells. Histograms represent mean; $n = 2$ for empty vector, *Ntn1*-KD and *Unc5b*-KD. **e**, mRNA expression of mesenchymal genes that are downregulated following *Ntn1* knockdown or *Unc5b* knockdown, determined by RNA-seq in EPCAM$^-$ cells 6 days after plating of 100% EPCAM$^+$ tumour cells. Histograms represent mean; $n = 2$. **f**,**g**, In situ hybridization (RNAscope) for *Nrp1* (**f**) and *Aqp5* (**g**) in empty vector control, *Ntn1*-KD and *Unc5B*-KD cell lines ($n = 2$ independent biological replicates). Scale bars, 20 µm.

NP137 prevents EMT in human cancer

To assess the human and clinical relevance of our findings, we first assessed the correlations between netrin-1 expression, UNC5B expression and the EMT signature in human non-small cell lung carcinoma (lung SCC and lung adenocarcinoma) and melanoma. We used several previously described human EMT signatures[11,38,40] and the gene expression dataset from the pan-TCGA (The Cancer Genome Atlas) version of lung SCC (LUSCC) (484 primary tumours), lung adenocarcinoma (LUAD) (510 primary tumours) and skin cutaneous melanoma (SKCM) (76 primary tumours and 367 metastases). Although netrin-1 expression was not strongly associated with the EMT score, there was a very good correlation between the expression of the netrin-1 receptor UNC5B and EMT scores for these three cancer types (Fig. 6a,b).

To assess the functional relevance of these data, we then assessed the effect of blocking netrin-1–UNC5B signalling on EMT in the A549 human non-small cell lung cancer (NSCLC) cell line, a commonly used human cancer cell line that can undergo EMT in a plastic manner upon TGFβ1 administration[8,9]. We treated A549 cells with recombinant TGFβ1 in vitro for 3 days, which promoted mesenchymal cell morphology, increased netrin-1 expression and promoted EMT as shown by the upregulation of vimentin and downregulation of E-cadherin expression (Fig. 6c,d). We next performed subcutaneous grafting of the A549 cells that underwent EMT into immunodeficient mice and administered NP137 every 2 days. Of note, immunostaining analysis revealed that NP137 significantly increased the number of tumour cells expressing high levels of epithelial marker E-cadherin (Fig. 6e,f), demonstrating that netrin-1 inhibition decreases EMT in human cancer cells in vivo. Treatment of Ishikawa cells—a human endometrial adenocarcinoma cell line—with NP137 following their transplantation into immunodeficient mice decreased tumour growth (Extended Data Fig. 7a) and resulted in an increase in epithelial gene expression (Extended Data Fig. 7b), further

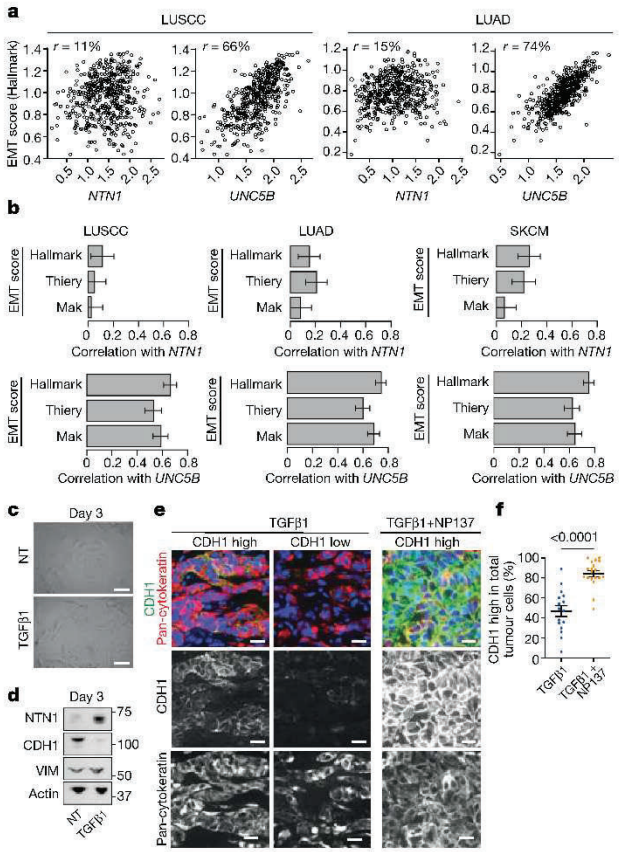

Fig. 6 | Anti-netrin-1 therapy inhibits EMT in human cancer cells. a, Scatter plots of *NTN1* and *UNC5B* expression versus Hallmark EMT signatures are shown for LUSCC ($n = 484$ primary tumours) and LUAD ($n = 510$ primary tumours) cancer types from the TCGA. Spearman correlations are shown at the top of each graph. **b**, Bar plots showing Spearman correlations between *NTN1*, *UNC5B* expression and three EMT signature scores[11,38,40] across LUSCC ($n = 484$ primary tumours), LUAD ($n = 510$ primary tumours) and SKCM ($n = 443$ tumours including 76 primary tumours and 367 metastases) cancer types from TCGA, with 95% confidence intervals (clipped at 0 for low correlations). To obtain EMT scores, the Hallmark signature was computed using single-sample Gene Set Enrichment Analysis[41] (ssGSEA) on genes from the HALLMARK_EPITHELIAL_MESENCHYMAL_TRANSITION signature, from MSigDB[38]; the Thiery signature was computed similarly using genes from ref. 11; the Mak signature was calculated from the gene sets in ref. 40 as the difference of two signatures: a mesenchymal signature defined as the mean of mesenchymal gene expression and an epithelial signature defined as the mean of epithelial gene expression. **c**, Microscopic appearance of A549 NSCLC cells, following no treatment or after 3 days of TGFβ1 treatment ($n = 3$). Scale bars, 20 µm. **d**, Western blot analysis of netrin-1, E-cadherin (CDH1) and vimentin expression in the A549 NSCLC cell line in control conditions or following 3 days of TGFβ1 treatment. **e**, Co-immunostaining of E-cadherin and pan-cytokeratin on tumours arising from subcutaneous grafting into immunodeficient mice of A549 cells pre-treated with TGFβ1 in vitro for 6 days. The mice were treated with physiologic serum or NP137 for 25 days and the tumours were collected for histological analysis. Scale bars, 20 µm. **f**, Tumour cells expressing high levels of E-cadherin as a percentage of pan-cytokeratin-positive tumour cells (each dot represents the mean of E-cadherin-high cells in 4 representative areas from each tumour; $n = 6$ control tumours and $n = 6$ NP137-treated tumours). Data are mean ± s.e.m. Two-tailed *t*-test.

demonstrating that targeting netrin-1 inhibits EMT. Consistent with the decrease of EMT induced by netrin-1 inhibition, NP137 administration decreased migration of these cells in vitro (Extended Data Fig. 7c).

Discussion

Our study demonstrates that pharmacological targeting of netrin-1 using NP137—a netrin-1-blocking monoclonal antibody currently being tested in phase II clinical trials for the treatment of different solid tumours—is a safe and effective strategy for targeting EMT in primary mouse and human tumours, decreasing lung metastasis and increasing the response of tumour cells to chemotherapy.

Our bioinformatic analysis of scRNA-seq data following netrin-1 inhibition combined with in situ characterization reveals the molecular mechanisms by which netrin-1 regulates EMT and promotes a late EMT differentiation trajectory. Inhibition of netrin-1 induces a switch in the lineage differentiation of tumour cells that redirects the tumour differentiation towards an epithelial tumour state that is more sensitive to chemotherapy and less prone to give rise to metastasis. Netrin-1 exerts its pro-EMT function by signalling to UNC5B, which promotes the expression of a mesenchymal transcriptional programme and downregulates the expression of genes controlling cell–cell adhesion and promoting the epithelial differentiation programme. The sensitization of tumour cells to chemotherapy following NP137 administration suggests that the combination of anti-netrin-1 antibody with other anti-cancer drugs might be beneficial for patients with cancer exhibiting EMT features.

We have also demonstrated the human relevance of pharmacologically targeting EMT following treatment with netrin-1-blocking antibody using a human lung cancer cell line and an endometrial adenocarcinoma line that presents EMT plasticity, demonstrating that pharmacological inhibition of EMT can be achieved in human cancers in vivo in pre-clinical settings.

In sum, our study provides a proof-of-principle that pharmacological targeting of EMT in a mouse model of primary cancer and in human cancers is possible. These results have important implications for the development of strategies for anti-cancer therapy combining netrin-1 inhibition in patients with cancer exhibiting EMT and for the development of novel biomarkers that will help to better stratify cases of cancer to identify those that are more likely to respond to anti-netrin-1 therapy.

Online content

Any methods, additional references, Nature Portfolio reporting summaries, source data, extended data, supplementary information, acknowledgements, peer review information; details of author contributions and competing interests; and statements of data and code availability are available at https://doi.org/10.1038/s41586-023-06372-2.

1. Ye, X. & Weinberg, R. A. Epithelial-mesenchymal plasticity: a central regulator of cancer progression. *Trends Cell Biol.* **25**, 675–686 (2015).
2. Shibue, T. & Weinberg, R. A. EMT, CSCs, and drug resistance: the mechanistic link and clinical implications. *Nat. Rev. Clin. Oncol.* **14**, 611–629 (2017).
3. Lambert, A. W. & Weinberg, R. A. Linking EMT programmes to normal and neoplastic epithelial stem cells. *Nat Rev. Cancer* **21**, 325–338 (2021).
4. Puisieux, A., Brabletz, T. & Caramel, J. Oncogenic roles of EMT-inducing transcription factors. *Nat. Cell. Biol.* **16**, 488–494 (2014).
5. Brabletz, S., Schuhwerk, H., Brabletz, T. & Stemmler, M. P. Dynamic EMT: a multi-tool for tumor progression. *EMBO J.* **40**, e108647 (2021).
6. Pastushenko, I. & Blanpain, C. EMT transition states during tumor progression and metastasis. *Trends Cell Biol.* **29**, 212–226 (2019).
7. Nieto, M. A., Huang, R. Y., Jackson, R. A. & Thiery, J. P. EMT: 2016. *Cell* **166**, 21–45 (2016).
8. Kasai, H., Allen, J. T., Mason, R. M., Kamimura, T. & Zhang, Z. TGF-β1 induces human alveolar epithelial to mesenchymal cell transition (EMT). *Respir Res.* **6**, 56 (2005).
9. Kim, J. H. et al. Transforming growth factor β1 induces epithelial-to-mesenchymal transition of A549 cells. *J. Korean Med. Sci.* **22**, 898–904 (2007).
10. Voon, D. C., Huang, R. Y., Jackson, R. A. & Thiery, J. P. The EMT spectrum and therapeutic opportunities. *Mol. Oncol.* **11**, 878–891 (2017).
11. Tan, T. Z. et al. Epithelial–mesenchymal transition spectrum quantification and its efficacy in deciphering survival and drug responses of cancer patients. *EMBO Mol. Med.* **6**, 1279–1293 (2014).
12. Lapouge, G. et al. Skin squamous cell carcinoma propagating cells increase with tumour progression and invasiveness. *EMBO J.* **31**, 4563–4575 (2012).
13. Latil, M. et al. Cell-type-specific chromatin states differentially prime squamous cell carcinoma tumor-initiating cells for epithelial to mesenchymal transition. *Cell Stem Cell* **20**, 191–204.e195 (2017).

14. Pastushenko, I. et al. Identification of the tumour transition states occurring during EMT. *Nature* **556**, 463–468 (2018).
15. Paradisi, A. et al. Combining chemotherapeutic agents and netrin-1 interference potentiates cancer cell death. *EMBO Mol. Med.* **5**, 1821–1834 (2013).
16. Paradisi, A. et al. Netrin-1 up-regulation in inflammatory bowel diseases is required for colorectal cancer progression. *Proc. Natl Acad. Sci. USA* **106**, 17146–17151 (2009).
17. Paradisi, A. et al. NF-κB regulates netrin-1 expression and affects the conditional tumor suppressive activity of the netrin-1 receptors. *Gastroenterology* **135**, 1248–1257 (2008).
18. Fitamant, J. et al. Netrin-1 expression confers a selective advantage for tumor cell survival in metastatic breast cancer. *Proc. Natl Acad. Sci. USA* **105**, 4850–4855 (2008).
19. Delloye-Bourgeois, C. et al. Netrin-1 acts as a survival factor for aggressive neuroblastoma. *J. Exp. Med.* **206**, 833–847 (2009).
20. Sung, P. J. et al. Cancer-associated fibroblasts produce netrin-1 to control cancer cell plasticity. *Cancer Res.* **79**, 3651–3661 (2019).
21. Park, K. W. et al. The axonal attractant Netrin-1 is an angiogenic factor. *Proc. Natl Acad. Sci. USA* **101**, 16210–16215 (2004).
22. Arakawa, H. Netrin-1 and its receptors in tumorigenesis. *Nat. Rev. Cancer* **4**, 978–987 (2004).
23. Brisset, M., Grandin, M., Bernet, A., Mehlen, P. & Hollande, F. Dependence receptors: new targets for cancer therapy. *EMBO Mol. Med.* **13**, e14495 (2021).
24. Hao, W. et al. The pan-cancer landscape of netrin family reveals potential oncogenic biomarkers. *Sci. Rep.* **10**, 5224 (2020).
25. Dumartin, L. et al. Netrin-1 mediates early events in pancreatic adenocarcinoma progression, acting on tumor and endothelial cells. *Gastroenterology* **138**, 1595–1606 (2010). 1606 e1591-1598.
26. Kefeli, U. et al. Netrin-1 in cancer: potential biomarker and therapeutic target? *Tumour Biol.* **39**, 1010428317698388 (2017).
27. Haerinck, J. & Berx, G. Partial EMT takes the lead in cancer metastasis. *Dev. Cell* **56**, 3174–3176 (2021).
28. Simeonov, K. P. et al. Single-cell lineage tracing of metastatic cancer reveals selection of hybrid EMT states. *Cancer Cell* **39**, 1150–1162.e1159 (2021).
29. Yang, J. et al. Guidelines and definitions for research on epithelial–mesenchymal transition. *Nat. Rev. Mol. Cell Biol.* **21**, 341–352 (2020).
30. Jin, X. et al. Netrin-1 interference potentiates epithelial-to-mesenchymal transition through the PI3K/AKT pathway under the hypoxic microenvironment conditions of non-small cell lung cancer. *Int. J. Oncol.* **54**, 1457–1465 (2019).
31. Zhang, X. et al. Netrin-1 elicits metastatic potential of non-small cell lung carcinoma cell by enhancing cell invasion, migration and vasculogenic mimicry via EMT induction. *Cancer Gene Ther.* **25**, 18–26 (2018).
32. Yan, W. et al. Netrin-1 induces epithelial-mesenchymal transition and promotes hepatocellular carcinoma invasiveness. *Dig. Dis. Sci.* **59**, 1213–1221 (2014).
33. Han, P. et al. Netrin-1 promotes cell migration and invasion by down-regulation of BVES expression in human hepatocellular carcinoma. *Am. J. Cancer Res.* **5**, 1396–1409 (2015).
34. Revenco, T. et al. Context dependency of epithelial-to-mesenchymal transition for metastasis. *Cell Rep.* **29**, 1458–1468.e1453 (2019).
35. DeConti, R. C. Chemotherapy of squamous cell carcinoma of the skin. *Semin. Oncol.* **39**, 145–149 (2012).
36. Khansur, T. & Kennedy, A. Cisplatin and 5-fluorouracil for advanced locoregional and metastatic squamous cell carcinoma of the skin. *Cancer* **67**, 2030–2032 (1991).
37. Chen, Q. Y. et al. miR-206 regulates cisplatin resistance and EMT in human lung adenocarcinoma cells partly by targeting MET. *Oncotarget* **7**, 24510–24526 (2016).
38. Liberzon, A. et al. The Molecular Signatures Database (MSigDB) hallmark gene set collection. *Cell Syst* **1**, 417–425 (2015).
39. Grandin, M. et al. Structural decoding of the Netrin-1/UNC5 interaction and its therapeutical implications in cancers. *Cancer Cell* **29**, 173–185 (2016).
40. Mak, M. P. et al. A patient-derived, pan-cancer EMT signature identifies global molecular alterations and immune target enrichment following epithelial-to-mesenchymal transition. *Clin. Cancer Res.* **22**, 609–620 (2016).
41. Subramanian, A. et al. Gene set enrichment analysis: a knowledge-based approach for interpreting genome-wide expression profiles. *Proc. Natl Acad. Sci. USA* **102**, 15545–15550 (2005).

Methods

Compliance with ethical regulations

Mouse colonies were maintained in a certified animal facility in accordance with the European guidelines. All the experiments were approved by the corresponding ethical committee (Commission d'Etique et du Bien-Être Animal CEBEA, Faculty of Medicine, Université Libre de Bruxelles). CEBEA follows the European Convention for the Protection of Vertebrate Animals Used for Experimental and Other Scientific Purposes (2010/63/UE). The mice were checked every day and were euthanized when tumours reached the endpoint size (2 cm^3), if the tumour was ulcerated (independently of the size), or if the mouse lost >20% of its initial weight or showed any other sign of distress (based on general health status and spontaneous activity). None of the experiments performed in this study surpassed the size limit of the tumours. All the experiments complied strictly with the protocols approved by ethical committee. The housing conditions of all animals were strictly following the ethical regulations. The room temperature ranged from 20 and 24 °C. The relative ambient humidity at the level of mouse cages was 55 ± 10%. Each cage was provided with food, water and two types of nesting material. A semi-natural light cycle of 12:12 was used. All the experiments complied strictly with the protocols approved by ethical committee.

For subcutaneous grafting using Ishikawa cells, female Swiss nude mice, six weeks of age, were purchased from Janvier Laboratories and maintained in specific pathogen-free conditions (P-PAC) and kept in sterilized filter-topped cages. Their care and housing were in accordance with institutional European guidelines as put forth by the CECCAP local ethical committee.

Mouse strains

Rosa26-YFP mice[42], *Lgr5-cre^{ER}* mice[43], *Kras$^{LSL-G12D}$* mice[44] and *Trp53$^{fl/fl}$* mice[45] were imported from the NCI mouse repository and Jackson Laboratories. NOD/SCID/Il2Rγ null mice were purchased from Charles River. All mouse groups used in this study were composed of males and females with mixed genetic background. No randomization and no blinding were performed in this study. The Rosa26LSL-NTN1 transgenic mice (for LKPR-NTN1 gain of function) were imported from Mehlen Laboratory–Apoptosis, Cancer and Development, Centre de Recherche en Cancérologie, Lyon, France[46].

LKPR and LKPR-NTN1 induced SCC model

The model LKPR mice were obtained by crossing *Rosa26-YFP* (ref. 42), *Lgr5-cre^{ER}* (ref. 43), *Kras$^{LSL-G12D}$* (ref. 44) and *Trp53$^{fl/fl}$* (ref. 45) mice[12]. Intraperitoneal administration of tamoxifen (an oestrogen analogue) (Sigma, T5648-1G) was used to activate specifically in hair follicle cells expressing LGR5 the CreERT2 recombinase fused to oestrogen receptor. Irreversible Cre-*lox* recombination results in expression of *Kras* oncogene, loss of the *Trp53* suppressor gene, and expression of the *YFP* reporter gene as tool for lineage tracing of tumour cells. Tamoxifen was diluted at 25 mg ml^{-1} in sunflower seed oil, 10% ethanol (Sigma). Four daily intraperitoneal injections of 2.5 mg tamoxifen were administered at postnatal day (P) 28 as previously described[12] to LKPR mice. Seven to nine weeks after tamoxifen injection, tumours were detected by daily observation and palpation. Mice were euthanized when the endpoint or maximum tumour size was reached or when mice presented signs of distress (see 'Compliance with ethical regulations'). Skin tumours were measured using a precision calliper. Tumour volumes were measured on the first day of appearance of the tumour and then every week until the death of the animal or every 2 days during chemotherapy assays in combination with anti-netrin-1 antibody. To generate the LKPR-NTN1 model, we crossed the LKPR mice with *Rosa26^{LSL}-NTN1* transgenic mice. These mice conditionally overexpress Flag-tagged netrin-1 under the control of a *Rosa26* promoter[46].

Cell culture

FACS-isolated EPCAM$^+$ and EPCAM$^-$ cells were cultured in Modified Eagle Medium (Capricorn Scientific, SP-2002-500 ml) supplemented with 10% fetal bovine serum (FBS) (Serana, S-FBS-SA-015), 4 μg ml^{-1} hydrocortisone (Sigma, H0888) 1% penicillin/streptomycin (100×) (Capricorn Scientific, PS-B), 2 mM L-glutamine, 2 ml amphotericin B (100×) (Capricorn Scientific, AMP-B) and 500 μl T3 (Sigma, T6397). Cells were washed with Dulbecco's phosphate buffered saline (PBS 1×) and detached from the cell culture plate with trypsin (Capricorn Scientific, TRY-2B10).

The A549 cell line was donated by R. Derynck and has been used in vitro as model in which EMT is plastic and can be induced by TGFβ1[9]. These cells were cultured in DMEM (Gibco, 11965092) with 10% FBS and 1% penicillin/streptavidin. For EMT induction, cells were plated, deprived in FBS the following day for 24 h, then treated with recombinant TGFβ1 (Peprotech, 100-21) at 5 μg ml^{-1} in vitro for 3 days or 6 days (treatment every 2 days) in DMEM 1.5% FBS.

The Ishikawa cell line, a well-differentiated endometrial adenocarcinoma cell line with netrin-1 and UNC5B expression, was purchased from the American Type Culture Collection (ATCC). They were grown in Minimum Essential Medium (Ozyme, COR10-009-CV), supplemented with 1% of penicillin/streptomycin and 5% FBS at 37 °C with saturating humidity and 5% CO_2.

In vitro invasion assays

For invasion assays on Ishikawa cell line, experiments were carried out using the xCELLigence RTCA DP instrument (Agilent, 56665817001), which was placed in a humidified incubator at 37 °C and 5% CO_2. Invasion experiments were performed using 16-well integrated Boyden chamber RTCA CIM plates (Agilent, 5665817001). Wells were prepared by depositing 190 μl of cell-free culture medium (5% FBS) in lower chambers and 20 μl of cell-free serum-free culture medium complemented with 2.5% Matrigel (Corning) on the porous membranes. CIM plates were placed in the humidified incubator (37 °C, 5% CO_2) for 1 h to let the Matrigel polymerize. Ishikawa cells that had been treated with NP137 or its isotypic control NP001 at 20 ng ml^{-1} for 72 h were collected, suspended in serum-free medium and counted, and 150,000 cells were seeded in 170 μl serum-free medium complemented with NP137 or its isotypic control NP001 at 20 ng ml^{-1} in the upper chambers of the CIM plates. The CIM plates were then placed in the xCELLigence RTCA DP instrument and cell invasion was monitored by detection of cells passing through the porous membrane and attaching to the impedance microelectrode in the lower chamber.

In vitro migration assays

For migration assays with EPCAM$^-$ cells (primary LKPR mouse skin SCC cell lines), experiments were carried out using Transwell migration plates (6.5 mm Transwell with 8.0 μm pore, Corning, 3422). Cells were deprived in FBS (0.5%) for 12 h before plating in migration plates. Wells were prepared by depositing 150 μl of cell culture medium (10% FBS) in the lower chamber (control or supplemented with NP137 at 20 μg ml^{-1}) and 50 μl serum-free culture medium containing 5,000 cells. Plates were placed in the humidified incubator (37 °C, 5% CO_2) for 18 h for migration progression. To detect cells that had passed through the porous membrane, the lower side of Transwell was fixed using fresh PFA (4%). Transwells were washed with PBS and the top sides of the Transwells were cleaned. The lower side of membrane was then stained with 0.2% crystal violet (in 20% methanol) for 20 min. After several washes, migrated cells were counted using an inverted microscope.

Lentiviral transduction using shRNA

HEK 293T cells (ATCC) were used as packaging cells. Transfer plasmid pLKO.1-puro (Sigma) carrying our gene of interest (*Unc5b* or *Ntn1*), TRC1 as empty vector and PPAX and PMDG packaging plasmids were

transfected into the cells with Lipofectamine 2000 (Thermo Fisher Scientific) using Opti-medium (Capricorn Scientific). The cell line of interest ($EPCAM^+$ primary mouse skin SCC cell lines derived from LKPR mice) was plated and transduced with the lentiviral shRNA with additional polybrene (Sigma, T2-1003G). A puromycin resistance test was performed after transduction.

Anti-netrin-1 treatment of LKPR mice

For in vivo experiments, to determine the effect of anti-netrin-1 on primary tumour progression and metastasis, LKPR mice were treated intraperitoneally with netrin-1 monoclonal antibody at 10 mg kg^{-1} every 2 days from 4 weeks after tamoxifen injection until the mouse was euthanized (see 'Compliance with ethical regulations'). 5-FU was used at 10 mg kg^{-1} and cisplatin was used at 4.4 mg kg^{-1} once a week for 2 weeks, and mice were treated with anti-netrin-1 every 2 days.

FACS isolation of tumour cells

Skin tumours from LKPR mice were dissected, rinsed and digested in collagenase type I (Sigma) at 3.5 mg ml^{-1} in HBSS (Gibco) for 1 h at 37 °C on a rocking plate protected from the light. Collagenase was blocked by the addition of EDTA (5 mM), and then the cells were rinsed once in PBS supplemented with 10% FBS and the cell suspension was filtered through a 70-µm cell strainer (BD Bioscience). For the next wash and antibody incubation, cells were resuspended in PBS supplemented with 2% FBS (FACS buffer). For cell sorting, cells were also filtered through a 40-µm cell strainer (BD Bioscience). Cells were incubated with BV711-conjugated anti-EPCAM (rat, clone G8.8, BD Bioscience 563134, dilution 1:100), PE-conjugated anti-CD45 (rat, clone 30-F11, BD, 553081, dilution 1:100) and PE-conjugated anti-CD31 (rat, clone MEC 13.3, BD, 553373, dilution 1:100) antibodies for 30 min at 4 °C protected from light. Living single tumour cells were selected by forward and side scatter, doublet discrimination and Hoescht exclusion. Tumour cells were selected by YFP expression and the exclusion of CD45 and CD31 (Lin^-). Different tumour cell subpopulations were defined in $EPCAM^+$ and $EPCAM^-$ tumour cells. FACS and analysis were performed using FACSAria and LSRFortessa, using FACSDiva software (v.9.1, BD Bioscience). Sorted cells were collected in culture medium complemented with 50% FBS for in vivo tail vein injection experiments and generation of culture cell lines or lysis buffer for RNA extraction with the RNeasy Micro Kit (Qiagen).

To analyse EPCAM profile on FACS on the $EPCAM^+$ LKPR cell line, cells were washed in PBS and detached from the cell culture plate with trypsin. Cells were resuspended and washed with PBS supplemented with 2% FBS (FACS buffer) and incubated with BV711-conjugated anti-EPCAM (rat, clone G8.8, BD Bioscience 563134, dilution 1:200) 30 min at room temperature and protected from the light. For cell sorting, cells were washed two times in FACS buffer and filtered through a 40-µm cell trainer. Living single YFP^+EPCAM^+ tumour cells were selected by forward and side scatter, doublet discrimination and Hoescht exclusion.

Metastasis assay

Primary tumours from mice were generated as described above and collected. The FACS-isolated tumour $EPCAM^-$ cell subpopulation was resuspended in 50 µl PBS and injected into the tail vein of NOD/SCID/Il2Rγ-null mice (1,000 cells per injection). The mice were treated with NP137 every 2 days (10 mg kg^{-1}) for 1 month. The mice were killed after the last treatment and lungs were analysed. The number of metastases was quantified on ten cryosections per lung (separated by 100 µm) based on YFP expression (skin SCCs tumours) and presented as the number of metastases per lung.

Tumour transplantation assays

Female Swiss nude mice, six weeks of age, were purchased from Janvier Laboratories (France) and maintained in specific pathogen-free conditions (P-PAC) and kept in sterilized filter-topped cages. Their care and housing were in accordance with institutional European guidelines as put forth by the CECCAP local ethical committee as previously described (C2EA-15, CLB_2014_001; CLB_2014_012; CECCAPP_CLB_2016_017). The mice were subcutaneously injected in the flank with Ishikawa cells (5×10^6) suspended in 100 µl of PBS. Tumours were allowed to grow for 15 days. Once tumours reached a volume of 100 mm^3, mice were stratified into treatment groups with 1 tumour per mouse based on their tumour volume at the start of the experiment, such that the starting tumour volumes in each group were uniform. Mice were treated via intravenous injection of 100 µl of NP137 or its isotypic control NP001 diluted in PBS at 20 mg kg^{-1} for 3 days, then 10 mg kg^{-1} every 2 days thereafter for 1 month. Tumours were measured every 2 days with calipers. Tumour size was calculated using the following formula: tumour volume (in mm^3) = $(D \times d^2)/2$. D, long dimension; d, short dimension.

A549 tumour cells were pre-treated in vitro with TGFβ1 for 6 days (see 'Cell culture' section) and then collected in Matrigel (50%) + PBS (50%) for subcutaneous grafting into NOD/SCID mice (1×10^6 cells per grafting point). Secondary tumours were detected by palpation every week, and their sizes were monitored until they reached 1 cm in size or when mice presented signs of distress. The mice were killed at the same time and tumours were collected for histology analyses.

Immunofluoresence

All staining was performed on frozen sections. Tumour tissues and lungs were pre-fixed in 4% PFA for 2 h at room temperature, rinsed in PBS, incubated overnight in 30% sucrose at 4 °C and embedded in OCT (Tissue Tek) for cryopreservation. Tissues were cut into 6-µm sections using a CM3050S cryostat (Leica Microsystems GmbH) and rinsed with PBS three times (5 min). Non-specific antibody binding was blocked with 5% horse serum, 1% BSA and 0.2% Triton X-100 for 1 h at room temperature. Primary antibodies were incubated overnight at 4 °C in blocking buffer. Sections were rinsed in PBS 3 times (5 min) and incubated with secondary antibodies diluted in blocking buffer at 1:400 for 1 h at room temperature. Nuclei were stained with Hoechst (4 mM) and slides were mounted using SafeMount (Labonord). Image acquisition was performed on a Zeiss Axio Imager.M2 fluorescence microscope with a Zeiss Axiocam MRm camera using Axiovision release 4.8 software. Brightness, contrast and picture size were adjusted using Adobe Photoshop.

Antibodies for immunostaining

The following primary antibodies were used for immunofluorescence: anti-GFP (goat polyclonal, Abcam, ab6673, dilution 1:500), anti-KRT14 (chicken, polyclonal, Thermo Fisher Scientific, MA5-11599, dilution 1:1 000), anti-VIM (rabbit, clone ERP3776 Abcam, ab92547, dilution 1:500), anti-KRT8 (rat, TROMA clone 1/28/21, DSHB, AB_531828, dilution 1:1,000), anti-PDGFRA (rat, clone APA5, eBioscience, 13-1401, dilution 1:500), anti-CDH1 (mouse, clone 67A4, BD, 563570, dilution 1:500) and anti-pan-CK antibody (clone CKAE/1AE3, Dako Belgium, 1:150). The following secondary antibodies were used (dilution 1:400): anti-rabbit, anti-rat, anti-goat or anti-chicken conjugated to Rhodamine Red-X (Jackson ImmunoResearch), Cy5 (Jackson ImmunoResearch) or Alexa Fluor-A488 (Invitrogen).

Immunoblot analysis

Subconfluent cells were washed with cold PBS and lysed in a lysis buffer containing SDS. Lysates were sonicated five times for 10 min each using a Bioruptor Plus (Diagenode, UCD-300) and cellular debris was pelleted by centrifugation (10,000*g* 15 min at 4 °C). Protein quantifications were carried out using the Pierce 660 nm Protein Assay kit (Thermo Fisher, 22662) with an ionic detergent compatibility reagent (Thermo Fisher, 22663) and measured using a Bio-Rad iMark microplate. Protein extracts containing 30 or 40 µg protein were loaded onto 4–12% SDS–PAGE (Thermo Fisher) and blotted onto nitrocellulose

sheets. The membranes were then blocked with 5% non-fat dried milk + 0.05% BSA for 1 h at room temperature and incubated at 4 °C overnight with primary antibodies: anti-NTN1 (rabbit, clone EPR5428, Abcam, ab126729, dilution 1:10,000), anti-CDH1 (mouse, clone 4A2, Cell Signaling, 14472, dilution 1:1,000), anti-VIM (rabbit, clone ERP3776 Abcam, ab92547, dilution 1:1,000) and anti-β-actin (rabbit, Abcam, ab8227, dilution 1:2,000). After three washes with PBS-T, it was followed by incubation 1 h incubation with anti-rabbit secondary antibody (anti-rabbit IgG HRP NA9340V, 1:5,000, Sigma Aldrich, Gena9340) at room temperature. After washing in TBS-T, immunoreactive antibody–antigen complexes were visualized with enhanced chemiluminescence reagents, West Dura or ECL Chemiluminescence System (Pierce). Membranes were imaged using iBright FL1500, Invitrogen.

RNA fluorescence in situ hybridization

All staining was performed on frozen sections or on cytospin. Tumour tissues were pre-fixed in 4% paraformaldehyde for 2 h at room temperature, rinsed in PBS, incubated overnight in 30% sucrose at 4 °C and embedded in OCT (Tissue Tek) for cryopreservation. Cytospin cell cultures were generated using CellspinI (Tharmac) (20,000 cells for one cytospin). The in situ protocol was performed according to the manufacturer's instructions (Advanced Cell Diagnostics). The following mouse probes were used: Mm-Aqp1 (504741-C2), Mm-Nrp1 (471621), Mm-Aqp5, (430021-C2), Mm-Vim (457961-C2) and Mm-Krt14 (422521-C3). The LSM-780 (Carl Zeiss) confocal system and ZEN2012 software were used to acquire and analyse the images.

Bulk RNA-seq

RNA quality was evaluated by Bioanalyzer 2100 (Agilent) before sequencing. Indexed cDNA libraries were obtained using Ovation Solo RNA-seq Systems (NuGen) according to the manufacturer's recommendations. The multiplexed libraries (11 pM or 18 pM) were loaded onto flow cells and sequences were produced using a HiSeq PE Cluster Kit v4 and TruSeq SBS Kit v3-HS (250 cycles) on a Novaseq 6000 (Illumina). Approximately 20 million paired-end reads per sample were generated and quality checks were performed with FastQC (https://www.bioinformatics.babraham.ac.uk/projects/fastqc/). The adapter sequences and low-quality regions were trimmed by Trimmomatic. Trimmed reads were mapped against the mouse reference genome (Grcm38/mm10) using STAR software to generate read alignments. Duplicated reads were removed by Picard MarkDuplicates. Annotations for Grcm38.87 were obtained from ftp://ftp.ensembl.org/. After transcript assembly, gene level counts were obtained using HTseq and normalized to 20 million of aligned reads. Average expression for each gene in the different sample was computed using two biological replicates and fold changes were calculated between control sample (empty vector) and sample of interest (*Ntn1* knockdown or *Unc5b* knockdown). Genes for which all the mean expressions across the sample were lower than 100 reads per million mapped reads were considered not expressed and removed from further analysis. Genes having a fold change of expression greater than or equal to 2 were considered upregulated and those having a fold change of expression lower than or equal to 0.5 were considered downregulated.

RNA extraction and real-time PCR

RNA was extracted from FACS-isolated cells or culture cell lines using RNeasy micro kit (QIAGEN) according to the manufacturer's recommendations. For real-time PCR, after mRNA quantification using Nanodrop1000, the first-strand cDNA was synthesized using Superscript II (Invitrogen) and random hexamers (Roche) in 50 µl final volume. Control of genomic contamination was measured for each sample by performing the same procedure with or without reverse transcriptase. Quantitative PCR assays were performed using 1 ng cDNA as template and SYBRGreen mix (Applied Bioscience) on a Light Cycler 96 (Roche) real-time PCR system. *Tbp or HPRT* housekeeping genes were used for normalization. The following probes were used: *Ntn1* forward: GCAAGCTGAAGATGAACATGA, *Ntn1* reverse: CTTTGTCGGCCTTCAGGAT, *Unc5b* forward: TTCCAGCTGCACACAACG, *Unc5b* reverse: GCAGAGCAGAGAGCATCCA, *Tbp* forward: TGTACCGCAGCTTCAAAATATTGTAT, *Tbp* reverse: AAATCAACGCAGTTGTCCGTG, *NTN1* forward: AAAAGTACTGCAAGAAGGACTATGC, *NTN1* reverse: CCCTGCTTATACACGGAGATG, *CDH1* forward: CCCGGGACAACGTTTATT, *CDH1* reverse: GCTGGCTCAAGTCAAAGTCC, *HOOK1* forward: TGCTGCTGAGATTATGCCAGTGGA, *HOOK1* reverse: TCAGCCTCTGCTCAGTTTCCAGT, *MUC1* forward: GCCAGGATCTGTGGTGGTACAAT, *MUC1* reverse: TGTCTCCAGGTCGTGGACATTGAT, *HPRT* forward: TGACCTTGATTTATTTTGCATACC, *HPRT* reverse: CGAGCAAGACGTTCAGTCCT.

Single-cell transcriptomic data analysis

Single-cell RNA library preparation and gene expression analysis. After FACS isolation, living cells from fresh LKPR control and anti-netrin-1 treated skin SCC tumours were sorted and loaded onto each channel of the Chromium Single Cell 3′ microfluidic chips (V2-chemistry, 10x Genomics) and individually barcoded with a 10x Chromium controller according to the manufacturer's recommendations (10x Genomics). RNA from the barcoded cells was reverse transcribed, followed by amplification. The libraries were prepared using the Chromium Single Cell 3′ Library Kit (V2-chemistry, 10x Genomics), quantified using a low coverage Illumina NextSeq 550 run and sequenced on an Illumina NovaSeq. CellRanger (v3.0.2) was used with the default parameters to demultiplex, align, and annotate the obtained sequencing reads with the 10x Genomics mm10-3.0.0 reference dataset extended with the *Yfp* transgene. The Seurat R package was used to perform further downstream analysis of the gene expression matrices for the treated and control samples separately[47] (v3.1.5). Only cells passing the following criteria were considered for further analysis: between 600 and 8,000 uniquely expressed genes and less than 25% of the unique molecular identifier counts mapping to mitochondrial sequences. For the treated samples (NP1371 and NP137 2), respectively, 16,926 of the 19,288 cells and 14,104 of 17,620 passed quality control. For the control samples (control 1 and control 2), respectively, 10,986 of the 12,180 cells and 5,248 of the 8,327 cells were considered for downstream analysis.

scRNA-seq clustering leading to cell types. Default parameters of Seurat were used unless mentioned otherwise. Before determining the cell cycle state, the read counts were log-normalized and scaled. The scaled expression data for the 2,000 most highly variable genes (HVG) (identified using Seurat's FindVariableGenes function) served as input for principal component analysis (PCA). Next, the JackStraw methodology implemented in Seurat was used to determine the number of significant principal components for Leiden clustering[48] and UMAP dimensionality reduction (maximum of 30 principal components). Clustering resolutions ranging from 0.1–1.0 with steps of 0.1 were assessed for stability with the clustree[49] R package (v0.4.2). The lowest stable resolution was chosen for a general overview of the cell types present in both conditions (control: 0.1 and treated: 0.2). Following that, the Wilcoxon rank sum was used to identify marker genes for each subcluster, only reporting genes that were expressed in at least 25% of the cells in the cluster and had an average log fold change of at least 0.25. Batch integration was performed per condition using Harmony[50] (v1.0) with standard parameters. Cell-type clusters were subsequently annotated using Seurat's module scoring function and cell-type-specific marker genes obtained from the PanglaoDB[51] database (version of 27/03/2020). Our annotations were further confirmed by plotting the expression of canonical cell markers as *Ptprc* for immune cells, *Pecam* for endothelial cells, *Cd3d* for T cells and *Col6a3* for CAFs. The clusters containing the tumour cells were characterized by expression of the *Yfp* transgene. Afterwards, the two datasets, except

for the tumour cells, were integrated using Harmony with 30 principal components, and standard parameters or Leiden clustering was subsequently performed in steps of 0.1 for resolutions ranging from 0.1 to 1.0. The clustree R package was then used to determine the lowest stable resolution (0.2). Cell-type clusters were then annotated in the same way as previously described. To compare the abundance of the identified cell types between the control and treated conditions, we used the scCODA algorithm[52] implemented in the pertpy v4.0 Python package using the pericytes as the reference cell type and a FDR threshold of 0.2.

scRNA-seq clustering leading to cell subtypes for CAFs. After being rescaled, the combined CAFS cluster across the conditions was further subclustered by using the top 2,000 HVGs as input for PCA analysis. The number of significant principal components for clustering and UMAP calculation, which ranged from 1 to 30, was determined using the JackStraw methodology. Seurat's AddModuleScore was then used to identify clusters with a high enrichment of PanglaoDB-derived marker genes for other cell types using a resolution of 0.4 for the Leiden clustering. Following the removal of these clusters, the previous analysis steps were repeated, and stable clustering resolutions for the treated condition were determined using clustree. A resolution of 0.3 was used for the identification of the final CAF subclusters. Harmony was used with standard parameters to perform batch integration. The mouse MSigDB hallmark gene sets and the AUCell R package (v1.8.0). were used to calculate pathway activities. Clusters were assigned the apCAF, iCAF or myCAF label using Seurat's AddModuleScore function and the signatures obtained from Elyada et al.[53] Compositional analysis between the control and treated condition was performed with the scCODA algorithm, implemented in the pertpy v4.0 Python package using the 'glycolytic CAFS' as the reference and a FDR threshold of 0.2.

scRNA-seq clustering leading to EMT states for *YFP*-positive cells and pseudotime analysis. For both conditions, all *YFP*-positive cells (defined as at least having two transcripts assigned to the *YFP* transgene) were subclustered. The top 2,000 variable genes were used as input for PCA analysis after the counts were rescaled. The JackStraw methodology was then used to calculate the number of significant principal components in a range of 1 to 30. The lowest stable clustering resolution per condition was determined using clustree (control: 0.1, treated: 0.3). Based on PanglaoDB-derived marker genes, the AddModuleScore was used to score clusters that showed an enrichment of expression signatures related to other cell types. Following the removal of these clusters, the preceding steps were repeated, with clustering resolutions of 0.7 and 0.6 used for the control and treated conditions, respectively. Subsequently the obtained clusters were scored as epithelial (*Epcam*$^+$*Krt14*$^+$*Vim*$^-$), early hybrid (*Epcam*$^-$*Krt14*$^+$*Vim*$^+$), late hybrid (*Epcam*$^-$*Krt14*$^-$*Krt8*$^+$*Vim*$^+$*Pdgfra*$^-$) or full EMT (*Epcam Krt14 Krt8 Vim*$^+$*Pdgfra*$^+$) based on the expression of *Epcam*, *Krt14*, *Krt8*, *Vim* and *Pdgfra*. The mouse MSigDB hallmark gene sets and the AUCell R package[38] (v1.8.0). were used to analyse pathway activities. Before performing the Wilcoxon rank-sum test with Bonferroni correction for multiple testing between conditions, the AUC distributions were normalized per sample using linear regression. To compare the abundance of the identified cell subtypes and cell cycle distribution per EMT state between the control and treated conditions, the scCODA algorithm of the pertpy v4.0 Python package was used with the early hybrid EMT state as reference a FDR threshold of 0.2. Harmony with standard parameters was used for batch integration per condition. Pseudotime ordering of YFP-positive cells in the G1 cell-phase was calculated using monocle[54] (v2.14.0) with the DDRtree (v0.1.5) method for dimensionality reduction on the top 2,000 HVGs for each condition, controlling for sample effects. The dynplot[55] R-package (v1.0.2) was used to create the trajectory plots.

Visium spatial transcriptomic analysis

To analyse the spatial distribution and localization of different EMT tumour states previously described by scRNA-seq in control and anti-netrin-1-treated skin SCC tumours, we used 10x Visium technology for spatial transcriptomic analysis (10x Genomics). FFPE tissue section were places on Visium slides and prepared according to 10x Genomics protocols. After haematoxylin and eosin staining, imaging and decrosslinking steps, tissue sections were incubated with human specific probes targeting 10,551 genes (10x Genomics, Visium Mouse Transcriptome Probe Set v1.0). Probes hybridized on mRNA were captured onto Visium slides and gene expression libraries were prepared following the provided protocol and sequencing on an Illumina Novaseq 6000 with 50,000 reads per spot targeted sequencing depth. For each FFPE section, FASTQ files and histology images were processed using 10x Space Ranger v2.0 to obtain the matrix associated with each spot. The SCutility method was used to perform the analysis. Briefly, filtered matrices were loaded and merged per sample, and spots with less than 1,000 detected genes were removed.

EMT score

Three signatures were used to assess the EMT level. The Hallmark signature was computed using ssGSEA[41] on the genes from the HALLMARK_EPITHELIAL_MESENCHYMAL_TRANSITION signature from MSigDB[38]. The Thiery signature was computed similarly using genes from ref. 11.

The Mak signature was calculated from gene sets in ref. 40 as the difference of two signatures: a mesenchymal signature defined as the mean of mesenchymal gene expression and an epithelial signature defined as the mean of epithelial gene expression.

Statistical analysis

All statistical analyses are based on biological replicates (*n* indicated in the text, figures or figure legends). Multiple unpaired *t*-tests were performed using GraphPad Prism version 9.00 for Mac software. Bar graphs and dot plots were generated with mean ± s.e.m with GraphPad Prism. Wilcoxon rank-sum test and Fisher test with Bonferroni correction were used for multiple analyses in scRNA-seq.

Reporting summary

Further information on research design is available in the Nature Portfolio Reporting Summary linked to this article.

Data availability

All raw sequence data for mouse RNA-seq, single cell RNA-seq and 10x Visium have been deposited in the Gene Expression Omnibus under the accession number GSE234267. Source data are provided with this paper.

42. Srinivas, S. et al. Cre reporter strains produced by targeted insertion of EYFP and ECFP into the ROSA26 locus. *BMC Dev. Biol.* **1**, 4 (2001).
43. Barker, N. et al. Identification of stem cells in small intestine and colon by marker gene Lgr5. *Nature* **449**, 1003–1007 (2007).
44. Tuveson, D. A. et al. Endogenous oncogenic K-ras(G12D) stimulates proliferation and widespread neoplastic and developmental defects. *Cancer Cell* **5**, 375–387 (2004).
45. Jonkers, J. et al. Synergistic tumor suppressor activity of BRCA2 and p53 in a conditional mouse model for breast cancer. *Nat. Genet.* **29**, 418–425 (2001).
46. Boussouar, A. et al. Netrin-1 and its receptor DCC are causally implicated in melanoma progression. *Cancer Res.* **80**, 747–756 (2020).
47. Satija, R., Farrell, J. A., Gennert, D., Schier, A. F. & Regev, A. Spatial reconstruction of single-cell gene expression data. *Nat. Biotechnol.* **33**, 495–502 (2015).
48. Traag, V. A., Waltman, L. & van Eck, N. J. From Louvain to Leiden: guaranteeing well-connected communities. *Sci. Rep.* **9**, 5233 (2019).
49. Zappia, L. & Oshlack, A. Clustering trees: a visualization for evaluating clusterings at multiple resolutions. *Gigascience* **7**, giy083 (2018).
50. Korsunsky, I. et al. Fast, sensitive and accurate integration of single-cell data with Harmony. *Nat. Methods* **16**, 1289–1296 (2019).
51. Franzen, O., Gan, L. M. & Björkegren, J. L. M. PanglaoDB: a web server for exploration of mouse and human single-cell RNA sequencing data. *Database* **2019**, baz046 (2019).
52. Buttner, M., Ostner, J., Muller, C. L., Theis, F. J. & Schubert, B. scCODA is a Bayesian model for compositional single-cell data analysis. *Nat. Commun.* **12**, 6876 (2021).

53. Elyada, E. et al. Cross-species single-cell analysis of pancreatic ductal adenocarcinoma reveals antigen-presenting cancer-associated fibroblasts. *Cancer Discov.* **9**, 1102–1123 (2019).
54. Trapnell, C. et al. The dynamics and regulators of cell fate decisions are revealed by pseudotemporal ordering of single cells. *Nat. Biotechnol.* **32**, 381–386 (2014).
55. Saelens, W., Cannoodt, R., Todorov, H. & Saeys, Y. A comparison of single-cell trajectory inference methods. *Nat. Biotechnol.* **37**, 547–554 (2019).

Acknowledgements The authors thank the ULB animal facility; ULB genomic core facility (F. Libert and A. Lefort) for bulk RNA-seq and scRNA-seq; the Gilles Thomas bioinformatic platform; Centre de Recherche en Cancérologie de Lyon, Fondation Synergie Lyon cancer for the spatial transcriptomic sequencing; S. Bottieau for technical assistance; F. Lavial for *Unc5b* shRNA; and R. Derynck for the A549 cell line. J.L. is supported by NETRIS Pharma. I.P. is supported by FNRS and WELBIO. S.V. is supported by a PhD fellowship for Strategic Basic Research (1S93320N) from the Research Foundation Flanders (FWO). C. Decaestecker is a senior Research Associate with Fond National de la Recherche Scientifique (FNRS, Brussels, Belgium). DIAPath and the Department of Pathology are supported by the Fonds Yvonne Boël. The CMMI is supported by the European Regional Development Fund and the Walloon region (Wallonia-biomed; grant no. 411132–957270; project "CMMI-ULB" support the Center for Microscopy and Molecular Imaging and its DIAPath department). C.B. is supported by WELBIO, FNRS, TELEVIE, Fondation Contre le Cancer, ULB Foundation, Foundation Baillet Latour, FNRS/FWO EOS (40007513) and the European Research Council (AdvGrant 885093). This work was also supported by institutional grants from CNRS, University of Lyon1, Centre Léon Bérard and from the Ligue Contre le Cancer, INCA, ARC Sign'it and ANR (nos. ANR-10-LABX- 0061, ANR-17-CONV-0002 and ANR-18-RHUS-0009).

Author contributions J.L., I.P., S.V. and C.B. designed the experiments and performed data analysis. J.L. and I.P. performed most of the biological experiments. S.V. performed most of bioinformatic analysis for single-cell sequencing. N.R., Y.S. and A.S. helped with bioinformatic analysis. J.V.H. helped with 10x single-cell sequencing. R.M.S. helped with RNAscope analysis. V.M., A. Boinet., S.S., S.L., S.G. and S.B. helped with cell culture experiments, immunostaining, blocking antibody injection and follow-up with the mice. I.S., J.A., E.Z., C. Decaestecker. and A.C. performed immunostaining and quantification of EMT in human cancer samples. B.D., M.B. and N.B. performed biological in vivo and in vitro experiments on Ishikawa endometrial cell lines. C.S. and D.V. performed bioanalysis from TCGA. C. Dubois performed FACS sorting. T.V. helped and supervised the single-cell data analysis. P.M. and A. Bernet helped with the design of the experiments, data analysis and provided NP137 antibody. All authors read and approved the final manuscript.

Competing interests A. Bernet and P.M. declare a conflict of interest as founders and shareholders of NETRIS Pharma. J.L., P.M., B.D., M.B. and N.B. declare a conflict of interest as employees of NETRIS Pharma. A. Bernet. and N.R. declare a conflict of interest as consultants for NETRIS. T.V. is co-inventor on licensed patents WO/2011/157846 (*Methods for Haplotyping Single Cells*), WO/2014/053664 (*High-Throughput Genotyping by Sequencing Low Amounts of Genetic Material*) and WO/2015/028576 (*Haplotyping and Copy Number Typing Using Polymorphic Variant Allelic Frequencies*).

Additional information
Supplementary information The online version contains supplementary material available at https://doi.org/10.1038/s41586-023-06372-2.
Correspondence and requests for materials should be addressed to Patrick Mehlen, Agnès Bernet or Cédric Blanpain.
Peer review information *Nature* thanks the anonymous reviewers for their contribution to the peer review of this work.

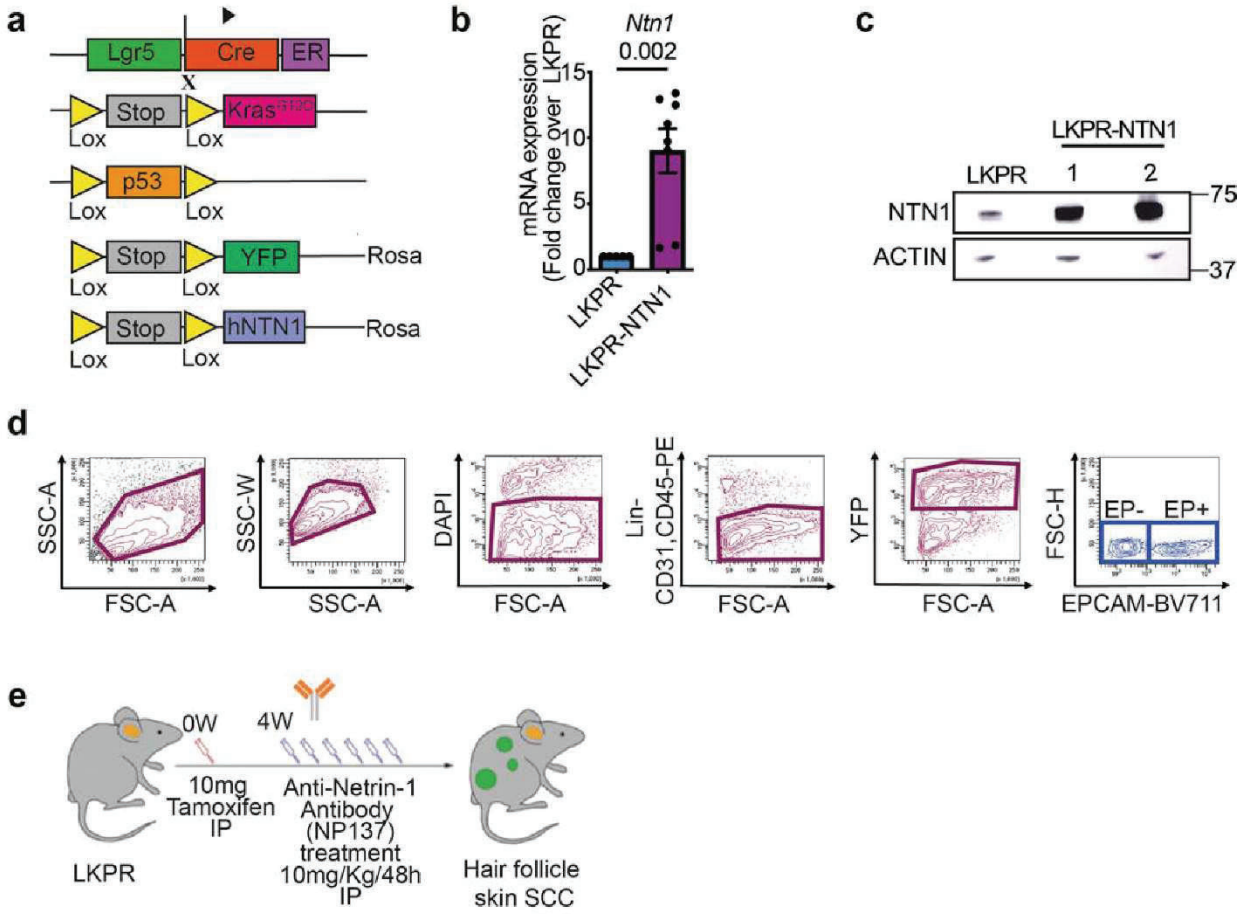

Extended Data Fig. 1 | Strategy to study the impact of Netrin-1 on EMT in mouse skin SCCs. a, Mouse model of skin SCC allowing the expression of *Kras*^{G12D}, *YFP*, *p53* deletion and overexpression of human NETRIN-1 in hair follicle stem cells and their progeny using *Lgr5CreER*. **b**, Relative mRNA expression of *Ntn1* in EPCAM- control LKPR (n = 5) and LKPR-NTN1 (n = 8) skin SCC defined by qRT-PCR (data are normalized to *Tbp* gene, mean ± s.e.m., two tailed Mann-Whitney U test). **c**, Western blot analysis of Netrin-1 expression in EPCAM- control LKPR and LKPR-NTN1 skin SCC TCs. **d**, FACS plots showing the gating strategy used to FACS-isolate or to analyse the proportion of YFP$^+$/EPCAM$^-$ and EPCAM$^-$ tumour cells. **e**, Drawing showing the experimental strategy of NP137 administration after Tamoxifen induction in *Lgr5CreER/Kras*$^{LSL\text{-}G12D}$*/p53*$^{fl/fl}$*/Rosa26-YFP*$^{l/l}$ mice. IP, intraperitoneal.

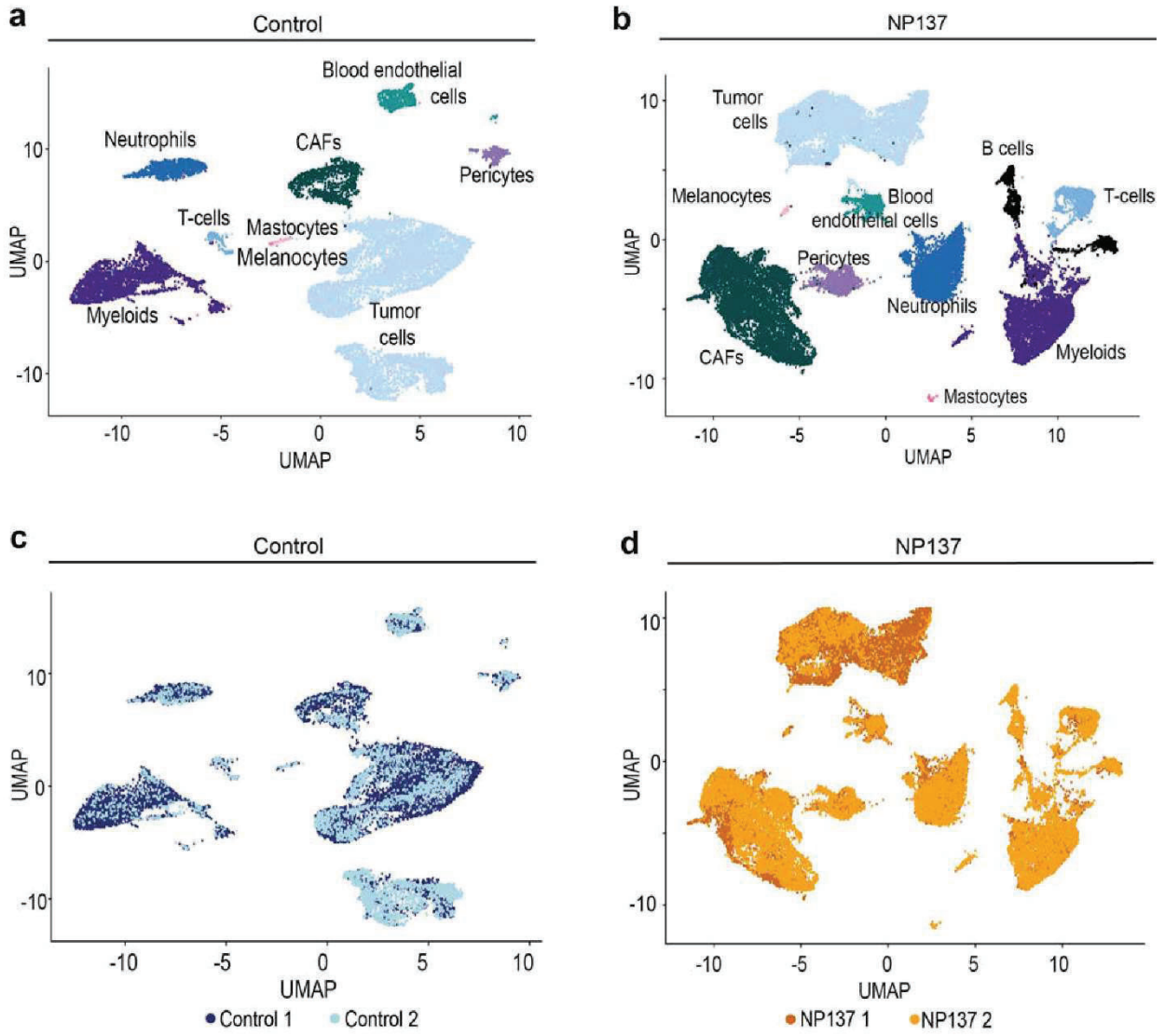

Extended Data Fig. 2 | Single cell analysis of the cellular composition of control and NP137-treated skin SCCs. a,b Uniform Manifold Approximation and Projection (UMAP) plot for control (**a**) and NP137-treated skin SCC (**b**) coloured by the identified cell types. **c,d**, UMAP plot for control (c) and NP137-treated skin SCC (d) coloured by the sample of origin for each cell. CAFs, cancer-associated fibroblasts.

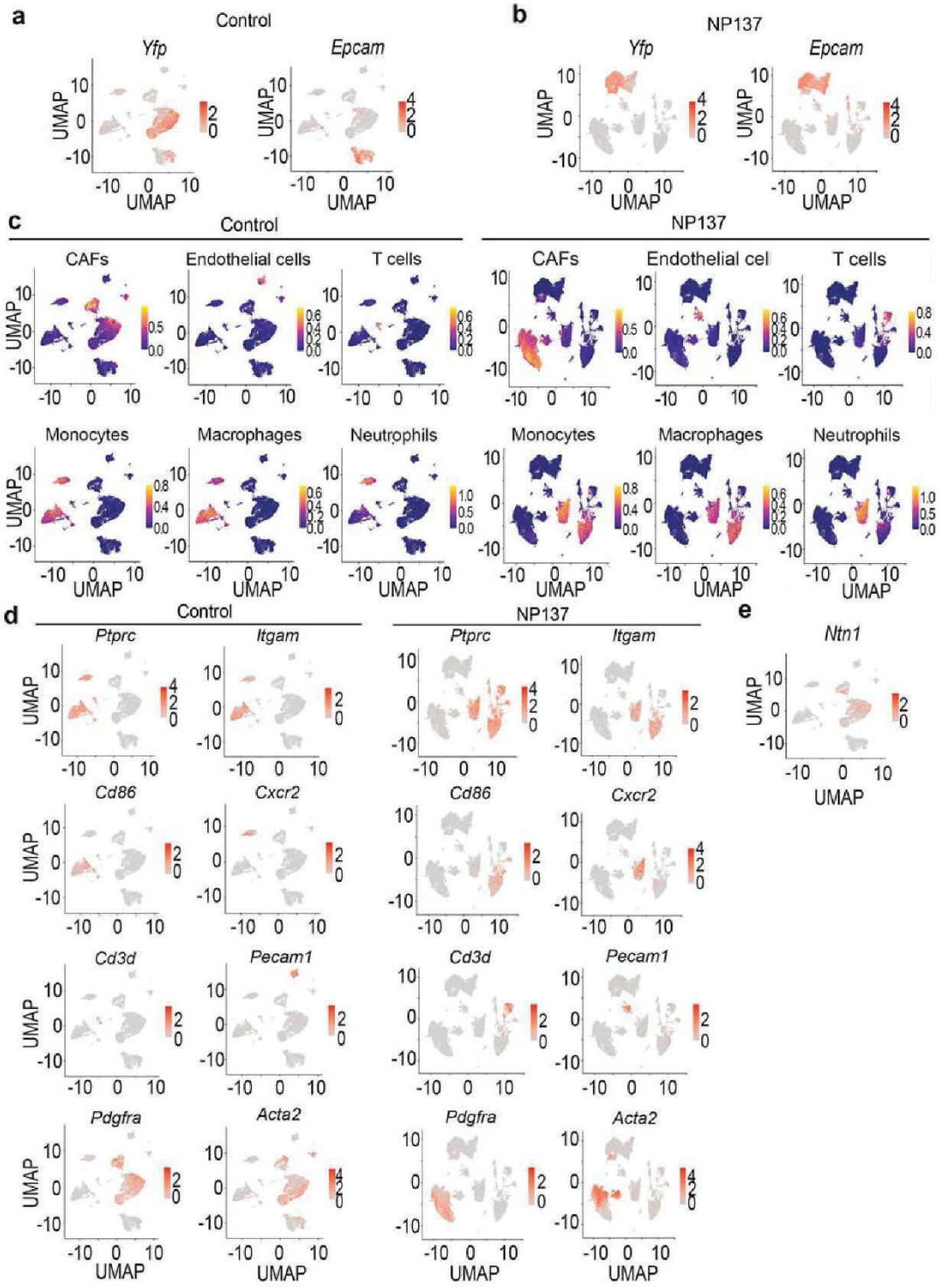

Extended Data Fig. 3 | Annotation of the cell types found by single cell RNA-seq in control and NP137-treated skin SCCs. a, UMAP plots coloured by normalized *Yfp* and *Epcam* expression in the control tumours. Gene expression values are visualized as colour gradient with grey indicating no expression and red indicating the maximum expression. **b**, UMAP plots coloured by normalized *Yfp* and *Epcam* in NP137-treated samples. **c**, UMAP plots coloured by the activity of modules containing the mouse-specific marker genes of the different cell types including CAFs, Macrophages, Neutrophils, Endothelial cells and T cells obtained from the PanglaoDB database in control samples (left) and anti-Netrin-1 treated samples (right). Module activity visualized as a colour gradient with blue indicating no expression and yellow indicating maximum activity. **d**, UMAP plots coloured by normalized *Pdgfra*, *Acta2*, *Pecam1*, *Cd3d*, *Ptprc*, *Itgam*, *Cd86* and *Cxcr2* expression in the control samples (left) and NP137-treated samples (right). CAFs, cancer-associated fibroblasts. **e**, UMAP plot coloured by normalized *Ntn1* expression in control condition.

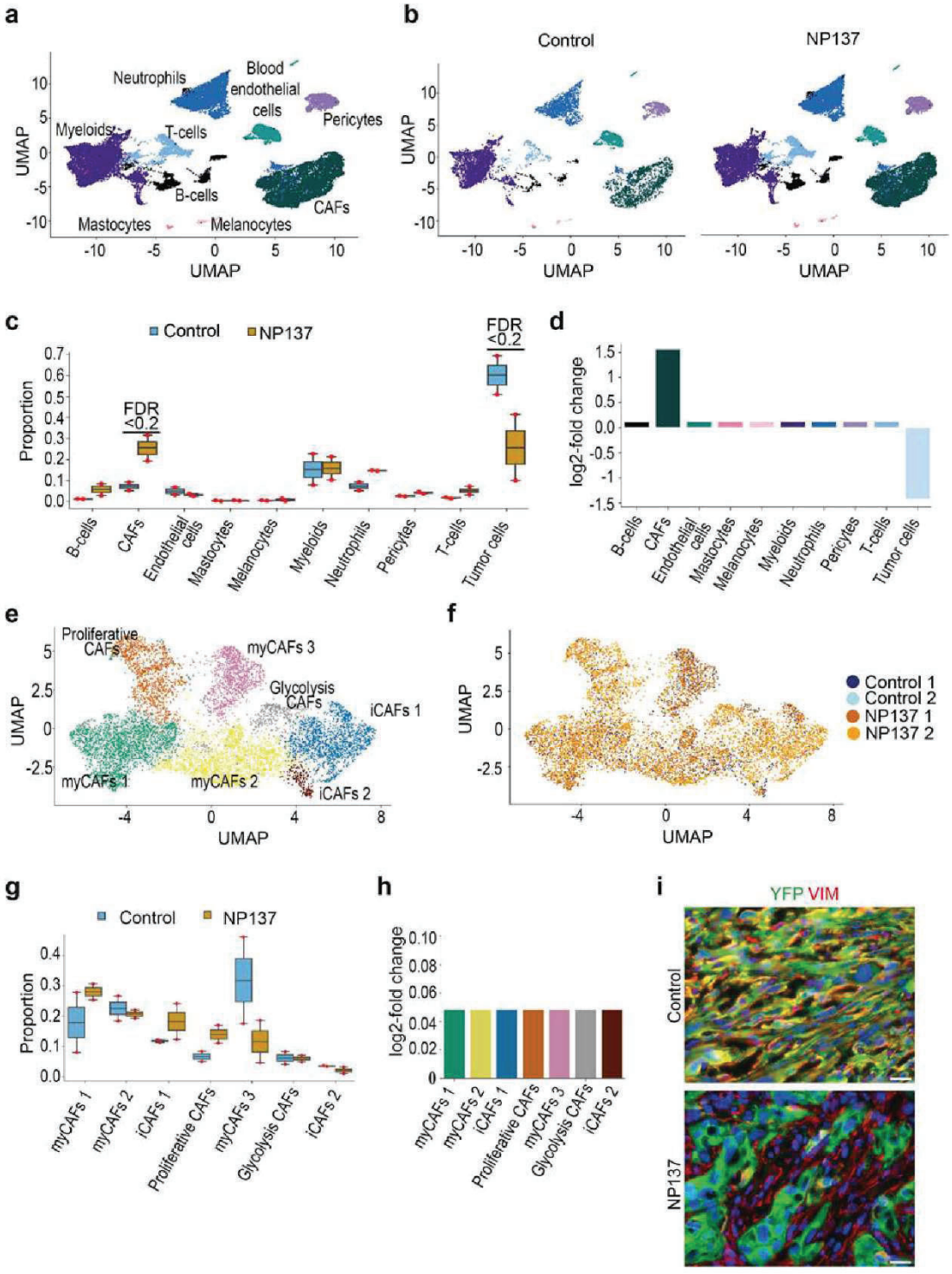

Extended Data Fig. 4 | See next page for caption.

Extended Data Fig. 4 | Impact of anti-Netrin antibody administration on the cellular composition of skin SCCs. a,**b**, Uniform Manifold Approximation and Projection (UMAP) plots coloured by the cell type labels obtained from the analysis of the microenvironment for the integration of all the samples in total **(a)** and split per sample **(b)**, respectively. **c**, Boxplot depicting the proportions of the different cell types for the 4 samples, split by their condition. The boxplots are coloured by their condition, and the individual measurements are visualized as red dots. The centre line, top and bottom of the boxplots represent respectively the median, 25th and 75th percentile and whiskers are 1.5 × IQR. Significant proportion changes are indicated by FDR < 0.2. **d**, barplot depicting the relative log fold change of the relative abundance of the different cell types after NP137-treated samples compared to the pericytes. Bars are coloured according to their cell type. **e**,**f**, UMAP plot of the CAFS subclustering, coloured by the identified seven subclusters and the sample the cell originated from, respectively. **g**, Boxplot depicting the proportions of the different CAF subclusters for the 4 samples, split by their condition. The boxplots are coloured by their condition, and the individual measurements are visualized as red dots. The centre line, top and bottom of the boxplots represent respectively the median, 25th and 75th percentile and whiskers are 1.5 × IQR. **h**. barplot depicting the relative log fold change of the relative abundance of the different CAF subclusters after NP137 treatment compared to the glycolysis CAFs subcluster. **i**, Co-immunostaining of YFP and Vimentin in control (top) (n = 5 tumours) and NP137- treated skin SCC (bottom) (n = 5 tumours) that defines YFP-/VIM+ CAFs as cells (Scale bars, 20 μm).

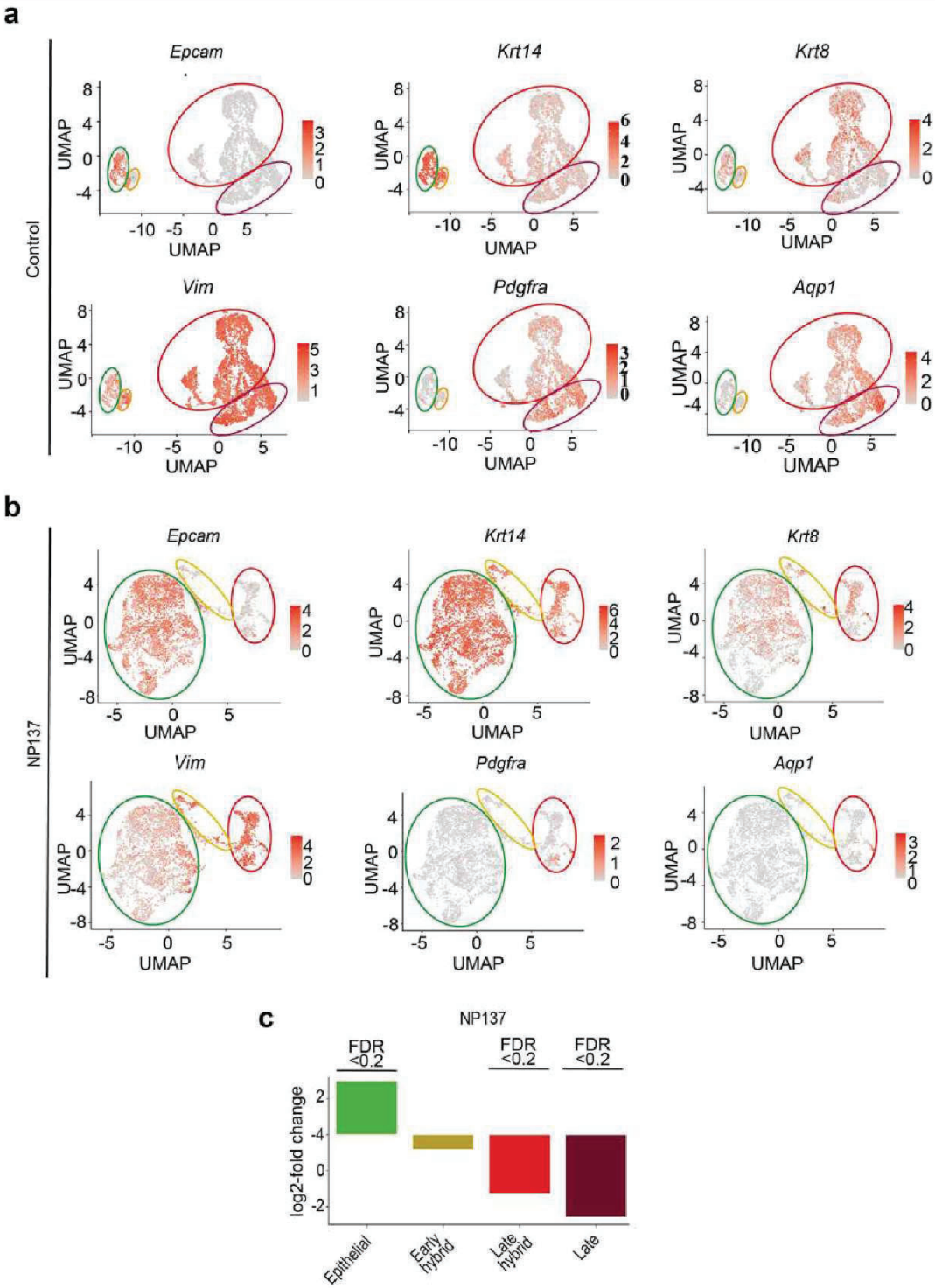

Extended Data Fig. 5 | Expression of markers of the different EMT states in control and NP137-treated skin SCCs. a, b, UMAP plots coloured by normalized gene expression values for the indicated genes in the control (**a**) and treated samples (**b**). Gene expression values are visualized as colour gradient with grey indicating no expression and red indicating the maximum expression. Circles represent TCs groups with a different degree of EMT based on the expression of *Epcam*, *Krt14*, *Krt8*, *Vim*, *Pdgfra* (green: *Epcam*+/*Krt14*+/*Vim*− as epithelial state; orange: *Epcam*−/*Krt14*+/*Vim*+ as early hybrid EMT state; red: *Epcam*−/*Krt14*−/*Krt8*+/*Vim*+ as late hybrid EMT state; dark red: *Epcam*−/*Krt14*−/*Krt8*−/*Vim*+ as late full EMT state expressing *Pdgfra* and *Aqp1*). **c**, Barplot depicting the relative log fold change of the relative abundance of the different EMT states after NP137-treatment compared to the early hybrid state. Significant proportion changes are indicated by FDR < 0.2.

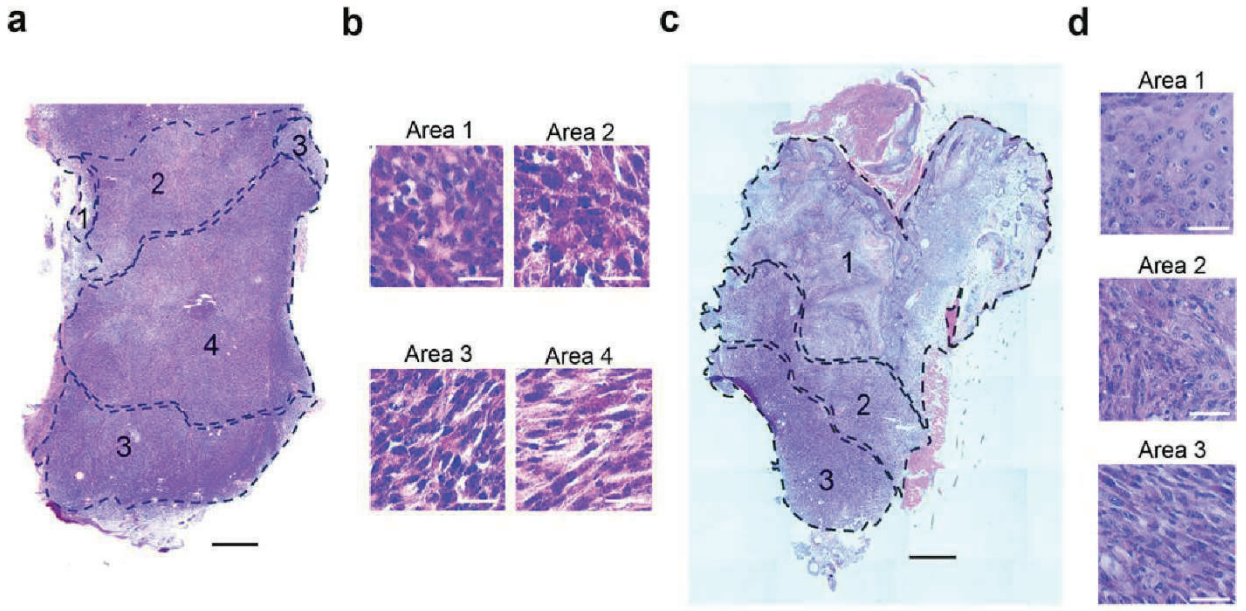

Extended Data Fig. 6 | Histological analysis of the control and NP137-treated tumors. a–d, Haematoxylin and Eosin staining showing the control (n = 1) (**a**,**b**) or NP137-treated (n = 1) (**c**,**d**) tumour skin SCC analysed in Visium spatial transcriptomic method. The annotated areas represent the EMT states previously defined by the expression of *Epcam*, *Krt14*, *Krt8* and *Vim* (1: epithelial, 2: early hybrid, 3, late hybrid, 4: full late EMT) (scale bars in a, c, 500 µm, scale bars in b, 20 µm).

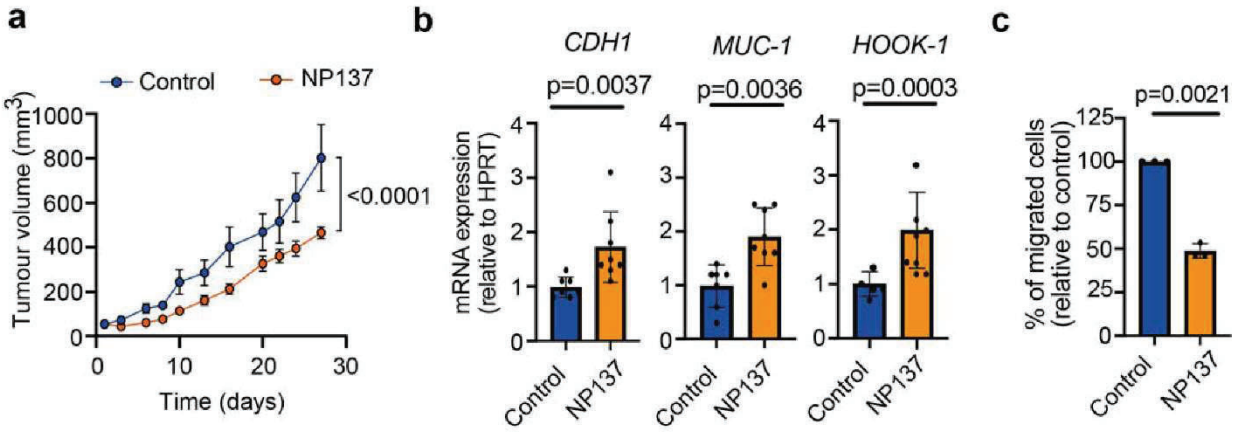

Extended Data Fig. 7 | Analysis of NP137 treatment on tumour growth, EMT and migration in endometrial human cancer cell line. a, Tumor growth quantification of human Ishikawa endometrial carcinoma cells grafted in nude mice treated with either control (n = 9) or NP137 (n = 9) (mean ± s.e.m., 2-way ANOVA). **b**, Relative mRNA expression of epithelial markers *CDH1*, *MUC1* and *HOOK1* by qRT-PCR in Ishikawa human cells grafted in nude mice treated with control (n = 7) or NP137 (n = 8) (data are normalized to *HPRT* gene, mean +/− s.e.m., two tailed Mann-Whitney U test). **c**, Percentage of migrated Ishikawa cells treated with NP137 relative to the migration of control condition through serum deprived culture medium complemented with 2.5% Matrigel between 5 and 24 h of invasion. (n = 3) (mean ± s.e.m, two tailed t test).

ARTICLE 3

Netrin-1 Mediated Feedforward Mechanism Promotes Pancreatic Cancer Liver Metastasis through Hepatic Stellate Cell Activation, Retinoid, and ELF3 Signalling.

Crissy Dudgeon[1]*, Anthony Casabianca[2,3]*, Charline Ogier[4], Chris Harris[2,3], Mélanie Bellina[5,6], Stephany Fiore[5], Agnes Bernet[5,6], Benjamin Ducarouge[6], David Goldschneider[6], Xiaoyang Su[1], Jason Pitarresi[8], Aram Hezel[7], Subhajyoti De[1], Wade Narrow[2,3], Fady Soliman[9], Cory Shields[3], Debora Barbosa Vendramini-Costa[4], Orjola Prela[2], Lan Wang[10], Igor Astsaturov[4], Patrick Mehlen[5,6], and Darren R. Carpizo[2,3,**]

*Co-first authors
**Corresponding Author

[1] Rutgers Cancer Institute of New Jersey [2] Department of Surgery, Division of Surgical Oncology, University of Rochester School of Medicine and Dentistry [3] Wilmot Cancer Center, University of Rochester [4] Department of Medical Oncology, Fox Chase Cancer Center [5] Apoptosis, Cancer and Development Laboratory - Equipe labellisée 'La Ligue', LabEx DEVweCAN, Institut Convergence PLAsCAN, Centre de Recherche en Cancérologie de Lyon (CRCL), INSERM U1052-CNRS UMR5286, Université de Lyon, Université Claude Bernard Lyon1, Centre Léon Bérard, 69008 Lyon, France. [6] Netris Pharma, 69008 Lyon. [7] Department of Medicine, Division Medical Oncology, University of Rochester School of Medicine and Dentistry [8] Department of Medicine, Division of Hematology/Oncology University of Massachusetts [9] Rutgers Robert Wood-Johnson Medical School [10] Department of Pathology and Laboratory Medicine, University of Rochester School of Medicine and Dentistry

Correspondence: darren_carpizo@urmc.rochester.edu

Highlights:

1) Netrin-1 is upregulated in metastatic pancreatic cancer.
2) The mechanism of Netrin-1 regulation involves activated hepatic stellate cell secreted retinoic acid signaling through RXR/RAR and ELF3 signaling.
3) Netrin-1 is present on the surface of extracellular vesicles which function to condition the pre-metastatic niche in the liver by activating HSCs.
4) Targeting Netrin-1 inhibits metastasis and improves survival in models of pancreatic cancer supporting the translation of anti-Netrin-1 therapy clinically in pancreatic cancer.

Summary

The biology of metastatic pancreatic ductal adenocarcinoma (PDAC) is distinct from that of the primary tumor. We detected an upregulation of the secreted axon guidance molecule Netrin-1 (Ntn1) in human and mouse PDAC metastases that signals through its receptor, uncoordinated-5b (Unc5b) to facilitate metastasis in vitro and in vivo. The mechanism of Ntn1 induction in liver metastasis is mediated by hepatic stellate cell (HSC) secreted retinoic acid through RXR/RAR and ELF3 signaling. Ntn1 is present in PDAC-derived extracellular vesicles (EVs) and facilitates metastasis

by inducing HSC activation. Importantly, administration of a neutralizing monoclonal NTN1 antibody decreased metastases and increased survival in several murine PDAC models (autochthonous and metastatic). Our studies reveal a new metabolic feed-forward loop for metastatic niche formation in the liver involving NTN1 in PDAC-secreted EVs and retinoic acid released from HSCs which is targetable using anti-NTN1 therapy.

INTRODUCTION

One of the defining features of pancreatic adenocarcinoma (PDAC) is its proclivity for early metastatic dissemination. This is underscored by several facts: 1) the majority of patients (85%) are stage IV at diagnosis and 2) the overwhelming majority (>80%) of patients with early-stage resectable disease succumb to metastatic recurrence. This highlights the need to better understand the biology of metastatic PDAC and identify novel therapeutic strategies for this major component of the disease. Recent next generation sequencing studies of pancreatic tumor progression have revealed that metastatic pancreatic cancer is driven more by global epigenetic reprogramming than by metastasis specific gene mutations with some exceptions such as parathyroid hormone related protein (PTHrP) (McDonald et al., 2017; Pitarresi et al., 2021). Epigenetic reprogramming leads to the selection of genetic programs that confer survival for disseminated tumor cells. One such category of genetic programs in advanced PDAC is that of axonal guidance genes, which include members of four canonical families (netrins, semaphorins, slits, and ephrins) (Biankin et al., 2012). These gene families were originally described for their involvement in neuronal development but have recently been implicated in cancer biology, particularly later stages of tumor progression and metastasis (Mehlen et al., 2011).

Netrin-1 is a secreted, laminin-like protein that was initially described for its role as both an axon attractant and repellent across a diverse number of organisms from C. elegans to D.melanogaster to H.sapiens (Lai Wing Sun et al., 2011; Serafini et al., 1994) . The netrin-1 receptors DCC (deleted in colon cancer) and Unc5 (in mammals there are five: Unc5A-D) belong to the family of Dependence Receptors (DRs) that mediate different functions depending on whether they are ligand bound or unbound (Gibert and Mehlen, 2015). In the presence of ligand, cells receive positive signals (survival, proliferation, migration) while in the absence of ligand, cells receive negative signals (apoptosis) (Mehlen et al., 2011). Through their death-inducing pathway, DRs function as tumor suppressors with three described means of inactivating this pathway for tumor progression and metastasis: 1) upregulation of the ligand (i.e. Netrin-1), 2) loss of expression of its receptor (through LOH or epigenetic silencing), and 3) loss of downstream death signaling partners (Delloye-Bourgeois et al., 2009; Mehlen et al., 2011). In metastasis, upregulation of Netrin-1 in breast cancer has been reported as a survival mechanism though the mechanism of this upregulation is unknown (Fitamant et al., 2008).

While Netrin-1 has been found to be upregulated in PDAC (Dumartin et al., 2010), its role in PDAC tumor progression is poorly understood. Here we describe that Netrin-1 becomes upregulated to drive PDAC metastasis through the dependence receptor Unc5b. For the first time we show that Netrin-1 is detected on the surface of EVs which function to facilitate liver metastasis through the activation of hepatic stellate cells. The mechanism of Netrin-1 upregulation in disseminated tumor cells is mediated by a novel feed-forward mechanism whereby EV's containing Netrin-1 activate hepatic stellate cells to secrete retinoic acid which upregulates Netrin-1 by both RAR/RXR and Elf3-mediated mechanisms. Disruption of Netrin-1/Unc5b signaling both

genetically and pharmacologically prevents metastasis and increases survival in murine and human PDAC models validating Netrin-1 as a novel therapeutic target for metastatic PDAC.

RESULTS

Netrin-1 is upregulated in metastatic PDAC.

We identified Netrin-1 as a gene that is upregulated in metastatic tumors from a murine PDAC model (INK4.1^{syn_Luc}) whereby immunocompetent FVB mice were orthotopically injected with a primary pancreatic cancer cell line (Ink4a.1) derived from the Pdx-1-Cre; Kras$^{G12D/+}$; p16$^{-/-}$; p19$^{-/-}$ murine model (Bardeesy et al., 2006; Collisson et al., 2012). This spontaneously disseminating model was used to harvest liver and peritoneal metastases for RNA sequencing and cell line establishment. When we compared the liver metastases to the primary tumors in this model, we observed marked differences in morphology. The histology of the primary tumors was poorly differentiated, with scattered glandular appearing cells consistent with the quasi-mesenchymal subtype that this cell line was previously classified (Collisson et al., 2011) (Figure 1Ai). E- cadherin staining of primary tumors exhibited a lack of staining in the mesenchymal-like tumor cells and positive staining in the well-differentiated cells which were sparse (Figure 1A*ii*). Collagen deposition was observed at the stromal border along the tumor edge (Figure 1A*iii*), similar to other orthotopic models of pancreatic cancer (Erstad et al., 2018; Erstad et al., 2020; Takahashi et al., 2018). While the primary tumors resembled the quasi-mesenchymal subtype of PC, liver metastases displayed hallmarks consistent with the 'classic' molecular subtype of PC including appearing more well differentiated areas with more tumor cells forming glandular structures (Figure 1A*iv*) with high expression of E-cadherin (Figure 1A*v*) and robust collagen stroma (Figure 1A*vi*).

We hypothesized that the observed plasticity in morphology in the metastatic tumors is a consequence of epigenetic reprogramming, like that reported in human metastatic PCs (McDonald et al., 2017). We compared the transcriptomes from metastatic and primary tumor tissue (n=5 for both) by total RNAseq and found the transcriptomes to be substantially different, as evident from the volcano plot showing p-value and fold change of gene expression between groups (Figure S1A). We then examined a cell line derived from a liver metastasis (Met38) for differential open chromatin regions in comparison to the parental cells using the assay for transposase accessible chromatin (ATAC-seq). While genome-wide higher order chromatin accessibility patterns were largely comparable (see example of chromosome 1, Figure S1B), a total of 238 loci showed significant changes in chromatin accessibility. The primary tumor cell line, Ink4a.1, had 51 regions of open chromatin which were not observed in the metastatic line, Met38, whereas the latter had gain of open chromatin in 187 regions (Figure S1C). Taken together, these data indicate that this model faithfully recapitulates the cellular plasticity characteristic of epithelial to mesenchymal (EMT) and mesenchymal to epithelial (MET) transition in human metastatic biology (Thiery et al., 2009; Tsai and Yang, 2013).

Differential gene expression analysis comparing hepatic metastases to primary tumors revealed several genes up and downregulated that involve pathways important in metastasis. Pathway enrichment analysis for Biological Processes showed top upregulated pathways included Developmental Biology, Nervous System Development, Axon Guidance, Extracellular Matrix Organization, Regulation of IGF uptake, and Signaling by PDGF (Figure 1B left, Figure S1D left). Top downregulated enriched pathways include Cell-Cell Signaling, Biological and Cellular Adhesion, Small Molecule Biosynthetics Process, and Epithelial Cell Differentiation (Figure 1B

right, Figure S1D right). Taken together, these pathways have been shown by others as part of the metastatic process for pancreatic cancer (Krebs et al., 2022; Lu et al., 2019; Wu et al., 2020; Zu et al., 2020). Differential gene expression involved in pancreatic cancer metastasis included upregulation of *Pdgfrb* (Weissmueller et al., 2014), and *Cldn9* (and downregulation of *Cldn1* (Chao et al., 2009)) . Interestingly metastatic tumors were high in Col6a3 (Type VI collagen) which has previously been shown to be highly expressed in human PDAC as part of the desmoplastic stroma (Arafat et al., 2011), consistent with what we observed morphologically (Figure 1A*vi*). We also observed the axon guidance gene Netrin-1 was amongst the most upregulated genes (Figure 1B). Previous reports have shown expression of multiple axon guidance genes in PDAC, including Slit, Robo, and Sema3, and there importance regulating perineural invasion, a common feature of PDAC (Biankin et al., 2012; Foley et al., 2015; Jurcak et al., 2019; Yong et al., 2016). Homing in on the expression of this pathway from our dataset shows that Ntn1 was the most upregulated (Figure 1B, bottom). We validated this result on a small subset of these genes by quantitative PCR (qPCR) using four cell lines derived from separate hepatic metastases (Met 25,35,36,38). We found that compared to the parental Ink4a.1 cell line, *Ntn1*, *Selp*, and *Pdgfb* were all significantly upregulated while expression of *Basp1* trended downward, validating the RNAseq results (Figure S1E). To confirm this result at the protein level we examined Netrin-1 expression by immunohistochemistry of primary and metastatic tumor tissue. We found greater Netrin-1 expression in hepatic metastasis compared to primary tumors in the orthotopic model (Figure S1F). We created primary cell lines from a number of metastatic liver tumors and found that Netrin-1 protein was upregulated when compared to the Ink4a.1 primary tumor cell line. (Figure 1C). To validate this in human PDAC, we performed Netrin-1 immunohistochemical staining on a tissue microarray (TMA) composed of 93 PDAC samples containing 18 metastatic and 75 primary tumors in which Netrin-1 expression was significantly greater in the metastatic tumors ($p=0.03$) (Figure 1D). To confirm this finding, we evaluated a separate TMA composed of 25 PDAC specimens taken from patients with stage II primary cancers and stage IV metastatic disease. Similarly, we found that Netrin-1 expression was greatest in metastatic tumors as compared to primaries (Figure S1G). Due to the Ink4a.1's QM status, we looked to see if high Netrin-1 expression differs amongst PDAC molecular subtypes. Interestingly in the Collisson *et. al*. dataset, *NTN1* expression is significantly greater in both the QM and exocrine as compared to classical subtypes (Figure 1E).

Unc5b is the dominant Netrin-1 receptor in PDAC and functions as a Dependence Receptor to promote metastasis.

We examined the Ink4a.1 RNAseq data set and found the Netrin-1 receptor that was primarily expressed in PDAC was Unc5b. We found no detectable levels of DCC and minimal to no detectable levels of Unc5a, Unc5c, and Unc5d (Figure 2A). We confirmed this by western blot in the Ink4a.1, Met25, and Met38 metastatic clones (Figure S2A). We also detected Unc5b in all cell lines of a larger panel of murine and human PDAC cells that also lacked DCC expression (Figure S2B). Using the TCGA dataset in human PDAC, we also found the dominant Netrin-1 receptor is Unc5b (Figure S2C). We then determined the impact of Netrin-1/Unc5b signaling on PDAC metastasis both *in vitro* and *in vivo*. We first confirmed the cell death mechanism of the Unc5b receptor was intact whereby downregulation of the ligand using siRNA in both the Ink4a.1 and Met38 cell lines led to increased apoptosis by Annexin V staining (Figure 2B). To demonstrate Unc5b functioned positively when ligand bound, we performed *in vitro* migration and invasion assays in the presence of recombinant Netrin-1 using the Ink4a.1 line and found that Netrin-1 significantly increased both migration and invasion (Figure 2C). Conversely, when we knocked down (KD) the expression of Netrin-1 using siNtn1 we observed a significant decrease in migration

and invasion (Figure 2D). We validated Ntn1 KD in these cell lines by western blot (Figure S2D). We created a stable KD of *Ntn1* in the Met38 cell line by sh*Ntn1* (KD verified by western blot, Figure S2E) whose proliferation was unchanged by Ntn1 KD (Figure S2F) and evaluated this cell line's ability to form pseudopodia during a 3D tumor spheroid invasion assay. We found that in the control shRNA Met38 cells, the cells form abundant pseudopods in 7 days that were significantly attenuated in the *Ntn1* KD cells (Figure 2E). When we deleted the *Unc5b* gene from another mouse PDAC cell line, A1925, and from the Met38 cells, we also observed a significant reduction in both pseudopodia formation and cell invasion (Figure 2E and F respectively). We validated these *in vitro* findings *in vivo* using a liver metastasis assay where Met38 *Ntn1* WT and *Ntn1* KD cells were injected into the spleen followed by splenectomy. After 10 days, mice were sacrificed, and liver metastases were quantitated from H&E-stained tissue sections. We found that *Ntn1* KD significantly decreased the percent tumor area of metastatic tumor growth (Figure 2G). We found a similar finding when we evaluated the *Unc5b* knock out cells by the same liver metastasis assay (Figure 2H). Taken together these experiments demonstrate that Unc5b is the dominant Dependence Receptor in PDAC and as such, facilitates metastasis when ligand bound and cell death when ligand unbound.

Hepatic stellate cell secretion of retinoids causes upregulation of Netrin-1 through RAR/RXR signaling.

While upregulation of Netrin-1 as a survival mechanism in metastatic cancer has previously been described, the mechanism for this is unknown (Fitamant et al., 2008). During liver metastasis hepatic stellate cells transdifferentiate into myofibroblasts, which then secrete factors that promote tumor cell migration/invasion through a variety of mechanisms (Kang et al., 2011). We hypothesized that HSCs might also be involved in promoting Netrin-1 mediated liver metastasis. To address this, we isolated and cultured HSCs to produce conditioned media that was fed to the Ink4a.1 cell line over a 24-hour time period. Netrin-1 expression by western blot was analyzed. The HSC conditioned media induced a time-dependent increase in Netrin-1 at 3, 6, and 24 hours (Figure 3A). This upregulation was specific to HSCs as we did not observe a similar increase in Netrin-1 when we incubated conditioned media from other cell types in the liver including hepatocytes and liver sinusoidal endothelial cells with the Ink4a.1cells (Figure S3A). *In vitro*, fresh isolates of HSCs cultured on plastic dishes become spontaneously activated to myofibrobasts over a period of 8 days (Jophlin et al., 2018). Naïve HSCs contain lipid droplets which are specialized organelles for the storage of retinoids (they store 60% of the body's vitamin A) and upon activation, HSC-derived myofibroblasts lose these lipid droplets due to extracellular secretion. This process can be visualized by microscopy as the intracellular droplets auto fluoresce and are lost upon activation (D'Ambrosio et al., 2011; Friedman et al., 1993). We observed this process in isolated HSCs in vitro over a 15-day period (Figure 3B, top), confirming the loss of retinoids. We found an increase of Ink4a.1 Netrin-1 levels when cells were incubated with HSC conditioned media from days 2-15, corresponding with decreasing HSC intracellular retinoids (Figure 3B, bottom). We believed this increase was due to a molecule secreted by activated HSCs (Figure 3B). To identify this molecule, we used size exclusion chromatography using filters with cutoff sizes of 3,000 Daltons (3K), and 1000 Daltons (1K). Fractions were collected of the filtered and flow through and analyzed for Netrin-1 upregulation by incubating them with the Ink4a.1 cells. Based upon induction of Netrin-1 by the flow through fractions of the 3K and 1K filters, we concluded that the molecule was less than 1000 Daltons which ruled out a macromolecule, such as a protein or peptide and hypothesized it to be a small molecule, likely a metabolite (Figure S3B). Given that the major component of the HSC lipid droplets are retinoid species within this size range, we examined fractions of our HSC

conditioned media collected for evidence of retinoid species using LC/MS. Conditioned media at days 8, 11, and 15 contained both retinal and retinoate (9-cis-retinoic acid) (M.W. 285 and 301 respectively) while these compounds were minimally present at day 4 indicating the presence of retinoid metabolites in the CM of activated HSCs (Figure S3C). To confirm that retinoid metabolites were the molecule(s) in question we incubated retinoic acid (RA), retinoate (9-cis-retinoic acid) and retinal with the Ink4a.1 cells over 24 hours and examined Netrin-1 levels and found that all three exhibited a time-dependent increase that was observed as early as 3 hours (Figure 3C, S3D). The finding that retinoic acid upregulates Netrin-1 was observed in multiple murine PDAC cell lines other than the Ink4a.1 cells suggesting this to be a common mechanism (Figure S3E).

To determine if the upregulation of Netrin-1 in PDAC cell lines by HSC-secreted retinoic acid was mediated by retinoic acid receptors RAR/RXRs, we first examined the expression levels of RAR-α, RARγ, RXRα, RXRβ, and RXRγ in three murine PDAC cell lines (Ink4a.1, K8484, and K8483). We found that all three cell lines expressed RARα and RXRα, while RARγ was expressed in the Ink4a.1 and K8383 lines but not in the K8484. RXRβ and RXRγ were only expressed in the K8383 line (Figure S3F). Using chromatin immunoprecipitation (ChIP), we detected the binding of RXR in the Netrin-1 promoter in response to treatment with retinoic acid (10 mM) (Figure 3D). We next performed knockdown experiments of both RAR-α and RXRα using an siRNA approach and found that knockdown of both led to a decrease in HSC-mediated Netrin-1 induction, and a combination of si*RARα/RXRα* led to the greatest decrease in Netrin-1 induction (Figure 3E). Consistent with this result we used a small molecule antagonist of RXR signaling (UVI 3003) in combination with either all trans retinoic acid (RA) or 9-cis-retinoic acid (9RA) and found that UVI 3003 suppressed the induction of these retinoids in the Ink4a.1 cells (Figure 3F). Together, these experiments indicate that activated HSCs secrete retinoic acid which in turn upregulates Netrin-1through RAR/RXR signaling. RXR signaling appears to be more important as 9-cis-retinoic acid has the biggest effect on Netrin-1 induction (Figure 3C) and it targets RXR preferentially over RAR.

Retinoic acid induces transcription factor Elf3 to increase expression of Netrin 1 in human and mouse pancreatic cancer cells.

We noted that a number of cell lines derived from liver metastases from Ink4a.1 primary tumors retained upregulated expression of Netrin-1 despite no longer being in the presence of HSC's or retinoic acid (Figure 1C) suggesting that these cells underwent epigenetic reprogramming, possibly in response to retinoic acid as this has been shown to modulate chromatin (Pattison et al., 2018). We examined our ATACseq data (Figure S1B) at the Ntn1 locus for evidence of differential peaks between the metastatic and parental cells and did not find a difference (Figure S3G), however, we did find the locus of transcription factor Elf3 to be to be more open in the Met38 cell line (Figure 4A). Elf3 mRNA expression was also upregulated in the Met38 cell line, as well as in all other cell lines (Met25, Met35, Met36 and Met72) derived from metastatic Ink4a.1 tumors (Figure S3H).

Like Ntn1, transcription of Elf3 was strongly induced by retinoic acid in pancreatic cell lines (Figure 4B). Binding of RAR to the Elf3 promoter by also detected by ChIP (Figure 4C). Since ELF3 has been shown to cause epithelial-mesenchymal transition (EMT) in hepatocellular cancer cells (Zheng et al., 2018), we tested whether retinoic acid can also promote EMT in pancreatic cancer cells using a set of cell lines derived from an alternative PDAC model (Ptf1a-Cre; LSL-Kras^{G12D}; Arid1a$^{f/f}$ (KPCA)) (Wang et al., 2019). As shown in Figure 4D, the epithelial marker protein E-cadherin was decreased by retinoic acid treatment, while the mesenchymal marker protein vimentin increased in a dose dependent manner. We hypothesized that Elf3 may upregulate Netrin-1 directly as there are several Elf3 consensus binding sites in the *Ntn1* promoter conserved across species.

Using ChIP, we confirmed that Elf3 bound the *Ntn1* promoter (Figure 4E). We observed an induction of *Ntn1* when Elf3 was overexpressed in the Ink4a.1 cells (Figure 4F). Alternatively, when CRISPR-Cas9 was used to reduce expression of *Elf3* in the MET38 cell line, there was decreased induction of *Ntn1* by retinoic acid (Figure 4G). In a human PDAC cell line, Miapaca-2, siRNA-dependent knockdown of *ELF3* expression (Figure S3I, right) caused a sharp decrease in *NTN1* expression (Figure S3I, left). Note, we did not concomitantly silence expression of the retinoic acid receptors in these experiments. These results demonstrate that retinoic acid can regulate *Ntn1* directly as well as indirectly through *Elf3*.

Netrin-1 on the surface of extracellular vesicles promotes hepatic metastasis by activating HSCs.

Netrin-1 and its receptors have been shown to be expressed on a variety of cell types including cancer associated fibroblasts (CAFs) (Sung et al., 2019) , thus we hypothesized that tumor cell-secreted Netrin-1 might be involved in HSC activation. We incubated recombinant Netrin-1 with freshly isolated hepatic stellate cells and observed a time-dependent increase in the expression of genes associated with the activated HSC phenotype (*Acta2*, *Col1a1*, and *Lox*) (Figure 5A). To see if this effect could be observed *in vivo*, we created a *Ntn1* KO in the Ink4a.1 cell line. We confirmed a lack of *Ntn1* expression in two different KO clones (P2A4, P5E11) by qPCR analysis (Figure S4A). We implanted the Ink4a.1 *Ntn1* WT and KO cells orthotopically and allowed primary pancreatic tumors to develop. After 20 days the mice were sacrificed, and their livers were harvested to assess for in vivo HSC activation. Of note, there was no significant difference in size of the *Ntn1* KO primary tumors compared to the *Ntn1* WT (Figure S4B), in addition the livers of these mice did not show evidence of macro or microscopic metastases (data not shown). Since the Ink4a.1 cells express the Cre-recombinase and the FVB host mice that are used to create pancreatic tumors do not, we developed a QPCR based assay for Cre-recombinase DNA in liver tissue as a sensitive means of detecting metastatic cells in the liver particularly when it is difficult to detect them by immunofluorescent techniques. We found that at 20 days post injection the amount of Cre recombinase in the liver of mice injected with either *Ntn1* WT vs. KO cells was not significantly different, in fact there was a trend toward an increase in the *Ntn1* KO group (Figure S4C). This indicates that at this early stage of primary tumor development there was evidence of distant metastasis that was not significantly different in either the *Ntn1* WT or KO tumors.

To determine if there was a difference in HSC activation in vivo, we performed dual immunofluorescence on the livers of mice harboring either *Ntn1* WT vs. KO pancreatic tumors using the HSC marker desmin. We used smooth muscle actin (SMA) to indicate transdifferentiation to the myofibroblast state. We quantified double positive Desmin/SMA cells and found a significant increase in the mice with *Ntn1* WT vs. KO tumors (Figure 5B). As an alternative approach to evaluating the activation state of HSCs in the liver, we used flow cytometry to identify HSCs by high scatter (SSC) (Geerts et al., 1998). We repeated the orthotopic pancreatic tumor experiment with either *Ntn1* WT vs. KO cells and at 20 days post injection, harvested livers for cell isolation and stained the cells with an antibody to SMA. We gated the top 10% of high side scatter events for HSC isolation as previously described and then quantified the SMA+ population. This population of HSCs represent the early activated state before the HSCs have fully released their Vitamin A stores. We found a significantly greater number of high SSC/SMA+ cells in the livers of mice harboring the Ntn1 WT vs. KO tumors (Figure 5C). This indicates that Ntn1 activates HSCs both *in vitro* and *in vivo*. This also suggests that this intercellular communication could not only be through short range but also a long-range mechanism.

Although Netrin-1 is a secreted protein, its laminin structure causes it to tightly associate with extracellular matrix proteins rather than enter the blood. Interestingly, however, we did detect the presence of Netrin-1 in tumor-derived extracellular vesicles (EVs), which have been shown to enter the blood stream and to play a role in pre-metastatic niche formation in pancreatic and other cancers (Costa-Silva et al., 2015; Peinado et al., 2012). We isolated EVs from conditioned media of Netrin-1 expressing cells (Ink4a.1, Met38) using modified ultracentrifugation protocols suitable for EVs isolation from conditioned media (Menck et al., 2013; Thery et al., 2006). We determined the size distribution of the different pellets and concentration using NanoSight software (NTA) analysis. All EV populations present a peak in particles size around 100nm (Figure 5C). Western blot analysis was used to assess Netrin-1 presence in EVs in each of these cell lines (Figure 5C). To investigate Netrin-1's localization, Transmission Electron Microscopy analysis (TEM) was performed using a commercial anti-netrin-1 antibody coupled with 15 nm golden beads and used to analyze EVs derived from lnK4a and Met38 cell lines. In parallel, a commercial CD63 tetraspanin antibody was coupled with 5 nm golden beads as a positive control of EV labelling. We performed this analysis without permeabilization such that detection of a positive signal indicated that Netrin-1 is located at the vesicle surface. TEM detected Netrin-1 localization at the surface of EVs of lnK4a and Met38 cells respectively with a frequency of 10% and 50% of all EVs (Figure 5E,F). As Netrin-1 is upregulated in the Met38 cell line as compared to Ink4a.1, we detected a significantly higher number of Netrin-1+ EVs amongst the CD63+ EVs (Figure S4D). As an alternative approach, we harvested EVs from conditioned media by immunoaffinity isolation in both both Ink4a.1 and Met38 cells and verified the presence of EVs with expression of alix, a known EV marker. Netrin-1 was detected in the EV fraction, with the Met38 cells showing a greater yield of Netrin-1 (Figure S4E). We also prepared EVs from Ink4a.1 *Ntn1* WT and KO cells and demonstrated Netrin-1 detection in the CM as well as the EV fraction from *Ntn1* WT cells, while *Ntn1* KO EVs were devoid of Netrin-1 expression (Figure S4F). We further confirmed that this fraction contained EVs by transmission electron microscopy, revealing that both the preparation from *Ntn1*-WT and *Ntn1*-KO cells exhibited similar size particles (Figure S4G). To determine the generality of Netrin-1 presence in EVs, we isolated EVs from three human lung cancer cell lines (A549, H322, H358) that were of similar size (100 nM) by NTA analysis to EVs from the Ink4a.1 and Met38 lines (Figure S5A). Netrin-1 was present in EVs of H322 and H358 but not in A549 (Figure S5B, with CD9 and Flottilin-1 as EV markers). TEM analysis on the H358 and A549 cells for CD63 demonstrated the presence of CD63 on the surface of all EVs while Netrin-1 was only present in the H358 EVs (Figure S5C). This suggests a general mechanism of Netrin-1 localization in EVs of cancer cells.

We then employed the splenic liver metastasis assay to determine if Netrin-1+ EVs functionally contributed to the metastatic process. To do this, we harvested EVs from Ink4a.1 *Ntn1* WT and *Ntn1* KO cells by immunoaffinity isolation. For this *in vivo* experiment, mice were pre-treated with EVs prepared from Ink4a.1 *Ntn1* WT and *Ntn1*KO cells for two weeks prior to injecting the Met38 cells intrasplenically. The dose and schedule of EVs was previously shown to facilitate liver metastatic niche in pancreatic cancer (Costa-Silva et al., 2015). After 14 days, the mice were sacrificed, and livers harvested to assay for differences in metastatic burden. We found that the mice injected with the *Ntn1*-KO EVs exhibited a marked decrease in the metastatic burden as evident by gross examination of the liver, and histologic quantitation (Figure 5G). These data indicate that Netrin-1 is present at the surface of EVs from tumor cells and that these EVs are functionally relevant to liver metastasis through HSC activation.

Netrin-1 interference suppresses metastasis and increases survival in murine PDAC models.

While the Unc5b receptor facilitates metastasis, due to its function as a dependence receptor, it also provides a pathway to therapeutically target these metastatic tumor cells by interfering with Netrin-1 signaling to initiate apoptosis. We evaluated the potential of Netrin-1 as a novel therapeutic target in PDAC by first using the in vivo Ink4a.1 liver metastasis assay to assess quantitation of metastatic burden and overall survival as endpoints. One day before splenic injection of the Ink4a.1 tumor cells, mice were treated with a monoclonal antibody to Netrin-1 (mAbNtn1) every other day for 14 days before sacrificing the mice and quantifying the metastatic burden from the livers. We found that Netrin-1 interference significantly decreased the number of metastatic colonies as compared to the vehicle control (Figure 6A). Likewise, when we evaluated the same model for overall survival, we found that Netrin-1 interference significantly improved overall survival. All of the PBS-treated mice succumbed to their PDACs by day 46 days while 3/9 mice in the mAbNtn1 group were alive past 200 days. The median survival of the control was 37 days and 56 days for the mAb-Ntn1 group, $p \leq 0.008$ (Figure 6B). To confirm these results, we turned to another liver metastatic model using a cell line (KPC3) derived from the Pdx1-Cre;LSL-$Kras^{G12D}$;$Trp53^{f/f}$ model injected directly into the portal vein of C57Bl/6J mice and treated with either IgG control vs. mAbNtn1 twice per week for 3 weeks prior to sacrifice. We quantified sections of liver stained for CK17 as a marker for tumor cells and found that anti-Netrin-1 therapy significantly reduced the metastatic burden (Figure 6C). The Netrin-1 levels in the KPC3 cell line were not detectable by Western blot (Figure 6D), but when the cells engrafted in the liver and formed tumors in both the IgG control and mAbNtn1 treated mice, Netrin-1 levels significantly increased consistent with what we observed with the Ink4a.1 model (Figure 1C). There was a marked decrease in Netrin-1 levels in the livers of mAbNtn1 treated mice versus the IgG controls (Figure 6D). To evaluate the efficacy of anti-Netrin-1 on survival in an autochthonous mouse model, we used the Pdx-1; $Kras^{G12D/+}$; $p53^{R172H/+}$ (KPC) model in which mice were monitored for primary tumor growth and randomized to either vehicle control vs. mAbNtn1 when a dominant tumor was detected by ultrasound at 4-5mm. We found that the mAbNtn1 significantly improved the median survival, from 18 days in the control vs. 42 days in mAb-Ntn1, $p=0.018$ (Figure 6E). Taken together, these data suggest that anti-Netrin-1 decreases metastasis and improves survival in pre-clinical pancreatic cancer models.

DISCUSSION

The biology of metastatic PDAC remains poorly understood but evidence now exists that it is largely driven by epigenetic mechanisms that govern cell plasticity (McDonald et al., 2017). The source of these mechanisms and their timing during tumor progression remains unclear. Here we demonstrate that one source of this plasticity is driven by the microenvironment of the metastatic niche as evidenced by the upregulation of the axon guidance molecule, Netrin-1, signaling through its receptor Unc5b to promote dissemination and metastatic tumor cell survival. Most importantly because of the unique cell death mechanism of dependence receptors triggered upon interference with ligand binding, this upregulation also confers a therapeutic vulnerability to metastatic PDAC.

While Netrin-1 has been shown to be upregulated in metastases of other solid organ cancers such as breast and colon (Fitamant et al., 2008; Paradisi et al., 2009), the feed-forward mechanism we have found through Netrin-1 activating hepatic stellate cells to then secrete retinoic acid to upregulate Netrin-1 is the first to describe this and emphasizes the role of the metastatic niche in driving this aspect of PDAC biology (Figure 7). Given the only source of retinoic acid in the body comes from the hepatic stellate cell population, this raises the question as to, “What is the mechanism of upregulation in metastases in other organs such as the lung, brain or peritoneum?”

Given that the microenvironment of other organs is vastly different, it is likely that other drivers of cell plasticity are likely driving Netrin-1 upregulation. Our data suggest that inhibition of RXR or dual RXR/RAR signaling could potentially be useful for hepatic metastases either alone or in combination with anti-Netrin-1 therapy. There are currently no inhibitors of RXR or RAR signaling available in the clinic and the inhibitors that exist for research purposes (such as the one used here) are not optimized for in vivo use. Another strategy would be to combine Netrin-1 inhibitors with inhibitors of hepatic stellate cell activation, which are currently being investigated to treat liver fibrosis (Hong et al., 2018). Interestingly dietary intake of retinol or oleic acid has been shown to inhibit liver fibrosis by inhibiting HSC (Li et al., 2015; Murakami et al., 2011) but has not been investigated as a strategy to inhibit liver metastasis.

The finding of Netrin-1 on the surface of extracellular vesicles is novel and represents a significant contribution to the Netrin-1 field as it shows that Netrin-1 can function in both long- and short-range intercellular communication. This fits well with previous reports showing secreted Netrin-1 that is not associated with EVs binds to the surface of cells through heparin-sulfate functioning in an autocrine manner to guide axons making it difficult to perform this type of intercellular communication (Matsumoto et al., 2007; Serafini et al., 1994).

The discovery that Netrin-1 positive EVs activate hepatic stellate cells and contribute to liver metastasis through hepatic stellate cell activation indicates that EV associated Netrin-1 is functionally relevant to liver metastasis. It is possible this occurs through both long- and short-range mechanisms. While it has been shown that exosomes from pancreatic cancer can facilitate liver metastasis by preparing the metastatic niche, the mechanism was shown to be distinct from ours in that the exosomes were taken up by Kupffer cells which lead to the secretion of cytokines that acted locally within the liver to activate HSCs (Costa-Silva et al., 2015). Both investigations suggest the importance of HSC activation to contribute to making a more hospitable environment for the survival of metastatic PDAC cells.

The vast majority of PDAC patients harbor disseminated disease, thus a novel therapy that targets the biology of metastatic PDAC (such as Netrin-1 signaling) could have a significant clinical impact. NP137 is the first in class humanized monoclonal antibody specific to Netrin-1 which targets the V2 sub-domain that is critical for binding to the UNC5 receptors (Grandin et al., 2016). NP137 was shown to be safe in a phase I clinical trial in multiple solid organ cancers and is now being evaluated in phase II in patients with advanced gynecological cancers with a follow up study in locally advanced PDAC patients in combination with FOLFIRINOX (NCT05546853) (Cassier P., 2019). Our data provide pre-clinical evidence to support a trial of NP137 in metastatic PDAC patients. We speculate that the clinical setting that would most benefit from Netrin-1 therapy would be in patients undergoing surgical resection where anti-Netrin-1 therapy can prevent the progression of micrometastatic disease to clinically detectable disease.

Metastatic relapse occurs in the majority (>80%) of patients following curative intent surgery due to a large burden of disseminated tumor cells present at the time of surgery. Our data suggest that anti-Netrin-1 therapy could potentially have a significant impact in this circumstance. We have now entered the era where molecular subtype in PDAC has shown to correlate with differences in survival in response to chemotherapy with basal or quasi-mesenchymal tumors being associated with chemotherapy resistance and a worse survival. Novel therapies for QM tumors are needed and the finding that Netrin-1 is upregulated in QM tumors supports the investigation of NP137 in PDAC for differential responses in classical vs. basal/QM tumors.

MATERIALS AND METHODS

Cell lines. Ink4a.1 (gift from Dr. Eric Collisson) is a mouse pancreatic cancer cell line derived from the p48cre, KrasLSL_G12D, p16-/-/p19-/- mouse model (Bardeesy et al., 2006). The cell lines MET25, MET35, MET36, MET38 and MET72 were derived from Ink4a.1 as described in Figure 1. K8483 and K8484 are mouse pancreatic cancer cell lines derived from Pdx-1-Cre, KrasLSL_G12D, Trp53R172/H/+animals, and were a gift from Dr. David Tuveson. 2838c3 and 6419c5 are mouse pancreatic cell lines derived from KPC-YFP animals and were a gift from Dr. Ben Stanger. KP2 is a mouse pancreatic cell line derived from KPC mice and was a gift from Dr. David Linehan. BXPC3, CAPAN2, PANC1 and MIAPACA-2 are human pancreatic cell lines that were purchased from ATCC. A1809, A2031 and A2441 are mouse pancreatic cancer cell lines derived from Ptf1a-Cre; LSL- KrasG12D; Arid1af/f (KPCA) mice from Dr. Aram Hezel. A knockout of UNC5B was generated in the MET38 cell line by CRISPR-Cas9, using the Edit-R lentivirus VSGM11942-247910466 (Horizon Discovery). All copies of Unc5b were completely removed, as confirmed by Western blot and by DNA sequence analysis near the gRNA target site. A knockdown of Elf3 was generated in the MET38 cell line by CRISPR-Cas9, using the Edit-R lentivirus VSGM11942-248070215 (Horizon Discovery). This reduced but did not remove Elf3 expression, as judged by Western blot. A knockdown of Ntn1 was generated in the MET38 cell line by CRISPR-Cas9, using the Edit-R lentivirus VSGM10144-246774776 (Horizon Discovery). Isolated mouse hepatocytes (C57- 6224F) and sinusoidal endothelial cells (C57-6017) were purchased from Cell Biologics and were cultured as recommended by the manufacturer. To treat INK4A cells, conditioned media from 72-hour cultures of hepatocytes and sinusoidal endothelial cells were added in equal volume to DMEM/10% FBS. For proliferation analysis, cells were grown in 96 well plates and assayed at various time using CCK8 solution (Dojindo).

Knockdown and overexpression experiments. Lipofectamine 3000 (Lifetechnologies) was used to transfect INK4A.1 cells with either pCMV6 control vector or with pCMV6- ELF3 (Origene #RC200631). RNA was harvested from transfected cells after 72 hours. siRNAs were purchased from Horizon Discovery. MIAPACA2 cells were treated with On- TargetPlus SmartPool directed against human ELF3 (L-016080–00-0005), or with On- TargetPlus non-targeting pool (D-001810-10-05). RNAIMAX was used as a transfection reagent. 72 hours after transfection, RNA was collected using RNAeasy columns (Qiagen).

Drug treatments. All trans retinoic acid (ATRA or RA) and 9-cis retinoic acid (9RA) were purchased from Sigma and resuspended in ethanol. Cells were treated with 1-10 μM of various retinoids at various times and harvested for protein or RNA analysis. To inhibit RXR, 10 μM UVI 3003 (SelleckChem) was used to pretreat cells for 1 hour prior to addition of retinoic acids for 24 hours. Cells were then harvested for Western blotting analysis.

Migration,nvasion, and 3D Tumor Spheroid Sprouting Assays. Cells were plated a day prior to overnight starvation in media containing 0.1% FBS (serum starvation media, SSM). The next day, 100,000 cells in serum starvation media were placed in the top of a transwell (8 μm filter, Falcon, 353097), with the bottom chamber containing either SSM, SSM+ 150 ng/mL recombinant human Netrin-1 in PBS/0.2% BSA (R&D Systems, 1109- N1-025), or media + 10% FBS. For invasion assays, transwells were coated with 1 mg/mL growth factor reduced matrigel (Corning) and allowed to solidify 1 hr at 37°C prior to loading cells into the chamber. Cells were allowed to migrate/invade for 24 hrs. Transwells were removed and cells fixed and stained using Diff-Qwik (FisherSci) per the manufacturer's protocol. After 3x PBS washing of transwells, a pre-wetted q-tip was used to remove

cells from the upper part of the filter, while the bottom, where cells had migrated through, were not disturbed. The filter was removed from the transwell using a razorblade and laid cell-side down and mounted with a glass coverslip in permount on a glass slide. Slides were cured overnight at room temperature and images taken with the light microscope at 100X. Cells were quantitated per 100X field (n=10 fields). For the sprouting assay, a single cell suspension in 1:1 matrigel/media was plated at low density (1000- 5000 cells/well of 96-well plate) onto a hardened bed of matrigel and allowed to grow for 7-14 days. Cells were re-fed in complete media + 2% matrigel every 3 days.

ATAC-seq analysis. ATAC-Seq analysis. Cells were harvested and frozen in culture media containing 5% DMSO. Frozen cells were sent to Active Motif to perform the ATAC- seq assay. The cells were then thawed in a 37oC water bath, pelleted, washed with cold PBS, and fragmented as previously described (Buenrostro et al., 2013) with some modifications (Corces et al., 2017). Briefly, cell pellets were resuspended in lysis buffer, pelleted, and tagmented using the enzyme and buffer provided in the Nextera Library Prep Kit (Illumina). Tagmented DNA was then purified using the MinElute PCR purification kit (Qiagen), amplified with 10 cycles of PCR, and purified. Resulting material was quantified using the KAPA Library Quantification Kit for Illumina platforms (KAPA Biosystems), and sequenced with PE42 sequencing on the NextSeq 500 sequencer (Illumina). Analysis of ATAC-seq data was very similar to the analysis of ChIP-Seq data. Reads were aligned to the human genome (hg38) using the BWA algorithm (MEME mode; default settings). Duplicate reads were removed, only reads mapping as matched pairs and only uniquely mapped reads (mapping quality >= 1) were used for further analysis. Alignments were extended in silico at their 3'-ends to a length of 200 bp and assigned to 32-nt bins along the genome. The resulting histograms (genomic "signal maps") were stored in bigWig files. Peaks were identified using the MACS 2.1.0 algorithm at a cutoff of p-value 1e-7, without control file, and with the –nomodel option. Peaks that were on the ENCODE blacklist of known false ChIP-Seq peaks were removed. Signal maps and peak locations were used as input data to Active Motifs proprietary analysis program, which creates Excel tables containing detailed information on sample comparison, peak metrics, peak locations, and gene annotations. Data tracks were loaded on the Integrated Genome Browser (Bioviz.org) to visualize chromatin open peaks.

RNAseq Analysis Ink4a.1 and Met cell lines were profiled using standard RNA-seq completed by Azenta Life Sciences (formally known as Genewiz, South Plainfield, NJ). After quality check of the reads using FastQC (https://www.bioinformatics.babraham.ac.uk/projects/fastqc/). We used Salmon (A) to quantify transcript-level expression and EdgeR (B) to identify genes with significantly differential expression between pairs of conditions based on replicated count data from bulk RNA-seq profiling. The normalized data were applied to R package GAGE (C) for gene-set enrichment and pathway analysis. The p-values were corrected for multiple testing using FDR. Heat maps were created using Morpheus from the Broad Institute (https://software.broadinstitute.org/morpheus/). Pathway enrichment was analyzed by ShinyGO 0.77 (http://bioinformatics.sdstate.edu/go/).

Size exclusion chromatography Ink4a.1 cells were plated at a density of 30,000 cells/well of a 12-well plate. Prior to treatment, media was aspirated and the cells were washed with 1X PBS. A control well of Ink4a.1 was maintained in RPMI+10% FBS. Pooled HSC conditioned media (CM) from HSCs (Day 6) was filtered with a 0.45 μm filter and added directly to Ink4a.1 cells as a positive control. For size exclusion chromatography for treatments, CM was fractionated with an Amicon Ultra-4 Ultracel-3K MWCO or Ultra-cel-1K MWCO filter and centrifuged at 4°C. 200 μL of CM

3K or 1K concentrate was diluted in 400 μL media and placed in a well of Ink4a.1 cells in order to determine Netrin-1 induction 24 hrs later.

Identification of Retinoid species by LC/MS The retinoid measurement was performed on a Vanquish Horizon UHPLC system (Thermo Fisher Scientific, Waltham, MA) with a Poroshell 120 EC-C18 column (150 mm × 2.1 mm, 2.7 μm particle size, Agilent InfinityLab, Santa Clara, CA) using a gradient of solvent A (90%:10% H2O:MeOH with 34.2 mM acetic acid, 1 mM ammonium acetate, pH 9.4), and solvent B (75%:25% IPA:methanol with 34.2 mM acetic acid, 1 mM ammonium acetate, pH 9.4). The gradient was 0 min, 25% B; 2 min, 25% B; 5.5 min, 65% B; 12.5 min, 100% B; 19.5 min, 100% B; 20.0 min, 25% B; 30 min, 25% B. The flow rate was 200 μl/min. Injection volume was 5 μL and column temperature was 55 °C. The autosampler temperature was set to 4°C and the injection volume was 5μL. The full scan mass spectrometry analysis was performed on a Thermo Q Exactive PLUS with a HESI source which was set to a spray voltage of -2.7kV under negative mode and 3.5kV under positive mode. The sheath, auxiliary, and sweep gas flow rates of 40, 10, and 2 (arbitrary unit) respectively. The capillary temperature was set to 300°C and aux gas heater was 360°C. The S-lens RF level was 45. The m/z scan range was set to 100 to 1200m/z under positive ionization mode. The AGC target was set to 1e6 and the maximum IT was 200ms. The resolution was set to 140,000.

Antibodies. NTN1 antibody (1:1000; clone EPR5428; cat #ab126729; Abcam) was used for western blotting and immunohistochemistry (IHC). ELF3 antibody (#AF5787) was purchased from R&D Biosystems and used for Western blots. For immunoprecipitation experiments and western blotting, rabbit polyclonal antibodies against RXRα and ELF3 were purchased from Cell Signaling (3085S) and Invitrogen (PA5-89261), respectively, and compared with normal mouse IgG purchased from Cell Signaling (2729P). For chromatin immunoprecipitation experiments and western blotting, mouse monoclonal against RARα was purchased from Santa Cruz Biotechnology (sc-515796) and compared to an isotype control purchased from Cell Signaling (5415). For IHC , desmin antibody was from Abcam (ab32362), smooth muscle actin was from Proteintech (14395-1-AP), and secondary goat anti-rabbit antibodies were purchased from Invitrogen (A-11009 and A-21428). Other antibodies included CD9 (1:2000; clone EPR2949; cat #ab92726; Abcam); Unc5b (1:1000; clone D9M7Z; cat# 13851; Cell Signaling), mouse polyclonal flotillin-1 (1:500; cat #610820; BD Bioscience); CK17; cat# 606-540; Thermo Fisher), RARy1 (1:500; clone D3A4; cat# 8965, Cell Signaling), RXRβ (1:500; cat# ab221115; Abcam), RXRy (clone G-6, cat# sc-514134, Santa Cruz Biotechnology, actin (1:5000; clone H-6; cat# sc-376421; Santa Cruz), and Alix (1:1000; clone 3A9; cat # 2171; Cell Signaling).

Quantitative PCR analysis. Cells were prepared for RNA extraction using the RNAeasy kit (Qiagen). RNA was converted into cDNA using Reverse Transcription Reagents (LifeTechnologies). qPCR assays for Ntn1, Elf3 , Dcc, Unc5a, Unc5b, Unc5c, Unc5d, Acta2, Col1a1, Lox, and ActB were purchased from Life Technologies. RNA was assayed in using an Applied Biosystems 7500 Real Time PCR System. Beta-actin was used as a normalizing control.

Promoter analysis. Chromatin immunoprecipitation experiments were performed using a SimpleChip Plus Sonication kit from Cell Signaling Technology. INK4a cells were treated for 7hr or 19hr treatment with 10 □M ATRA then formaldehyde crosslinked chromatin was generated as recommended by the manufacturer. Quantitative PCR was performed using a 7500 Real Time machine from Applied Biosystems, and QPCR assays were designed and synthesized by Integrated DNA Technologies. PCR amplification of the ELF3 promoter was detected in real time using SYBR

Green reagents (Thermofisher) and oligonucleotides 5'CTGACAATCATTAAACCAGCCA 3' and 5'CTCTAAATAGAGCAAAGCAGGAG 3'. PCR amplification of NTN1 Intron 1 was detected in real time using the probe oligonucleotide 5'FAM- AACCTGGGA/ZEN/GCCGGAGAAAGAAC-IABkFQ-3' and outside primers 5'AAGAAGAAAGTTAAAGCCAACGG 3' and 5'TGCTTTCTCTTTGTCTCTGCT-3'.

Flow cytometry. Mouse cell lines were treated for seven days either with DMSO, 10 micromolar ATRA or 67 micromolar ATRA. Cells were then gently trypsinized, washed twice in PBS, and resuspended in PBS/0.5% bovine serum albumin. Half of the cells were stained with a fluorescently labeled antibody against native mouse E-cadherin (Biolegend #147307), while the remaining cells were fixed and permeabilized before being stained with an antibody against mouse vimentin (Cell Signaling Technologies #5741S) that had been labeled with AF647 using a Lightning-Link kit (Abcam #ab269823). For flow cytometry using single cell suspensions, fixed and permeabilized single cell liver suspensions were stained for alpha-Smooth-Muscle-Actin (Novus Biologicals, 1A4/asm- 1), as well as DAPI prior to imaging. An 18-color LSR Fortessa (nicknamed "Dr Teeth") was used for flow cytometry analysis.

Quantitation of disseminated tumor cells by Cre qPCR. Orthotopic pancreatic tumors were generated by injecting FVB mice with 100 cells of Met38 or Met38 NTNKO cell lines in Matrigel. After three weeks, mice were euthanized and genomic DNA was isolated from the entire liver. Quantitation of disseminated tumor cells was performed by qPCR analysis for the presence of cre DNA, which was specific to the cell line and not to the mouse line. The cre probe sequence was 5'-6FAM-AAACATGCTTCATCGTCGGTCCGG-BHQ-3' and outside primer sequences were 5'GCGGTCTGGCAGTAAAAACTATC-3' and 5'GTGAAACAGCATTGCTGTCACTT-3'.

Ex**tracellular vesicle isolation by immunobead prec**ipitation: Ink4a.1 and Met38 cells were grown to 80% confluence on 10cm dishes before being washed in PBS and placed in serum free media for 24 hours. The conditioned media was then collected and centrifuged first at 500g for 10 minutes, then 1000g for 10 minutes to remove any cells and debris. This clarified conditioned media was then filtered using a 20μM syringe-tip filter, and concentrated 1:60 using a centrifugal filter unit (Amicon Ultra-15, Merk- Millipore). Extracellular vesicles were isolated from conditioned media concentrates per manufacturer instructions using 0.4 μm immunobeads for overall exosome isolation kit (Novus biologicals, cat: NBP2-49833). Sizing of EVs was evaluated by transmission electron microscopy by the Department of Pathology's Core Imaging Laboratory at Rutgers University.

EVs isolation by ultracentrifugation. For EVs isolation, cells were seeded in 150 cm2 dishes at 8 million cells/plate following a 12h attachment period, were washed three times with PBS before supplying 10 mL of serum free media to prevent contamination from serum-derived EVs. After 72h conditioned media was collected and EVs were purified: conditioned media was centrifuged at 2500g for 30min at 4°C to remove cells and debris. The remaining supernatant was ultracentrifuged at 100 000g for 1h at 4°C to recover EVs.

Animal studies: All animal protocols were approved by the Rutgers Biomedical and Health sciences Animal Care and Use Committee, or the University of Rochester Committee on Animal Resources. Five- to six-week-old female FVB mice were purchased from The Jackson Laboratory (Bar Harbor, ME), or bred in-house following established vivarium approved protocols. For orthotopic studies,

100 Ink4a.1 luc/mcherry pancreatic cells in a mixture of 50% matrigel/50% DMEM +10% FBS were injected into the tail of the pancreas. Buprenorphine and bupivacaine were given for pain management and the mouse was allowed to recover under a heating lamp until ambulatory. For intrasplenic injections, 20-50k cells (see figure legend) in DMEM +10%FBS were injected into the spleen near the hilum. The spleen was then divided distal to the clip and a second clip was placed across the splenic vessels to ensure hemostasias prior to removing the injected hemi-spleen. Buprenorphine and bupivacaine were given for pain management and the mouse was allowed to recover under a heating lamp until ambulatory. Mice were monitored for survival and study end-points daily post-surgery. KPC mice (KrasG12D/+, Trp53R172H/+,Pdx-1-Cre) were bred following University of Rochester Committee on Animal Resources approved protocols. KPC mice began screening with twice weekly palpation and once weekly abdominal ultrasound to identify pancreas tumors. Upon identification of mice with tumors greater than 5mm mice were randomized into treatment arms with anti-netrin-1 therapy, or vehicle control and started immediately on twice weekly treatment with 10mg/kg mAbNtn1, or vehicle control. Mice were monitored daily for survival endpoints.

Liver metastasis assay by portal vein injection: For portal vein injection of pancreatic tumor cells, mice were anaesthetized using continuous inhalation of 2-5% isoflurane in O2. The abdominal incision site was sterilized with iodine and ethanol and injected with 1% xylocaine. A dose of at a dose of 0.05-0.1 mg/kg of buprenorphine was administered subcutaneously immediately prior, at the end of operation, and every 4–6 h for 12 h and then every 6–8 h for 3 additional days after surgery. Following laparotomy, the peritoneal cavity was exposed and the loops of intestines exteriorized onto a sterile towel wetted with sterile saline and maintained hydrated with sterile PBS. The portal vein was visualized and injected with a 100 uL of suspension of 5×105 PDAC cells suspended in sterile PBS via a 30-gauge needle (Covidien, USA). Successful injection was confirmed by partial blanching of the liver. After removing the needle from the vein, hemostasis was obtained by applying gentle pressure with a Q-tip on a 5x5 mm piece of Rapid Hemostatic Gauze (Medtrade Products Ltd.) for 5-10 minutes. Once no bleeding was seen, the intestines were placed back into the peritoneal cavity, and the peritoneum was closed with resorbable 5-0 PDS II violet suture (Ethicon). Skin was closed using the AutoClip system (Reflex; CellPoint Scientific, Inc.). Following surgery, mice were given buprenorphine and were analyzed after 3 weeks unless indicated otherwise in study designs.

Generation of single-cell suspension of murine livers: freshly harvested liver tissue was digested in 37˚ DMEM/F12 solution with a combination of collagenase type I (200u/ml), Hyaluronidase (60u/ml), and DAase I (30µg/ml) for 20 minutes with gentle vortexing. The solution was then strained through a 100µm filter and washed in PBS with 0.5% bovine serum albumin. ACK lysis buffer was added and cells were washed again in PBS with 0.5% bovine serum with DNase I prior counting and dilution to 1000000 cells/ml for antibody staining, and analysis.

Anti-Netrin-1 treatment: humanized monoclonal anti-netrin-1 (mAbNtn1) was obtained as a gift from Dr. Patrick Mehlen. mAbNtn1 was delivered via twice weekly intraperitoneal injection at 10mg/ml concentration diluted in phosphate buffered saline. For murine survival surgery experiments, anti-netrin-1 therapy was initiated 2 days before cell line injection.

Murine Hepatic Stellate Cell isolation: Hepatic stellate cells were isolated from healthy 9-week-old FVB mice using the protocol previously described (Mederacke et al., 2015). Briefly, mice are anesthetized for non-survival surgery using ketamine and xylazine. A laparotomy incision is made

in the abdomen and the inferior vena cava is cannulated using a 26g needle attached to a peristaltic pump. The liver is then perfused in-situ with pronase-collagenase prior to being removed and further processed in-vitro. The single cell suspension is then subjected to density gradient centrifugation and stellate cells are collected for experimental use.

H&E staining, Immunofluorescence, Immunohistochemistry. H&E staining was completed using xylene for deparaffinization and reducing percentages of ethanol for rehydration. Gill's hematoxylin (Vector Labs) and Eosin-Y Alcoholic stain (Richard-Allan Scientific) was used according to manufacturer's instructions. Slides were dehydrated in increasing percentages of ethanol, placed in 3 washes of xylene for 30 seconds each and mounted using ClearMount (American Mastertech Scientific, Inc). Immuno-staining was completed with deparaffinization and rehydration as above. For IHC on human PDX samples, Netrin-1 expression was measured with indicated antibodies at manufacturer's recommended dilutions and visualized by Liquid DAB chromogen (Dako) and hematoxylin. Slides were scanned (Aperio CS scanner) and regions of interest were outlined manually to enumerate Netrin-1 strong positive cells in ImageScope software (Leica Biosystems Imaging, Inc.). The images were independently validated by a certified pathologist.

Quantitation of liver metastases: Livers were fixed in 4% paraformaldehyde prior to sectioning and H&E staining. Whole slide images were captured at 20x magnification using an Aperio whole slide scanner (Leica Biosystems). Images were then analyzed by pixel classification to identify tumor versus stroma using VisioPharm® 19, and QuPath digital pathology analysis software.

Statistical analysis. All experiments were completed in triplicate. Data was analyzed in Excel or GraphPad Prism by students two-tailed t-test. Survival statistical analysis was completed in GraphPad by logrank test. * is $p<0.05$, ** is $p<0.01$, *** is $p<0.001$, and **** is $p<0.0001$.

ACKNOWLEDGEMENTS

This work was partially funded by a grant from the Pancreatic Cancer Action Network to DRC and PM as well as funds provided by the Wilmot Cancer Institute to DRC. Funding from the following were also provided to PM (Ligue Contre Le Cancer, INCA, ANR, and Institut Convergence Plascan. IA acknowledges funding from NCI (CA-06927, R01CA188430, K22CA160725, R21CA164205, R21CA231252. SF received a fellowship from Ligue Contre Le Cancer. Funding support from the Pancreatic Cancer Action Network was also provided to CO by the Francoise Wallace Monahan fund. We thank Alain Brisson for advice on exosome isolation and identification. We thank Guy Montelione for assistance with size-exclusion chromatography. We would like to acknowledge Tracy Withers and Aizhan Surumbayeva for their assistance with animal studies and Asra Asad for her assistance with in vitro migration studies. We would like to acknowledge the URMC Wilmot Cancer Institute flow cytometry shared resource. Services, results and/or products in support of the research were generated by Rutgers Cancer Institute of New Jersey Flow Cytometry & Cell Sorting Shared Resource P30CA072720-5921 and Metabolomics Shared Resource supported, in part, with funding from NCI-CCSG P30CA072720-5923. We acknowledge the contribution of SFR Santé Lyon-Est (UAR3453 CNRS, US7 Inserm, UCBL) facility: CIQLE (a LyMIC member), especially Elisabeth ERRAZURIZ-CERDA for their help on the TEM imaging.

FIGURE LEGENDS

Figure 1. Netrin 1 is upregulated in metastatic PDAC. (A) Histology of a representative primary and metastatic pancreatic tumor to the liver displaying both mesenchymal (M) and epithelial (well-differentiated) features (D). Left: H&E (i,iv), E-cadherin (ii, v), Masson's trichrome stain (iii, vi). (B) Heat maps of over (left) and under (right) expressed genes as well as the axon guidance gene family determined by RNAseq comparing the log2 fold change from primary to metastatic tumor transcriptomes. Enriched pathways are marked on the right side of the heatmaps. (C) Western blot analysis of Netrin-1 and actin (loading control) expression in primary tumor cell line (Ink4a.1) and 4 separate metastatic cell lines obtained from liver metastases. (D) Top Representative immunohistochemistry images of Netrin-1 expression in human primary pancreatic tumor biopsy (i), primary PDX pancreatic tumor (ii), and two metastatic pancreatic PDX tumors (iii, iv). Scale bar: 100 μm. Below: quantification of Netrin-1 expression in the TMA of PDX pancreatic tumors; n=75 for primary, n=18 for metastases. (E) Expression of netrin 1 in Collison et al.'s RNAseq dataset of different pancreatic cancer phenotypes based on expression profiling. Statistical analysis was completed using two-tailed student's t-test (*=$p<0.05$).

Figure 2. Unc5b is the dominant Netrin-1 receptor in PDAC and functions as Dependece Receptor to promote metastasis. (A) RNAseq analysis of primary and metastatic pancreatic cancer cell line expression of Netrin-1 receptors. (B) Annexin V staining of primary Ink4a and metastatic Met38 cell lines transiently transfected with a non-targeting control siRNA or Ntn1 siRNA. (C) Left: Graphs of the migration and invasion analysis of serum starved Ink4a cells treated with recombinant Netrin-1. Representative images of fixed and stained cells are on the right. (D) Left: Graphs of the migration and invasion analysis of Met38 cells transiently transfected with a control or Ntn1 siRNA. Representative images of fixed and stained cells are on the right. (E) 3D in vitro sprouting assay for Met38 control KD (a, b) or Ntn1 KD cells (c,d) and A1925 control (e,f) and ΔUnc5b (g,h) expressing cells. Netrin 1 knockdown was confirmed by netrin 1 expression analysis (far right). Scale bar 100 μm. (F) Top: Graphs of the invasion analysis of Met38 cKO (control knockout) and Met38 Unc5b KO cells. Representative images of fixed and stained cells are below, as well as the Western blot showing Unc5b depletion in Unc5b KO cells. (dG) H&E stain of livers after intrasplenic injection of Met38 control KD and Met38 Ntn1 KD cells. Right: quantitation of tumor area using VisioPharm software. Statistical analysis was completed using two-tailed student's t-test (*$p<0.05$; **$p<0.01$, ***$p<0.001$, ****$p<0.0001$).

Figure 3. Hepatic stellate cell secretion of retinoids causes upregulation of Netrin- 1 through RAR/RXR signaling. (A) Netrin-1 expression was analyzed by Western blot following treatment with HSC conditioned media for the indicated time points. Actin served as a loading control. The fold change of netrin 1 expression is shown below the Netrin 1 blot. (B) (Top) HSCs were imaged on the indicated days by brightfield or retinoid autofluorescence using the DAPI filter. Scale bar: 20 μm. (Bottom) Ink4a.1 cells were treated for 24 hours with HSC conditioned media from the top experiment. Netrin-1 expression was determined by Western blot with actin as a loading control. (C) Ink4a.1 cells were treated with retinoic acid (ATRA) and 9-cis retinoic acid for the indicated times. Netrin-1 and actin expression was analyzed as before. (D) ATRA-treated Ink4a cells were subjected to ChIP analysis of the Ntn1 exon 1 promoter region using an isotype control or RXRα antibody. (E) Ink4a.1 cells were transfected with siRNA to RARα, RXRα, and the combination and then treated for 24 hours with HSC conditioned media. Netrin-1 and actin expression was analyzed as before. (F) Ink4a.1 cells were treated with ATRA (RA) or 9-cis RA (9RA) +/- UVI 3003 for 24 hrs.

Netrin-1 and actin were blotted as before. Statistical analysis was completed using two-tailed student's t-test (**p<0.01).

Figure 4. Retinoic acid induces transcription factor Elf3 to increase expression of Netrin-1 in human and mouse pancreatic cancer cells. (A) ATAC-seq analysis of the Elf3 promoter shown in duplicates for metastatic Met38 and primary Ink4a.1 pancreatic cancer cells. (B) Expression of Elf3 was determined by qPCR in multiple primary and metastatic mouse (left) and human (right) pancreatic cancer cell lines treated with 10 μM ATRA for 18 hours. Actin expression was used for normalization. In all cases except for Miapaca-2, the increase in Elf3 mRNA was statistically significant by two-tailed t test. (C) ChIP experiment to demonstrate that RAR interacts with the Elf3 promoter. (D) Following 7 days of treatment with DMSO or varying concentrations of ATRA, the percentages of E-cadherin positive (left) and vimentin positive (right) cells were determined by flow cytometry in three cell lines, each of which had been developed from pancreatic tumors generated by different KPC-Arid1a-/- mice. (E) The top panel shows conservation of consensus Elf3 transcription factor binding sequence within the Netrin-1 promoter in a variety of species, while the bottom panel shows results of a ChIP experiment indicating that Elf3 interacts with this region on the mouse Ntn1 gene (F) Ink4a.1 cells were transfected for 72 hours with pCMV6 or with pCMV6-Elf3, followed by qPCR to assay Netrin-1 transcription. Actin was used as a normalization control. (G) Met38 sgControl and sgElf3 were treated with DMSO or 10 μM ATRA for 18 hours and analyzed for Netrin-1 RNA expression. The top graph shows the fold change of Netrin-1 expression for ATRA vs DMSO. In the bottom panel the reduction of Elf3 protein is demonstrated by Western blot analysis. Statistical analysis was completed using two- tailed student's t-test (*p<0.05; **p<0.01, ***p<0.001, ****p<0.0001).

Figure 5. Netrin-1 on the surface of extracellular vesicles promotes hepatic metastasis by activating HSCs. (A) Expression of HSC activation markers was determined by qPCR following treatment of HSCs with recombinant Netrin-1 at the indicated time points. (B) In vivo activation of HSCs was determined by Desmin and SMA immunofluorescence staining of livers from mice orthotopically injected with Ink4a.1 WT and Ntn1 KO cells (left). Quantitation of Desmin+/SMA+ HSC cells (right) was determined. (C) Activated HSCs were identified and quantitated by flow cytometry using high side scatter and SMA staining. (D) NanoSight software analysis on EVs from lnk4a and Met38 cells showing the size of the analyzed EVs. Netrin 1 expression analysis of cellular and EV fraction by Western blot. (inset) (E) TEM analysis on EVs EVs harvested from Ink4a.1 and Met38 cells using netrin 1 antibody coupled to 15 nm gold beads. Representative images showing the frequency of EVs labeled with netrin 1 and specific EV marker, CD63. (F) Enlargement of representative Netrin-1 positive EVs. (G) Schema for the in vivo experimental metastasis model used to demonstrate EV priming of the liver for pancreatic cancer metastatic seeding (top). H&E stain of livers obtained from mice primed with netrin-1-containing or netrin-1 null EVs prior to pancreatic cancer cell seeding. (Bottom, left). Percentage of tumor area (bottom, right) compared to total liver lobe area shows significant decrease of priming the microenvironment with Ntn1 KO EVs compared to WT EVs. Statistical analysis was completed using two-tailed student's t-test (***p<0.001, ****p<0.0001).

Figure 6. Netrin-1 interference suppresses metastasis and increases survival in murine PDAC models. (A) Mice were pretreated with mAbNtn1 for two days and then intrasplenically injected with 50,000 Ink4a.1 cells. Antibody treatment (10mg/kg) continued every 2 days until liver harvest at day 14. Percentage tumor area in the liver was quantified as before. (B) Survival of mice injected intrasplenically with 20,000 INK4.1syn_Luc cells using mAbNtn1 as adjuvant treatment. Note that

3 mice have not recurred beyond day 200. Treatment groups were compared with Kaplan-Meier analysis. (C) IHC of CK17-stained livers from C57Bl/6J mice injected via portal vein injection with KPC3 cells (left) and treated with IgG control or mAbNtn1. Percentage of tumor metastasis area was quantified as before. Note the significant reduction in mice treated with anti-netrin-1 antibody (right). (D) Normalized Netrin-1 expression in KPC3 cells, normal liver, hepatic KPC3 metastases from IgG control treated mice, and hepatic KPC3 metastases from mAbNtn1 treated mice as quantified by Western blot. (E) Kaplan-Meier plot showing survival of KPC mice treated with IgG vehicle and mAbNtn1 antibodies. The vehicle group had an MS=18 days, while the mAbNtn1 group had an MS~42 days, a doubling of lifespan. Statistical analysis was completed using two-tailed student's t-test (***$p<0.001$, ****$p<0.0001$).

Figure 7. Netrin 1 facilitates liver metastasis by a feedforward mechanism involving Netrin-1 mediated HSC activation and retinoid mediated Netrin-1 upregulation through RXR/RAR and Elf signaling. EVs containing Netrin-1 activate HSCs through both long-range (A) and possibly short-range communication upon dissemination in the liver (B). Upon activation by Netrin-1, HSCs dump their retinoic acid stores (C). The free retinoic acid is taken up by DTCs by their retinoic acid receptors (D), leading to upregulation of Netrin-1 directly and indirectly through Elf3 upregulation. Through autocrine signaling (E) by Unc5b receptors, newly arrived DTCs increase survival potential through netrin 1 excretion. In addition, activated hepatic stellate cells deposit collagen into the microenvironment (F), which over time allows macrometastases to become established in the liver (G).

Supplemental Figure Legends

Figure S1. Netrin-1 is upregulated in hepatic metastases of pancreatic cancer. (A) Volcano plot showing bulk RNA sequencing of matched hepatic metastases (n=5) versus primary tumors (n=5) from INK4.1syn_Luc mice. (B) ATACseq analysis of open regions (blue peaks) of chromosome 1 in the Ink4a.1 (primary) cell line versus the early metastatic cell line Met38 (metastasis) using the Integrated Genome Browser (Bioviz.org). Reference genes are in green, genomic coordinates are in black. (C) ATACseq analysis of primary tumor cell line, Ink4a.1, in comparison with metastatic pancreatic cell line, Met38. n=2 each cell line. Dark blue denotes regions of open areas of chromatin. Genes within the euchromatin are listed to the right. (D) Pathway enrichment analysis of upregulated and downregulated differentially expressed genes (DEGs). (E) qPCR validation of genes found upregulated by bulk RNAseq in Ink4a.1 and Met cell lines. Only Ntn1 and Pdgfb were shown to be upregulated in metastasis versus primary tumor. (F) IHC staining with Netrin-1 antibody of primary and hepatic metastasis of pancreatic cancer from INK4.1syn_Luc mice. (G) Netrin 1 expression in a TMA of human primary and metastatic cancer (n=25). Statistical analysis was completed by two-tailed student's t-test (****$p<0.0001$).

Figure S2. Unc5b is the dominant netrin 1 receptor in murine and human pancreatic cancer. (A) Unc5b and DCC expression analysis in Ink4a.1, Met25, and Met38 cell lines by Western blotting. Actin was used as a loading control. (B) Unc5b expression in multiple mouse (left) pancreatic cancer cell lines, and UNC5B and DCC expression in human (right) pancreatic cancer cell lines. Actin was used as a loading control. (C) TCGA analysis of UNC5B and DCC mRNA expression in human pancreatic cancer. Note that the X axis for the UNC5B graph has a larger range than for DCC (D) Western blot analysis of the efficacy of Ntn1 siRNA knockdown in the Ink4a.1 and Met38 cell lines, with actin as a loading control. (E) Expression of Netrin-1 in multiple stable Ntn1 knockdown clones by shRNA, as compared to parental (WT). Actin served as a loading

control. (F) CCK8 proliferation analysis on Met38 WT and Ntn1 KD clones A4, A5, and D5 over 4 days showing no significant changes in proliferation rate with Ntn1 knockdown.

Figure S3. Retinoids isolated from activated hepatic stellate cells can induce Ntn1 and Elf3 expression. (A) Ink4a.1 cells were treated with conditioned media from cultures of hepatocytes or sinusoidal epithelial cells for 0-24 hrs, as indicated. Western blot analysis of Netrin-1 expression is shown. (B) Ink4a.1 cells were treated with HSC conditioned media filtered using a size exclusion column. Netrin 1 expression was assayed 24 hours later, with actin as a loading control. (C) Mass spectrometry chromatograph showing presence of retinal (top) and retinoate (bottom), two forms of retinoids, in HSC conditioned media taken from days 4-15 after HSC isolation and plating. Each day of isolation is represented by a color. Note the majority of detection of both retinal and retinoate is during the days 11 and 15 (post HSC activation) as opposed to days 4 and 8 (pre-activation) (D) Ink4a.1 cells were treated with 10 □M of retinol or Vitamin A for 0-24 hrs, as indicated. Western blot analysis of Netrin-1 expression is shown. (E) qPCR analysis of Ntn1 expression in multiple mouse pancreatic cancer cell lines treated with DMSO or 10 μM ATRA, with mRNA expression normalized to Actb. Three of the four cell lines showed a significant increase in Ntn1 expression as determined by two-tailed T test. (F) Western blotting analysis of various RXRs and RARs in mouse pancreatic cancer cell lines Ink4a.1, K8484, and K8483. Actin was used as a loading control. Note that all the cell lines expressed RARα and RXRα. (G) ATACseq analysis of the Ntn1 promoter region showing open chromatin (arrow pointing to peak) of Ink4a.1 and Met38 cell lines, n=2 each. (H) qPCR analysis of Elf3 mRNA expression in Ink4a.1 and Met cell lines showing significant expression in Met cell lines compared to the primary cell line. mRNA expression was normalized to Actb. (I) qPCR analysis of Ntn1 (left) and Elf3 (right) expression in siCTRL and siElf3 knockdown Ink4a.1 cells.

Figure S4. Analysis of EVs from Ink4a.1 Ntn1 WT and KO cells. (A) Ntn1 expression validation in various Ink4a.1 Ntn1 KO clones, showing clones P2A4 and P5E11 clones as null. (B) Ink4a.1 WT and Ntn1 KO cells were injected orthotopically into the pancreas. Primary tumor size was measured, showing no significant difference in sizes between the two genotypes. (C) EV load as detected by Cre+ DNA between Netrin-1 WT and Netrin- 1 KO EVs shows no differences in liver seeding. (D) The amount of Netrin-1 containing EVs was compared in Ink4a.1 and Met38 PDAC cells. (E) Netrin-1 expression was measured in Ink4a.1 and Met38 cell lysates, 20X concentrated conditioned media, and EVs purified. Alix was used as an EV marker. (F) Expression of Netrin-1 is assessed in the media of Ink4a.1 Ntn1 WT and KO clones (left) as well as in purified EVs. Actin was used as a cytoplasm marker. (G) TEM of Ink4a.1 WT and Ntn1 KO EVs shows no significant difference in sizes (left). Representative images are shown on the right.

Figure S5. NSCLC EVs contain Netrin 1. (A) Nanosight measurement of EV size from 3 human lung cancer cell lines. (B) Netrin 1, CD9, and Flotillin-1 expression in the lysate and EVs of A549, H322, and H358, as shown in (A). Note the lack of Netrin-1 in A549. (C.) TEM of CD63 and Netrin-1 gold labeled antibodies on EVs purified from A549 and H358 cells. CD63 is an EV marker. Netrin-1 was not found in EVs of A549.

Figure 1

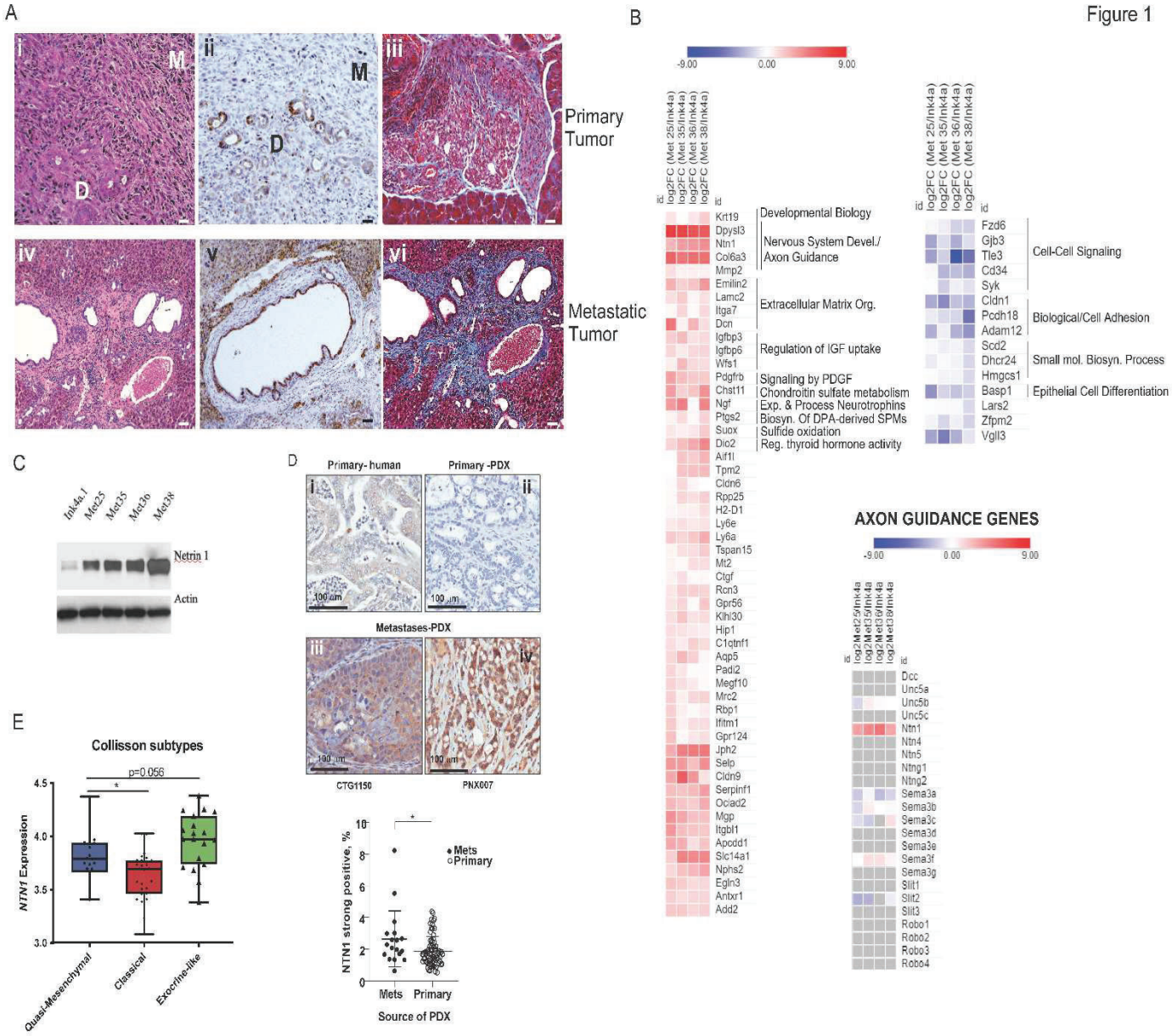
A
i
M
D
ii
M
D
iii
Primary Tumor
iv
v
vi
Metastatic Tumor
B
-9.00
0.00
9.00
log2FC (Met 25/Ink4a)
log2FC (Met 35/Ink4a)
log2FC (Met 36/Ink4a)
log2FC (Met 38/Ink4a)
id
Krt19
Dpysl3
Ntn1
Col6a3
Mmp2
Emilin2
Lamc2
Itga7
Dcn
Igfbp3
Igfbp6
Wfs1
Pdgfrb
Chst11
Ngf
Ptgs2
Suox
Dio2
Aif1l
Tpm2
Cldn6
Rpp25
H2-D1
Ly6e
Ly6a
Tspan15
Mt2
Ctgf
Rcn3
Gpr56
Klhl30
Hip1
C1qtnf1
Aqp5
Padi2
Megf10
Mrc2
Rbp1
Ifitm1
Gpr124
Jph2
Selp
Cldn9
Serpinf1
Ociad2
Mgp
Itgbl1
Apcdd1
Slc14a1
Nphs2
Egln3
Antxr1
Add2
Developmental Biology
Nervous System Devel./ Axon Guidance
Extracellular Matrix Org.
Regulation of IGF uptake
Signaling by PDGF
Chondroitin sulfate metabolism
Exp. & Process Neurotrophins
Biosyn. Of DPA-derived SPMs
Sulfide oxidation
Reg. thyroid hormone activity
Fzd6
Gjb3
Tle3
Cd34
Syk
Cldn1
Pcdh18
Adam12
Scd2
Dhcr24
Hmgcs1
Basp1
Lars2
Zfpm2
Vgll3
Cell-Cell Signaling
Biological/Cell Adhesion
Small mol. Biosyn. Process
Epithelial Cell Differentiation
AXON GUIDANCE GENES
-9.00
0.00
9.00
log2Met25/Ink4a
log2Met35/Ink4a
log2Met36/Ink4a
log2Met38/Ink4a
Dcc
Unc5a
Unc5b
Unc5c
Ntn1
Ntn4
Ntn5
Ntng1
Ntng2
Sema3a
Sema3b
Sema3c
Sema3d
Sema3e
Sema3f
Sema3g
Slit1
Slit2
Slit3
Robo1
Robo2
Robo3
Robo4
C
Ink4a.1
Met25
Met35
Met3o
Met38
Netrin 1
Actin
D
Primary- human
Primary -PDX
Metastases-PDX
100 um
CTG1150
PNX007
NTN1 strong positive, %
Mets
Primary
Source of PDX
E
Collisson subtypes
p=0.056
NTN1 Expression
4.5
4.0
3.5
3.0
Quasi-Mesenchymal
Classical
Exocrine-like

Figure 2

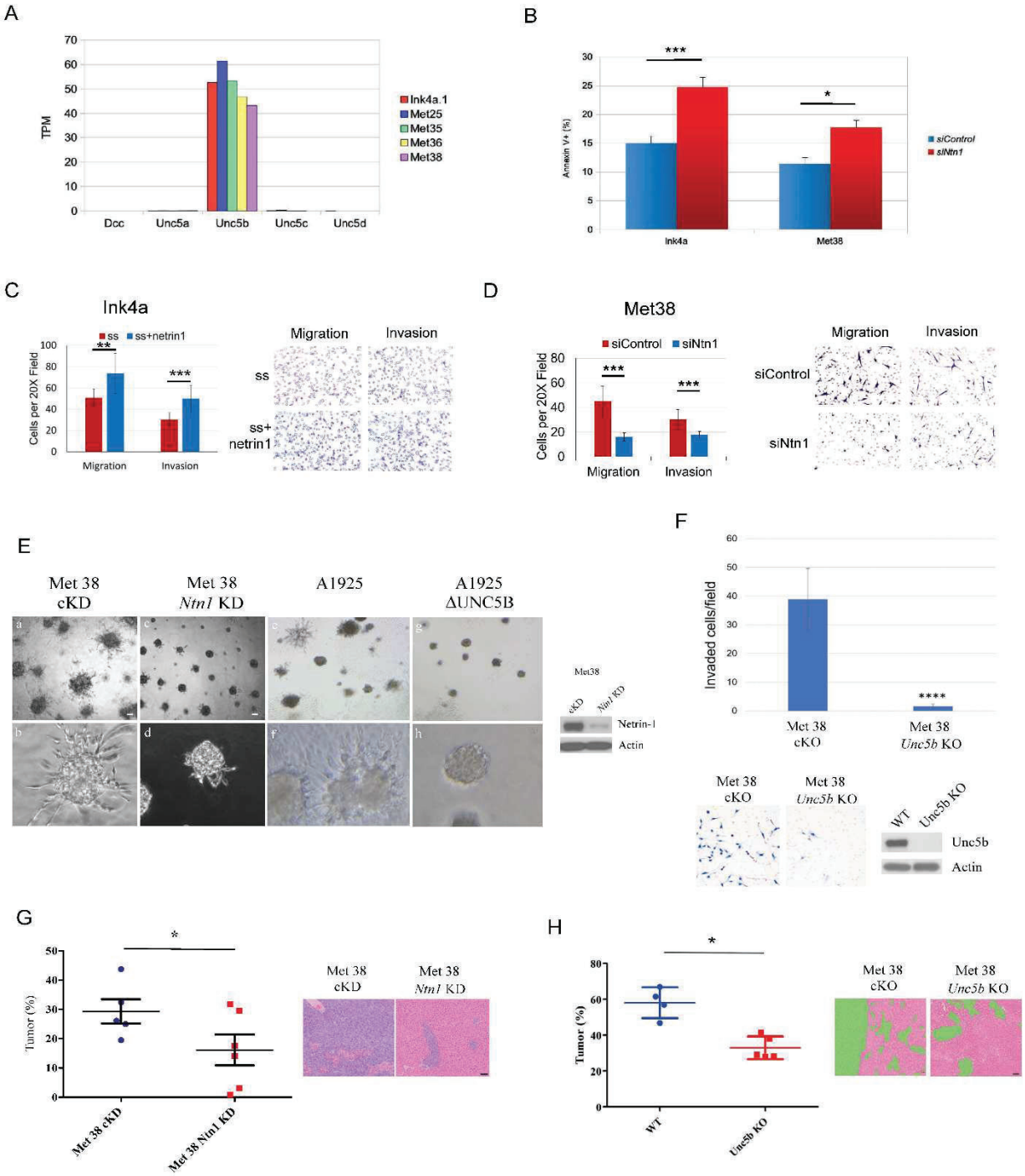
A
TPM
Dcc
Unc5a
Unc5b
Unc5c
Unc5d
Ink4a.1
Met25
Met35
Met36
Met38
B
Annexin V+ (%)
siControl
siNtn1
Ink4a
Met38
C
Ink4a
ss
ss+netrin1
Cells per 20X Field
Migration
Invasion
D
Met38
siControl
siNtn1
E
Met 38 cKD
Met 38 Ntn1 KD
A1925
A1925 ΔUNC5B
Met38
Netrin-1
Actin
F
Invaded cells/field
Met 38 cKO
Met 38 Unc5b KO
WT
Unc5b
G
Tumor (%)
Met 38 cKD
Met 38 Ntn1 KD
H
Tumor (%)
WT
Unc5b KO

Figure 3

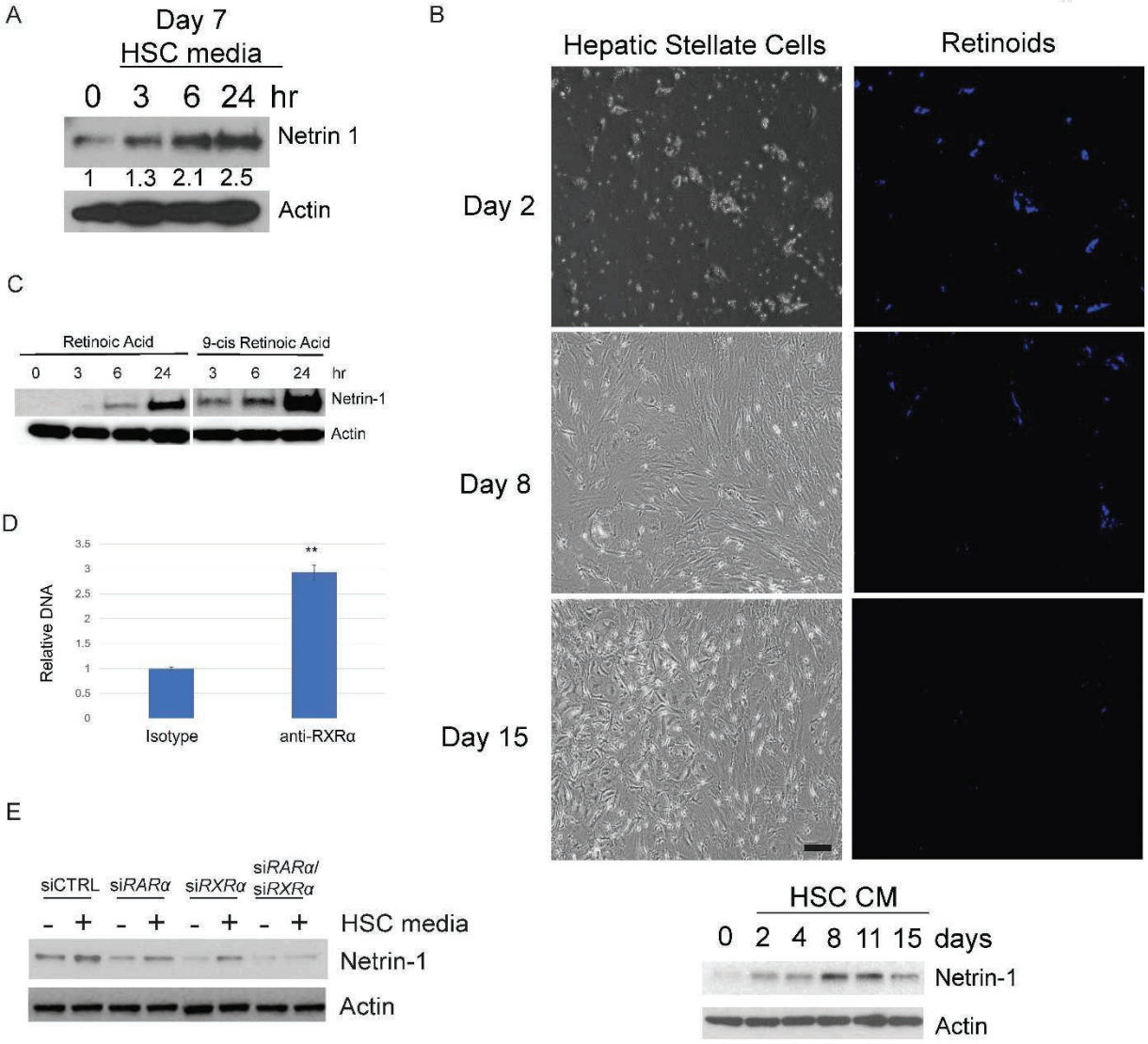
A
Day 7
HSC media
0 3 6 24 hr
Netrin 1
1 1.3 2.1 2.5
Actin
B
Hepatic Stellate Cells
Retinoids
Day 2
Day 8
Day 15
C
Retinoic Acid
9-cis Retinoic Acid
0 3 6 24 3 6 24 hr
Netrin-1
Actin
D
Relative DNA
3.5
3
2.5
2
1.5
1
0.5
0
**
Isotype
anti-RXRα
E
siCTRL siRARα siRXRα siRARα/ siRXRα
- + - + - + - +
HSC media
Netrin-1
Actin
HSC CM
0 2 4 8 11 15 days
Netrin-1
Actin
F
CTL CTL RA RA 9RA 9RA
– + – + – +
UVI 3003
Netrin-1
Actin

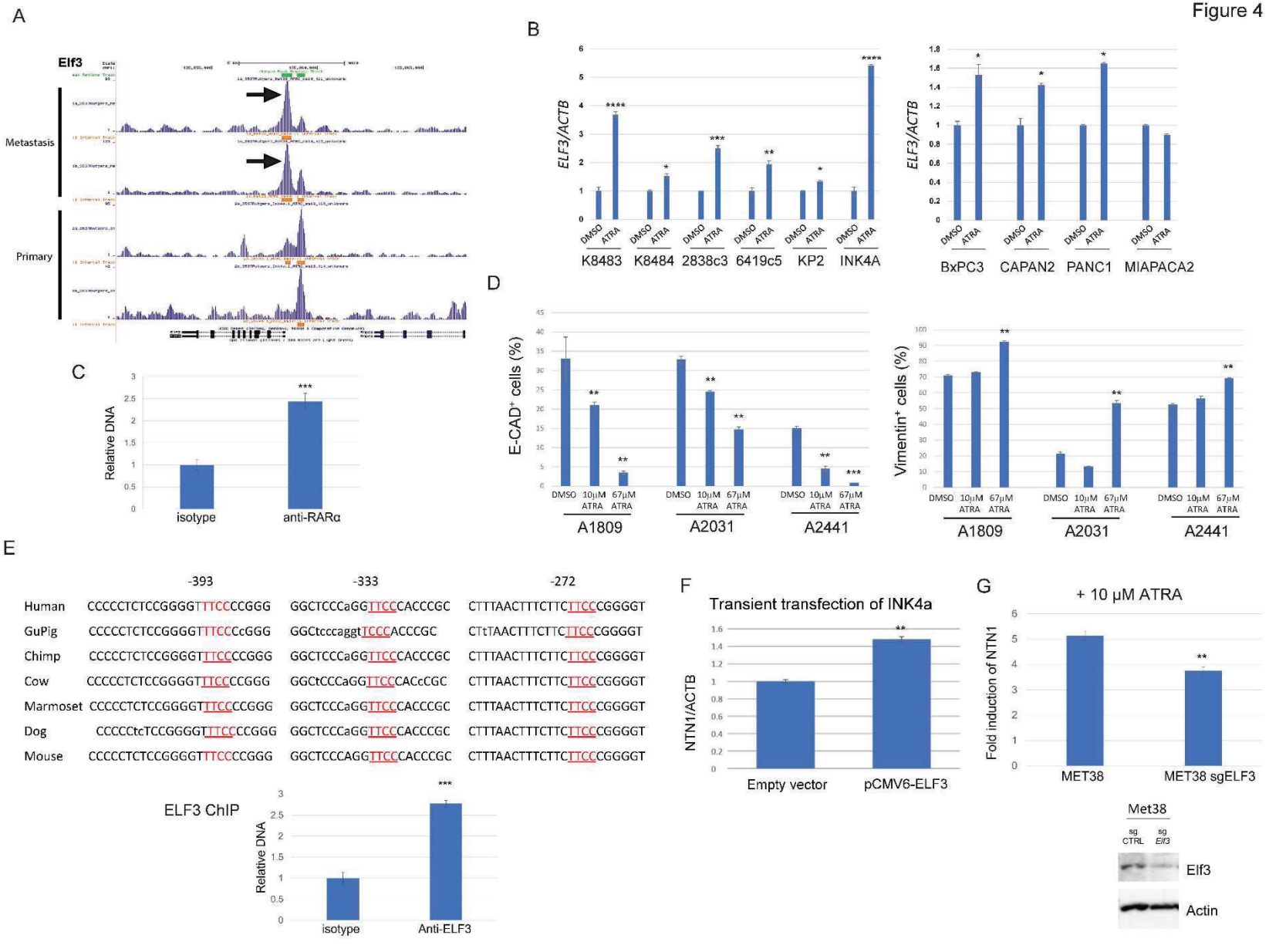
A
Elf3
Metastasis
Primary
B
ELF3/ACTB
DMSO
ATRA
K8483
K8484
2838c3
6419c5
KP2
INK4A
BxPC3
CAPAN2
PANC1
MIAPACA2
C
Relative DNA
isotype
anti-RARα
D
E-CAD+ cells (%)
Vimentin+ cells (%)
DMSO
10μM ATRA
67μM ATRA
A1809
A2031
A2441
E
-393
-333
-272
Human CCCCCTCTCCGGGGTTTCCCCGGG GGCTCCCaGGTTCCCACCCGC CTTTAACTTTCTTCTTCCCGGGGT
GuPig CCCCCTCTCCGGGGTTTCCCcGGG GGCtcccaggtTCCCACCCGC CTtTAACTTTCTTCTTCCCGGGGT
Chimp CCCCCTCTCCGGGGTTTCCCCGGG GGCTCCCaGGTTCCCACCCGC CTTTAACTTTCTTCTTCCCGGGGT
Cow CCCCCTCTCCGGGGTTTCCCCGGG GGCtCCCaGGTTCCCACCcGC CTTTAACTTTCTTCTTCCCGGGGT
Marmoset CCCCCTCTCCGGGGTTTCCCCGGG GGCTCCCaGGTTCCCACCCGC CTTTAACTTTCTTCTTCCCGGGGT
Dog CCCCCtcTCCGGGGTTTCCCCGGG GGCTCCCaGGTTCCCACCCGC CTTTAACTTTCTTCTTCCCGGGGT
Mouse CCCCCTCTCCGGGGTTTCCCCGGG GGCTCCCAGGTTCCCACCCGC CTTTAACTTTCTTCTTCCCGGGGT
ELF3 ChIP
Relative DNA
isotype
Anti-ELF3
F
Transient transfection of INK4a
NTN1/ACTB
Empty vector
pCMV6-ELF3
G
+ 10 μM ATRA
Fold induction of NTN1
MET38
MET38 sgELF3
Met38
sg CTRL
sg Elf3
Elf3
Actin

Figure 5

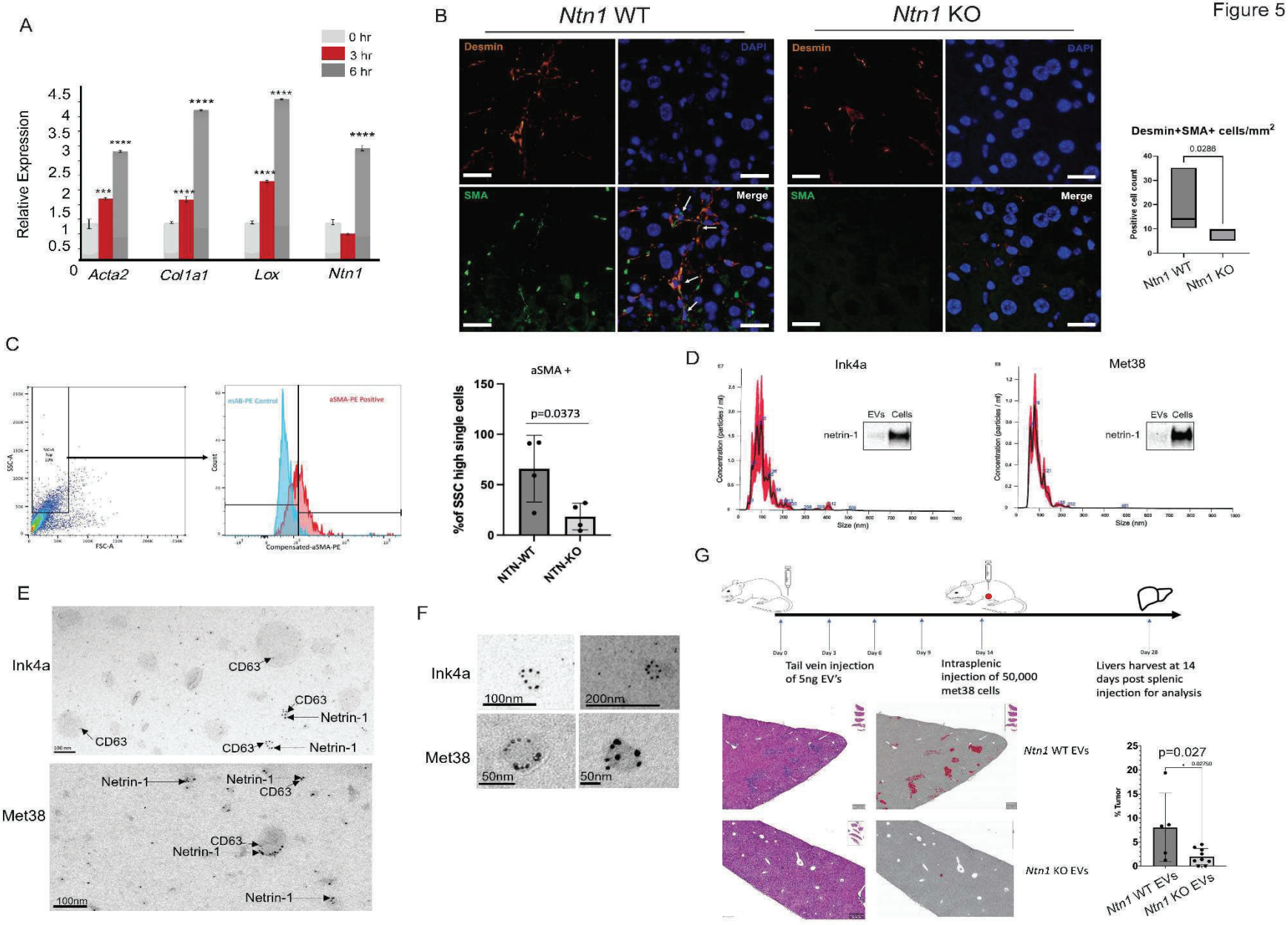
A
0 hr
3 hr
6 hr
Relative Expression
Acta2
Col1a1
Lox
Ntn1
B
Ntn1 WT
Ntn1 KO
Desmin
DAPI
SMA
Merge
Desmin+SMA+ cells/mm2
0.0288
Positive cell count
Ntn1 WT
Ntn1 KO
C
mAB-PE Control
aSMA-PE Positive
SSC-A
FSC-A
Count
Compensated-aSMA-PE
aSMA +
p=0.0373
%of SSC high single cells
NTN-WT
NTN-KO
D
Ink4a
Met38
EVs Cells
netrin-1
Concentration (particles / ml)
Size (nm)
E
Ink4a
Met38
CD63
Netrin-1
100nm
F
Ink4a
Met38
100nm
200nm
50nm
50nm
G
Day 0
Day 3
Day 6
Day 9
Day 14
Day 28
Tail vein injection of 5ng EV's
Intrasplenic injection of 50,000 met38 cells
Livers harvest at 14 days post splenic injection for analysis
Ntn1 WT EVs
Ntn1 KO EVs
p=0.027
0.02750
% Tumor
Ntn1 WT EVs
Ntn1 KO EVs

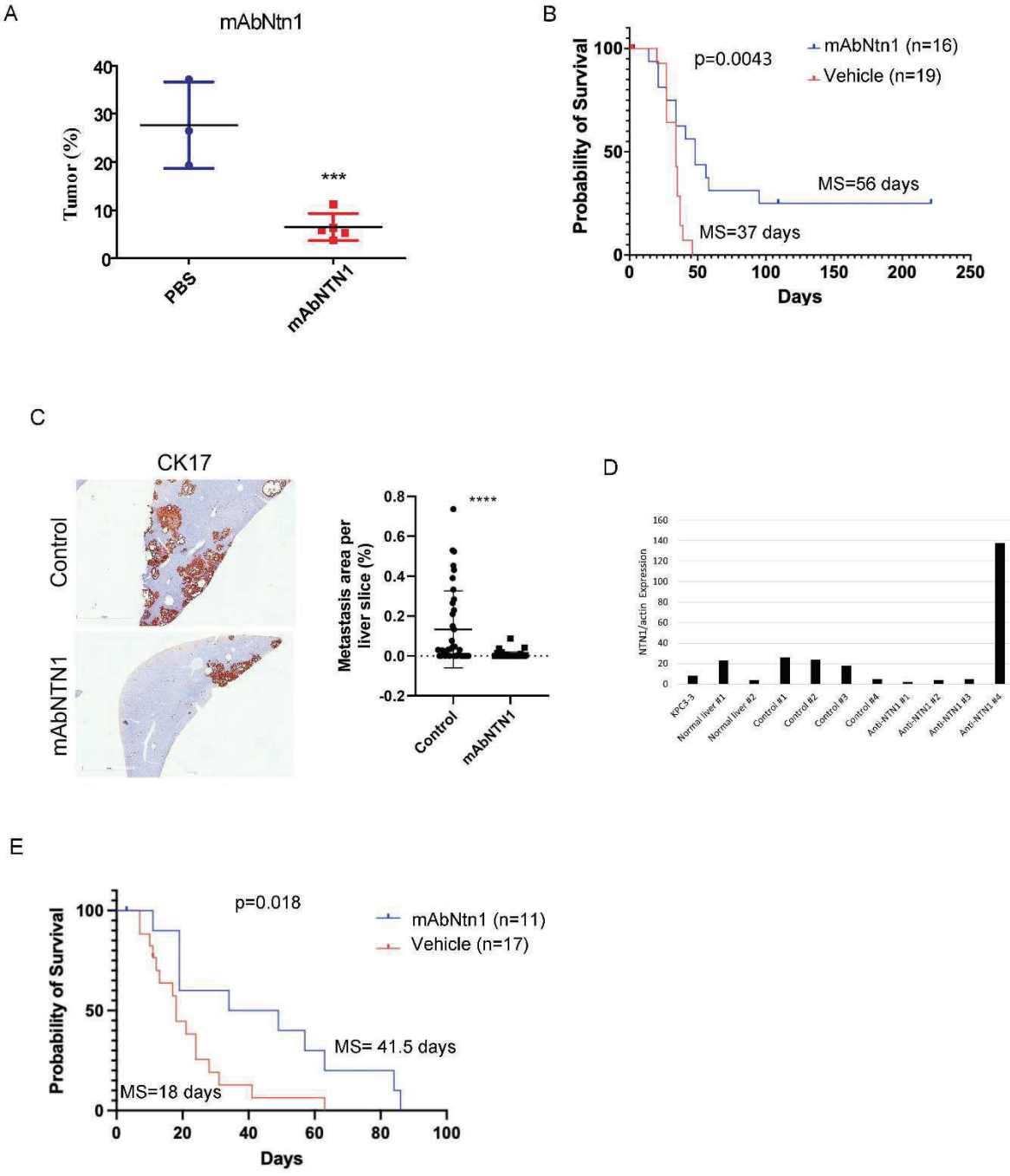
A
mAbNtn1
Tumor (%)
40
30
20
10
0
***
PBS
mAbNTN1
B
Probability of Survival
100
50
0
p=0.0043
mAbNtn1 (n=16)
Vehicle (n=19)
MS=56 days
MS=37 days
0
50
100
150
200
250
Days
C
CK17
Control
mAbNTN1
Metastasis area per liver slice (%)
0.8
0.6
0.4
0.2
0.0
-0.2
****
Control
mAbNTN1
D
NTN1/actin Expression
160
140
120
100
80
60
40
20
0
KPC3-3
Normal liver #1
Normal liver #2
Control #1
Control #2
Control #3
Control #4
Anti-NTN1 #1
Anti-NTN1 #2
Anti-NTN1 #3
Anti-NTN1 #4
E
Probability of Survival
100
50
0
p=0.018
mAbNtn1 (n=11)
Vehicle (n=17)
MS= 41.5 days
MS=18 days
0
20
40
60
80
100
Days

Figure 7

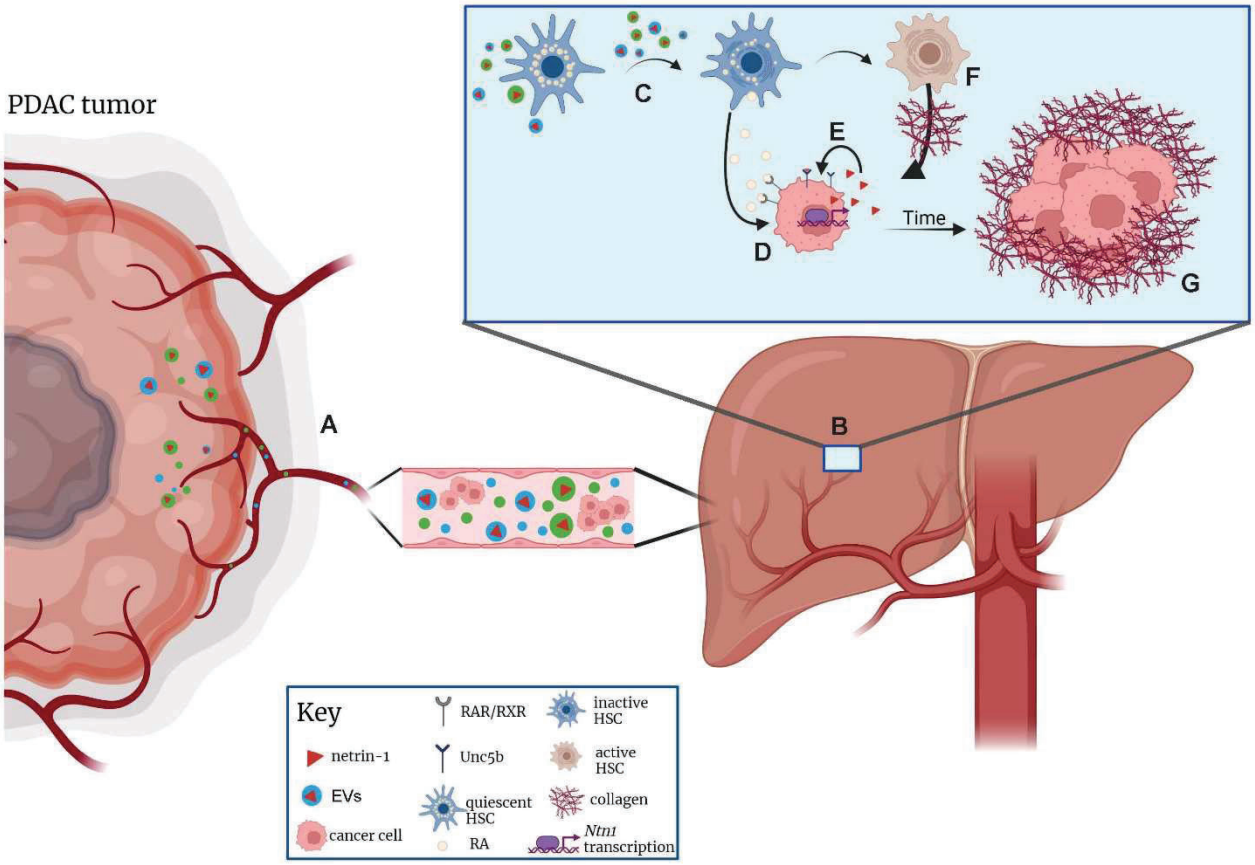
PDAC tumor
A
B
C
D
E
F
G
Time
Key
netrin-1
EVs
cancer cell
RAR/RXR
Unc5b
quiescent HSC
RA
inactive HSC
active HSC
collagen
Ntn1 transcription

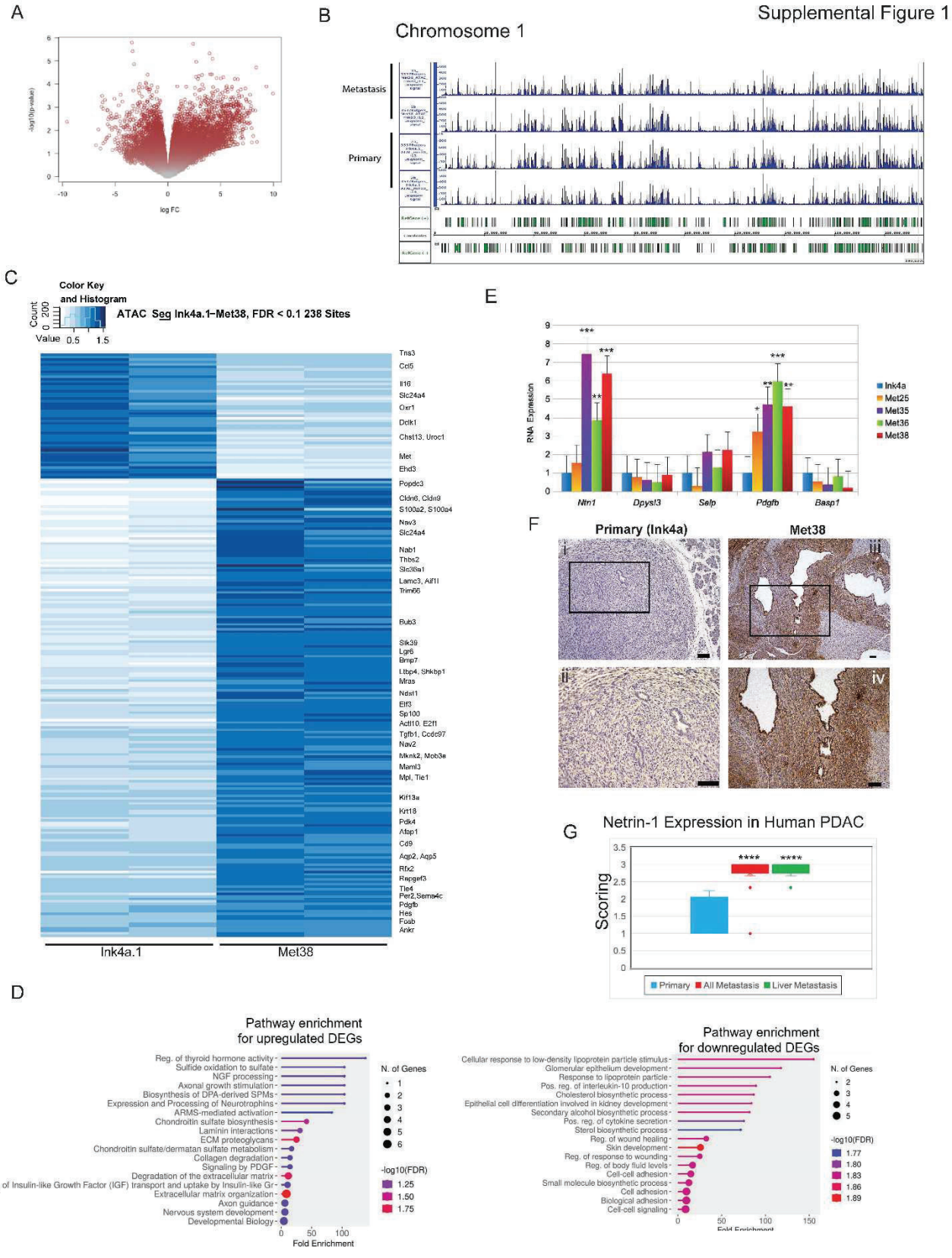
A
-log10(p-value)
log FC
B
Chromosome 1
Metastasis
Primary
C
Color Key and Histogram
Count
Value
ATAC Seq Ink4a.1–Met38, FDR < 0.1 238 Sites
Tns3
Ccl5
Il16
Slc24a4
Oxr1
Ddk1
Chst13, Uroc1
Met
Ehd3
Popdc3
Cldn6, Cldn9
S100a2, S100a4
Nav3
Slc24a4
Nab1
Thbs2
Slc38a1
Lamc3, Aif1l
Trim66
Bub3
Slk39
Lgr6
Bmp7
Ltbp4, Shkbp1
Mras
Ndst1
Eif3
Sp100
Actl10, E2f1
Tgfb1, Ccdc97
Nav2
Mknk2, Mob3a
Maml3
Mpl, Tie1
Kif13a
Krt18
Pdk4
Afap1
Cd9
Aqp2, Aqp5
Rfx2
Rapgef3
Tie4
Per2,Sema4c
Pdgfb
Hes
Fosb
Ankr
Ink4a.1
Met38
D
Pathway enrichment for upregulated DEGs
Reg. of thyroid hormone activity
Sulfide oxidation to sulfate
NGF processing
Axonal growth stimulation
Biosynthesis of DPA-derived SPMs
Expression and Processing of Neurotrophins
ARMS-mediated activation
Chondroitin sulfate biosynthesis
Laminin interactions
ECM proteoglycans
Chondroitin sulfate/dermatan sulfate metabolism
Collagen degradation
Signaling by PDGF
Degradation of the extracellular matrix
of Insulin-like Growth Factor (IGF) transport and uptake by Insulin-like Gr
Extracellular matrix organization
Axon guidance
Nervous system development
Developmental Biology
Fold Enrichment
N. of Genes
-log10(FDR)
Pathway enrichment for downregulated DEGs
Cellular response to low-density lipoprotein particle stimulus
Glomerular epithelium development
Response to lipoprotein particle
Pos. reg. of interleukin-10 production
Cholesterol biosynthetic process
Epithelial cell differentiation involved in kidney development
Secondary alcohol biosynthetic process
Pos. reg. of cytokine secretion
Sterol biosynthetic process
Reg. of wound healing
Skin development
Reg. of response to wounding
Reg. of body fluid levels
Cell-cell adhesion
Small molecule biosynthetic process
Cell adhesion
Biological adhesion
Cell-cell signaling
Fold Enrichment
N. of Genes
-log10(FDR)
E
RNA Expression
Ntn1
Dpysl3
Selp
Pdgfb
Basp1
Ink4a
Met25
Met35
Met36
Met38
F
Primary (Ink4a)
Met38
i
ii
iii
iv
G
Netrin-1 Expression in Human PDAC
Scoring
Primary
All Metastasis
Liver Metastasis

Supplemental Figure 2

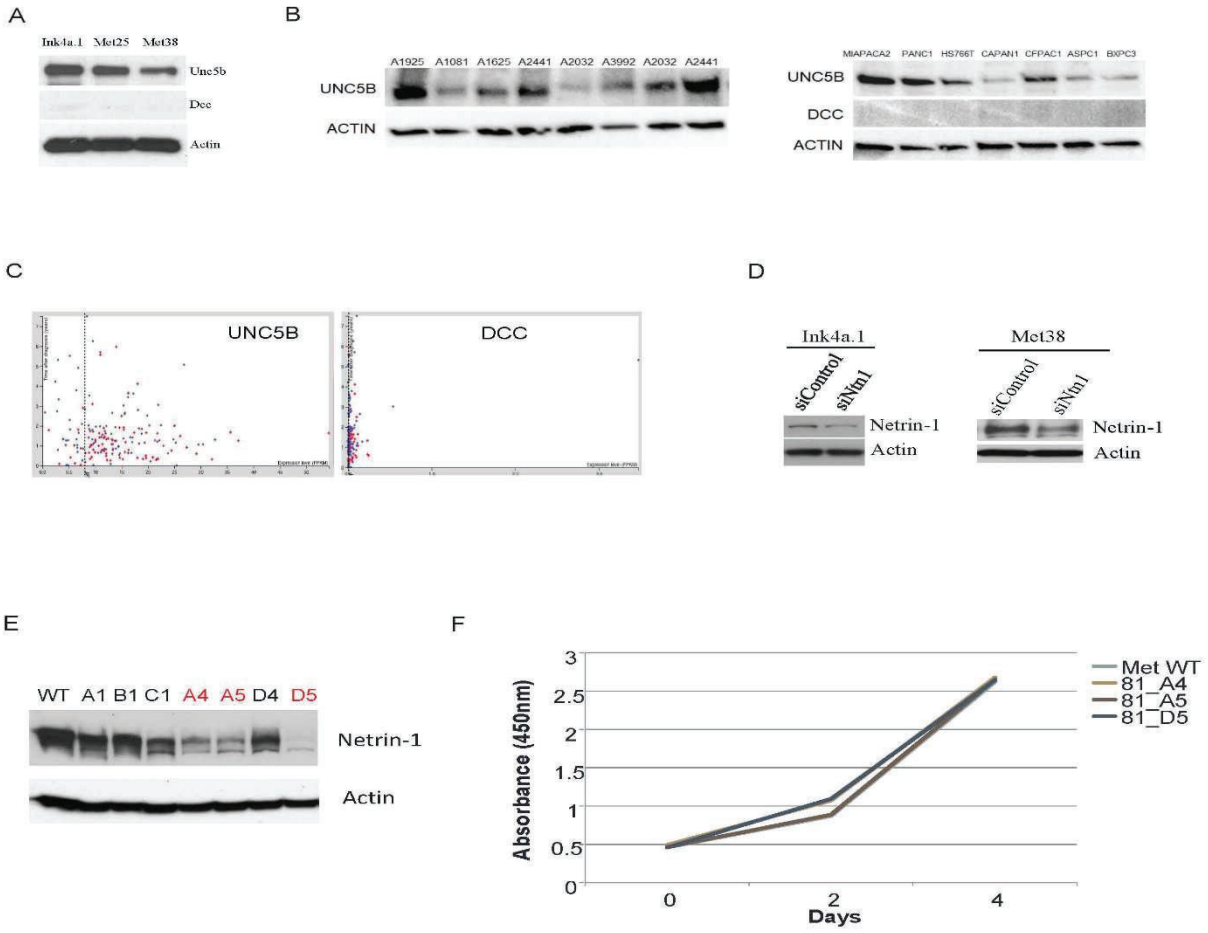

Supplemental Figure 3

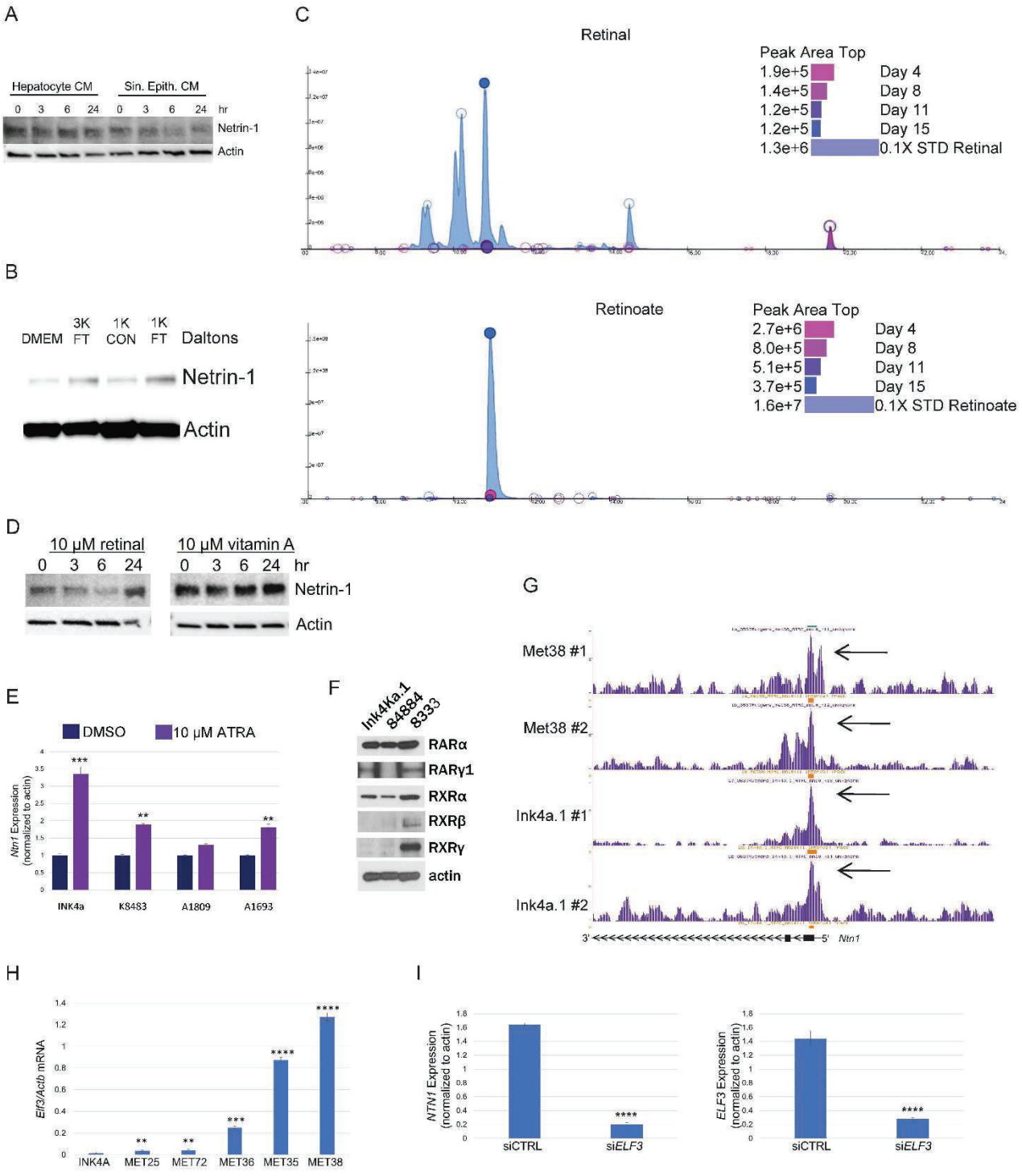

Supplemental Figure 4

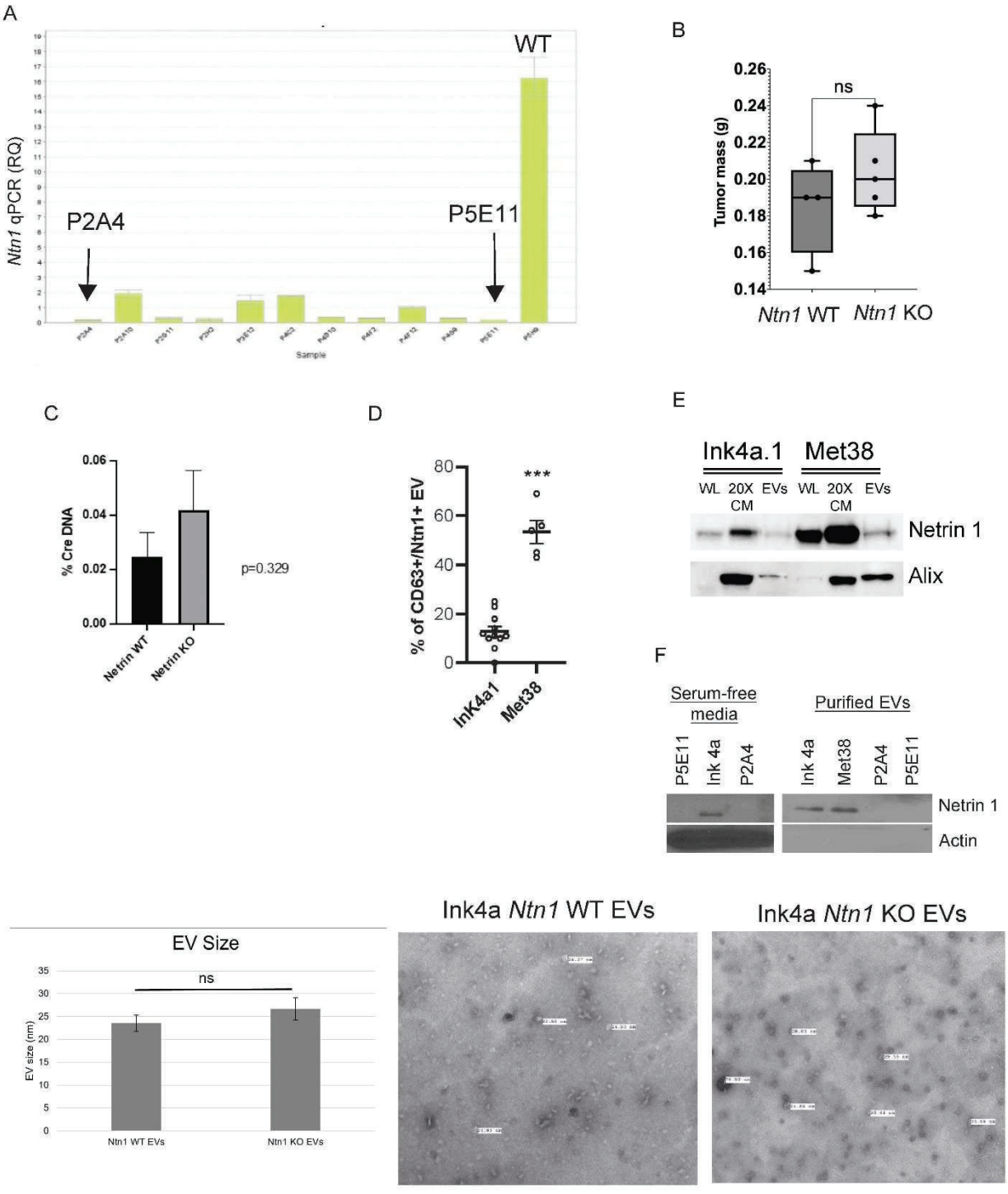

Supplemental Figure 5

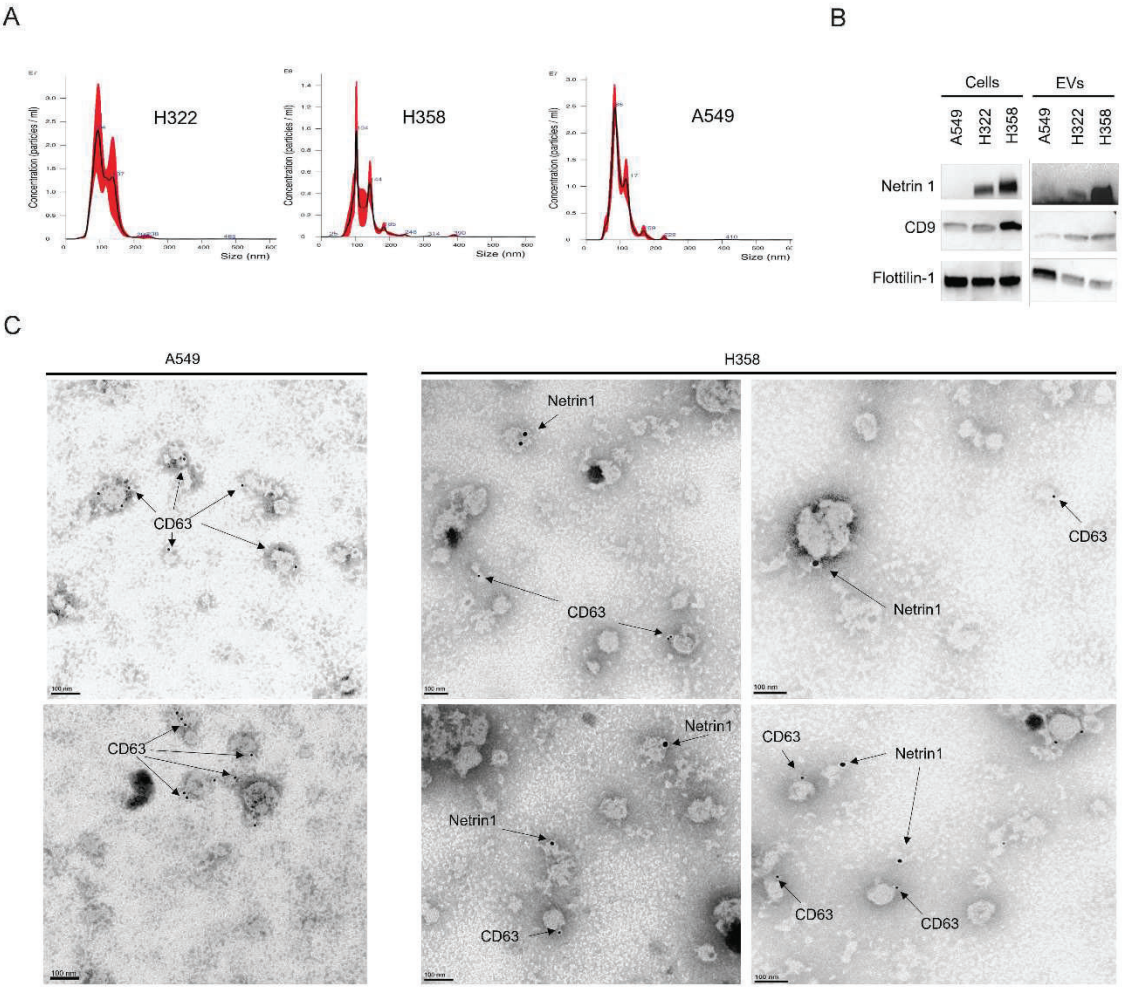

REFERENCES

Arafat, H., Lazar, M., Salem, K., Chipitsyna, G., Gong, Q., Pan, T. C., Zhang, R. Z., Yeo, C. J., and Chu, M. L. (2011). Tumor-specific expression and alternative splicing of the COL6A3 gene in pancreatic cancer. Surgery *150*, 306-315.

Bardeesy, N., Aguirre, A. J., Chu, G. C., Cheng, K. H., Lopez, L. V., Hezel, A. F., Feng, B., Brennan, C., Weissleder, R., Mahmood, U.*, et al.* (2006). Both p16(Ink4a) and the p19(Arf)-p53 pathway constrain progression of pancreatic adenocarcinoma in the mouse. Proc Natl Acad Sci U S A *103*, 5947-5952.

Biankin, A. V., Waddell, N., Kassahn, K. S., Gingras, M. C., Muthuswamy, L. B., Johns, A. L., Miller, D. K., Wilson, P. J., Patch, A. M., Wu, J.*, et al.* (2012). Pancreatic cancer genomes reveal aberrations in axon guidance pathway genes. Nature *491*, 399-405.

Cassier P., E. L., Garin G., Courbebaisse Y., Terret C., Robert M., Frenel J-S., Depil S., Delord J-P., Perol D., Ray-Coquard I.L., Bidaux A-S., Tabone-Eglinger S., Gilles-Afchain L., Treilleux I., Wang Q., Ducarouge B., Mehlen P., Blay J-Y., Gomez-Roca C.A. (2019). A first in human, phase I trial of NP137, a first in class antibody targeting Netrin-1, in patients with advanced refractory solid tumors. Annals of Oncology *v159-v193*.

Chao, Y. C., Pan, S. H., Yang, S. C., Yu, S. L., Che, T. F., Lin, C. W., Tsai, M. S., Chang, G. C., Wu, C. H., Wu, Y. Y.*, et al.* (2009). Claudin-1 is a metastasis suppressor and correlates with clinical outcome in lung adenocarcinoma. Am J Respir Crit Care Med *179*, 123-133.

Collisson, E. A., Sadanandam, A., Olson, P., Gibb, W. J., Truitt, M., Gu, S., Cooc, J., Weinkle, J., Kim, G. E., Jakkula, L.*, et al.* (2011). Subtypes of pancreatic ductal adenocarcinoma and their differing responses to therapy. Nat Med *17*, 500-503.

Collisson, E. A., Trejo, C. L., Silva, J. M., Gu, S., Korkola, J. E., Heiser, L. M., Charles, R. P., Rabinovich, B. A., Hann, B., Dankort, D.*, et al.* (2012). A central role for RAF-->MEK-->ERK signaling in the genesis of pancreatic ductal adenocarcinoma. Cancer Discov *2*, 685-693.

Costa-Silva, B., Aiello, N. M., Ocean, A. J., Singh, S., Zhang, H., Thakur, B. K., Becker, A., Hoshino, A., Mark, M. T., Molina, H.*, et al.* (2015). Pancreatic cancer exosomes initiate pre-metastatic niche formation in the liver. Nat Cell Biol *17*, 816-826.

D'Ambrosio, D. N., Walewski, J. L., Clugston, R. D., Berk, P. D., Rippe, R. A., and Blaner, W. S. (2011). Distinct populations of hepatic stellate cells in the mouse liver have different capacities for retinoid and lipid storage. PLoS One *6*, e24993.

Delloye-Bourgeois, C., Brambilla, E., Coissieux, M. M., Guenebeaud, C., Pedeux, R., Firlej, V., Cabon, F., Brambilla, C., Mehlen, P., and Bernet, A. (2009). Interference with netrin-1 and tumor cell death in non-small cell lung cancer. J Natl Cancer Inst *101*, 237-247.

Dumartin, L., Quemener, C., Laklai, H., Herbert, J., Bicknell, R., Bousquet, C., Pyronnet, S., Castronovo, V., Schilling, M. K., Bikfalvi, A., and Hagedorn, M. (2010). Netrin-1 mediates early events in pancreatic adenocarcinoma progression, acting on tumor and endothelial cells. Gastroenterology *138*, 1595-1606, 1606 e1591-1598.

Erstad, D. J., Sojoodi, M., Taylor, M. S., Ghoshal, S., Razavi, A. A., Graham-O'Regan, K. A., Bardeesy, N., Ferrone, C. R., Lanuti, M., Caravan, P.*, et al.* (2018). Orthotopic and heterotopic murine models of pancreatic cancer and their different responses to FOLFIRINOX chemotherapy. Dis Model Mech *11*.

Erstad, D. J., Sojoodi, M., Taylor, M. S., Jordan, V. C., Farrar, C. T., Axtell, A. L., Rotile, N. J., Jones, C., Graham-O'Regan, K. A., Ferreira, D. S.*, et al.* (2020). Fibrotic Response to Neoadjuvant Therapy Predicts Survival in Pancreatic Cancer and Is Measurable with Collagen-Targeted Molecular MRI. Clin Cancer Res *26*, 5007-5018.

Fitamant, J., Guenebeaud, C., Coissieux, M. M., Guix, C., Treilleux, I., Scoazec, J. Y., Bachelot, T., Bernet, A., and Mehlen, P. (2008). Netrin-1 expression confers a selective advantage for tumor cell survival in metastatic breast cancer. Proc Natl Acad Sci U S A *105*, 4850-4855.

Foley, K., Rucki, A. A., Xiao, Q., Zhou, D., Leubner, A., Mo, G., Kleponis, J., Wu, A. A., Sharma, R., Jiang, Q.*, et al.* (2015). Semaphorin 3D autocrine signaling mediates the metastatic role of annexin A2 in pancreatic cancer. Sci Signal *8*, ra77.

Friedman, S. L., Wei, S., and Blaner, W. S. (1993). Retinol release by activated rat hepatic lipocytes: regulation by Kupffer cell-conditioned medium and PDGF. Am J Physiol *264*, G947-952.

Geerts, A., Niki, T., Hellemans, K., De Craemer, D., Van Den Berg, K., Lazou, J. M., Stange, G., Van De Winkel, M., and De Bleser, P. (1998). Purification of rat hepatic stellate cells by side scatter-activated cell sorting. Hepatology *27*, 590-598.

Gibert, B., and Mehlen, P. (2015). Dependence Receptors and Cancer: Addiction to Trophic Ligands. Cancer Res *75*, 5171-5175.

Grandin, M., Meier, M., Delcros, J. G., Nikodemus, D., Reuten, R., Patel, T. R., Goldschneider, D., Orriss, G., Krahn, N., Boussouar, A.*, et al.* (2016). Structural Decoding of the Netrin-1/UNC5 Interaction and its Therapeutical Implications in Cancers. Cancer Cell *29*, 173-185.

Hong, Y., Li, S., Wang, J., and Li, Y. (2018). In vitro inhibition of hepatic stellate cell activation by the autophagy-related lipid droplet protein ATG2A. Sci Rep *8*, 9232.

Jophlin, L. L., Koutalos, Y., Chen, C., Shah, V., and Rockey, D. C. (2018). Hepatic stellate cells retain retinoid-laden lipid droplets after cellular transdifferentiation into activated myofibroblasts. Am J Physiol Gastrointest Liver Physiol *315*, G713-G721.

Jurcak, N. R., Rucki, A. A., Muth, S., Thompson, E., Sharma, R., Ding, D., Zhu, Q., Eshleman, J. R., Anders, R. A., Jaffee, E. M.*, et al.* (2019). Axon Guidance Molecules Promote Perineural Invasion and Metastasis of Orthotopic Pancreatic Tumors in Mice. Gastroenterology *157*, 838-850 e836.

Kang, N., Gores, G. J., and Shah, V. H. (2011). Hepatic stellate cells: partners in crime for liver metastases? Hepatology *54*, 707-713.

Krebs, N., Klein, L., Wegwitz, F., Espinet, E., Maurer, H. C., Tu, M., Penz, F., Kuffer, S., Xu, X., Bohnenberger, H.*, et al.* (2022). Axon guidance receptor ROBO3 modulates subtype identity and prognosis via AXL-associated inflammatory network in pancreatic cancer. JCI Insight *7*.

Lai Wing Sun, K., Correia, J. P., and Kennedy, T. E. (2011). Netrins: versatile extracellular cues with diverse functions. Development *138*, 2153-2169.

Li, Y., Liu, F., Ding, F., Chen, P., and Tang, M. (2015). Inhibition of liver fibrosis using vitamin A-coupled liposomes to deliver matrix metalloproteinase-2 siRNA in vitro. Mol Med Rep *12*, 3453-3461.

Lu, W., Li, N., and Liao, F. (2019). Identification of Key Genes and Pathways in Pancreatic Cancer Gene Expression Profile by Integrative Analysis. Genes (Basel) *10*.

Matsumoto, Y., Irie, F., Inatani, M., Tessier-Lavigne, M., and Yamaguchi, Y. (2007). Netrin-1/DCC signaling in commissural axon guidance requires cell-autonomous expression of heparan sulfate. J Neurosci *27*, 4342-4350.

McDonald, O. G., Li, X., Saunders, T., Tryggvadottir, R., Mentch, S. J., Warmoes, M. O., Word, A. E., Carrer, A., Salz, T. H., Natsume, S.*, et al.* (2017). Epigenomic reprogramming during pancreatic cancer progression links anabolic glucose metabolism to distant metastasis. Nat Genet *49*, 367-376.

Mehlen, P., Delloye-Bourgeois, C., and Chedotal, A. (2011). Novel roles for Slits and netrins: axon guidance cues as anticancer targets? Nat Rev Cancer *11*, 188-197.

Menck, K., Klemm, F., Gross, J. C., Pukrop, T., Wenzel, D., and Binder, C. (2013). Induction and transport of Wnt 5a during macrophage-induced malignant invasion is mediated by two types of extracellular vesicles. Oncotarget *4*, 2057-2066.

Murakami, K., Kaji, T., Shimono, R., Hayashida, Y., Matsufuji, H., Tsuyama, S., Maezono, R., Kosai, K., and Takamatsu, H. (2011). Therapeutic effects of vitamin A on experimental cholestatic rats with hepatic fibrosis. Pediatr Surg Int *27*, 863-870.

Paradisi, A., Maisse, C., Coissieux, M. M., Gadot, N., Lepinasse, F., Delloye-Bourgeois, C., Delcros, J. G., Svrcek, M., Neufert, C., Flejou, J. F.*, et al.* (2009). Netrin-1 up-regulation in inflammatory bowel diseases is required for colorectal cancer progression. Proc Natl Acad Sci U S A *106*, 17146-17151.

Pattison, J. M., Melo, S. P., Piekos, S. N., Torkelson, J. L., Bashkirova, E., Mumbach, M. R., Rajasingh, C., Zhen, H. H., Li, L., Liaw, E.*, et al.* (2018). Retinoic acid and BMP4 cooperate with p63 to alter chromatin dynamics during surface epithelial commitment. Nat Genet *50*, 1658-1665.

Peinado, H., Aleckovic, M., Lavotshkin, S., Matei, I., Costa-Silva, B., Moreno-Bueno, G., Hergueta-Redondo, M., Williams, C., Garcia-Santos, G., Ghajar, C.*, et al.* (2012). Melanoma exosomes educate bone marrow progenitor cells toward a pro-metastatic phenotype through MET. Nat Med *18*, 883-891.

Pitarresi, J. R., Norgard, R. J., Chiarella, A. M., Suzuki, K., Bakir, B., Sahu, V., Li, J., Zhao, J., Marchand, B., Wengyn, M. D*., et al.* (2021). PTHrP Drives Pancreatic Cancer Growth and Metastasis and Reveals a New Therapeutic Vulnerability. Cancer Discov *11*, 1774-1791.

Serafini, T., Kennedy, T. E., Galko, M. J., Mirzayan, C., Jessell, T. M., and Tessier-Lavigne, M. (1994). The netrins define a family of axon outgrowth-promoting proteins homologous to C. elegans UNC-6. Cell *78*, 409-424.

Sung, P. J., Rama, N., Imbach, J., Fiore, S., Ducarouge, B., Neves, D., Chen, H. W., Bernard, D., Yang, P. C., Bernet, A*., et al.* (2019). Cancer-Associated Fibroblasts Produce Netrin-1 to Control Cancer Cell Plasticity. Cancer Res *79*, 3651-3661.

Takahashi, K., Ehata, S., Koinuma, D., Morishita, Y., Soda, M., Mano, H., and Miyazono, K. (2018). Pancreatic tumor microenvironment confers highly malignant properties on pancreatic cancer cells. Oncogene *37*, 2757-2772.

Thery, C., Amigorena, S., Raposo, G., and Clayton, A. (2006). Isolation and characterization of exosomes from cell culture supernatants and biological fluids. Curr Protoc Cell Biol *Chapter 3*, Unit 3 22.

Thiery, J. P., Acloque, H., Huang, R. Y., and Nieto, M. A. (2009). Epithelial-mesenchymal transitions in development and disease. Cell *139*, 871-890.

Tsai, J. H., and Yang, J. (2013). Epithelial-mesenchymal plasticity in carcinoma metastasis. Genes Dev *27*, 2192-2206.

Wang, W., Friedland, S. C., Guo, B., O'Dell, M. R., Alexander, W. B., Whitney-Miller, C. L., Agostini-Vulaj, D., Huber, A. R., Myers, J. R., Ashton, J. M*., et al.* (2019). ARID1A, a SWI/SNF subunit, is critical to acinar cell homeostasis and regeneration and is a barrier to transformation and epithelial-mesenchymal transition in the pancreas. Gut *68*, 1245-1258.

Weissmueller, S., Manchado, E., Saborowski, M., Morris, J. P. t., Wagenblast, E., Davis, C. A., Moon, S. H., Pfister, N. T., Tschaharganeh, D. F., Kitzing, T*., et al.* (2014). Mutant p53 drives pancreatic cancer metastasis through cell-autonomous PDGF receptor beta signaling. Cell *157*, 382-394.

Wu, M., Li, X., Liu, R., Yuan, H., Liu, W., and Liu, Z. (2020). Development and validation of a metastasis-related Gene Signature for predicting the Overall Survival in patients with Pancreatic Ductal Adenocarcinoma. J Cancer *11*, 6299-6318.

Yong, L. K., Lai, S., Liang, Z., Poteet, E., Chen, F., van Buren, G., Fisher, W., Mo, Q., Chen, C., and Yao, Q. (2016). Overexpression of Semaphorin-3E enhances pancreatic cancer cell growth and associates with poor patient survival. Oncotarget *7*, 87431-87448.

Zheng, L., Xu, M., Xu, J., Wu, K., Fang, Q., Liang, Y., Zhou, S., Cen, D., Ji, L., Han, W., and Cai, X. (2018). ELF3 promotes epithelial-mesenchymal transition by protecting ZEB1 from miR-141-3p-mediated silencing in hepatocellular carcinoma. Cell Death Dis *9*, 387.

Zu, F., Liu, P., Wang, H., Zhu, T., Sun, J., Sheng, W., and Tan, X. (2020). Integrated analysis identifies a pathway-related competing endogenous RNA network in the progression of pancreatic cancer. BMC Cancer *20*, 958.

SUPPLEMENTARY DATA

During my PhD, I have produced additional data which support the soon-to-be published work and helped in its acceptance. Indeed, it has enabled me to observe the inhibition of pro-tumoural-EMT functions that NTN1 targeting induces in murine and human cancer cells, most likely through an alteration of the PI3K/AKT pathway. Furthermore, I have observed the effect of the anti-NTN1 antibody NP137 on EMT features *in vitro* through migration, invasion and organoid assays, and the potential role of TFF3 as a potential biomarker of cancer development in endometrial cancer patients. These results are presented in the following paragraphs.

***

1- NTN1 blockade inhibits organoid growth.

Based on the previously published data of Eritja et al. in 2017 demonstrating that PTEN-deficient endometrial cell 3D cultures show increased glandular perimeter compared to WT cells [280], we investigated whether NP137 could attenuate this inducing effect. After replicating the effect of PTEN deletion on organoid growth as already seen, we observed a significant inhibition of glandular cell growth when cultures were treated with NP137 (Figure 1ab). As PTEN WT cells are capable of forming organoids but of smaller volume, this data supports the view that NTN1 blockade disrupts the growth of EC cells in a 3D formation, a setting phenocopying that of glands in the endometrial tissue, and suggests a possible effect of NTN1 blockade on stem-like properties.

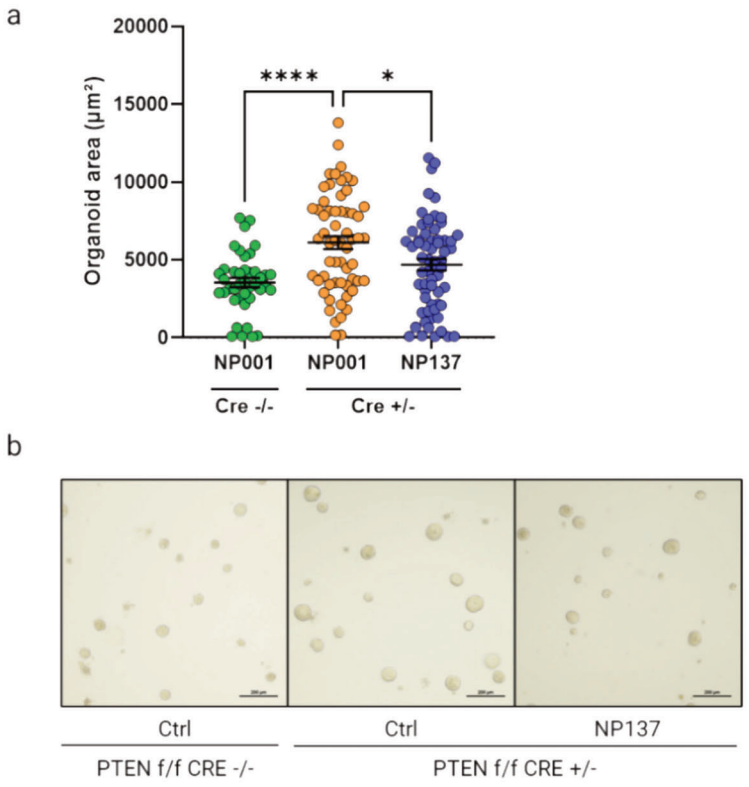

Figure 1: In vitro, NP137 inhibits organoid formation induced by PTEN deletion.

a. *Glandular area measurements of organoid cultures of Cre:ER-/- PTENf/f mice endometrial cells untreated with tamoxifen (WT) or Cre:ER+/-;PTENf/f (PTEN knock-out) mice endometrial cells treated with tamoxifen and* ***b.*** *associated phase contrast pictures. Values are mean, and error bars represent mean +/- s.e.m. *p<0.05, ****p< 0.0001 by T-test (n=1). Data are shown for 1 experiment with more than 100 measured glands per condition. Scale bars: 200 µm.*

2- NTN1 blockade impacts functional EMT.

To investigate the effect of NP137 on EMT-associated features such as migration and invasion, wound healing assays and Transwell invasion assays were carried out on human EC cell lines Ishikawa, ARK1 and ARK2. After optimization of wound closure experiments using the Incucyte® Scratch Wound software and the associated Imagelock plates and scratch module, and in line with the results observed in the Ishikawa cell line (presented in the extended figure 7a of Lengrand *et al.* Accepted in Nature), I observed an inhibition of wound closure in wound healing/scratch assays in both ARK1 and ARK2 NTN1 expressing serous EC cell lines following NP137 treatment (Figure 2ab). As cell migration is a net sum of cell movement, multiplication, and death, the monitoring of the two latter parameters under identical culture conditions and time frames allowed us to see that this inhibitory effect was due to a decrease in migratory properties and not explained by a modulation in cell death (figure 2c) or in cell proliferation (figure 2d). Furthermore, RTqPCR quantification of transcriptional activity of specific genes of Ishikawa cells xenografted tumours in NMRI Nude female adult mice showed an increased expression of epithelial markers when mice were treated intravenously with NP137 for 28 days (Figure 2e, in part present in extended data Figure 7b of Lengrand et al.). Altogether, these data are complementary to the ones already described in the Lengrand *et al.* article, which demonstrate the effect of NP137 on EMT properties such as migration and invasion. This data thus supports the view that NTN1 blockade inhibits mesenchymal cell behaviour and phenotypes.

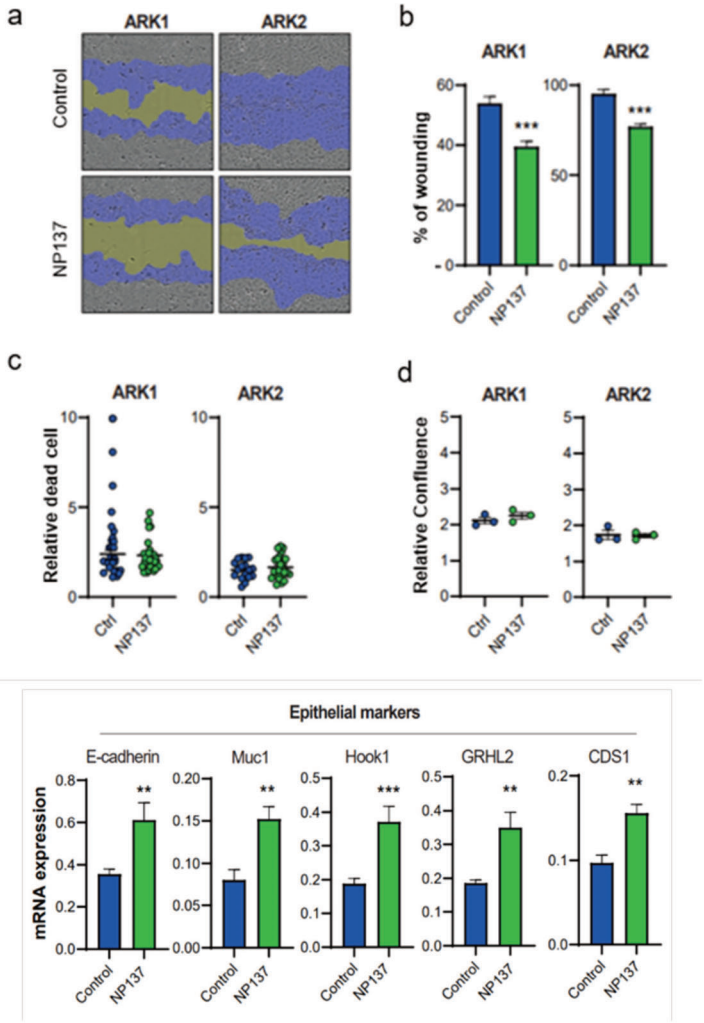

Figure 2: NTN1 blockade impacts EC cell EMT features.

a, *Representative fields of in vitro closure of the wound healing assay area in 3 different indicated cell lines with real-time monitoring of cell migration pre-treated or with NP137 or control. The blue surfaces represent wounded areas. Scale bar (represented by a line), (100 µm).* ***b,*** *Percentage of wounded surface in ARK1 or ARK2 (at 48h) cell lines treated with NP137 or control. Bars are mean values of more than 10 wells +/- s.e.m. *** p<0,001 by T-test.* ***c,d,*** *Measurement of relative ARK1 and ARK2* ***c,*** *cell death or* ***d,*** *proliferation in culture conditions of the wound healing from 3 independent experiments.* ***e,*** *Relative mRNA expression of main epithelial markers (E-cadherin, Muc1, Hook1, GRHL2 and CDS1) by qRT-PCR in mice tumours harvested from Ishikawa human cells treated with control (n=7) or NP137 (n=8) (Bars are mean values mean +/- s.e.m., data are normalized to HPRT gene). * p<0.05; ** p<0.01; *** p<0.001 by Mann-Whitney.*

3- NTN1 is exposed at the surface of EVs, and its blockade impacts tumour cell EVs secretion and profile.

Due to the implication of EVs in the induction of EMT and the progression of cancer, we analysed the effect of NP137 treatment on the *in vitro* secretion of EVs by cancer cells. Prior data generated by Dr. Stephany Fiore, a former doctoral student at the laboratory, demonstrated the presence of NTN1 at the surface of EVs in H358 and H322 NTN1-expressing lung cancer cell lines (as opposed to the absence of NTN1 in the EVS of the A549 lung cells that do not express NTN1 (figure 3abc and supplementary figure 5 from Dudgeon et al. submitted in Cell Report). Additionally, treatment of the H358 NTN1-expressing lung cell line with NP137 led to a significant decrease in the amount of EVs secreted in the conditioned media (figure 3d). The reason for this decrease in the amount of EVs after NP137 treatment may be due to cell death induced by NP137 or by another mechanism, which remains to be determined. However, it is important to note that this effect is of the greatest interest as the NTN1 positive EVs seem to participate in the formation of metastasis (Dudgeon *et al*., submitted in Cell Report). As EVs are representative of the cells from which they derive, we investigated whether NP137 treatment altered the proteomic composition of tumour derived EVs. Mass spectrometry analysis conducted on EVs derived from NP137 treated and untreated H358 cells highlighted a shift EV profile, with 54 proteins that appear to be differentially expressed with a downregulation of proteins implicated in cellular junctions and cellular interaction with the ECM such as laminin subunit beta 3 (MALB3) and laminin subunit gamma 2 (LAMC2). Additionally, NP137 treatment also upregulated immunoglobulin proteins such as IGKC or intracellular trafficking proteins such as ANFY1, MUO5C and SNX5 that is implicated in the inhibition of E-cadherin endosomal degradation [281] (figure 3e). Altogether, these data support the anti-tumoural effect of NTN1 blockade through EVs and the alteration of their composition, representative of the EMT blockade within cells in favour of tumour epithelialization.

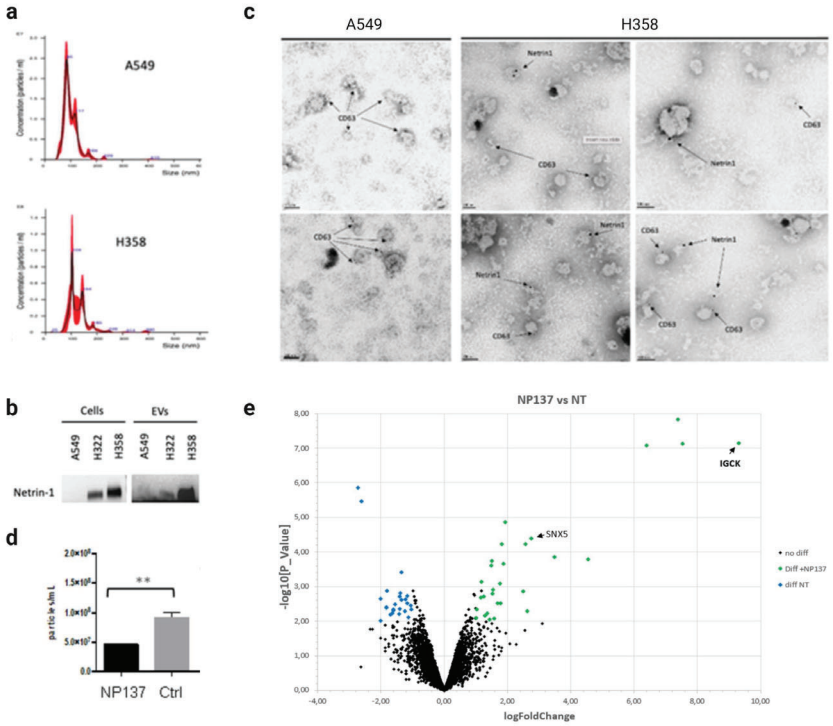

Figure 3: NTN1 is exposed at the surface of EVs isolated from human pulmonary cell line conditioned media, whose expression is influenced by NP137 treatment.

a. *Quantification of EVs isolated from human pulmonary cancer cell line; nanoparticle tracking analysis (NTA) distribution of EVs isolated from A549 and H358 cells.* ***b.*** *Immunoblot showing the expression of NTN1 in A549 (negative control), H322 and H358 cells (NTN1 positive) and associated EVs.* ***c.*** *Transmission electron microscopy (TEM) images of representative fields of EVs marked for NTN1 and CD63 (marker specific of EVs) in A549 (negative control) and H358 cells. Immunolabelling realized with an anti-NTN1 antibody coupled to 15 nm gold beads and an anti-CD63 antibody coupled to 5 nm gold beads. Scale bar = 100 nm.* ***d.*** *Quantification with NTA of EVs isolated from H358 cells after treatment with NP137 antibody or isotypic antibody control (Ctrl).* ***e.*** *Volcano plot of the mass spectrometry analysis of EVs derived from NP137 treated (NP137) and untreated (NT) H358 cells. Increased proteins are in green, decreased are in blue. IGCK (Immunoglobulin Kappa Constant) protein is described to be found in extracellular vesicles and is found increased after NP137 treatment along with SNX5 (sorting nexin-5), a vesicular transport protein.*

4- EMT inhibition by NTN1 blockade implicates the PI3K-AKT pathway.

Several published *in vitro* studies have suggested an involvement of NTN1 in EMT associated with the PI3K/AKT pathway [282–284], which is also frequently altered in EC. We hence investigated whether the *in vitro* inhibitory effect observed on migration and invasion of cells treated with NP137 was linked to a regulation of the PI3K/AKT pathway. We first induced EMT by adding TGFb and EGF to Ishikawa cells' culture medium. Western Blot analysis of PI3K/AKT effector activation by phosphorylation and EMT markers that indicated an inhibitory effect of NP137 on mesenchymal transformation and AKT activating phosphorylation of EMT induced cells (Figure 4ab). Furthermore, chemical blocking of the PI3K/AKT pathway by the inhibitor LY294002 resulted in an inhibition of cell migration, but no additive effect was observed compared to that of NP137 when the two were combined (Figure 4cd). Along with the previously described preclinical data, the *in vitro* inhibitory effect of NTN1 blockade on EMT features appears to be intrinsically linked to a regulation of the PI3K/AKT pathway. Altogether, these preclinical data support the dual action of NTN1 blockade on tumour cells: triggering cancer cell death and inhibiting EMT features, rendering the overall NP137-treated tumours more epithelial.

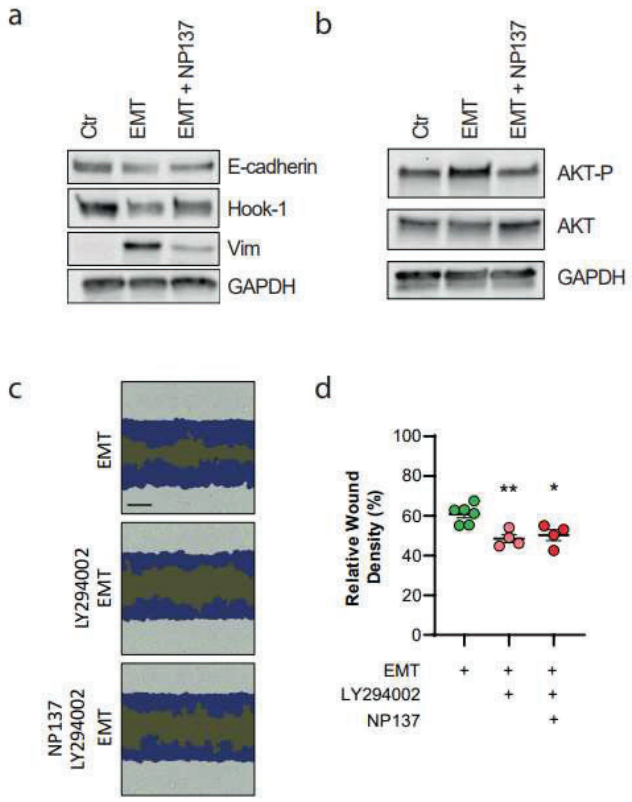

Figure 4: In vitro, NP137 blocks EMT features through the inhibition of PI3K/AKT pathway.

a,b*, EMT was induced by adding TGFβ and EGF in Ishikawa cells culture medium for 72 hours, NP137 was also added during 72h. Western blot of EMT markers and phosphorylated AKT (AKT-P) shows a decrease of Vim and AKT-P and an increase of E-caderin (CDH1) and Hook-1 after NP137 treatment.* ***c,d*** *Ishikawa cells were treated with EMT inducers TGFβ and EGF alone or in combination with the inhibitor LY294002 (during 24h) and with or without NP137, c. Representative fields of wound healing assays in the presence or not of the PI3K/AKT inhibitor LY294002 and of NP137. The blue surfaces represent wounded areas. Scale bar (represented by a line), (25 µm). d, Percentage of the wounded surface. Bars are mean values of more than 10 wells +/- s.e.m., * p<0.05, **p<0.01 by T-test (n=4).*

5- TFF3 as a potential biomarker of gynaecological cancer.

With the aim of identifying a biomarker able to predict clinical response to NP137, we analysed the biopsies of 14 EC patients from the phase I NP137 clinical trial by bulk RNA sequencing, comparing expression profiles in responsive (stable diseases or partial responses) and unresponsive patients. The major differentially expressed gene identified was TFF3, a secreted molecule driver of tumour development through the promotion of proliferation, invasion, angiogenesis, and apoptosis resistance also linked to hormone receptor expression [285]. To verify if this difference is translated at the protein level, an ELISA quantification of TFF3 expression was carried out in the serum of these same patients. The results showed a higher expression of TFF3 in EC serum, but not in a statistically significant manner (figure 5b). We then chose to look at more EC patients as well as cervical cancer patient samples, accessible to us thanks to the phase I extension cohorts. We first compared EC patient serum before treatment (C1D1) to that of 10 healthy individuals with the aim of determining if TFF3 could be a prognostic marker (figure 5c). In comparison to the healthy individuals, the results showed a significantly higher expression of TFF3 in EC patient samples, as well as in cervical cancer patient samples (Figure 5c). Unfortunately, when looking at the prediction potential of TFF3 serum levels regarding patient response to NP137 treatment, we were unable to identify any significant difference between serum TFF3 levels of responding and non-responding patients nor in the EC population or the cervical cancer population (figure 5de).

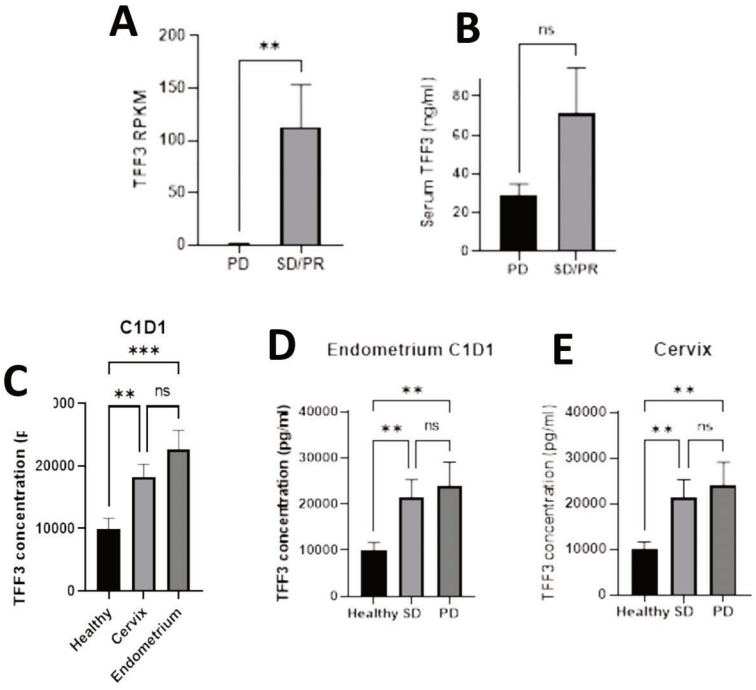

Figure 5: TFF3 as a biomarker of cancer progression.

A. Quantification of TFF3 RNA expression from RNA sequencing of biopsies from EC patients, only sorted by their progression. PD: Progressive disease, SD: stable disease, PR: partial response. Mean values for both PD and SD/PR groups (RPKM) are presented (PD: n=8; SD/PR: n=6) ***B****. Quantification of circulant TFF3 protein by ELISA. Mean values for both response groups (ng/ml), plotted with SEM bars, same number of patients as RNA expression in A.* ***C.*** *ELISA quantification of TFF3 concentration in serum samples of healthy individuals (n=10), cervical cancer patients (n=11) and EC patients (n=21) before NP137 injection.* ***D****. ELISA quantification of TFF3 concentration in serum samples before NP137 injection of healthy individuals (n=10), EC patients showing signs of stable disease (SD, n=12) and EC patients showing signs of progressive disease (PD, n=9) after 2 cycles of NP137 treatment.* ***E.*** *ELISA quantification of TFF3 concentration in serum samples before NP137 injection of healthy individuals (n=10), cervical cancer patients showing signs of stable disease (SD, n=5) and cervical cancer patients showing signs of progressive disease (PD, n=6) after 2 cycles of NP137 treatment. * $p<0.05$, ** $p<0.01$ by T-test.*

METHODS

Cell line and culture

The Ishikawa cell line, a well-differentiated endometrial adenocarcinoma cell line with NTN1 and UNC5B expression, was purchased from the American Type Culture Collection (ATCC). They were grown in Minimum Essential Medium (Ozyme), supplemented with 1% of penicillin/streptomycin (Life Technologies) and 5% FBS (Life Technologies) at 37 °C with saturating humidity and 5% CO2. The ARK1 and ARK2 cell lines were donated from Dr. Alessandro Santin (Yale University), and were grown in RPMI Glutamax (Life Technologies), supplemented with 1% of penicillin/streptomycin (Life Technologies), 10% FBS (Life Technologies), 25mM HEPES (Life Technologies), 1mM Sodium Pyruvate (Life Technologies), 2mM L-Glutamine (Life Technologies) at 37 °C with saturating humidity and 5% CO2.

In vitro endometrial cell line assays

Ishikawa, ARK1 and ARK2 cells were seeded (respectively 5x10^4, 4x10^4 and 2x10^4 cells/well) in 96-well Imagelock Plate (Sartorius) and treated with NP137 or its isotypic control NP001 at 10 ng/ml for respectively 72h, 48h and 48h at 37 °C (48 NP137 wells, 48 NP001 wells). Using the Woundmaker (Sartorius), the cell monolayer was scratched in each well. Wells were then washed with cell culture medium to remove free-floating cells and debris. 100 µl of culture medium was then added to each well, supplemented in NP137 at 10ng/ml (or its isotypic control), and plates were placed in the Incucyte at 37 °C, 5% CO2 for 24h for observation. Images of the wells were taken every 2h. Cytox Green was added to the wells after wound scratching to monitor cell death throughout the 24h of observation. PI3K inhibitor LY294002 was administered at 20µM for 24h before wound scratching. Regarding proliferation assays, Ishikawa, ARK1 and ARK2 cells were seeded in petri dished (10^6 cells/dish) and treated with NP137 or its isotypic control NP001 at 10ng/ml for respectively 72h, 48h and 48h at 37 °C. Cells were then harvested and seeded (respectively 10x10^3, 8x10^3 and 6x10^3 cells/well) in 100µl of culture medium in 96- well cell culture plate (Corning-Falcon) supplemented with NP137 at 10 ng/ml (or its isotypic control), and plates were placed in the Incucyte at 37 °C, 5% C02 for 24h for observation. EMT was induced by adding TGFβ (10ng/ml) and EGF (50ng/ml) in Ishikawa cells culture medium for 72h.

Isolation of endometrial epithelial cells and organoid culture

Cell culture experiments were performed in the Cell Culture Scientific and Technical Service from Universitat de Lleida, Lleida, Catalonia, Spain. Isolation and culture of endometrial organoids was performed as previously described with minor modifications [31,32]. Mice were killed by cervical dislocation and uterine horns were dissected, washed with HBSS and chopped in 3–4 mm length fragments. Uterine fragments were digested with 1% trypsin (Invitrogen) in HBSS (Invitrogen) for 1 h at 4 °C and 45 min at room temperature and epithelial sheets were squeezed-out of the uterine pieces. Epithelial sheets were washed twice with PBS and resuspended in 1 mL of DMEM/F12 (Invitrogen) supplemented with 1 mM Sodium Pyruvate (Thermo Scientific), 1% of penicillin/streptomycin (Sigma) and fungizone (Invitrogen) (basal medium). Epithelial sheets were disrupted mechanically in basal medium, and cells were diluted in basal medium containing 2% of dextran-coated charcoal-stripped serum (Invitrogen) and plated into culture dishes (BD Falcon). Cells were cultured for 24 h in an incubator at 37 °C with 5% CO2 and saturating humidity. Twenty-four hours later, cells were washed with HBSS and incubated with trypsin/EDTA solution (Sigma) for 5 min at 37 °C. Cells were collected resuspended in HBSS, and mechanically disrupted cells were centrifuged and plated in matrigrel-coated tissue culture plates in basal medium containing 3% of matrigel. Twenty-four hours after plating, the medium was replaced by basal medium supplemented with 5 ng/mL EGF and 1/100 dilution of Insulin−Transferrin−Sodium Selenite (ITS)

Supplement (Invitrogen) and 3% of fresh matrigel. Medium was replaced every 2–3 days. Organoid size was monitored by microscopy images (Nikon) and ImageJ software.

EV isolation from conditioned media

For EV isolation, cells were seeded in 150 cm^2 petri dishes at 4 million cells per plate and, following a 12h attachment period, were washed three times with PBS before supplying 10 mL of serum free media to prevent contamination from serum derived EVs. After 72h conditioned media was collected and EVs were purified following different protocols.

Differential ultracentrifugation

Following the protocol of Menck et al.2013, conditioned media was centrifuged at 750 g (5 minutes) and 1500 g (15 minutes) to remove cells and debris. An ultracentrifugation at 14 000 g for 35 minutes precipitated macrovesicles (MV). The remaining supernatant ultracentrifuged at 100 000g for at 4°C to recover exosome (EXO). All centrifuges were performed at 4°C (Menck et al., 2013). Following the protocol of Théry *et al*. 2006, to clear conditioned media from cells, a centrifuge at 300 g for 10 minutes was performed. Supernatant was collected and centrifuged 70 minutes at 100 000 g. Once supernatant was removed, the pellet was resuspended in PBS and centrifuged 1 hour at 100 000 g.

Immunoblotting

Cells as well as purified EVs were lysed in lysis buffer (10mM Tris pH 7,6, 10% glycerol, 5% SDS, 1% Triton X-100 and 0,1M DTT supplemented with a cocktail of protease inhibitors (Roche Applied Science)). After sonication, cell lysate total protein content was quantified using Pierce 660 nm Protein Assay Reagent (Life Technologies, cat #22660). Samples were boiled and loaded onto 4%-15% SDS-polyacrylamide gel (Biorad). SDS-PAGE electrophoresis was followed by transfer to a nitrocellulose membrane using Trans-Blot Turbo Transfer System (Biorad) and membranes were blocked 1 hour at room temperature using 10% non-fat dried milk in PBS/0.1% Tween 20 (PBS-T). Overnight incubation at 4 °C was performed using the following primary antibodies: rabbit monoclonal NTN1 (1:1000; clone EPR5428; cat #ab126729; Abcam); rabbit monoclonal UNC5B (1:1000; clone D9M7Z; cat #13851; Cell Signalling Technology). After three washes with PBS-T, membranes were incubated with the appropriate HRP-conjugated secondary antibodies (1:10 000; Jackson ImmunoResearch) for 1 hour at room temperature. Detection was performed using SuperSignal West Dura Chemoluminescent System (cat #34075; ThermoFisher Scientific). Membranes were imaged on the ChemiDoc Touch Imaging System (Biorad).

Transmission electron microscopy (CIQLE-Lyon Bio Image)

Suspensions were adsorbed on 200 Mesh Nickel grids coated with formvar-C for 10 min at RT. Immunogold labelling was performed the nest day by flotation the grids on drops of reactive media. Nonspecific sites were coated with 1% BSA in 50 mM Tris-HCl, pH7.4 for 10 min at RT. The incubation was carried 2 hours at RT in wet chamber with primary antibody (anti-NTN1) diluted 1/300 in 1% BSA, 50 mM Tris-HCl, pH 7.4. They were successively washed in 50 mM Tris-HCl, pH 7.4 and pH 8.2 at RT. Then, grids were incubated in a wet chamber in 1% BSA, 50 mM Tris-HCl, pH 8.2 for 10 min at RT, and labelled with 15 nm gold conjugated goat anti mouse IgG (Aurion) diluted 1/50 in 1% BSA, 50 mM Tris-HCl pH 8.2 for 45 minutes. They were successively washed in 50 Mm Tris-HCl pH8.2 and pH 7.4. The immunocomplex was fixed with glutaraldehyde 2% diluted in 50 mM Tris-HCl, pH7.4 for 2 min. Grids with suspension were then coloured with uranyl acetate in methylcellulose for 10 min in the dark and observed on a transmission electron microscope (Jeol 1400 JEM, Tokyo, Japan) equipped with a Gatan camera (Orius 1000) and Digital Micrograph Software.

Mass spectrometry

Mass spectrometry analysis was conducted in the Institute of Interdisciplinary Research of Grenoble (IRIG) by the "Exploring the Dynamics of Proteomes" (EDyP) team (INSERM U1292, CEA, UGA). Extracted proteins for mass spectrometry were stacked in the top of an SDS-PAGE gel (NuPAGE 4-12% gel, Invitrogen) before in-gel digestion was performed using trypsin (sequencing-grade, Promega). Resulting peptides were analyzed by nanoliquid chromatography couples to tandem MS (Ultimate 3000 RSLCnano system couples to Q-Exactive HF Quadripole-Orbitrap, Thermo Scientific) using a 120-min gradient. To do so, peptides were sampled on a 300 µm x 5 mm PepMap C18 precolumn and separated on a 75 µm x 250 mm C18 column (Reprosil-Pur 120 C18-AQ 1.9uM, Dr. A. Maisch, HPLC-GMBH). Mass spectrometry (MS) and MS/MS data were acquired using Xcalibur software. Peptides and proteins have been identified using MASCOT software (Matrix Science) through searches against Uniprot_human database and the frequently observed contaminant database. Trypsin was chosen as the enzyme and two missed cleavages were allowed. Peptide modifications allowed during the search were: carbamidomethylation (C, fixed), acetyl (Protein N-ter, variable) and oxidation (M, variable). Peptides and proteins have been validated and quantified with Proline software (2.0 version).

Statistical analysis

Statistical analyses were performed on Prism (GraphPad Software, San Diego, California). In the figure legends, n defines the total number of replicates. All statistical tests were two-sided. Cell migration assays were compared by T-test.

METHODS REFERENCES

Menck, K., Klemm, F., Gross, J.C., Pukrop, T., Wenzel, D., and Binder, C. (2013). Induction and transport of Wnt 5a during macrophage-induced malignant invasion is mediated by two types of extracellular vesicles. Oncotarget *4*, 2057–2066.

Théry, C., Amigorena, S., Raposo, G., and Clayton, A. (2006). Isolation and characterization of exosomes from cell culture supernatants and biological fluids. Curr Protoc Cell Biol *Chapter 3*, Unit 3.22.

Discussion, Conclusion & Perspectives

The results obtained over the course of my PhD have enabled us to showcase the true potential and therapeutic benefit of NTN1 targeting in EC, not only through the induced cell death by the activation of its DR associated apoptosis, but also through the disruption of the EMT process that NTN1 normally elicits. Indeed, by preventing the binding of NTN1 with UNC5B, NP137 also leads to the inhibition of EMT progression, a positive NTN1/UNC5B associated signalling. Bulk and single cell RNA analysis of patient metastatic lesions and multiple cancer mouse model samples have enabled us to identify an alteration of the EMT profile of cancer cells in favour of an epithelialization of the tissue after NP137 treatment. These findings were deepened through *in vitro* studies analysing the functional aspects of EMT in cancer cell lines, such as cell migration and invasion, where a significant inhibition was observed thanks to NP137. With this work, we have not only put into light the promoting role of NTN1 for the progression of EMT in cancer cells, but also that of a humanized anti-NTN1 monoclonal antibody to counter this effect that is currently undergoing multiple phase II clinical trials including gynaecological indication in combo with chemotherapy and/or immunotherapy.

In this discussion, we will address into somewhat detail hypotheses and interrogations concerning the mechanistical aspects of the mode of action of NTN1 on EMT and will contextualize the therapeutic benefit NP137 shows for the management of cancer, EC in particular, but also potentially other diseases.

1. Targeting and monitoring patient response to NP137.

As mentioned in the introduction of the manuscript, patient staging and classification greatly influence the choice of treatment they receive and their response to the latter. The emergence of molecular classification through MMR deficiency, p53 and POLE mutation identification - amongst others – has allowed to better personalize treatment options and improve patient outcome. Although in our phase I study biological cohort patients are all considered as high-risk as their cancer had progressed to form metastases, knowledge of the molecular classification of their primary and secondary tumours and comparing this information to their response to treatment and the intensity of EMT variation observed after treatment may provide us with valuable information. From a preclinical standpoint, most experiments regarding human EC cell lines have been carried out on human Ishikawa cells that represent the most common type of EC: type I according to Bokhman and ultra-mutated EC according to the molecular classification as cells bear POLE, PTEN, P53 and PIK3R1 genetic alterations. Although NP137 effect on EMT features has also been observed on serous type II EC cell lines ARK1 and ARK2, providing encouraging indications of a generalized effect of NP137 on various types of EC, it doesn't provide sufficient proof to establish or not a link between EC classification and NP137 effect. Furthermore, the clinical outcome of patients from the phase I RH+ extension cohort as well as the ELISA experiments quantifying TFF3 in patient serum samples suggest that the NP137 mediated effect on patient response doesn't seem to be linked with hormone receptor expression as observed in the preliminary cohort. As the TCGA molecular characterization of EC tumours had admittedly been published in 2014 but not yet considered as a new classification method by the WHO nor FIGO for EC at the start of the NP137 phase I trial in 2016, such criteria were not systematically investigated in these patients. Additionally, the correlation of molecular classification with treatment response requires a great deal more samples, meaning a great deal more patients. With the trial having progressed to phase II in 2020, such information has since been added to patients' case report form (CRF) to deepen our understanding of the putative implication of molecular alterations on response to NP137 treatment. To conclude,

no matter how complex the classifications are, the only thing that matters as with most targeted therapies is the presence of NTN1 in the tumour, so it can respond to NP137 treatment.

Furthermore, in our efforts to identify a circulating biomarker for the monitoring of patient response to NP137 treatment, and as the circulating protein NTN1 is impossible to detect by ELISA or classical techniques in blood, probably related to its "sticky" laminin-like protein functions possibly trapping it in the ECM, we have managed to observe through TEM analysis NTN1 localization at the surface of pancreatic and lung cancer cell EVs isolated from conditioned media. However, not only do we now know that it is expressed at EV level, but we have managed to detect it by Mass Spectrometry *in vitro* by spiking of healthy blood samples with EVs isolated from a NTN1 expressing cell line. By which means NTN1 is attached to these membranes remains to be elucidated. Cryo-electron microscopy experiments locating NTN1 with gold-tagged NP137 has shown an agglomeration of golden beads away from vesicles derived from NTN1 EVs, suggesting that UNC5B may be involved as NP137 was designed to specifically inhibit the NTN1/UNC5B interaction. Due to a lack of material, we were not able to conduct such experiments on phase I EC patients' samples. However, the detection of NTN1 on the EVs is not technically something easy to do for a companion clinical test, so we will have to find other predictive biomarkers of NP137 response, and we hope that the clinical studies have started will allow us to find some.

2. NP137, an effective inhibitor of NTN1 mediated EMT, but through which processes?

Inhibition of EMT by NP137 has been observed in both EC and skin SCC, consolidating its relevance in an array of cancer indications at a preclinical level. We have been able to observe a blockade of cancer development by NP137 treatment *in vivo* due to a hindrance of pathogenic tissue evolution in the PTEN mutated mouse model, tumour growth in the SCC mouse model and the NUDE mice xenografting experiments and a diminished amount of metastasis formation by orthotopic intravenous injection of MECPK mouse endometrial cells. The blocking effect of NP137 on cancer development was also observed *in vitro* through a weakened ability of cancer cell to invade Matrigel coated porous membranes and to migrate to re-establish cell contacts after the development of an artificial wound in scratch assays. In addition, we have also observed a clear epithelialization of tumour phenotypes both at the transcript and protein levels through a multitude of techniques, whether it be bulk or scRNA sequencing, RTqPCR, 10x Visium analysis or IHC. One might next wonder which specific molecular interactions and signalling pathways lead to these observed effects. In other words, what are the intracellular effectors of NTN1/Unc5B?

My in vitro work using a human EC cell line has put into evidence the potential implication of the PI3K/AKT pathway due to an inhibition of AKT phosphorylation after NP137 treatment, and the impeded migration of cells with PI3K chemical inhibition that was not potentiated by NP137. However, these experiments required the induction of EMT *in vitro* using TGFβ and epidermal growth factor (EGF) *inter alia*. TGFβ and EGF are known to induce alternative intracellular pathways such as JAK/STAT and RAS/MAPK, both implicated in EMT. As a matter of fact, NTN1/UNC5B is known to regulate the MAPK signalling pathway in mouse embryonic stem cells [286]. Additional wound healing experiments carried out in the Ishikawa cell line showed an additive effect on inhibition of Ishikawa cell migration when treated with an inhibitor of the MAPK pathway in combination with NP137 as opposed to NP137 alone (not shown in this manuscript). These results suggest that in our *in vitro* model, the MAPK pathway is not implicated in the observed effect of NP137. However, many more pathways remain to be investigated to confidently postulate about the implication of PI3K/AKT in this NTN1 mediated effect on EMT, and these experiments

also need to be carried out in murine models and human samples, not only on immortalized *in vitro* cell lines. Furthermore, Prof. Blanpain's research team have pointed out the differential expression of gene signatures associated with hypoxia, angiogenesis as well as inflammation in their SCC mouse model when treated with NP137 (figure 3 from Lengrand et al.), our bioinformatic analyses on patient samples in scRNA sequencing or Spatial Visium allowed us to find the involvement of the same pathways in EC (data not published), given the role of NTN1 already described in these pathways, this is not surprising but should be explored in the future, as part of therapy. This further complexifies the issue, opening the door to a multitude of other possibly involved effectors.

3. Involvement of the tumour microenvironment.

It is without a doubt that the tumour microenvironment plays a great role in tumour development and cancer progression. In our case, the implication of NTN1 in macrophage driven inflammation, for example, is very well described in a plethora of diseases such as lung injury, inflammatory bowel disease, pancreatitis, atherosclerosis, etc. As presented in the published review displayed in this manuscript's introduction, NTN1 has been described as a bivalent protein regarding inflammatory processes and the recruitment of immune cells [287]. The impact of NTN1 and UNC5B, both expressed in leucocytes, on inflammation, has made them targets of interest for the treatment of inflammatory conditions such as arthritis [288]. Furthermore, current work conducted in the lab on CTLA-4 resistant breast cancer cells showed that combination of anti-CTLA-4 therapy with NP137 increased CD8+ T cell and a decreased immunosuppressive PMN-MDSC neutrophils infiltration of tumours, events supporting the observed tumour re-sensitisation to immunotherapy (Ducarouge et al., Cell Death and Differentiation, 2023, in press). This also emphasizes the potential of standard treatment combinations with NP137 for non-responding aggressive cancers. In this manuscript's presented work, NTN1 targeting in EC not only acted upon cell death and EMT cell phenotype and behaviour, but also upon the nature of the tumoural stroma by printing a new anti-tumour immune landscape, which I will now discuss.

a. Cancer associated fibroblasts.

Cancer associated fibroblasts (CAFs) are cells known to be implicated in the progression of cancer through the expression of soluble factors and functions like the remodelling of the matrix or immune crosstalk [289]. Furthermore, in our laboratory, Sung et al. published in 2019 data demonstrating the role of NTN1 expressing CAFs in the maintenance of cancer cell stemness through coculture experiments, and linked this effect to the expression of CAF secreted IL6 known to be involved in the promotion of a stem cell-like phenotype, and that NP137 treatment leads to the decrease of stemness of cancer cells [290]. NTN1's expression in CAF populations as it has been seen in the skin SCC model (extended data figure 3, Lengrand et al.) supports its function of pro-tumoural signalling described in the literature, and the decrease in CAF populations in the human biopsy samples and the reduced strength of interaction of CAFs with tumour cells after NP137 treatment corroborate with the previously published data. However, when comparing this data with the stromal modulations observed in the SCC mouse model after NP137 treatment, heterogeneities emerge. Indeed, Prof. Blanpain's team has observed quite the opposite in their SCC mouse model, with a relative increase in CAFs after NP137 treatment. It is important to note that both study models (human vs murine) and the nature of tumour (metastatic vs primary) are varying parameters in these experiments. Further investigations need to be carried out to determine whether this difference in CAF population after NP137 treatment is a matter of study model, of variation in CAF subpopulations, or of the primary or metastatic nature of tumours. Moreover, when analysing the

subpopulation of CAF in SSC model (extended data figure 4, Lengrand et al), subpopulation of CAFs (myCAF, iCAFs, …) react differently to NP137, indeed a subpopulation of myCAF seems to be reduced. A decrease in a subpopulation of iCAF has also been observed in the scRNA sequencing analysis in human C. The subpopulation of CAFs is really complicated to identify due to the marker used. More in-depth studies on CAF subpopulations will be interesting to carry out because CAFs are the cells that secrete a lot of cytokines that vary EMT. Additionally, when looking at the interaction between CAFs and other immune cells in patient biopsies, we observe an increase in the crosstalk between CAFs and T cells. Could it be possible that the increasing population of cytotoxic T cells impacts CAF population, leading to its decrease and inhibiting its pro-tumoural functions? That is another hypothesis that remains to be demonstrated.

b. The myeloid lineage: neutrophil and macrophage fate

The variation observed in the myeloid immune population of by RNA sequencing in the patient samples corroborate with the previously demonstrated impact of NTN1 in the chemotaxis of a variety of immune cells such as monocytes, macrophages, and neutrophils [291]. However, additional work conducted in the laboratory also put to light the inhibitory effect of NTN1 interference on the presence of PMN-MDSCs (tumour associated neutrophils) in EMT6 engrafted tumours, an immune checkpoint inhibitor resistant breast cancer cell line. PMN-MDSCs are immature myeloid-derived suppressor cells able to inhibit T cell function [292] and therefore drivers of tumour development and resistance to therapy. The increase in neutrophils observed in our patient samples after treatment does not support this data. One may hypothesize that the functions of tumour associated neutrophils may be dependent on the nature of the model studied, or that the observed effect is mirroring that of a single moment in time and that modulation of neutrophil recruitment may be time-dependent. Another more probable hypothesis is that again there are many subpopulations of neutrophils, and some are increased by NP137, and others decreased, like immunosuppressive PMN-MDSCs. Therefore, further investigations need to be carried out to truly comprehend the effect of NTN1 interference with the modulation of the tumour microenvironment's myeloid immune population. Neutrophil staining could be performed on the FFPE tumour blocks from NP137 treated patients, but again, we still need to determine which markers should be used to make these stainings.

Furthermore, these same biopsies have also demonstrated that NP137 treatment decreased the proportion of M2 macrophages in the tumoural stroma of patient biopsies. M2 macrophages are regarded as "friends" by cancer cells as they support angiogenesis and express immunosuppressive molecules, effectively carrying out an anti-inflammatory function and promoting cancer progression [293]. Previous studies have demonstrated NTN1's ability to maintain macrophage accumulation in adipose tissue [294], however, the protein's capacity to modulate macrophage polarization per se is still unclear. Very recently, Fang and colleagues have pointed out the implication of UNC5B in the maturation of monocytes into macrophages by the binding of FLRT2 to its extracellular domain [295], demonstrating that NTN1's receptor can act upon immune cell fate. Whether NTN1 can itself induce such associated signalling through UNC5B to guide macrophage polarization towards a M2 phenotype remains to be investigated.

c. A closer look at lymphoid cells

When looking at the lymphoid compartment of immune cell, our work has shown that NTN1 blockade leads to an increase of cytotoxic CD8+ T lymphocytes (also observed in the PTENf/f

mouse model) and Natural Killer (NK) cells, as well as antigen presenting cells (APC). This data is replicated in SCC by Prof. Cedric Blanpain's team as they also observe an increase in T cells in the SCC mouse model, although the different subpopulations variations are not described in detail. As the presence of NTN1 dependence receptors has been observed at the surface of CD4+ T cells [296], one might wonder whether the blockade of its signalling by NP137 treatment leads to the induction of apoptosis in this population. Such speculations need to be further investigated. Furthermore, not only did the amount of CD8+ T cells increase, but so did their interactions with tumour cells. This might be explained to some extent by the coordinated increase in the efficiency of antigen presenting cells (APCs) as the interaction of tumour cells with monocytes before treatment weakens after treatment in favour of that with dendritic cells, but once again, further experiments are required to fully comprehend the molecular mechanisms implicated in such phenomena.

4. What's next for NP137?

One of the main challenges conventional cancer therapies like chemotherapy and radiotherapy face today is that of EMT-associated resistance. We have shown that NP137 is able to block the progression of EMT, effectively pushing cells to a more epithelial profile and making them more sensitive to chemotherapy treatment, as shown in both the induced PTEN mutated and SSC mouse models. One might now wonder about the potential of NTN1 targeting to sensitize chemo- and immune therapy resistant cancers in patients. As nicely summarized by the expert opinion Angela Green in the clinical briefing part and the summary "The unmet medical need" associated with the two articles in the Nature journal (put below), NP137 offers a possible means to overcome resistance to current chemotherapy and the safety and efficacy of the anti-netrin 1 antibody as therapy should be evaluated in further preclinical and clinical experiments, alone and in combination with other therapies. In this sense, a phase II clinical trial for NP137 subbed "GYNET" is underway, testing the efficiency of NP137 in combination with standard chemotherapy (Carboplatin + Paclitaxel) and an immunotherapy (anti-PD-L1) in endometrial and cervical cancer patients. Additionally, another phase Ib/II clinical trial called "IMMUNONET" opened to inclusions since late 2022, investigates the potential of NP137 in combination with anti-PD-1 or anti-PD-L1 in advanced or metastatic solid tumours displaying various sensitivity to immunotherapy.

Two additional phase Ib trials were initiated in 2023 to investigate the added benefit of NP137 treatment in both pancreatic adenocarcinoma and hepatocellular carcinoma in combination with their respective standard therapy options that are respectively mFOLFIRINOX and Atezolizumab with Bevacizumab, their first results being eagerly awaited as the first patients have been enrolled. Finally, two other indications are soon planned to test NP137, a phase Ib monocentric study on AML in combination with Vidaza and Venetoclax and another phase Ib on sarcomas. All these clinical results associated with ancillary studies should shed light on the efficacy of inhibiting netrin-1 in the cancer pathologies.

Finally, preclinical trials on indications other than cancer where netrin-1 is involved are also underway. Indeed, since netrin-1 is involved in many pathological processes, NP137, which does not show any toxic profile, could be useful, we hope, in many fields in the future.

Blockade of netrin-1 is a promising strategy against endometrial cancer

The protein netrin-1 is involved in embryonic development and is upregulated in various cancers, including endometrial cancer. In mouse models and a first-in-human trial, blocking netrin-1 with a humanized monoclonal antibody, NP137, prevents a cellular change called the epithelial–mesenchymal transition and inhibits tumour growth.

This is a summary of:
Cassier, P. A. *et al.* Netrin-1 blockade inhibits tumour growth and EMT features in endometrial cancer. *Nature* https://doi.org/10.1038/s41586-023-06367-z (2023).

Cite this as:
Nature https://doi.org/10.1038/d41586-023-02181-9 (2023).

At a glance

Study design: phase I trial of NP137, an antibody that blocks netrin-1.

Population: fourteen people with advanced endometrial cancer.

End points: preliminary safety and efficacy, pharmacokinetics and pharmacodynamics.

Analysis: NP137 was safe; preliminary signs of antitumour activity in nine individuals.

Conclusion: netrin-1 blockade as an antitumour strategy warrants further investigation.

The unmet medical need

Endometrial cancer, which affects the lining of the uterus, is the sixth most common cancer in women globally[1]. More than 417,000 new cases were reported worldwide in 2020 (ref. 1). Over the past three decades, the incidence of endometrial cancer and the number of deaths related to the disease have increased – especially in western countries, reflecting rising rates of obesity and ageing populations. The treatment for early-stage endometrial cancer is usually hysterectomy, and can also include radiotherapy and chemotherapy. People with advanced disease are treated with the chemotherapies carboplatin and paclitaxel, and the median progression-free survival for those receiving this combination is 8.7 months. Adding the immunotherapies pembrolizumab[2] or dostarlimab[3] to carboplatin–paclitaxel can significantly prolong survival. However, there are few other effective options if these first-line therapies fail.

Netrin-1 is a glycoprotein, produced mainly during embryonic development, that has key roles in neuronal navigation, blood-vessel formation and cell survival[4]. It is also expressed in some cancers, and protects cancer cells from death. We wanted to understand the role of netrin-1 in endometrial cancer.

The study and its findings

We found that netrin-1 was expressed at high levels in endometrial tumour samples from humans and mice. In a genetically engineered mouse model of endometrial cancer, blocking the interaction between netrin-1 and its receptor on cancer cells triggered the death of these cells and inhibited the epithelial–mesenchymal transition (EMT), a process in which cells lose their epithelial characteristics and acquire mesenchymal features. Blocking netrin-1 also inhibited the EMT in a mouse model of skin cancer[5]. In tumours, the EMT is associated with resistance to chemotherapy and immunotherapy. On the basis of these results, we developed NP137, an anti-netrin-1 antibody.

We conducted a first-in-human phase I clinical trial to investigate the safety and efficacy of NP137. Fourteen individuals with advanced endometrial cancer received NP137 intravenously once every 2 weeks for as long as the therapy controlled the disease and was tolerable (12 weeks, on average). NP137 was well tolerated overall; the main adverse event, in seven people, was reactions related to infusion of the therapy. After at least six weeks of treatment, the disease had stabilized in eight people, and one person's liver metastases had shrunk by more than 50% (Fig. 1a). We analysed gene expression in endometrial tumour biopsies from 12 individuals, and found that NP137 inhibited the EMT (Fig. 1b). Further studies in mice showed that combining NP137 with carboplatin–paclitaxel produced a stronger response than did the standard chemotherapy alone. These observations are supported by those made in the skin-cancer model, in which NP137 sensitized cancer cells to chemotherapy[5].

This work is one of the first to test netrin-1 blockade in humans, and provides preliminary evidence that NP137 is safe and has clinical activity. Further development and testing of this antibody is warranted.

Outlook for the future

- The safety and efficacy of NP137 as a therapy for endometrial cancer should be evaluated in further preclinical and clinical experiments, alone and in combination with other therapies.
- A randomized phase II study investigating NP137 together with carboplatin, paclitaxel and pembrolizumab for endometrial and cervical cancer is currently recruiting (clinical trial ID: NCT04652076).
- Inhibition of netrin-1 could be used as an approach to treat other cancers. Studies are being planned or already under way.

Philippe A. Cassier is at the Léon Bérard Centre, Lyon, France, and **Patrick Mehlen** is at the Cancer Research Center of Lyon, Lyon, France.

EXPERT OPINION

"In their summary of the preclinical and early clinical experience with netrin-1 blockade for the treatment of endometrial cancers, the authors describe compelling results, including the upregulation of netrin-1 in endometrial cancer, its efficacy in mouse models and an experience with an exceptional responder. Interestingly, netrin-1 blockade also leads to reversion of the EMT and is a possible means to overcome resistance to current chemotherapy."

Angela Green is at the Memorial Sloan Kettering Cancer Center, New York City, New York, USA.

FIGURE

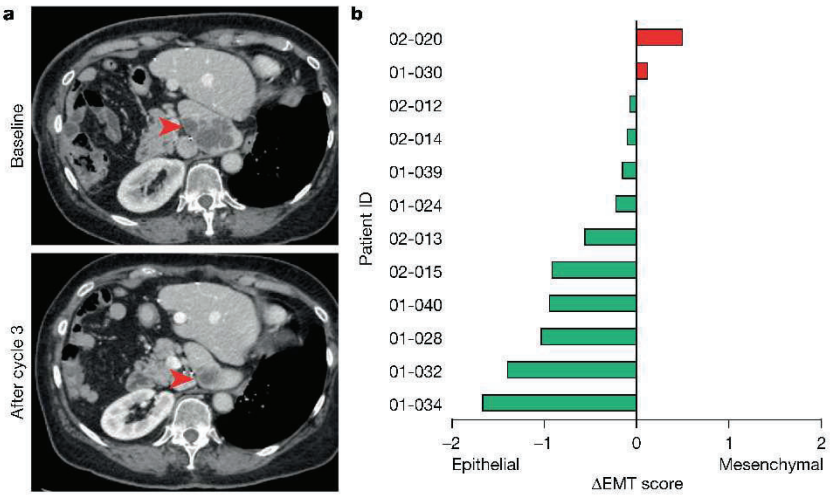

Figure 1 | An antibody that blocks netrin-1 could be used as a therapy for endometrial cancer. **a**, NP137, an anti-netrin-1 antibody, was administered to an individual who had endometrial cancer that had metastasized to the liver. Axial images of computed tomography scans show a liver metastasis at baseline (top) and at six weeks, after three infusions of the antibody (bottom). The red arrowheads indicate cancer lesions. **b**, Genetic analyses of biopsies from 12 people with endometrial cancer were used to produce an epithelial–mesenchymal transition (EMT) score that indicates how 'mesenchymal' the tumour is. ΔEMT score represents the change in the EMT score between the start of treatment and after three cycles of NP137. Most of the biopsies show a reduction in the EMT score, indicating an inhibition of cell transition. Red, tumours that become more mesenchymal after NP137 treatment (as indicated by the positive change in the EMT score); green, tumours that become more epithelial. Cassier, P. A. *et al./Nature* (CC BY 4.0).

REFERENCES

1. Crosbie, E. J. *et al. Lancet* **399**, 1412–1428 (2022).
2. Eskander, R. N. *et al. N. Engl. J. Med.* **388**, 2159–2170 (2023).
3. Mirza, M. R. *et al. N. Engl. J. Med.* **388**, 2145–2158 (2023).
4. Mehlen, P., Delloye-Bourgeois, C. & Chédotal, A. *Nature Rev. Cancer* **1**, 188–197 (2011).
5. Lengrand, J. *et al. Nature* https://doi.org/10.1038/s41586-023-06372-2 (2023).

FROM THE EDITOR

The EMT is seen as a key step in the progression of cancers to metastasis. Although the EMT has been well characterized at the biological level, developing therapies that specifically target the process has been difficult. It was therefore exciting to receive this paper reporting results from a phase I trial, and an accompanying preclinical paper by Lengrand *et al.*[5]. The hope is that NP137 will find its way into clinical care.

Barbara Marte, Senior Editor, *Nature*

General conclusion

To conclude, this work provides the first evidence that NTN1, an axon guidance molecule normally only expressed during embryonic development, is re-expressed in cancer and implicated in the EMT process of cancer cells. However, the molecular mechanisms underlying this induction of EMT by NTN1 remain to be elucidated. Many pathways seem to be implicated in the complex change of tumour heterogeneity and its microenvironment, and it will require further exploration to elucidate all the mechanisms implicated in these important changes in tumour plasticity. EV based experiments have enabled us to observe the localization of NTN1 at the surface of EVs utilized by cancer cells to prep the metastatic niche and observe the inhibitory potential of NTN1 blockade to inhibit the progression of EMT through mass spectrometric analysis of EV proteome which mimics that of cancer cells. We have also demonstrated that preventing the binding of NTN1 in cancer using a novel humanized monoclonal antibody epithelializes metastatic and primary tumours in both mouse and human models, allowing important and promising combination therapy perspectives. Furthermore, murine studies have shown the potential of such targeting on tumour sensitization to standard chemotherapy. In this sense, the NP137 antibody that has previously undergone safety and preliminary efficacy assessment studies is now evaluated in phase II clinical trials to demonstrate its efficacy in combination with chemotherapies and/or immunotherapies in the treatment of advanced / metastatic and difficult-to-treat cancers.

Annexes

Inclusion Criteria:

- Adult men and women ≥ 18 years at time of inform consent signature.
- For dose escalation cohorts, biological cohorts and extension parts: Histological confirmed locally advanced/metastatic solid tumours of any histological types.

For second expansion part only: patients with histologically confirmed locally advanced / metastatic endometrial carcinoma and who positively expressed Hormone Receptors (with a positivity threshold value ≥ 10%). Estrogene receptors (ER) and Progesterone Receptors (PR) expression rates must be assessed by immunohistochemistry and fully documented.

- Documented disease progression after at least one prior line of treatment in the metastatic/advanced setting.
- Patient must be, in the judgment of the investigator, an appropriate candidate for an experimental therapy i.e. with no available curative options.
- At least one measurable lesion as per RECIST 1.1.
- For Expansion part only: Availability of at least 2 pre-treatment scans prior to C1D1 including the screening scan (i.e. within 28 days before C1D1) and the most recent scan prior to screening to evaluate tumour growth kinetics.
- Mandatory for Biological collection cohorts and Expansion part #1 and #2 only (optional for dose escalation): Availability of a representative archival tumour specimen in formalin-fixed paraffin embedded (FFPE) block with an associated pathology report. Optional for Expansion part #2 only (RH+ endometrial carcinoma] Biopsable disease i.e. at least one lesion with a diameter ≥10 mm, visible by medical imaging and accessible to percutaneous sampling.
- Life expectancy ≥ 12 weeks.
- ECOG PS 0-1
- Adequate haematological function: Haemoglobin ≥ 9 g/dL, Absolute neutrophil count (ANC) ≥ 1.5 x 109/L, Platelet count ≥ 100 x 109/L (without transfusion within 21 days before C1D1).
- Adequate renal function: Calculated creatinine clearance by MDRD or CDK-EPI ≥50 mL/min/1.73m2 or serum creatinine ≤ 1.5 ULN
- Adequate liver function: AST and ALT ≤ 2.5 ULN (up to 5 ULN may be tolerated in case of liver metastases), Total serum bilirubin ≤ 1.5 x ULN (except for patients with Gilbert disease for whom a total serum bilirubin ≤3mg/dL is acceptable).
- Adequate coagulation function: INR≤ 1.5, aPTT≤ 1.5 ULN.
- Adequate cardiovascular function: QTc ≤470ms, Resting BP systolic <160mmHg and diastolic<100mmHg, LVEF ≥50% as determined by multiple-gated acquisition (MUGA) scan or transthoracic echocardiogram.
- Minimal wash-out period for prior treatment before C1D1: For chemotherapy, tyrosine kinase inhibitor > 2 weeks, Radiation therapy >4 weeks, For monoclonal antibodies >4 weeks, For immunosuppressive medication > 2 weeks, with the exceptions of intranasal and inhaled corticosteroids or systemic corticosteroids at doses which are not to exceed 10 mg/day of prednisone, or an equivalent corticosteroid, Major surgery >4 weeks, For hormonotherapy > 2 weeks with exception of GnRH analogues for prostate cancer patients who should continue on GnRH analogues throughout the study.
- Women of child-bearing potential must have a negative serum pregnancy test at screening (7 days before C1D1).
- Women of child-bearing potential must agree to remain abstinent or to use 2 effective forms of contraception from the time of the negative pregnancy test up to 3 months after the last dose of study drug. Effective forms of contraception are listed in Protocol.
- Men must agree to remain abstinent or to use an effective contraceptive method during the study and for up to 3 months after the last dose of study drug.

- Patient should understand, sign, and date the written voluntary informed consent form prior to any protocol-specific procedures.
- Patient should be able and willing to comply with study visits and procedures as per protocol.
- Patients must be covered by a medical insurance.

Exclusion Criteria:

- Persistence of CTCAE ≥ Grade 2 toxicity due to prior anti-cancer therapy (except alopecia (any grades), blood tests values according to inclusion criteria, Grade ≥3 peripheral neuropathy.
- History of severe allergic anaphylactic reactions to one of the components of the study drug or to humanized mAbs
- Any known neurodegenerative (Alzheimer's disease, Parkinson's disease and related disorders, amyotrophic lateral sclerosis, prion disease, motor neuron diseases, Huntington's disease, spinocerebellar ataxia, spinal muscular atrophy,) or neuroinflammatory disease (multiple sclerosis, …).
- Active or untreated CNS metastases. Patients with radiographically stable, asymptomatic previously irradiated lesions are eligible provided that patient is ≥ 4 weeks beyond completion of cranial irradiation and ≥ 3 weeks off of corticosteroid therapy are eligible.
- Any uncontrolled intercurrent illness that would limit compliance with protocol requirements including, but not limited to: Ongoing or active infection including acute or chronic hepatitis B, hepatitis C or human immunodeficiency virus (HIV), History of chronic liver disease or hepatic cirrhosis, Impaired cardiovascular function or clinically significant cardiovascular diseases including but not limited to symptomatic congestive heart failure, history of acute myocardial infection, acute coronary syndromes; history or current evidence of clinically significant cardiac arrhythmia and/or conduction abnormality within 6 months prior to C1D1, Psychiatric illness / specific social situations.
- Other invasive malignancy in the last 2 years except for those with a minimal risk of metastasis or death such as adequately managed in-situ carcinoma of the cervix, basal or squamous cell skin cancer, localized prostate cancer or ductal carcinoma in situ treated with curative intent.
- Needs to be treated with a forbidden concomitant/concurrent therapies/procedures including: Any investigational anticancer therapy other than the study drug, Any concurrent chemotherapy, radiotherapy (except palliative radiotherapy performed on non-target lesion and following sponsor's approval), immunotherapy, biologic or hormonal therapy* for cancer treatment. *: for prostate cancer patients, treatment with GnrH analogues is allowed, Immunosuppressive medications including methotrexate, azathioprine, and TNF-α blockers. Use of immunosuppressive medications including steroids for the management of AEs or in subjects with contrast allergies is acceptable, Major surgery, Any hematopoietic growth factor (during the DLT period)
- Female subjects who are pregnant or breast-feeding.

***Annex 1: Eligibility criteria of the phase I NP137 clinical trial** [297].*

TNM	FIGO[a]	Description
T1	I	Carcinoma confined to the uterus
T1a	IA	Carcinoma limited to endometrium
T1b	IB	Invasion less than or equal to half of the myometrium
T1c	IC	Invasion of more than half of the myometrium
T2	II	Invasion of cervix
T2a	IIA	Invasion of endocervical glands
T2b	IIB	Invasion of cervical stroma
T3 and/or N1	III	Local regional or local and regional spread
T3a	IIIA	Involvement of serosa, adnexa, or both serosa and adnexa with or without positive peritoneal cytology
T3b	IIIB	Vaginal involvement
T3c	IIIC	Metastatic to pelvic, paraaortic, or both pelvic and paraaortic nodes
T4	IV	Tumor extends outside pelvis or invades bladder or rectal mucosa
T4a	IVA	Invasion of bladder, bowel mucosa, or both
M1	IVB	Distant metastasis

[a]FIGO staging system is based on surgical and pathologic findings alone; imaging, although useful in preoperative assessment of tumor stage, is not recognized as a method for definitive staging.

***Annex 2: Classification of EC using TNM and FIGO staging systems** [298].*

Risk group	Tumour characteristics	Tumour characteristics with molecular classification
Low	• Stage IA EEC grade 1/2 without substantial LVSI	• Stage I-II **POLEmut** EC without residual disease • Stage IA **MMRd/NSMP** EEC grade 1/2 without substantial LVSI
Intermediate	• Stage IB EEC grade 1/2 without substantial LVSI • Stage IA EEC grade 3 without substantial LVSI • Stage IA NEEC without myometrial invasion	• Stage IB **MMRd/NSMP** EEC grade 1/2 without substantial LVSI • Stage IA **MMRd/NSMP** EEC grade 3 without substantial LVSI • Stage IA **p53abn** and/or NEEC without myometrial invasion
High-intermediate	• Stage I EEC with substantial LVSI regardless of grade and depth of invasion • Stage IB EEC grade 3 regardless of LVSI status • Stage II	• Stage I **MMRd/NSMP** EEC with substantial LVSI regardless of grade and depth of invasion • Stage IB **MMRd/NSMP** EEC grade 3 regardless of LVSI status • Stage II **MMRd/NSMP** EEC
High	• Stage III-IVA with no residual disease • Stage I-IVA NEEC with myometrial invasion, and with no redisual disease	• Stage III-IVA **MMRd/NSMP** EEC without residual disease • Stage I-IVA **p53abn** EC with myometrial invasion without residual disease • Stage I-IVA **NSMP/MMRd** NEEC without residual disease
Advanced metastatic	• Stage III-IVA with residual disease • Stage IVB	• Stage III-IVA with residual disease of any molecular subtypes • Stage IVB of any molecular subtype

Annex 3: Table of EC patients prognostic risk groups of according to the ESGO/ESTRO/ESP guidelines.

EEC: endometrioid EC, LVSI: lymph-vascular space invasion, NEEC: non-endometrioid EC [78,299,300].

Cancer	Cytokine	Mechanism of EMT
Endometrial	TGF-β	Epithelial downregulation: E-cadherin [65,96]. Mesenchymal upregulation: Vimentin [80,96] and N-cadherin [65,96,99]. EMT-TF activation/suppression: *TWIST* [96] and *SNAI2*/Slug [65,80,98]. Mesenchymal morphological changes: [65,96,97].
	IL-6	Epithelial downregulation: E-cadherin [65]. Mesenchymal upregulation: Vimentin and N-cadherin [65]. EMT-TF activation/suppression: *TWIST* [65] and *SNAI1* [65]. Mesenchymal morphological changes: [65].
	AMF	Epithelial downregulation: E-cadherin [103]. Mesenchymal upregulation: Vimentin [103]. Mesenchymal morphological changes: [103].
	RANK/RANKL/CCL20	Epithelial downregulation: E-cadherin [102]. Mesenchymal upregulation: Vimentin [102] and N-cadherin [102]. EMT-TF activation/suppression: *SNAI1*/2 and *TWIST* [102]. Mesenchymal morphological changes: [102].
	CCL18	Epithelial downregulation: E-cadherin [100]. Mesenchymal upregulation: Vimentin [100] and N-cadherin [100]. EMT-TF activation/suppression: *TWIST* [100]. Mesenchymal morphological changes: [100].
	CXCR4/CXCL12	Mesenchymal upregulation: N-cadherin [101] and α-SMA [101].

Annex 4: EMT changed associated with cytokines / chemokines in endometrial cancer.

Markers of EMT

Acquired markers		Attenuated markers	
Name	**EMT type**	**Name**	**EMT type**
Cell-surface proteins			
N-cadherin	1, 2	E-cadherin	1, 2, 3
OB-cadherin	3	ZO-1	1, 2, 3
α5β1 integrin	1, 3		
αVβ6 integrin	1, 3		
Syndecan-1	1, 3		
Cytoskeletal markers			
FSP1	1, 2, 3	Cytokeratin	1, 2, 3
α-SMA	2, 3		
Vimentin	1, 2		
β-Catenin	1, 2, 3		
ECM proteins			
α1(I) collagen	1, 3	α1(IV) collagen	1, 2, 3
α1(III) collagen	1, 3	Laminin 1	1, 2, 3
Fibronectin	1, 2		
Laminin 5	1, 2		
Transcription factors			
Snail1 (Snail)	1, 2, 3		
Snail2 (Slug)	1, 2, 3		
ZEB1	1, 2, 3		
CBF-A/KAP-1 complex	2, 3		
Twist	1, 2, 3		
LEF-1	1, 2, 3		
Ets-1	1, 2, 3		
FOXC2	1, 2		
Goosecoid	1, 2		
MicroRNAs			
miR10b	2	Mir-200 family	2
miR-21	2, 3		

ZEB1, zinc finger E-box binding homeobox 1.

Annex 5: Markers of EMT *[301]*

	E vs M	Basal	BLCA	BRCA	COAD	HNSC	KIRC	LUAD	LUSC	OVCA	READ	UCEC
ADAM12	M	0.812	0.816	0.814	0.858	0.821	0.779	0.778	0.659	0.842	0.824	0.581
ADAMTS12	**M**	**0.686**	**0.758**	**0.607**	**0.806**	**0.776**	**0.626**	**0.629**	**0.761**	**0.838**	**0.875**	**0.380**
ADAMTS2	M	0.758	0.784	0.773	0.827	0.834	0.634	0.615	0.810	0.817	0.872	0.625
AEBP1	**M**	**0.817**	**0.822**	**0.822**	**0.820**	**0.845**	**0.640**	**0.636**	**0.858**	**0.844**	**0.910**	**0.831**
ANGPTL2	M	0.761	0.784	0.848	0.884	0.754	0.393	0.769	0.847	0.787	0.932	0.633
ANTXR1	**M**	**0.702**	**0.816**	**0.785**	**0.782**	**0.710**	**0.621**	**0.639**	**0.771**	**0.733**	**0.879**	**0.595**
AP1G1	E	-0.056	-0.330	-0.343	-0.002	-0.179	-0.523	-0.394	-0.135	-0.181	-0.625	-0.525
ATP8B1	**E**	**-0.055**	**-0.547**	**-0.351**	**-0.136**	**-0.363**	**0.466**	**-0.409**	**-0.469**	**-0.090**	**-0.397**	**-0.490**
AXL	M	0.698	0.782	0.813	0.835	0.674	0.528	0.624	0.656	0.542	0.954	0.604
BNC2	**M**	**0.805**	**0.798**	**0.813**	**0.709**	**0.813**	**0.202**	**0.756**	**0.831**	**0.249**	**0.799**	**0.519**
CALD1	M	0.536	0.799	0.780	0.663	0.813	0.499	0.748	0.826	0.625	0.779	0.597
CDH1	**E**	**-0.196**	**-0.440**	**-0.407**	**-0.379**	**-0.462**	**-0.518**	**-0.367**	**-0.317**	**-0.317**	**-0.405**	**-0.539**
CDH2	M	0.507	0.685	0.490	0.734	0.705	-0.224	0.560	0.492	0.030	0.793	0.501
CDS1	**E**	**-0.151**	**-0.360**	**-0.422**	**-0.384**	**-0.413**	**-0.801**	**-0.443**	**-0.354**	**-0.268**	**-0.536**	**-0.383**
CGN	E	-0.105	-0.417	-0.304	-0.099	-0.427	-0.563	-0.416	-0.228	-0.179	-0.235	-0.592
CLDN4	**E**	**-0.061**	**-0.444**	**-0.187**	**-0.150**	**-0.524**	**-0.471**	**-0.246**	**-0.294**	**-0.174**	**0.249**	**-0.258**
CMTM3	M	0.624	0.548	0.828	0.728	0.807	0.599	0.605	0.621	0.584	0.881	0.488
CNOT1	**E**	**-0.033**	**-0.104**	**-0.231**	**-0.429**	**-0.262**	**-0.275**	**-0.226**	**-0.159**	**-0.215**	**-0.574**	**-0.307**
CNRIP1	M	0.785	0.772	0.809	0.701	0.823	0.520	0.726	0.733	0.810	0.869	0.658
COL10A1	**M**	**0.728**	**0.660**	**0.724**	**0.793**	**0.758**	**0.660**	**0.549**	**0.836**	**0.770**	**0.819**	**0.469**
COL1A1	M	0.855	0.779	0.861	0.834	0.878	0.855	0.666	0.803	0.856	0.888	0.782
COL1A2	**M**	**0.843**	**0.812**	**0.866**	**0.916**	**0.880**	**0.837**	**0.724**	**0.844**	**0.780**	**0.913**	**0.657**
COL3A1	M	0.832	0.803	0.851	0.814	0.881	0.825	0.756	0.831	0.872	0.920	0.668
COL5A1	**M**	**0.817**	**0.777**	**0.846**	**0.837**	**0.859**	**0.876**	**0.678**	**0.825**	**0.875**	**0.866**	**0.819**
COL5A2	M	0.814	0.836	0.849	0.800	0.859	0.798	0.748	0.856	0.875	0.863	0.739
COL6A1	**M**	**0.697**	**0.769**	**0.820**	**0.828**	**0.874**	**0.790**	**0.710**	**0.752**	**0.730**	**0.910**	**0.564**
COL6A2	M	0.669	0.784	0.840	0.802	0.884	0.807	0.730	0.819	0.847	0.914	0.709
COL6A3	**M**	**0.833**	**0.815**	**0.822**	**0.888**	**0.856**	**0.830**	**0.652**	**0.793**	**0.844**	**0.863**	**0.770**
COL8A1	M	0.465	0.737	0.730	0.825	0.773	0.409	0.387	0.755	0.753	0.929	0.574
CTNND1	**E**	**-0.035**	**-0.370**	**-0.146**	**-0.229**	**-0.519**	**-0.306**	**-0.346**	**-0.192**	**-0.129**	**-0.296**	**-0.349**
DACT1	M	0.818	0.753	0.850	0.564	0.839	0.595	0.760	0.863	0.686	0.341	0.671
DYNC1LI2	**E**	**0.030**	**-0.194**	**-0.078**	**-0.098**	**0.095**	**-0.005**	**-0.296**	**0.004**	**-0.163**	**-0.450**	**-0.088**
EMP3	M	0.515	0.786	0.760	0.839	0.587	0.422	0.625	0.717	0.585	0.939	0.647
ERBB3	**E**	**-0.379**	**-0.600**	**-0.289**	**-0.294**	**-0.612**	**-0.536**	**-0.602**	**-0.391**	**-0.348**	**-0.167**	**-0.452**
ESRP1	E	-0.293	-0.503	-0.324	-0.356	-0.429	0.071	-0.421	-0.477	-0.016	-0.287	-0.307
ESRP2	**E**	**-0.288**	**-0.599**	**-0.382**	**-0.334**	**-0.567**	**-0.304**	**-0.639**	**-0.444**	**-0.324**	**-0.272**	**-0.279**
F11R	E	-0.252	-0.334	-0.166	-0.338	-0.459	-0.357	-0.481	-0.382	-0.212	-0.550	-0.299
FAP	**M**	**0.839**	**0.798**	**0.830**	**0.825**	**0.843**	**0.847**	**0.731**	**0.847**	**0.855**	**0.777**	**0.618**
FBN1	M	0.793	0.862	0.827	0.886	0.820	0.687	0.704	0.846	0.864	0.936	0.736

	E vs M	Basal	BLCA	BRCA	COAD	HNSC	KIRC	LUAD	LUSC	OVCA	READ	UCEC
FN1	**M**	**0.664**	**0.820**	**0.728**	**0.691**	**0.837**	**0.691**	**0.659**	**0.805**	**0.830**	**0.742**	**0.581**
FSTL1	**M**	**0.758**	**0.815**	**0.876**	**0.677**	**0.846**	**0.451**	**0.759**	**0.618**	**0.683**	**0.876**	**0.444**
GALNT3	**E**	**-0.017**	**-0.173**	**-0.088**	**-0.191**	**-0.274**	**-0.083**	**-0.081**	**-0.362**	**-0.225**	**-0.290**	**-0.536**
GPC6	M	0.564	0.797	0.652	0.715	0.781	0.084	0.720	0.804	0.501	0.816	0.394
GPR56	**E**	**-0.163**	**-0.325**	**-0.237**	**-0.145**	**-0.012**	**-0.107**	**-0.255**	**-0.252**	**-0.081**	**0.029**	**0.015**
GRHL2	E	-0.082	-0.494	-0.379	-0.275	-0.381	0.093	-0.527	-0.470	-0.142	-0.222	-0.314
GYPC	**M**	**0.407**	**0.785**	**0.663**	**0.724**	**0.668**	**0.220**	**0.625**	**0.585**	**0.514**	**0.914**	**0.629**
HOOK1	E	-0.365	-0.253	-0.378	-0.205	-0.441	-0.570	-0.354	-0.245	-0.402	-0.475	-0.373
HTRA1	**M**	**0.782**	**0.697**	**0.853**	**0.805**	**0.587**	**0.697**	**0.702**	**0.710**	**0.604**	**0.773**	**0.642**
INHBA	M	0.572	0.589	0.657	0.815	0.476	0.683	0.683	0.798	0.817	0.820	0.686
IRF6	**E**	**-0.194**	**-0.218**	**-0.126**	**-0.264**	**-0.345**	**-0.542**	**-0.298**	**0.027**	**-0.362**	**-0.303**	**-0.295**
ITGA11	M	0.759	0.648	0.717	0.733	0.781	0.694	0.629	0.794	0.842	0.905	0.778
LOXL2	**M**	**0.543**	**0.754**	**0.767**	**0.822**	**0.731**	**0.710**	**0.652**	**0.787**	**0.756**	**0.872**	**0.629**
LRRC15	M	0.720	0.719	0.774	0.688	0.768	0.599	0.690	0.802	0.781	0.865	0.509
MAP7	**E**	**-0.112**	**-0.601**	**-0.398**	**-0.246**	**-0.454**	**-0.613**	**-0.445**	**-0.407**	**-0.254**	**-0.436**	**-0.488**
MARVELD2	E	-0.228	-0.476	-0.397	-0.297	-0.490	-0.524	-0.554	-0.186	-0.374	-0.480	-0.429
MARVELD3	**E**	**-0.093**	**-0.425**	**-0.352**	**-0.184**	**-0.256**	**-0.594**	**-0.501**	**-0.305**	**-0.276**	**-0.471**	**-0.292**
MMP2	M	0.820	0.687	0.876	0.867	0.812	0.700	0.688	0.853	0.868	0.945	0.694
MSRB3	**M**	**0.642**	**0.807**	**0.772**	**0.743**	**0.822**	**0.602**	**0.681**	**0.713**	**0.759**	**0.841**	**0.696**
MYO5B	E	-0.206	-0.405	-0.207	-0.098	-0.481	-0.615	-0.273	-0.259	-0.082	-0.284	-0.232
NAP1L3	**M**	**0.661**	**0.623**	**0.756**	**0.626**	**0.734**	**0.358**	**0.580**	**0.623**	**0.339**	**0.863**	**0.445**
NID2	M	0.814	0.768	0.795	0.702	0.865	0.532	0.741	0.844	0.693	0.719	0.652
OCLN	**E**	**-0.089**	**-0.442**	**-0.270**	**-0.075**	**-0.429**	**-0.537**	**-0.448**	**-0.179**	**-0.206**	**-0.279**	**-0.548**
OLFML2B	M	0.772	0.802	0.843	0.869	0.886	0.844	0.829	0.811	0.818	0.915	0.677
PCOLCE	**M**	**0.817**	**0.793**	**0.865**	**0.824**	**0.891**	**0.820**	**0.738**	**0.840**	**0.829**	**0.956**	**0.630**
PDGFRB	M	0.818	0.807	0.789	0.848	0.857	0.607	0.594	0.834	0.796	0.918	0.769
PMP22	**M**	**0.543**	**0.594**	**0.519**	**0.812**	**0.843**	**0.450**	**0.705**	**0.816**	**0.805**	**0.847**	**0.676**
POSTN	M	0.734	0.750	0.741	0.647	0.865	0.727	0.778	0.843	0.812	0.806	0.407
PRSS8	**E**	**-0.255**	**-0.188**	**-0.194**	**-0.305**	**-0.464**	**-0.488**	**-0.455**	**-0.144**	**-0.071**	**-0.023**	**-0.177**
SPARC	M	0.811	0.807	0.876	0.880	0.871	0.622	0.816	0.878	0.876	0.959	0.733
SPINT1	**E**	**-0.299**	**-0.420**	**-0.273**	**-0.099**	**-0.488**	**-0.472**	**-0.360**	**-0.329**	**-0.011**	**-0.157**	**-0.189**
SPOCK1	M	0.604	0.477	0.696	0.864	0.627	0.355	0.635	0.320	0.551	0.841	0.624
SULF1	**M**	**0.740**	**0.748**	**0.596**	**0.807**	**0.784**	**0.701**	**0.719**	**0.781**	**0.598**	**0.869**	**0.633**
SYT11	M	0.508	0.720	0.658	0.778	0.713	0.293	0.630	0.461	0.130	0.869	0.326
THBS2	**M**	**0.748**	**0.600**	**0.836**	**0.902**	**0.703**	**0.702**	**0.756**	**0.857**	**0.869**	**0.930**	**0.737**
VCAN	M	0.696	0.688	0.809	0.810	0.848	0.414	0.715	0.798	0.887	0.891	0.476
VIM	**M**	**0.426**	**0.836**	**0.857**	**0.909**	**0.834**	**0.503**	**0.645**	**0.802**	**0.557**	**0.947**	**0.310**
ZEB2	M	0.619	0.866	0.664	0.705	0.786	0.481	0.553	0.704	0.670	0.752	0.514

Annex 6: Correlation of Pan-Cancer signature genes by tumour type. (Mak et al. 2016)

Tumor	Abbreviation	Sample size
Basal-like breast cancer	Basal	103
Bladder urothelial carcinoma	BLCA	88
Breast invasive carcinoma	BRCA	503
Colon adenocarcinoma	COAD	89
Head and neck squamous cell carcinoma	HNSC	203
Kidney renal clear cell carcinoma	KIRC	354
Lung adenocarcinoma	LUAD	131
Lung squamous cell carcinoma	LUSC	104
Ovarian carcinoma	OVCA	123
Rectum adenocarcinoma	READ	47
Uterine corpus endometrial carcinoma	UCEC	189

Annex 7: Summary of TCGA analysis for the Pan-Cancer EMT signature. (Mak et al. 2016)

References

[1] Grandin M, Meier M, Delcros JG, *et al.* Structural Decoding of the Netrin-1/UNC5 Interaction and its Therapeutical Implications in Cancers. *Cancer Cell* 2016 ; 29 : 173–185.
[2] Mhawech-Fauceglia P, Wang D, Samrao D, *et al.* Trefoil factor family 3 (TFF3) expression and its interaction with estrogen receptor (ER) in endometrial adenocarcinoma. *Gynecol Oncol* 2013 ; 130 : 174–180.
[3] Ameer MA, Fagan SE, Sosa-Stanley JN, *et al.* Anatomy, Abdomen and Pelvis, Uterus. *StatPearls*. Treasure Island (FL) : StatPearls Publishing, 2022 :
[4] Casarini L, Simoni M. Recent advances in understanding gonadotropin signaling. *Fac Rev* 2021 ; 10 : 41.
[5] Survival Rates for Endometrial Cancer n.d. ;.
[6] Endometrial Cancer 2021 ;.
[7] Koskas M, Amant F, Mirza MR, *et al.* Cancer of the corpus uteri: 2021 update. *Int J Gynaecol Obstet* 2021 ; 155 Suppl 1 : 45–60.
[8] Bakkum-Gamez JN, Wentzensen N, Maurer MJ, *et al.* Detection of endometrial cancer via molecular analysis of DNA collected with vaginal tampons. *Gynecologic Oncology* 2015 ; 137 : 14–22.
[9] Fiegl H, Gattringer C, Widschwendter A, *et al.* Methylated DNA Collected by Tampons—A New Tool to Detect Endometrial Cancer. *Cancer Epidemiology, Biomarkers & Prevention* 2004 ; 13 : 882–888.
[10] Shen Y, Yang W, Liu J, *et al.* Minimally invasive approaches for the early detection of endometrial cancer. *Molecular Cancer* 2023 ; 22 : 53.
[11] Vizza E, Corrado G, De Angeli M, *et al.* Serum DNA integrity index as a potential molecular biomarker in endometrial cancer. *J Exp Clin Cancer Res* 2018 ; 37 : 16.
[12] Tanaka H, Tsuda H, Nishimura S, *et al.* Role of circulating free alu DNA in endometrial cancer. *Int J Gynecol Cancer* 2012 ; 22 : 82–86.
[13] Beinse G, Borghese B, Métairie M, *et al.* Highly Specific Droplet-Digital PCR Detection of Universally Methylated Circulating Tumor DNA in Endometrial Carcinoma. *Clin Chem* 2022 ; 68 : 782–793.
[14] Maritschnegg E, Wang Y, Pecha N, *et al.* Lavage of the Uterine Cavity for Molecular Detection of Müllerian Duct Carcinomas: A Proof-of-Concept Study. *Journal of clinical oncology : official journal of the American Society of Clinical Oncology* 2015 ; 33 .
[15] Du J, Li Y, Lv S, *et al.* Endometrial sampling devices for early diagnosis of endometrial lesions. *J Cancer Res Clin Oncol* 2016 ; 142 : 2515–2522.
[16] Wang Y, Li L, Douville C, *et al.* Evaluation of liquid from the Papanicolaou test and other liquid biopsies for the detection of endometrial and ovarian cancers. *Sci Transl Med* 2018 ; 10 : eaap8793.
[17] Raffone A, Raimondo D, Raspollini A, *et al.* Accuracy of cytological examination of Tao Brush endometrial sampling in diagnosing endometrial premalignancy and malignancy. *International Journal of Gynecology & Obstetrics* 2022 ; 159 .
[18] Bolivar AM, Luthra R, Mehrotra M, *et al.* Targeted Next-Generation Sequencing of Endometrial Cancer and Matched Circulating Tumor DNA: Identification of Plasma-Based, Tumor-Associated Mutations in Early Stage Patients. *Mod Pathol* 2019 ; 32 : 405–414.
[19] Arnold M, Pandeya N, Byrnes G, *et al.* Global burden of cancer attributable to high body-mass index in 2012: a population-based study. *Lancet Oncol* 2015 ; 16 : 36–46.
[20] Beavis AL, Smith AJB, Fader AN. Lifestyle changes and the risk of developing endometrial and ovarian cancers: opportunities for prevention and management. *Int J Womens Health* 2016 ; 8 : 151–167.
[21] Pérez-Martín AR, Castro-Eguiluz D, Cetina-Pérez L, *et al.* Impact of metabolic syndrome on the risk of endometrial cancer and the role of lifestyle in prevention. *Bosn J Basic Med Sci* 2022 ; 22 : 499–510.
[22] Byrne FL, Martin AR, Kosasih M, *et al.* The Role of Hyperglycemia in Endometrial Cancer Pathogenesis. *Cancers (Basel)* 2020 ; 12 : 1191.
[23] Saed L, Varse F, Baradaran HR, *et al.* The effect of diabetes on the risk of endometrial Cancer: an updated a systematic review and meta-analysis. *BMC Cancer* 2019 ; 19 : 527.

[24] Wu Q-J, Li Y-Y, Tu C, *et al.* Parity and endometrial cancer risk: a meta-analysis of epidemiological studies. *Sci Rep* 2015 ; 5 : 14243.
[25] Yang HP, Cook LS, Weiderpass E, *et al.* Infertility and incident endometrial cancer risk: a pooled analysis from the epidemiology of endometrial cancer consortium (E2C2). *Br J Cancer* 2015 ; 112 : 925–933.
[26] Brinton LA, Westhoff CL, Scoccia B, *et al.* Fertility drugs and endometrial cancer risk: results from an extended follow-up of a large infertility cohort. *Hum Reprod* 2013 ; 28 : 2813–2821.
[27] Hall JE. Endocrinology of the Menopause. *Endocrinol Metab Clin North Am* 2015 ; 44 : 485–496.
[28] Sun X, Zhang Y, Shen F, *et al.* The histological type of endometrial cancer is not associated with menopause status at diagnosis. *Biosci Rep* 2022 ; 42 : BSR20212192.
[29] Wu Y, Sun W, Liu H, *et al.* Age at Menopause and Risk of Developing Endometrial Cancer: A Meta-Analysis. *Biomed Res Int* 2019 ; 2019 : 8584130.
[30] Gambacciani M, Levancini M. Hormone replacement therapy and the prevention of postmenopausal osteoporosis. *Prz Menopauzalny* 2014 ; 13 : 213–220.
[31] Gambrell RD. The menopause: benefits and risks of estrogen-progestogen replacement therapy. *Fertil Steril* 1982 ; 37 : 457–474.
[32] Jordan VC. The 38th David A. Karnofsky Lecture: The Paradoxical Actions of Estrogen in Breast Cancer—Survival or Death? *JCO* 2008 ; 26 : 3073–3082.
[33] Emons G, Mustea A, Tempfer C. Tamoxifen and Endometrial Cancer: A Janus-Headed Drug. *Cancers (Basel)* 2020 ; 12 : 2535.
[34] Bokhman JV. Two pathogenetic types of endometrial carcinoma. *Gynecol Oncol* 1983 ; 15 : 10–17.
[35] Levine DA. Integrated genomic characterization of endometrial carcinoma. *Nature* 2013 ; 497 : 67–73.
[36] PTEN Gene - GeneCards | PTEN Protein | PTEN Antibody n.d. ;.
[37] Ali IU, Schriml LM, Dean M. Mutational Spectra of PTEN/MMAC1 Gene: a Tumor Suppressor With Lipid Phosphatase Activity. *JNCI Journal of the National Cancer Institute* 1999 ; 91 : 1922–1932.
[38] Fedorova O, Parfenyev S, Daks A, *et al.* The Role of PTEN in Epithelial–Mesenchymal Transition. *Cancers (Basel)* 2022 ; 14 : 3786.
[39] Ho J, Cruise ES, Dowling RJO, *et al.* PTEN Nuclear Functions. *Cold Spring Harb Perspect Med* 2020 ; 10 : a036079.
[40] Fusco N, Sajjadi E, Venetis K, *et al.* PTEN Alterations and Their Role in Cancer Management: Are We Making Headway on Precision Medicine? *Genes (Basel)* 2020 ; 11 : 719.
[41] Masson GR, Williams RL. Structural Mechanisms of PTEN Regulation. *Cold Spring Harb Perspect Med* 2020 ; 10 : a036152.
[42] Marchiò C, De Filippo MR, Ng CKY, *et al.* PIKing the type and pattern of PI3K pathway mutations in endometrioid endometrial carcinomas. *Gynecologic Oncology* 2015 ; 137 : 321–328.
[43] Chalhoub N, Baker SJ. PTEN and the PI3-Kinase Pathway in Cancer. *Annual Review of Pathology: Mechanisms of Disease* 2009 ; 4 : 127–150.
[44] Yehia L, Eng C. PTEN Hamartoma Tumor Syndrome. In : Adam MP, Mirzaa GM, Pagon RA, et al., editors. *GeneReviews®*. Seattle (WA) : University of Washington, Seattle, 1993 :
[45] Henninger EE, Pursell ZF. DNA polymerase ε and its roles in genome stability. *IUBMB Life* 2014 ; 66 : 339–351.
[46] Nick McElhinny SA, Gordenin DA, Stith CM, *et al.* Division of Labor at the Eukaryotic Replication Fork. *Mol Cell* 2008 ; 30 : 137–144.
[47] POLD1 DNA polymerase delta 1, catalytic subunit [Homo sapiens (human)] - Gene - NCBI n.d. ;.
[48] Evaluation of POLE and POLD1 Mutations as Biomarkers for Immunotherapy Outcomes Across Multiple Cancer Types | Cancer Biomarkers | JAMA Oncology | JAMA Network n.d. ;.

[49] León-Castillo A, Britton H, McConechy MK, *et al.* Interpretation of somatic *POLE* mutations in endometrial carcinoma. *J. Pathol.* 2020 ; 250 : 323–335.
[50] Myers AP. New strategies in endometrial cancer: targeting the PI3K/mTOR pathway--the devil is in the details. *Clin Cancer Res* 2013 ; 19 : 5264–5274.
[51] Bianco B, Barbosa CP, Trevisan CM, *et al.* Endometrial cancer: a genetic point of view. *Translational Cancer Research* 2020 ; 9 .
[52] Long H-Z, Cheng Y, Zhou Z-W, *et al.* PI3K/AKT Signal Pathway: A Target of Natural Products in the Prevention and Treatment of Alzheimer's Disease and Parkinson's Disease. *Front Pharmacol* 2021 ; 12 : 648636.
[53] Slomovitz BM, Coleman RL. The PI3K/AKT/mTOR pathway as a therapeutic target in endometrial cancer. *Clin Cancer Res* 2012 ; 18 : 5856–5864.
[54] Timar J, Kashofer K. Molecular epidemiology and diagnostics of KRAS mutations in human cancer. *Cancer Metastasis Rev* 2020 ; 39 : 1029–1038.
[55] Huang L, Guo Z, Wang F, *et al.* KRAS mutation: from undruggable to druggable in cancer. *Sig Transduct Target Ther* 2021 ; 6 : 386.
[56] Jančík S, Drábek J, Radzioch D, *et al.* Clinical Relevance of KRAS in Human Cancers. *Journal of Biomedicine and Biotechnology* 2010 ; 2010 : 1–13.
[57] Pylayeva-Gupta Y, Grabocka E, Bar-Sagi D. RAS oncogenes: weaving a tumorigenic web. *Nat Rev Cancer* 2011 ; 11 : 761–774.
[58] Temko D, Tomlinson IPM, Severini S, *et al.* The effects of mutational processes and selection on driver mutations across cancer types. *Nat Commun* 2018 ; 9 : 1857.
[59] Wilsker D, Patsialou A, Dallas PB, *et al.* ARID proteins: a diverse family of DNA binding proteins implicated in the control of cell growth, differentiation, and development. *Cell Growth Differ* 2002 ; 13 : 95–106.
[60] Bell DW, Ellenson LH. Molecular Genetics of Endometrial Carcinoma. *Annu. Rev. Pathol. Mech. Dis.* 2019 ; 14 : 339–367.
[61] Mullen J, Kato S, Sicklick JK, *et al.* Targeting ARID1A mutations in cancer. *Cancer Treatment Reviews* 2021 ; 100 : 102287.
[62] Mrf-2 (human) n.d. ;.
[63] Lecarpentier Y, Schussler O, Hébert J-L, *et al.* Multiple Targets of the Canonical WNT/β-Catenin Signaling in Cancers. *Frontiers in Oncology* 2019 ; 9 .
[64] Ledinek Ž, Sobočan M, Knez J. The Role of CTNNB1 in Endometrial Cancer. *Dis Markers* 2022 ; 2022 : 1442441.
[65] Zhang C, Liu J, Xu D, *et al.* Gain-of-function mutant p53 in cancer progression and therapy. *J Mol Cell Biol* 2020 ; 12 : 674–687.
[66] Hu J, Cao J, Topatana W, *et al.* Targeting mutant p53 for cancer therapy: direct and indirect strategies. *J Hematol Oncol* 2021 ; 14 : 157.
[67] Vermij L, Smit V, Nout R, *et al.* Incorporation of molecular characteristics into endometrial cancer management. *Histopathology* 2020 ; 76 : 52–63.
[68] Mould RF. The early history of x-ray diagnosis with emphasis on the contributions of physics 1895-1915. *Phys Med Biol* 1995 ; 40 : 1741–1787.
[69] Koka K, Verma A, Dwarakanath BS, *et al.* Technological Advancements in External Beam Radiation Therapy (EBRT): An Indispensable Tool for Cancer Treatment. *Cancer Manag Res* 2022 ; 14 : 1421–1429.
[70] Arneson AN. An Evaluation of the Use of Radiation in the Treatment of Endometrial Cancer. *Bull N Y Acad Med* 1953 ; 29 : 395–410.
[71] Uyeda M, Friedrich F, Pellizzon ACA. High dose rate (HDR) brachytherapy in gynecologic cancer regression: a review of the literature. *Applied Cancer Research* 2018 ; 38 : 19.
[72] Autorino R, Tagliaferri L, Campitelli M, *et al.* EROS study: evaluation between high-dose-rate and low-dose-rate vaginal interventional radiotherapy (brachytherapy) in terms of overall survival and rate of stenosis. *J Contemp Brachytherapy* 2018 ; 10 : 315–320.
[73] Kong A, Johnson N, Kitchener HC, *et al.* Adjuvant radiotherapy for stage I endometrial cancer. *Cochrane Database Syst Rev* 2012 ; 2012 : CD003916.
[74] Onsrud M, Cvancarova M, Hellebust TP, *et al.* Long-Term Outcomes After Pelvic Radiation for Early-Stage Endometrial Cancer. *Journal of Clinical Oncology* 2013 ;.

[75] Sunil RA, Bhavsar D, Shruthi MN, *et al.* Combined external beam radiotherapy and vaginal brachytherapy versus vaginal brachytherapy in stage I, intermediate- and high-risk cases of endometrium carcinoma. *J Contemp Brachytherapy* 2018 ; 10 : 105–114.
[76] Wang W, Zou L, Wang T, *et al.* Treatment optimization of pelvic external beam radiation and/or vaginal brachytherapy for patients with stage I to II high-risk Endometrioid adenocarcinoma: a retrospective multi-institutional analysis. *BMC Cancer* 2021 ; 21 : 774.
[77] Wortman BG, Creutzberg CL, Putter H, *et al.* Ten-year results of the PORTEC-2 trial for high-intermediate risk endometrial carcinoma: improving patient selection for adjuvant therapy. *Br J Cancer* 2018 ; 119 : 1067–1074.
[78] Concin N, Matias-Guiu X, Vergote I, *et al.* ESGO/ESTRO/ESP guidelines for the management of patients with endometrial carcinoma. *International Journal of Gynecologic Cancer* 2021 ; 31 .
[79] Keys HM, Roberts JA, Brunetto VL, *et al.* A phase III trial of surgery with or without adjunctive external pelvic radiation therapy in intermediate risk endometrial adenocarcinoma: a Gynecologic Oncology Group study. *Gynecologic Oncology* 2004 ; 92 : 744–751.
[80] Adjuvant external beam radiotherapy in the treatment of endometrial cancer (MRC ASTEC and NCIC CTG EN.5 randomised trials): pooled trial results, systematic review, and meta-analysis *The Lancet* 2009 ; 373 : 137–146.
[81] Tacar O, Sriamornsak P, Dass CR. Doxorubicin: an update on anticancer molecular action, toxicity and novel drug delivery systems. *Journal of Pharmacy and Pharmacology* 2013 ; 65 : 157–170.
[82] Dasari S, Tchounwou PB. Cisplatin in cancer therapy: molecular mechanisms of action. *Eur J Pharmacol* 2014 ; 740 : 364–378.
[83] Weaver BA. How Taxol/paclitaxel kills cancer cells. *Mol Biol Cell* 2014 ; 25 : 2677–2681.
[84] Verweij J, Clavel M, Chevalier B. Paclitaxel (TaxolTM) and docetaxel (TaxotereTM): Not simply two of a kind. *Annals of Oncology* 1994 ; 5 : 495–505.
[85] Miller DS, Filiaci VL, Mannel RS, *et al.* Carboplatin and Paclitaxel for Advanced Endometrial Cancer: Final Overall Survival and Adverse Event Analysis of a Phase III Trial (NRG Oncology/GOG0209). *J Clin Oncol* 2020 ; 38 : 3841–3850.
[86] Chambers SK. Advances in Chemotherapy and Targeted Therapies in Endometrial Cancer. *Cancers* 2022 ; 14 : 5020.
[87] Maggi R, Lissoni A, Spina F, *et al.* Adjuvant chemotherapy vs radiotherapy in high-risk endometrial carcinoma: results of a randomised trial. *Br J Cancer* 2006 ; 95 : 266–271.
[88] Susumu N, Sagae S, Udagawa Y, *et al.* Randomized phase III trial of pelvic radiotherapy versus cisplatin-based combined chemotherapy in patients with intermediate- and high-risk endometrial cancer: A Japanese Gynecologic Oncology Group study. *Gynecologic Oncology* 2008 ; 108 : 226–233.
[89] Randall ME, Filiaci VL, Muss H, *et al.* Randomized Phase III Trial of Whole-Abdominal Irradiation Versus Doxorubicin and Cisplatin Chemotherapy in Advanced Endometrial Carcinoma: A Gynecologic Oncology Group Study. *JCO* 2006 ; 24 : 36–44.
[90] Boer SM de, Powell ME, Mileshkin L, *et al.* Adjuvant chemoradiotherapy versus radiotherapy alone in women with high-risk endometrial cancer (PORTEC-3): patterns of recurrence and post-hoc survival analysis of a randomised phase 3 trial. *The Lancet Oncology* 2019 ; 20 : 1273–1285.
[91] Mikuła-Pietrasik J, Witucka A, Pakuła M, *et al.* Comprehensive review on how platinum- and taxane-based chemotherapy of ovarian cancer affects biology of normal cells. *Cell Mol Life Sci* 2019 ; 76 : 681–697.
[92] Wagner VM, Backes FJ. Do Not Forget about Hormonal Therapy for Recurrent Endometrial Cancer: A Review of Options, Updates, and New Combinations. *Cancers (Basel)* 2023 ; 15 : 1799.
[93] Hormonothérapie - Cancer de l'endomètre n.d. ;.
[94] Mitra S, Lami MS, Ghosh A, *et al.* Hormonal Therapy for Gynecological Cancers: How Far Has Science Progressed toward Clinical Applications? *Cancers* 2022 ; 14 : 759.

[95] Rehman O, Jaferi U, Padda I, *et al.* Overview of lenvatinib as a targeted therapy for advanced hepatocellular carcinoma. *Clin Exp HEPATOL* 2021 ; 7 : 249–257.
[96] PubChem. KIT - KIT proto-oncogene, receptor tyrosine kinase (human). n.d. ;.
[97] Lenvatinib : substance active à effet thérapeutique *VIDAL* n.d. ;.
[98] Makker V, Colombo N, Casado Herráez A, *et al.* Lenvatinib plus Pembrolizumab for Advanced Endometrial Cancer. *New England Journal of Medicine* 2022 ; 386 : 437–448.
[99] Flynn JP, Gerriets V. Pembrolizumab. *StatPearls*. Treasure Island (FL) : StatPearls Publishing, 2023 :
[100] Definition of pembrolizumab - NCI Drug Dictionary - NCI 2011 ;.
[101] Eskander RN, Sill MW, Beffa L, *et al.* Pembrolizumab plus Chemotherapy in Advanced Endometrial Cancer. *N Engl J Med* 2023 ; 388 : 2159–2170.
[102] Apte RS, Chen DS, Ferrara N. VEGF in Signaling and Disease: Beyond Discovery and Development. *Cell* 2019 ; 176 : 1248–1264.
[103] Chen H, Liang M, Min J. Efficacy and Safety of Bevacizumab-Combined Chemotherapy for Advanced and Recurrent Endometrial Cancer: A Systematic Review and Meta-analysis. *Balkan Med J* 2021 ; 38 : 7–12.
[104] Stelloo E, Nout RA, Osse EM, *et al.* Improved Risk Assessment by Integrating Molecular and Clinicopathological Factors in Early-stage Endometrial Cancer—Combined Analysis of the PORTEC Cohorts. *Clinical Cancer Research* 2016 ; 22 : 4215–4224.
[105] Leslie KK, Filiaci VL, Mallen AR, *et al.* Mutated p53 portends improvement in outcomes when bevacizumab is combined with chemotherapy in advanced/recurrent endometrial cancer: an NRG Oncology study. *Gynecol Oncol* 2021 ; 161 : 113–121.
[106] Mitric C, Bernardini MQ. Endometrial Cancer: Transitioning from Histology to Genomics. *Current Oncology* 2022 ; 29 : 741–757.
[107] Molecular Classification of Endometrial Cancer and Targeted Therapy Considerations 2022 : p.
[108] Bell MR. Comparing Postnatal Development of Gonadal Hormones and Associated Social Behaviors in Rats, Mice, and Humans. *Endocrinology* 2018 ; 159 : 2596–2613.
[109] Ajayi AF, Akhigbe RE. Staging of the estrous cycle and induction of estrus in experimental rodents: an update. *Fertility Research and Practice* 2020 ; 6 : 5.
[110] Bellofiore N, Cousins F, Temple-Smith P, *et al.* A missing piece: the spiny mouse and the puzzle of menstruating species. *Journal of Molecular Endocrinology* 2018 ; 61 : R25–R41.
[111] Podsypanina K, Ellenson LH, Nemes A, *et al.* Mutation of Pten/Mmac1 in mice causes neoplasia in multiple organ systems. *Proc Natl Acad Sci U S A* 1999 ; 96 : 1563–1568.
[112] Mirantes C, Eritja N, Dosil MA, *et al.* An inducible knockout mouse to model the cell-autonomous role of PTEN in initiating endometrial, prostate and thyroid neoplasias. *Dis Model Mech* 2013 ; 6 : 710–720.
[113] Dosil MA, Mirantes C, Eritja N, *et al.* Palbociclib has antitumour effects on Pten-deficient endometrial neoplasias. *J Pathol* 2017 ; 242 : 152–164.
[114] Kalluri R, Weinberg RA. The basics of epithelial-mesenchymal transition. *J Clin Invest* 2009 ; 119 : 1420–1428.
[115] Ray I, Michael A, Meira LB, *et al.* The Role of Cytokines in Epithelial–Mesenchymal Transition in Gynaecological Cancers: A Systematic Review. *Cells* 2023 ; 12 : 416.
[116] Marconi GD, Fonticoli L, Rajan TS, *et al.* Epithelial-Mesenchymal Transition (EMT): The Type-2 EMT in Wound Healing, Tissue Regeneration and Organ Fibrosis. *Cells* 2021 ; 10 : 1587.
[117] Zeisberg M, Neilson EG. Biomarkers for epithelial-mesenchymal transitions. *J Clin Invest* 2009 ; 119 : 1429–1437.
[118] Kim DH, Xing T, Yang Z, *et al.* Epithelial Mesenchymal Transition in Embryonic Development, Tissue Repair and Cancer: A Comprehensive Overview. *J Clin Med* 2017 ; 7 : 1.
[119] Bilyk O, Coatham M, Jewer M, *et al.* Epithelial-to-Mesenchymal Transition in the Female Reproductive Tract: From Normal Functioning to Disease Pathology. *Frontiers in Oncology* 2017 ; 7 .

[120] Savagner P. Chapter Eight - Epithelial–Mesenchymal Transitions: From Cell Plasticity to Concept Elasticity. In : Yap AS, editor. *Current Topics in Developmental Biology*. Cellular Adhesion in Development and Disease. Academic Press, 2015 : 273–300.
[121] Hüsemann Y, Geigl JB, Schubert F, *et al.* Systemic Spread Is an Early Step in Breast Cancer. *Cancer Cell* 2008 ; 13 : 58–68.
[122] Sugino T, Yamaguchi T, Ogura G, *et al.* Morphological evidence for an invasion-independent metastasis pathway exists in multiple human cancers. *BMC Medicine* 2004 ; 2 : 9.
[123] Huang RY-J, Guilford P, Thiery JP. Early events in cell adhesion and polarity during epithelial-mesenchymal transition. *Journal of Cell Science* 2012 ; 125 : 4417–4422.
[124] Liotta LA, Kohn E. Cancer and the homeless cell. *Nature* 2004 ; 430 : 973–974.
[125] Derksen PWB, Liu X, Saridin F, *et al.* Somatic inactivation of E-cadherin and p53 in mice leads to metastatic lobular mammary carcinoma through induction of anoikis resistance and angiogenesis. *Cancer Cell* 2006 ; 10 : 437–449.
[126] Grillet F, Bayet E, Villeronce O, *et al.* Circulating tumour cells from patients with colorectal cancer have cancer stem cell hallmarks in ex vivo culture. *Gut* 2017 ; 66 : 1802–1810.
[127] Krebs MG, Sloane R, Priest L, *et al.* Evaluation and Prognostic Significance of Circulating Tumor Cells in Patients With Non–Small-Cell Lung Cancer. *JCO* 2011 ; 29 : 1556–1563.
[128] Cohen SJ, Punt CJA, Iannotti N, *et al.* Prognostic significance of circulating tumor cells in patients with metastatic colorectal cancer. *Annals of Oncology* 2009 ; 20 : 1223–1229.
[129] Cristofanilli M, Budd GT, Ellis MJ, *et al.* Circulating Tumor Cells, Disease Progression, and Survival in Metastatic Breast Cancer. *New England Journal of Medicine* 2004 ; 351 : 781–791.
[130] Bakir B, Chiarella AM, Pitarresi JR, *et al.* EMT, MET, plasticity and tumor metastasis. *Trends Cell Biol* 2020 ; 30 : 764–776.
[131] Zhang N, Ng AS, Cai S, *et al.* Novel therapeutic strategies: targeting epithelial–mesenchymal transition in colorectal cancer. *The Lancet Oncology* 2021 ; 22 : e358–e368.
[132] Stemmler MP, Eccles RL, Brabletz S, *et al.* Non-redundant functions of EMT transcription factors. *Nat Cell Biol* 2019 ; 21 : 102–112.
[133] Ikenouchi J, Matsuda M, Furuse M, *et al.* Regulation of tight junctions during the epithelium-mesenchyme transition:direct repression of the gene expression of claudins/occludin by Snail. *Journal of Cell Science* 2003 ; 116 : 1959–1967.
[134] Martínez-Estrada OM, Cullerés A, Soriano FX, *et al.* The transcription factors Slug and Snail act as repressors of Claudin-1 expression in epithelial cells1. *Biochem J* 2006 ; 394 : 449–457.
[135] Batlle E, Sancho E, Francí C, *et al.* The transcription factor Snail is a repressor of E-cadherin gene expression in epithelial tumour cells. *Nat Cell Biol* 2000 ; 2 : 84–89.
[136] Whiteman EL, Fan S, Harder JL, *et al.* Crumbs3 Is Essential for Proper Epithelial Development and Viability. *Molecular and Cellular Biology* 2014 ; 34 : 43–56.
[137] Blechschmidt K, Sassen S, Schmalfeldt B, *et al.* The E-cadherin repressor Snail is associated with lower overall survival of ovarian cancer patients. *Br J Cancer* 2008 ; 98 : 489–495.
[138] Shioiri M, Shida T, Koda K, *et al.* Slug expression is an independent prognostic parameter for poor survival in colorectal carcinoma patients. *Br J Cancer* 2006 ; 94 : 1816–1822.
[139] Hardy RG, Vicente-Dueñas C, González-Herrero I, *et al.* Snail Family Transcription Factors Are Implicated in Thyroid Carcinogenesis. *The American Journal of Pathology* 2007 ; 171 : 1037–1046.
[140] Qin Q, Xu Y, He T, *et al.* Normal and disease-related biological functions of Twist1 and underlying molecular mechanisms. *Cell Res* 2012 ; 22 : 90–106.
[141] Nuti SV, Mor G, Li P, *et al.* TWIST and ovarian cancer stem cells: implications for chemoresistance and metastasis. *Oncotarget* 2014 ; 5 : 7260–7271.
[142] Yang J, Mani SA, Weinberg RA. Exploring a New Twist on Tumor Metastasis. *Cancer Research* 2006 ; 66 : 4549–4552.
[143] Gheldof A, Hulpiau P, Roy F van, *et al.* Evolutionary functional analysis and molecular regulation of the ZEB transcription factors. *Cell. Mol. Life Sci.* 2012 ; 69 : 2527–2541.
[144] Zhang P, Sun Y, Ma L. ZEB1: At the crossroads of epithelial-mesenchymal transition, metastasis and therapy resistance. *Cell Cycle* 2015 ; 14 : 481–487.

[145] Dave N, Guaita-Esteruelas S, Gutarra S, *et al.* Functional Cooperation between Snail1 and Twist in the Regulation of ZEB1 Expression during Epithelial to Mesenchymal Transition*. *Journal of Biological Chemistry* 2011 ; 286 : 12024–12032.
[146] Spaderna S, Schmalhofer O, Wahlbuhl M, *et al.* The Transcriptional Repressor ZEB1 Promotes Metastasis and Loss of Cell Polarity in Cancer. *Cancer Research* 2008 ; 68 : 537–544.
[147] Jang MH, Kim HJ, Kim EJ, *et al.* Expression of epithelial-mesenchymal transition–related markers in triple-negative breast cancer: ZEB1 as a potential biomarker for poor clinical outcome. *Human Pathology* 2015 ; 46 : 1267–1274.
[148] Kurahara H, Takao S, Maemura K, *et al.* Epithelial–mesenchymal transition and mesenchymal–epithelial transition via regulation of ZEB-1 and ZEB-2 expression in pancreatic cancer. *Journal of Surgical Oncology* 2012 ; 105 : 655–661.
[149] Prislei S, Martinelli E, Zannoni GF, *et al.* Role and prognostic significance of the epithelial-mesenchymal transition factor ZEB2 in ovarian cancer. *Oncotarget* 2015 ; 6 : 18966–18979.
[150] Montserrat N, Mozos A, Llobet D, *et al.* Epithelial to mesenchymal transition in early stage endometrioid endometrial carcinoma. *Human Pathology* 2012 ; 43 : 632–643.
[151] Sadlecki P, .Jozwicki J, Antosik P, *et al.* Expression of Selected Epithelial-Mesenchymal Transition Transcription Factors in Endometrial Cancer. *BioMed Research International* 2020 ; 2020 .
[152] Liu L, Zhang J, Yang X, *et al.* SALL4 as an Epithelial-Mesenchymal Transition and Drug Resistance Inducer through the Regulation of c-Myc in Endometrial Cancer. *PLOS ONE* 2015 ; 10 : e0138515.
[153] Hao Y, Li Y, Wu J, *et al.* Hypermethylation of the GRHL2 promoter region is associated with ovarian endometriosis. *Reproduction* 2022 ; 163 : 379–386.
[154] Chung VY, Tan TZ, Ye J, *et al.* The role of GRHL2 and epigenetic remodeling in epithelial–mesenchymal plasticity in ovarian cancer cells. *Commun Biol* 2019 ; 2 : 1–15.
[155] Wang Z, Coban B, Wu H, *et al.* GRHL2-controlled gene expression networks in luminal breast cancer. *Cell Communication and Signaling* 2023 ; 21 : 15.
[156] Xu X, Zhang Y, Wang X, *et al.* Substrate Stiffness Drives Epithelial to Mesenchymal Transition and Proliferation through the NEAT1-Wnt/β-Catenin Pathway in Liver Cancer. *Int J Mol Sci* 2021 ; 22 : 12066.
[157] Rice AJ, Cortes E, Lachowski D, *et al.* Matrix stiffness induces epithelial–mesenchymal transition and promotes chemoresistance in pancreatic cancer cells. *Oncogenesis* 2017 ; 6 : e352–e352.
[158] Hurwitz SN, Rider MA, Bundy JL, *et al.* Proteomic profiling of NCI-60 extracellular vesicles uncovers common protein cargo and cancer type-specific biomarkers. *Oncotarget* 2016 ; 7 : 86999–87015.
[159] Hornick NI, Huan J, Doron B, *et al.* Serum Exosome MicroRNA as a Minimally-Invasive Early Biomarker of AML. *Sci Rep* 2015 ; 5 : 11295.
[160] Lin S-Y, Chang C-H, Wu H-C, *et al.* Proteome Profiling of Urinary Exosomes Identifies Alpha 1-Antitrypsin and H2B1K as Diagnostic and Prognostic Biomarkers for Urothelial Carcinoma. *Sci Rep* 2016 ; 6 : 34446.
[161] György B, Szabó TG, Pásztói M, *et al.* Membrane vesicles, current state-of-the-art: emerging role of extracellular vesicles. *Cell Mol Life Sci* 2011 ; 68 : 2667–2688.
[162] Luga V, Zhang L, Viloria-Petit AM, *et al.* Exosomes mediate stromal mobilization of autocrine Wnt-PCP signaling in breast cancer cell migration. *Cell* 2012 ; 151 : 1542–1556.
[163] Costa-Silva B, Aiello NM, Ocean AJ, *et al.* Pancreatic cancer exosomes initiate pre-metastatic niche formation in the liver. *Nat Cell Biol* 2015 ; 17 : 816–826.
[164] Mahaweni NM, Kaijen-Lambers MEH, Dekkers J, *et al.* Tumour-derived exosomes as antigen delivery carriers in dendritic cell-based immunotherapy for malignant mesothelioma. *J Extracell Vesicles* 2013 ; 2 .
[165] Ristorcelli E, Beraud E, Verrando P, *et al.* Human tumor nanoparticles induce apoptosis of pancreatic cancer cells. *FASEB J* 2008 ; 22 : 3358–3369.

[166] Zhang Y, Luo C-L, He B-C, *et al.* Exosomes derived from IL-12-anchored renal cancer cells increase induction of specific antitumor response in vitro: a novel vaccine for renal cell carcinoma. *Int J Oncol* 2010 ; 36 : 133–140.
[167] Chen L, Guo P, He Y, *et al.* HCC-derived exosomes elicit HCC progression and recurrence by epithelial-mesenchymal transition through MAPK/ERK signalling pathway. *Cell Death Dis* 2018 ; 9 : 513.
[168] Franzen CA, Blackwell RH, Todorovic V, *et al.* Urothelial cells undergo epithelial-to-mesenchymal transition after exposure to muscle invasive bladder cancer exosomes. *Oncogenesis* 2015 ; 4 : e163.
[169] Rahman MA, Barger JF, Lovat F, *et al.* Lung cancer exosomes as drivers of epithelial mesenchymal transition. *Oncotarget* 2016 ; 7 : 54852–54866.
[170] Gabriel K, Ingram A, Austin R, *et al.* Regulation of the tumor suppressor PTEN through exosomes: a diagnostic potential for prostate cancer. *PLoS One* 2013 ; 8 : e70047.
[171] Al-Nedawi K, Meehan B, Micallef J, *et al.* Intercellular transfer of the oncogenic receptor EGFRvIII by microvesicles derived from tumour cells. *Nat Cell Biol* 2008 ; 10 : 619–624.
[172] Luhtala N, Aslanian A, Yates JR, *et al.* Secreted Glioblastoma Nanovesicles Contain Intracellular Signaling Proteins and Active Ras Incorporated in a Farnesylation-dependent Manner. *J Biol Chem* 2017 ; 292 : 611–628.
[173] Rojas A, Delgado-López F, Gonzalez I. Tumor-associated macrophages in gastric cancer: more than bystanders in tumor microenvironment. *Gastric Cancer* 2017 ; 20 : 215–216.
[174] Wu Y, Deng J, Rychahou PG, *et al.* Stabilization of Snail by NF-κB Is Required for Inflammation-Induced Cell Migration and Invasion. *Cancer Cell* 2009 ; 15 : 416–428.
[175] Taki M, Abiko K, Ukita M, *et al.* Tumor Immune Microenvironment during Epithelial–Mesenchymal Transition. *Clinical Cancer Research* 2021 ; 27 : 4669–4679.
[176] Szabo PM, Vajdi A, Kumar N, *et al.* Cancer-associated fibroblasts are the main contributors to epithelial-to-mesenchymal signatures in the tumor microenvironment. *Sci Rep* 2023 ; 13 : 3051.
[177] Soon PSH, Kim E, Pon CK, *et al.* Breast cancer-associated fibroblasts induce epithelial-to-mesenchymal transition in breast cancer cells. *Endocrine-Related Cancer* 2013 ; 20 : 1–12.
[178] Quintero-Fabián S, Arreola R, Becerril-Villanueva E, *et al.* Role of Matrix Metalloproteinases in Angiogenesis and Cancer. *Front Oncol* 2019 ; 9 : 1370.
[179] Bollrath J, Greten FR. IKK/NF-κB and STAT3 pathways: central signalling hubs in inflammation-mediated tumour promotion and metastasis. *EMBO reports* 2009 ; 10 : 1314–1319.
[180] Johnson DE, O'Keefe RA, Grandis JR. Targeting the IL-6/JAK/STAT3 signalling axis in cancer. *Nat Rev Clin Oncol* 2018 ; 15 : 234–248.
[181] Pankov R, Yamada KM. Fibronectin at a glance. *Journal of Cell Science* 2002 ; 115 : 3861–3863.
[182] Erdogan B, Ao M, White LM, *et al.* Cancer-associated fibroblasts promote directional cancer cell migration by aligning fibronectin. *J Cell Biol* 2017 ; 216 : 3799–3816.
[183] Zeng Z-Z, Jia Y, Hahn NJ, *et al.* Role of Focal Adhesion Kinase and Phosphatidylinositol 3′-Kinase in Integrin Fibronectin Receptor-Mediated, Matrix Metalloproteinase-1–Dependent Invasion by Metastatic Prostate Cancer Cells. *Cancer Research* 2006 ; 66 : 8091–8099.
[184] Neve A, Cantatore FP, Maruotti N, *et al.* Extracellular matrix modulates angiogenesis in physiological and pathological conditions. *Biomed Res Int* 2014 ; 2014 : 756078.
[185] Mitra A, Sawada K, Tiwari P, *et al.* Ligand independent activation of c-Met by fibronectin and α5β1-integrin regulates ovarian cancer invasion and metastasis. *Oncogene* 2011 ; 30 : 1566–1576.
[186] Cell Adhesion, Cell Communication | Learn Science at Scitable n.d. ;.
[187] Roy F van, Berx G. The cell-cell adhesion molecule E-cadherin. *Cell. Mol. Life Sci.* 2008 ; 65 : 3756–3788.
[188] Wang X, Dong B, Zhang K, *et al.* E-cadherin bridges cell polarity and spindle orientation to ensure prostate epithelial integrity and prevent carcinogenesis in vivo. *PLoS Genet* 2018 ; 14 : e1007609.

[189] Maître J-L, Heisenberg C-P. Three Functions of Cadherins in Cell Adhesion. *Curr Biol* 2013 ; 23 : R626–R633.
[190] Mrozik KM, Blaschuk OW, Cheong CM, *et al.* N-cadherin in cancer metastasis, its emerging role in haematological malignancies and potential as a therapeutic target in cancer. *BMC Cancer* 2018 ; 18 : 939.
[191] Shih H-C, Shiozawa T, Miyamoto T, *et al.* Immunohistochemical Expression of E-cadherin and ,-catenin in the Normal and Malignant Human Endometrium: An Inverse Correlation Between E-cadherin and Nuclear ,-catenin Expression. *ANTICANCER RESEARCH* 2004 ;.
[192] Cousins F, Pandoy R, Jin S, *et al.* The Elusive Endometrial Epithelial Stem/Progenitor Cells. *Frontiers in Cell and Developmental Biology* 2021 ; 9 .
[193] Loh C-Y, Chai JY, Tang TF, *et al.* The E-Cadherin and N-Cadherin Switch in Epithelial-to-Mesenchymal Transition: Signaling, Therapeutic Implications, and Challenges. *Cells* 2019 ; 8 : 1118.
[194] Kim YT, Choi EK, Kim JW, *et al.* Expression of E-Cadherin and α-, β-, γ-Catenin Proteins in Endometrial Carcinoma. *Yonsei Med J* 2002 ; 43 : 701.
[195] Yalta T, Atay L, Atalay F, *et al.* E-cadherin expression in endometrial malignancies: comparison between endometrioid and non-endometrioid carcinomas. *J Int Med Res* 2009 ; 37 : 163–168.
[196] Yadav S, Makkar A, Agarwal P, *et al.* Immunohistochemical expression of E-cadherin and N-cadherin in endometrioid endometrial carcinoma and its precursor lesions. *Clinical Epidemiology and Global Health* 2023 ; 21 : 101296.
[197] Lewczuk Ł, Pryczynicz A, Guzińska-Ustymowicz K. Expression level of E-, N- and P-cadherin proteins in endometrial cancer. *Oncol Lett* 2021 ; 21 : 261.
[198] Schnell U, Cirulli V, Giepmans BNG. EpCAM: Structure and function in health and disease. *Biochimica et Biophysica Acta (BBA) - Biomembranes* 2013 ; 1828 : 1989–2001.
[199] Brown TC, Sankpal NV, Gillanders WE. Functional Implications of the Dynamic Regulation of EpCAM during Epithelial-to-Mesenchymal Transition. *Biomolecules* 2021 ; 11 : 956.
[200] Maetzel D, Denzel S, Mack B, *et al.* Nuclear signalling by tumour-associated antigen EpCAM. *Nat Cell Biol* 2009 ; 11 : 162–171.
[201] Lu T-Y, Lu R-M, Liao M-Y, *et al.* Epithelial Cell Adhesion Molecule Regulation Is Associated with the Maintenance of the Undifferentiated Phenotype of Human Embryonic Stem Cells *. *Journal of Biological Chemistry* 2010 ; 285 : 8719–8732.
[202] Mohtar MA, Syafruddin, Nasir N, *et al.* Revisiting the Roles of Pro-Metastatic EpCAM in Cancer. *Biomolecules* 2020 ; 10 : 255.
[203] Wen K-C, Sung P-L, Chou Y-T, *et al.* The role of EpCAM in tumor progression and the clinical prognosis of endometrial carcinoma. *Gynecologic Oncology* 2018 ; 148 : 383–392.
[204] Hsu Y-T, Osmulski P, Wang Y, *et al.* EpCAM-Regulated Transcription Exerts Influences on Nanomechanical Properties of Endometrial Cancer Cells That Promote Epithelial-to-Mesenchymal Transition. *Cancer Research* 2016 ; 76 : 6171–6182.
[205] Huang R, Deng X, Zhang Z, *et al.* Lynch Syndrome-Associated Endometrial Cancer With Combined EPCAM-MSH2 Deletion: A Case Report. *Frontiers in Oncology* 2022 ; 12 .
[206] Datta A, Deng S, Gopal V, *et al.* Cytoskeletal Dynamics in Epithelial-Mesenchymal Transition: Insights into Therapeutic Targets for Cancer Metastasis. *Cancers (Basel)* 2021 ; 13 : 1882.
[207] Sharma P, Alsharif S, Fallatah A, *et al.* Intermediate Filaments as Effectors of Cancer Development and Metastasis: A Focus on Keratins, Vimentin, and Nestin. *Cells* 2019 ; 8 : 497.
[208] Vasilevska D, Rudaitis V, Adamiak-Godlewska A, *et al.* Cytokeratin Expression Pattern in Human Endometrial Carcinomas and Lymph Nodes Micrometastasis: a Mini-review. *J Cancer* 2022 ; 13 : 1713–1724.
[209] Schweizer J, Bowden PE, Coulombe PA, *et al.* New consensus nomenclature for mammalian keratins. *Journal of Cell Biology* 2006 ; 174 : 169–174.
[210] Ramms L, Fabris G, Windoffer R, *et al.* Keratins as the main component for the mechanical integrity of keratinocytes. *Proceedings of the National Academy of Sciences* 2013 ; 110 : 18513–18518.

[211] Bhattacharya R, Gonzalez AM, DeBiase PJ, *et al.* Recruitment of vimentin to the cell surface by β3 integrin and plectin mediates adhesion strength. *Journal of Cell Science* 2009 ; 122 : 1390–1400.
[212] Danielsson F, Peterson MK, Caldeira Araújo H, *et al.* Vimentin Diversity in Health and Disease. *Cells* 2018 ; 7 : 147.
[213] Jiu Y, Peränen J, Schaible N, *et al.* Vimentin intermediate filaments control actin stress fiber assembly through GEF-H1 and RhoA. *J Cell Sci* 2017 ; 130 : 892–902.
[214] Wang X, He L, Wu YI, *et al.* Light-mediated activation reveals a key role for Rac in collective guidance of cell movement in vivo. *Nat Cell Biol* 2010 ; 12 : 591–597.
[215] Caswell PT, Zech T. Actin-Based Cell Protrusion in a 3D Matrix. *Trends in Cell Biology* 2018 ; 28 : 823–834.
[216] Kuburich NA, Hollander P den, Pietz JT, *et al.* Vimentin and cytokeratin: Good alone, bad together. *Seminars in Cancer Biology* 2022 ; 86 : 816–826.
[217] Nisolle M, Casanas-Roux F, Donnez J. Coexpression of cytokeratin and vimentin in eutopic endometrium and endometriosis throughout the menstrual cycle: evaluation by a computerized method. *Fertil Steril* 1995 ; 64 : 69–75.
[218] Leong AS-Y. The Expression of Vimentin in Epithelial Neoplasms. In : Fenoglio-Preiser CM, Wolff M, Rilke F, editors. *Progress in Surgical Pathology: Volume XII*. Berlin, Heidelberg : Springer, 1992 : 31–48.
[219] Kröger C, Afeyan A, Mraz J, *et al.* Acquisition of a hybrid E/M state is essential for tumorigenicity of basal breast cancer cells. *Proceedings of the National Academy of Sciences* 2019 ; 116 : 7353–7362.
[220] Stefansson IM, Salvesen HB, Akslen LA. Loss of p63 and cytokeratin 5/6 expression is associated with more aggressive tumors in endometrial carcinoma patients. *International Journal of Cancer* 2006 ; 118 : 1227–1233.
[221] Lin J, Lu J, Wang C, *et al.* The prognostic values of the expression of Vimentin, TP53, and Podoplanin in patients with cervical cancer. *Cancer Cell International* 2017 ; 17 : 80.
[222] Khillare CD, Sinai Khandeparkar SG, Joshi AR, *et al.* Immunohistochemical Expression of Vimentin in Invasive Breast Carcinoma and Its Correlation with Clinicopathological Parameters. *Niger Med J* 2019 ; 60 : 17–21.
[223] Satelli A, Li S. Vimentin as a potential molecular target in cancer therapy Or Vimentin, an overview and its potential as a molecular target for cancer therapy. *Cell Mol Life Sci* 2011 ; 68 : 3033–3046.
[224] Zhang X, Cao G, Diao X, *et al.* Vimentin Protein In Situ Expression Predicts Less Tumor Metastasis and Overall Better Survival of Endometrial Carcinoma. *Dis Markers* 2022 ; 2022 : 5240046.
[225] Lien HE, Berg HF, Halle MK, *et al.* Single-cell profiling of low-stage endometrial cancers identifies low epithelial vimentin expression as a marker of recurrent disease. *eBioMedicine* 2023 ; 92 .
[226] Kong CS, Beck AH, Longacre TA. A Panel of 3 Markers Including p16, ProExC, or HPV ISH is Optimal for Distinguishing Between Primary Endometrial and Endocervical Adenocarcinomas. *Am J Surg Pathol* 2010 ; 34 : 915–926.
[227] Desouki MM, Kallas SJ, Khabele D, *et al.* Differential Vimentin Expression in Ovarian and Uterine Corpus Endometrioid Adenocarcinomas: Diagnostic Utility in Distinguishing Double Primaries from Metastatic Tumors. *Int J Gynecol Pathol* 2014 ; 33 : 274–281.
[228] Le Bras GF, Taubenslag KJ, Andl CD. The regulation of cell-cell adhesion during epithelial-mesenchymal transition, motility and tumor progression. *Cell Adhesion & Migration* 2012 ; 6 : 365–373.
[229] Maldonado-Báez L, Donaldson JG. Hook1, microtubules, and Rab22. *Bioarchitecture* 2013 ; 3 : 141–146.
[230] HOOK1 Gene - GeneCards | HOOK1 Protein | HOOK1 Antibody n.d. ;.
[231] HOOK1 hook microtubule tethering protein 1 [Homo sapiens (human)] - Gene - NCBI n.d. ;.
[232] Mamoor S. Differential expression of HOOK1 in cancers of the breast. 2022 ;.

[233] Yin L, Li W, Chen X, *et al.* HOOK1 Inhibits the Progression of Renal Cell Carcinoma via TGF-β and TNFSF13B/VEGF-A Axis. *Adv Sci (Weinh)* 2023 ; 10 : 2206955.
[234] Sun X, Zhang Q, Chen W, *et al.* Hook1 inhibits malignancy and epithelial–mesenchymal transition in hepatocellular carcinoma. *Tumour Biol.* 2017 ; 39 : 1010428317711098.
[235] Makker A, Goel MM. Tumor progression, metastasis, and modulators of epithelial–mesenchymal transition in endometrioid endometrial carcinoma: an update. *Endocrine-Related Cancer* 2016 ; 23 : R85–R111.
[236] Castellano E, Downward J. RAS Interaction with PI3K: More Than Just Another Effector Pathway. *Genes & Cancer* 2011 ; 2 : 261–274.
[237] Hsieh AC, Liu Y, Edlind MP, *et al.* The translational landscape of mTOR signalling steers cancer initiation and metastasis. *Nature* 2012 ; 485 : 55–61.
[238] McCubrey JA, Fitzgerald TL, Yang LV, *et al.* Roles of GSK-3 and microRNAs on epithelial mesenchymal transition and cancer stem cells. *Oncotarget* 2016 ; 8 : 14221–14250.
[239] Zhou H, Li X-M, Meinkoth J, *et al.* Akt Regulates Cell Survival and Apoptosis at a Postmitochondrial Level. *J Cell Biol* 2000 ; 151 : 483–494.
[240] Nelson AC, Lyons TR, Young CD, *et al.* AKT Regulates BRCA1 Stability in Response to Hormone Signaling. *Mol Cell Endocrinol* 2010 ; 319 : 129–142.
[241] Yang W-N, Ai Z-H, Wang J, *et al.* Correlation between the overexpression of epidermal growth factor receptor and mesenchymal makers in endometrial carcinoma. *J Gynecol Oncol* 2014 ; 25 : 36–42.
[242] Lelle RJ, Talavera F, Gretz H, *et al.* Epidermal growth factor receptor expression in three different human endometrial cancer cell lines. *Cancer* 1993 ; 72 : 519–525.
[243] Hipp S, Walch A, Schuster T, *et al.* Activation of epidermal growth factor receptor results in Snail protein but not mRNA overexpression in endometrial cancer. *J Cell Mol Med* 2009 ; 13 : 3858–3867.
[244] McCampbell AS, Broaddus RR, Loose DS, *et al.* Overexpression of the insulin-like growth factor I receptor and activation of the AKT pathway in hyperplastic endometrium. *Clin Cancer Res* 2006 ; 12 : 6373–6378.
[245] Pavelić J, Radaković B, Pavelić K. Insulin-like growth factor 2 and its receptors (IGF 1R and IGF 2R/mannose 6-phosphate) in endometrial adenocarcinoma. *Gynecol Oncol* 2007 ; 105 : 727–735.
[246] Wang Y, Hua S, Tian W, *et al.* Mitogenic and anti-apoptotic effects of insulin in endometrial cancer are phosphatidylinositol 3-kinase/Akt dependent. *Gynecol Oncol* 2012 ; 125 : 734–741.
[247] Roncolato F, Lindemann K, Willson ML, *et al.* PI3K/AKT/mTOR inhibitors for advanced or recurrent endometrial cancer. *Cochrane Database Syst Rev* 2019 ; 2019 : CD012160.
[248] Kim LC, Cook RS, Chen J. mTORC1 and mTORC2 in cancer and the tumor microenvironment. *Oncogene* 2017 ; 36 : 2191–2201.
[249] Darb-Esfahani S, Faggad A, Noske A, *et al.* Phospho-mTOR and phospho-4EBP1 in endometrial adenocarcinoma: association with stage and grade in vivo and link with response to rapamycin treatment in vitro. *J Cancer Res Clin Oncol* 2009 ; 135 : 933–941.
[250] Shen Q, Stanton ML, Feng W, *et al.* Morphoproteomic analysis reveals an overexpressed and constitutively activated phospholipase D1-mTORC2 pathway in endometrial carcinoma. *International journal of clinical and experimental pathology* 2011 ; 4 : 13–21.
[251] Yoshida Y, Kurokawa T, Horiuchi Y, *et al.* Localisation of phosphorylated mTOR expression is critical to tumour progression and outcomes in patients with endometrial cancer. *European Journal of Cancer* 2010 ; 46 : 3445–3452.
[252] Terrell EM, Morrison DK. Ras-Mediated Activation of the Raf Family Kinases. *Cold Spring Harb Perspect Med* 2019 ; 9 : a033746.
[253] Zhang M, Maloney R, Jang H, *et al.* The mechanism of Raf activation through dimerization. *Chem. Sci.* 2021 ; 12 : 15609–15619.
[254] McCubrey JA, Steelman LS, Chappell WH, *et al.* ROLES OF THE RAF/MEK/ERK PATHWAY IN CELL GROWTH, MALIGNANT TRANSFORMATION AND DRUG RESISTANCE. *Biochim Biophys Acta* 2007 ; 1773 : 1263–1284.

[255] Maik-Rachline G, Hacohen-Lev-Ran A, Seger R. Nuclear ERK: Mechanism of Translocation, Substrates, and Role in Cancer. *International Journal of Molecular Sciences* 2019 ; 20 : 1194.
[256] Warn-Cramer BJ, Cottrell GT, Burt JM, *et al.* Regulation of Connexin-43 Gap Junctional Intercellular Communication by Mitogen-activated Protein Kinase*. *Journal of Biological Chemistry* 1998 ; 273 : 9188–9196.
[257] Shin S, Buel GR, Nagiec MJ, *et al.* ERK2 regulates epithelial-to-mesenchymal plasticity through DOCK10-dependent Rac1/FoxO1 activation. *Proc. Natl. Acad. Sci. U.S.A.* 2019 ; 116 : 2967–2976.
[258] Kim TH, Yoo J-Y, Kim HI, *et al.* Mig-6 Suppresses Endometrial Cancer Associated with Pten Deficiency and ERK Activation. *Cancer Research* 2014 ; 74 : 7371–7382.
[259] Liu A, Zhang D, Yang X, *et al.* Estrogen receptor alpha activates MAPK signaling pathway to promote the development of endometrial cancer. *J Cell Biochem* 2019 ; 120 : 17593–17601.
[260] Kourea HP, Nikolaou M, Tzelepi V, *et al.* Expression of Phosphorylated Akt, mTOR and MAPK in Type I Endometrial Carcinoma: Clinical Significance. *ANTICANCER RESEARCH* 2015 ;.
[261] Mizumoto Y, Kyo S, Mori N, *et al.* Activation of ERK1/2 occurs independently of KRAS or BRAF status in endometrial cancer and is associated with favorable prognosis. *Cancer Science* 2007 ; 98 : 652–658.
[262] Swisher EM, Peiffer-Schneider S, Mutch DG, *et al.* Differences in patterns of TP53 and KRAS2 mutations in a large series of endometrial carcinomas with or without microsatellite instability. *Cancer* 1999 ; 85 : 119–126.
[263] Banno K, Yanokura M, Iida M, *et al.* Carcinogenic mechanisms of endometrial cancer: Involvement of genetics and epigenetics. *Journal of Obstetrics and Gynaecology Research* 2014 ; 40 : 1957–1967.
[264] Tsuda H, Jiko K, Yajima M, *et al.* Frequent occurrence of c-Ki-ras gene mutations in well differentiated endometrial adenocarcinoma showing infiltrative local growth with fibrosing stromal response. *Int J Gynecol Pathol* 1995 ; 14 : 255–259.
[265] Höckel M, Vaupel P. Tumor Hypoxia: Definitions and Current Clinical, Biologic, and Molecular Aspects. *JNCI: Journal of the National Cancer Institute* 2001 ; 93 : 266–276.
[266] Ke Q, Costa M. Hypoxia-Inducible Factor-1 (HIF-1). *Mol Pharmacol* 2006 ; 70 : 1469–1480.
[267] Emerling BM, Weinberg F, Liu J-L, *et al.* PTEN regulates p300-dependent hypoxia-inducible factor 1 transcriptional activity through Forkhead transcription factor 3a (FOXO3a). *Proceedings of the National Academy of Sciences* 2008 ; 105 : 2622–2627.
[268] Feng Z, Gan H, Cai Z, *et al.* Aberrant Expression of Hypoxia-inducible Factor 1α, TWIST and E-cadherin is Associated with Aggressive Tumor Phenotypes in Endometrioid Endometrial Carcinoma. *Japanese Journal of Clinical Oncology* 2013 ; 43 : 396–403.
[269] Tanaka Y, Terai Y, Kawaguchi H, *et al.* Prognostic impact of EMT (epithelial-mesenchymal-transition)-related protein expression in endometrial cancer. *Cancer Biol Ther* 2013 ; 14 : 13–19.
[270] Georgakopoulos-Soares I, Chartoumpekis DV, Kyriazopoulou V, *et al.* EMT Factors and Metabolic Pathways in Cancer. *Front Oncol* 2020 ; 10 : 499.
[271] Kurrey NK, Jalgaonkar SP, Joglekar AV, *et al.* Snail and slug mediate radioresistance and chemoresistance by antagonizing p53-mediated apoptosis and acquiring a stem-like phenotype in ovarian cancer cells. *Stem Cells* 2009 ; 27 : 2059–2068.
[272] Bruyere F, Namdarian B, Corcoran NM, *et al.* Snail expression is an independent predictor of tumor recurrence in superficial bladder cancers. *Urologic Oncology: Seminars and Original Investigations* 2010 ; 28 : 591–596.
[273] Ren S, Wu J, Yin W, *et al.* Researches on the Correlation Between Estrogen and Progesterone Receptors Expression and Disease-Free Survival of Endometrial Cancer. *CMAR* 2020 ; Volume 12 : 12635–12647.
[274] Chaudhry P, Asselin E. Resistance to chemotherapy and hormone therapy in endometrial cancer. *Endocrine-Related Cancer* 2009 ; 16 : 363–380.

[275] Ma L, Andrieu T, McKinnon B, *et al.* Epithelial-to-mesenchymal transition contributes to the downregulation of progesterone receptor expression in endometriosis lesions. *J Steroid Biochem Mol Biol* 2021 ; 212 : 105943.
[276] Shibue T, Weinberg RA. EMT, CSCs, and drug resistance: the mechanistic link and clinical implications. *Nat Rev Clin Oncol* 2017 ; 14 : 611–629.
[277] Kilic F, Unsal M, Cakir C, *et al.* Prognostic factors determining survival after extrapelvic recurrence in endometrioid type endometrial cancer. *Taiwanese Journal of Obstetrics and Gynecology* 2021 ; 60 : 1023–1030.
[278] Cancer today n.d. ;.
[279] Mak MP, Tong P, Diao L, *et al.* A Patient-Derived, Pan-Cancer EMT Signature Identifies Global Molecular Alterations and Immune Target Enrichment Following Epithelial-to-Mesenchymal Transition. *Clin Cancer Res* 2016 ; 22 : 609–620.
[280] Eritja N, Felip I, Dosil MA, *et al.* A Smad3-PTEN regulatory loop controls proliferation and apoptotic responses to TGF-β in mouse endometrium. *Cell Death Differ* 2017 ; 24 : 1443–1458.
[281] Schill NJ, Hedman AC, Choi S, *et al.* Isoform 5 of PIPKIγ regulates the endosomal trafficking and degradation of E-cadherin. *Journal of Cell Science* 2014 ; 127 : 2189–2203.
[282] Lv J, Sun X, Ma J, *et al.* Netrin-1 induces the migration of Schwann cells via p38 MAPK and PI3K-Akt signaling pathway mediated by the UNC5B receptor. *Biochemical and Biophysical Research Communications* 2015 ; 464 : 263–268.
[283] Yin K, Wang L, Zhang X, *et al.* Netrin-1 promotes gastric cancer cell proliferation and invasion via the receptor neogenin through PI3K/AKT signaling pathway. *Oncotarget* 2017 ; 8 : 51177–51189.
[284] Jin X, Luan H, Chai H, *et al.* Netrin-1 interference potentiates epithelial-to-mesenchymal transition through the PI3K/AKT pathway under the hypoxic microenvironment conditions of non-small cell lung cancer. *Int J Oncol* 2019 ; 54 : 1457–1465.
[285] Yang Y, Lin Z, Lin Q, *et al.* Pathological and therapeutic roles of bioactive peptide trefoil factor 3 in diverse diseases: recent progress and perspective. *Cell Death Dis* 2022 ; 13 : 1–14.
[286] Huyghe A, Furlan G, Ozmadenci D, *et al.* Netrin-1 promotes naive pluripotency through Neo1 and Unc5b co-regulation of Wnt and MAPK signalling. *Nat Cell Biol* 2020 ; 22 : 389–400.
[287] Bellina M, Bernet A. La nétrine-1, une nouvelle cible antitumorale. *Med Sci (Paris)* 2022 ; 38 : 351–358.
[288] Mediero A, Wilder T, Ramkhelawon B, *et al.* Netrin-1 and its receptor Unc5b are novel targets for the treatment of inflammatory arthritis. *FASEB J* 2016 ; 30 : 3835–3844.
[289] Sahai E, Astsaturov I, Cukierman E, *et al.* A framework for advancing our understanding of cancer-associated fibroblasts. *Nat Rev Cancer* 2020 ; 20 : 174–186.
[290] Sung P-J, Rama N, Imbach J, *et al.* Cancer-Associated Fibroblasts Produce Netrin-1 to Control Cancer Cell Plasticity. *Cancer Res* 2019 ; 79 : 3651–3661.
[291] Ly NP, Komatsuzaki K, Fraser IP, *et al.* Netrin-1 inhibits leukocyte migration in vitro and in vivo. *Proc Natl Acad Sci U S A* 2005 ; 102 : 14729–14734.
[292] Zhou J, Nefedova Y, Lei A, *et al.* Neutrophils and PMN-MDSCs: their biological role and interaction with stromal cells. *Semin Immunol* 2018 ; 35 : 19–28.
[293] Jayasingam SD, Citartan M, Thang TH, *et al.* Evaluating the Polarization of Tumor-Associated Macrophages Into M1 and M2 Phenotypes in Human Cancer Tissue: Technicalities and Challenges in Routine Clinical Practice. *Front Oncol* 2020 ; 9 : 1512.
[294] Ramkhelawon B, Hennessy EJ, Ménager M, *et al.* Netrin-1 promotes adipose tissue macrophage retention and insulin resistance in obesity. *Nat Med* 2014 ; 20 : 377–384.
[295] Fang Y, Ma K, Huang Y-M, *et al.* Fibronectin leucine-rich transmembrane protein 2 drives monocyte differentiation into macrophages via the UNC5B-Akt/mTOR axis. *Front Immunol* 2023 ; 14 : 1162004.
[296] Boneschansker L, Nakayama H, Eisenga M, *et al.* Netrin-1 Augments Chemokinesis in CD4+ T Cells In Vitro and Elicits a Proinflammatory Response In Vivo. *Journal of immunology (Baltimore, Md. : 1950)* 2016 ; 197 .

[297] Centre Leon Berard. *NP137 - An Open-label, First in Human, Phase I Trial Aiming to Evaluate the Safety, Pharmacokinetics, and Clinical Activity of a Humanized Monoclonal Antibody Targeting Netrin 1 (NP137) in Patients With Advanced/Metastatic Solid Tumors.* clinicaltrials.gov, 2022 : p.
[298] Sahdev A, Sohaib S, Jacobs I, *et al.* MR Imaging of Uterine Sarcomas. *AJR. American journal of roentgenology* 2002 ; 177 : 1307–11.
[299] Kasius JC, Pijnenborg JMA, Lindemann K, *et al.* Risk Stratification of Endometrial Cancer Patients: FIGO Stage, Biomarkers and Molecular Classification. *Cancers (Basel)* 2021 ; 13 : 5848.
[300] Marnitz S, Waltar T, Köhler C, *et al.* The brave new world of endometrial cancer. *Strahlenther Onkol* 2020 ; 196 : 963–972.
[301] Natarajan J, Chandrashekar C, Radhakrishnan R. Critical biomarkers of epithelial-mesenchymal transition in the head and neck cancers. *Journal of Cancer Research and Therapeutics* 2014 ; 10 : 512.

Researcher’s oath

In the presence of my peers. With the completion of my doctorate in oncology, in my quest for knowledge, I have carried out demanding research, demonstrated intellectual rigour, ethical reflection, and respect for the principles of research integrity. As I pursue my professional career, whatever my chosen field, I pledge to the greatest of my ability, to continue to maintain integrity in my relationship to knowledge, in my methods and in my results.

***

Serment du docteur

En présence de mes pairs. Parvenue à l'issue de mon doctorat en oncologie, et ayant ainsi pratiqué, dans ma quête du savoir, l'exercice d'une recherche scientifique exigeante, en cultivant la rigueur intellectuelle, la réflexivité éthique et dans le respect des principes de l'intégrité scientifique, je m'engage, pour ce qui dépendra de moi, dans la suite de ma carrière professionnelle quel qu'en soit le secteur ou le domaine d'activité, à maintenir une conduite intègre dans mon rapport au savoir, mes méthodes et mes résultats.

***